Reconstitution of Eukaryotic DNA Replication and Replication-Coupled Chromatin Assembly In Vitro

Hill, Jacob Hopkins

Awarding institution:
King's College London

Reconstitution of Eukaryotic DNA Replication Termination and Replication-Coupled Chromatin Assembly *In Vitro*

Jake Hill

King's College London

and

The Francis Crick Institute

PhD Supervisor: Dr John F.X. Diffley

A thesis submitted for the degree of

Doctor of Philosophy

King's College London

September 2018

Declaration

I, Jake Hill, confirm that the work presented in this thesis is my own. Where information has been derived from other sources, I confirm that this has been indicated in the thesis.

Abstract

Eukaryotic DNA replication machinery disrupts the structure of chromatin as the replication fork progresses through DNA. Importantly, the histone content must be duplicated every cell cycle in addition to the DNA. Whilst a number of insights into the initiation and elongation phases of replication on chromatin have been revealed from decades of work *in vivo* and *in vitro*, many mechanistic details of the later stages of replication remain poorly understood.

In this study, I used an *in vitro* biochemical approach to build upon the work described by Yeeles et al. (2017) and Kurat et al. (2017). I reconstituted Okazaki fragment maturation and identified the minimal set of proteins involved in this process on both naked and chromatinised DNA: Fen1, DNA ligase I, PCNA, and DNA polymerase δ. I then showed that these proteins – in addition to those required for replication initiation – are sufficient to generate relaxed, covalently closed daughter DNA. The process of termination is slow and inefficient relative to the rest of replication, however, and leads to the accumulation of late replication intermediates. I showed that Pif1 is able to enhance termination by (1) decreasing the amount of time it takes to occur and (2) resolving the late replication intermediates generated in the absence of Pif1.

Furthermore, I found that excess Mcm2-7 are inhibitory to replication on chromatin and must be removed from the DNA. I then identified a novel pathway for Mcm2-7 removal during replication involving Pif1. It has been known for many years that cells licence more origins of replication than are used in each cell cycle. In fact, many species (including humans) have been shown to load many more Mcm2-7 than there are origins on DNA. This is the first indication that they need to be removed during replication, and the data presented in this thesis provides a mechanism for how they are removed from the DNA.

Subsequently, I reconstituted replication-coupled chromatin assembly with purified proteins *in vitro* for the first time and identified the minimal set of proteins required for this process: histones, CAF-1, and Asf1. I also showed that regular spacing of nucleosomes on nascent DNA requires a nucleosome remodeller such as ISW1a. I then established a system for studying complete chromatin replication *in vitro*, including both the recycling of parental histones and *de novo* chromatin assembly by CAF-1 and Asf1.

Acknowledgements

Firstly, I would like to thank my supervisor, Dr John Diffley. This project would not have been possible without him, and his encouragement and guidance have helped me enormously throughout my PhD. Thanks also to the members of my thesis committee, Dr Simon Boulton, Dr Shaun Thomas, and Dr Hasan Yardimci, for their advice and support over the past four years.

Within the Francis Crick Institute, thanks to Ali Alidoust, Namita Patel, and Damini Patel in Fermentation Services and to Dr Bram Snjiders and Dr Steven Howell in Mass Spectrometry. I am also indebted to my collaborators Patrik Eikhoff and Dr Alessandro Costa for their expertise in EM.

Special thanks to all current and former members of the Diffley lab, including Joe Yeeles, Christoph Kurat, Steph Hills, Corella Casas-Delucchi, Gideon Coster, Max Douglas, Mona Yekezare, Anne Early, Lucy Drury, Tom Deegan, Belen Gomez-Gonzalez, Kerstin Kinkelin, Agnieszka Janska, Khalid Siddiqui, Theo van Laar, Allie McClure, Eiko Ozono, Agos Bertolin, Viktor Posse, Chris Smith, and Chew Theng Lim. I am especially grateful to Joe, Christoph, and Corella for their endless patience and invaluable scientific advice during my time at Clare Hall and later at the Francis Crick Institute. Thanks to Anne, Lucy, and Gideon for helping me to land on my feet in the early days of my project at Clare Hall. Additionally, I thank Steph for reading the first draft of this thesis and for being a wonderful bench mate over the course of my PhD.

I would like to thank my family and friends, many of whom have helped to keep me sane over the past four years. Special thanks to my parents and grandparents in particular for their constant encouragement and unwavering support, without which none of this would have been possible.

Finally, thanks to my partner, Zhou, for listening to my worrying over experiments, for keeping me focused, and for his love and support throughout my PhD.

Table of Contents

Table of Figures

List of Tables

Abbreviations

Acetyl-CoA	Acetyl-Coenzyme A
ACS	ARS consensus sequence
AEBSF	4-(2-aminoethyl)benzenesulfonyl fluoride hydrochloride
APC/C	anaphase Promoting Complex/Cyclosome
ARS	autonomously replicating sequence
Asf	anti-silencing function
ATP	adenosine 5'-triphosphate
ATPγS	adenosine 5'-O-(3-thio)triphosphate
βME	2-mercaptoethanol
Bp	base pair
BSA	bovine serum albumin
Cac	chromatin assembly complex
CBP	calmodulin binding peptide
Cdc	cell division cycle
CDK	cyclin-dependent kinase
Cdt	Cdc10-dependent transcript
Clb	cyclin B
CMG	Cdc45-Mcm2-7-GINS
CMGE	CMG-Pol ε
Csm	chromosome segregation in meiosis
Ctf	chromosome transmission fidelity
Cryo-EM	cryo-electron microscopy
CTD	C-terminal domain
Dbf	dumpbell forming
DDK	Dbf4-dependent kinase
Dna	DNA synthesis defective
DNA	deoxyribonucleic acid
dNTP	deoxynucleoside triphosphate
Dpb	DNA polymerase B possible subunit
dsDNA	double-stranded DNA

DTT	dithiothreitol
EDTA	ethylenediaminetetraacetic acid
EGTA	ethylene glycol tetraacetic acid
EM	electron microscopy
FACT	facilitates chromatin transcription
GST	glutathione S-transferase
HRP	horseradish peroxidase
IgG	immunoglobulin G
IPTG	isopropyl-1-thio-β-D-galactopyranoside
kDa	kilo Dalton
Mcm	minichromosome maintenance
MNase	micrococcal nuclease
Mrc	mediator of the replication checkpoint
MTBP	Mdm2 binding protein
NTD	N-terminal domain
NTP	ribonucleoside 5'-triphosphate
OCM	ORC-Cdc6-Mcm2-7
OCCM	ORC-Cdc6-Cdt1-Mcm2-7
Orc	origin recognition complex
PBS	phosphate buffered saline
PCR	polymerase chain reaction
PCNA	proliferating cell nuclear antigen
PEG	polyethylene glycol
PepA	Pepstatin A
Pif	petite integration frequency
PMSF	phenylmethylsulfonyl fluoride
Pol	polymerase
Pre-RC	pre-replicative complex
Psf	partner of Sld5
Rad	radiation sensitive
RLF	replication licensing factor
RPA	replication protein A
RPC	replisome progression complex

Rpm	revolutions per minute
Rtt	regulator of Ty1 transposition
SDS-PAGE	sodium dodecyl sulphate polyacrylamide gel electrophoresis
Sld	synthetically lethal with *dpb11-1*
Sic	substrate inhibitor of cyclin dependent kinase
ssDNA	single stranded DNA
STD	Sld3/Treslin domain
TAE	Tris acetate EDTA
TCP	TEV-CBP-protein A
TE	Tris-HCl EDTA
TEV	tobacco etch virus
TICRR	TopBP1 interacting checkpoint and replication regulator
Tof	topoisomerase I interacting factor
TopBP	topoisomerase II binding protein
Vps	vacuolar protein sorting
WT	wild type
YPD	yeast peptone glucose

Chapter 1. Introduction

1.1 Overview

The ability to duplicate genetic material is an essential requirement for any proliferating cell. In eukaryotic cells, genome duplication is tightly coupled to the four phases of the cell cycle: G_1, S, G_2, and M (Figure 1.1). The progression of a cell through the different phases is driven by oscillations in the activity of the cyclin-dependent kinases (CDKs). Chromosomal replication occurs during S (synthesis) phase of the cycle prior to chromosome segregation and cell division in the subsequent M (mitosis) phase (Morgan, 2007).

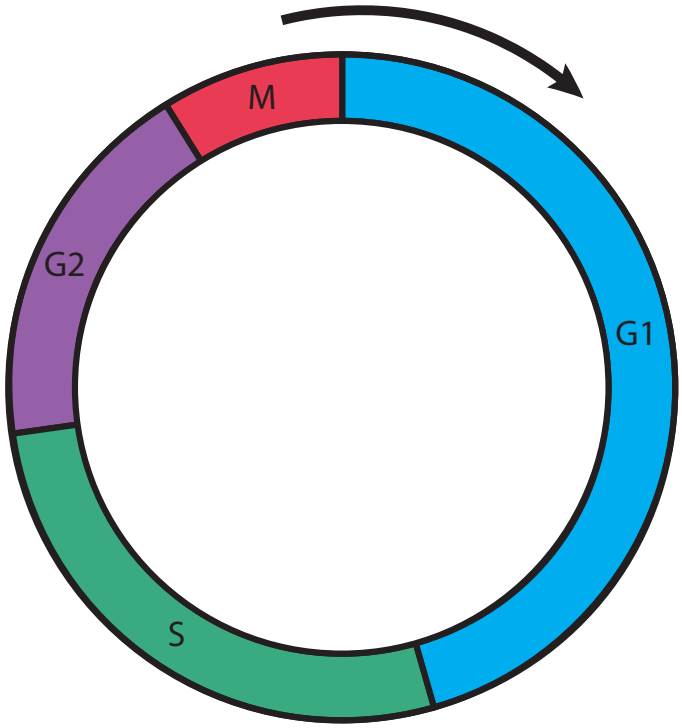

Figure 1.1 Schematic of the eukaryotic cell cycle
The human cell cycle lasts for approximately twenty-four hours, whereas budding yeast progress through the cycle in ninety minutes.

Notably, eukaryotic genomes are much larger than those of prokaryotes and are consequently more challenging to replicate; the forty-six chromosomes in the nuclei of most human cells contain approximately two metres of genetic material, or DNA. Importantly, under- or over- replication of the genome during S-phase can result in gene amplifications or chromosomal

rearrangements, which can ultimately lead to genomic instability and the onset of tumorigenesis (Arias and Walter, 2007; Blow and Gillespie, 2008; Green et al. 2010). Thus, this process must be tightly regulated to ensure that the genome is replicated free of errors only once per cell cycle.

This regulation is accomplished in large part during the early stages of replication. Whilst bacterial genomes can be replicated from a single site, or origin of replication, the vast size of eukaryotic genomes has led them to evolve such that replication initiates from numerous origins of replication across multiple chromosomes. In *Saccharomyces cerevisiae*, origins are called autonomously replicating sequences (ARS). The initiation of replication involves two conserved, mutually exclusive steps: origin licensing followed by origin activation (Blow and Laskey, 1988; Blow, 1993; Diffley et al. 1994).

1.1.1 Origin licensing and the Mcm2-7 paradox

The first step, origin licensing, occurs during late M and G_1 (gap 1) phases of the cell cycle and involves the recognition and binding of the hexameric Origin Recognition Complex (ORC) to origins of replication on DNA. ORC then recruits the Minichromosome-maintenance (MCM) complex (Mcm2-7) to these origins with the assistance of two additional proteins, Cdc6 and Cdt1. This process has also been called pre-Replicative Complex (pre-RC) assembly and was recently reconstituted with purified components *in vitro* (Bell and Dutta, 2002; Evrin et al. 2009; Remus et al. 2009). These studies revealed that licensed origins contain two copies of Mcm2-7 in a double hexamer configuration bound around double-stranded DNA (dsDNA) (Remus et al. 2009). Importantly, these Mcm2-7 double hexamers are inactive once they are loaded onto DNA.

In *S. cerevisiae* and in humans, many more origins are licensed than are used during normal replication. Unused licensed origins are called dormant origins, and they can be activated in the event of fork stalling (due to replication stress) in order to ensure that the genome is replicated in its entirety in any given cell cycle (Ge et al. 2007). Indeed, Mcm2-7 is loaded in

approximately twenty-fold excess over both replication origins and ORC (Burkhart et al. 1995; Lei et al. 1996; Rowles et al. 1996; Donovan et al. 1997; Mahbubani et al. 1997; Edwards et al. 2002), much of which has been found to be distributed at significant distances from ORC-bound DNA (Ritzi et al. 1998; Edwards et al. 2002; Harvey and Newport, 2003). Furthermore, reducing the amount of Mcm2-7 in cells has no effect on DNA synthesis unless cells are subjected to replication stress (Cortez et al. 2004; Tsao et al. 2004; Ge et al. 2007).

Despite recent advances in the field, it is unclear what happens to the excess unused Mcm2-7. In *Xenopus* and mammals, the MCM proteins do not co-localise with newly-replicated DNA (Krude et al. 1995; Todorov et al. 1995; Romanowski et al. 1996). Furthermore, in mammals it has been shown via immunofluorescence that Mcm2 is detectable at the end of G_1 phase but disappears (or is undetectable) at replication forks five minutes into S-phase (Dmitrova et al. 1999). This might be explained if all but the active Mcm2-7 was present at the replication fork (Takahashi et al. 2005).

1.1.2 CMG assembly and activation

Origin licensing occurs during G_1 phase of the cell cycle when CDK activity is low and the activity of the Anaphase Promoting Complex/Cyclosome (APC/C) E3 ubiquitin ligase is high (Arias and Walter, 2007; Siddiqui et al. 2013). Following a reduction in APC/C activity, the coordinated activities of CDK and Dbf4-dependent kinase (DDK) are then required to activate the loaded Mcm2-7 during S-phase of the cell cycle (Bousset and Diffley, 1998; Donaldson et al. 1998; Zou and Stillman, 1998). In eukaryotes, activation is strictly regulated by a temporal programme (Fangman and Brewer, 1992; Diller and Raghuraman, 1994). This process is initiated when DDK phosphorylates the Mcm4 and Mcm6 subunits of Mcm2-7, which in turn leads to the recruitment Sld3, Sld7, and Cdc45 (Deegan et al. 2016). CDK phosphorylation of Sld3 and Sld2 then precedes the recruitment of a number of 'firing factors' including Sld2, Dpb11, DNA polymerase ε, Mcm10, and the hetero-tetrameric GINS complex (Tanaka et al. 2007; Zegerman and Diffley,

2007; Yeeles et al. 2015). The inactive Mcm2-7 is thus converted into an active Cdc45-Mcm2-7-GINS (CMG) complex, encircling single stranded DNA (ssDNA). This complex comprises the core of the eukaryotic replisome. The reconstitution of this process *in vitro* with cell-free extracts and more recently with purified proteins has revealed these to be the minimal set of components required to form an active CMG (Gros et al. 2014; On et al. 2014; Yeeles et al. 2015). The current model for origin licensing and activation of the CMG is depicted in Figure 1.2. Though Sld2, Sld3, and Dpb11 are required for activation they are not thought to travel with the replisome (Gambus et al. 2006; Kanemaki and Labib, 2006; Tanaka et al. 2007). In contrast, DNA polymerase ε is essential for activation and remains associated with the CMG (Tanaka and Araki, 2013; Sengupta et al. 2013; Pellegrini and Costa, 2016). Whilst Mcm10 does not co-purify with CMG, it has been shown to associate with both Mcm2-7 and DNA polymerase α (Ricke and Bielinsky, 2004; Douglas and Diffley, 2016; Quan et al. 2015).

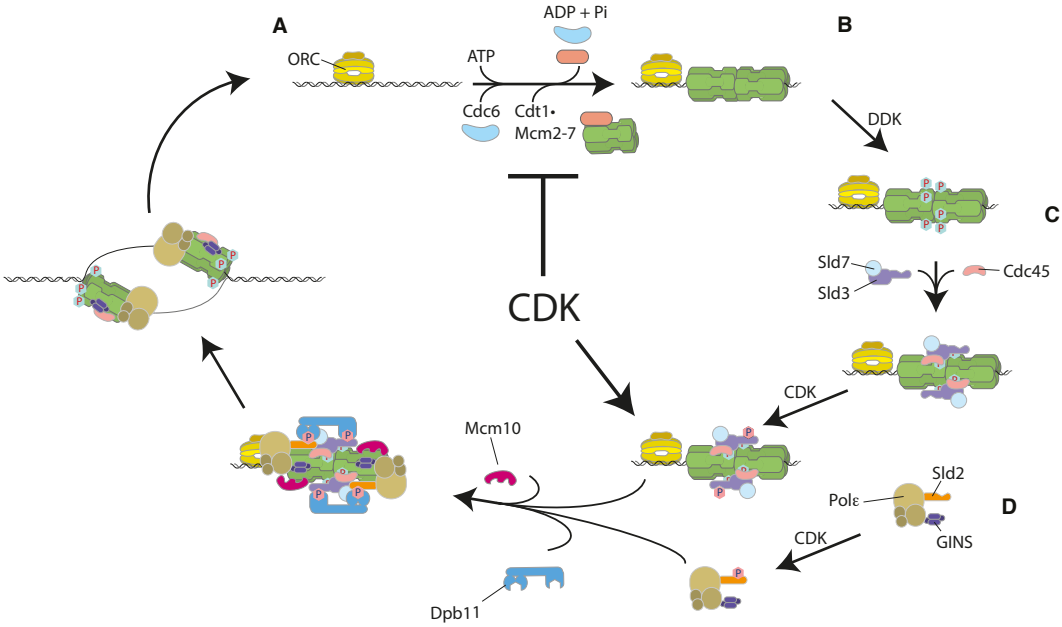

Figure 1.2 Model for origin licensing and activation of the CMG
(A) Origin licensing. (B) DDK phosphorylation of Mcm2-7. (C) Recruitment of Sld3, Sld7, and Cdc45. (D) CDK phosphorylation of Sld2 and Sld3, and recruitment of DNA polymerase ε and GINS.

Importantly, CDK plays a dual role in ensuring that replication occurs only once per cell cycle. In addition to its function in assembling the CMG, it also

prevents additional licensing outside of G_1 by phosphorylating ORC, Cdc6, and Mcm2-7 (Nguyen et al. 2001).

Furthermore, an additional set of factors has been shown to co-purify with CMG from S-phase cells in *S. cerevisiae*. These comprise the replisome progression complex (RPC) and include Ctf4, DNA polymerase α, Csm3, Tof1, Mrc1, FACT, and Topoisomerase I (Gambus et al. 2006). Mrc1, Csm3, and Tof1 have recently been shown to be required for the establishment of *in vivo* replication rates (Yeeles et al. 2017). Topoisomerase II, DNA polymerase δ, replication factor C (RPC), and the sliding clamp proliferating cell nuclear antigen (PCNA) have also been found to associate with replication forks, though they do not co-purify with the RPC (Yu et al. 2014).

Chromosome transmission fidelity 4 (Ctf4) forms a heterotrimer and has been shown to interact with DNA polymerase α, DNA polymerase ε, and GINS (Simon et al. 2014; Villa et al. 2016). In light of these observations, it has been proposed to link the leading and lagging strand machineries at the replication fork (Burgers and Kunkel, 2017). Ctf4 also interacts with chromosome loss 1 (Chl1), a protein known to play a role in the establishment of cohesion (Samora et al. 2016). This indicates that it may be important for coupling this process to replication. Interestingly, deletions of Ctf4 are viable, although they lead to an increase in genomic instability (Hanna et al. 2001; Fumasoni et al. 2015; Calzada et al. 2005).

1.2 Okazaki fragment maturation

Following establishment of an active CMG, synthesis proceeds bi-directionally from origins of replication. Given the intrinsic directionality of the CMG, the template is unwound and read in a 3' to 5' direction along the DNA. The nascent strands are then elongated by DNA polymerases that incorporate dNTPs in the 5' to 3' direction along the DNA. This means that one strand can be synthesised continuously (leading strand) whereas the other must be synthesised discontinuously and in the opposite direction (lagging strand). The DNA polymerase α/primase complex synthesises and elongates short

RNA primers (~20 nucleotides in total) that are extended on the leading strand primarily by DNA polymerase ε and on the lagging strand by DNA polymerase δ (Daigaku et al. 2015; Georgescu et al. 2015; Burgers and Kunkel, 2017). Recently, it was suggested that DNA polymerase δ also plays a role in the establishment of leading strand synthesis (Yeeles et al. 2017). Unlike the leading strand, replication on the lagging strand is achieved through the synthesis of short fragments, which are eventually processed (matured) to form a single, continuous strand of DNA. These are called Okazaki fragments in honour of Reji and Tuneko Okazaki, who first proposed a model for their synthesis in 1968 (Okazaki et al. 1968). Roughly 50 million Okazaki fragments are synthesised during a single S-phase in mammalian cells, underlying the need for rapid yet accurate maturation (Balakrishnan and Bambara, 2011).

In addition, DNA polymerase α/primase lacks 3'-5' exonuclease ('proofreading') activity and is thus considered to be an error-prone polymerase (Balakrishnan and Bambara, 2013). It is therefore important that the RNA primer and any DNA synthesised by DNA polymerase α/primase is removed and replaced by a high fidelity polymerase, such as DNA polymerase δ or DNA polymerase ε (Balakrishnan and Bambara, 2013).

1.2.1 Strand displacement by DNA polymerase δ

In *S.* cerevisiae, DNA polymerase δ is a complex consisting of three subunits: Pol3, Pol31, and Pol32 (Gerik et al. 1998). Pol3 is the catalytic subunit and it contains both polymerase and exonuclease (3'-5') activities (Stodola and Burgers, 2016). Furthermore, all three subunits contain PIP-box motifs (QxxhxxFF) for interacting with PCNA (Lu et al. 2002; Acharya et al. 2011). Interactions with PCNA have been shown to increase the processivity of both DNA polymerase δ and DNA polymerase ε *in vitro* (Chilkova et al. 2007; Yeeles et al. 2017).

During replication on the lagging strand, PCNA is loaded onto primer termini by RFC in a reaction that requires the hydrolysis of ATP (Tsurimoto and Stillman, 1990). DNA polymerase δ interacts with PCNA to extend primers synthesised by DNA polymerase α/primase until it reaches the 5'-end of a downstream Okazaki fragment, at which point it begins to displace the RNA/DNA. Importantly, the rate of synthesis decreases with each displaced nucleotide. This ensures that the flaps generated by the polymerase do not become too long for downstream processing (Burgers and Kunkel, 2017). In addition, DNA polymerase δ has been shown to switch between its polymerase and nuclease activities, leading to a cycle of continuous elongation and degradation of the nascent DNA (Burgers, 2009). This process has been termed 'idling' and is another mechanism through which the polymerase is restricted from excessive strand displacement.

Unlike DNA polymerase δ, DNA polymerase ε is very poor at strand displacement synthesis (Georgescu et al. 2014; Garg et al. 2004; Podust et al. 1993). Recently, it was shown that DNA polymerase ε is unable to carry out extensive strand displacement synthesis unless its 3'-5' exonuclease activity is first removed (Ganai et al. 2016).

1.2.2 The role of nucleases in Okazaki fragment maturation

Following the onset of strand displacement synthesis, the displaced nucleotides form a single-stranded flap structure that must be removed in preparation for downstream ligation (Bambara et al. 1997; Liu et al. 2004; Burgers et al. 2009). Two pathways exist for removing these displaced nucleotides, depending on the length of the flap generated by DNA polymerase δ. In one pathway, flap endonuclease 1 (Fen1) removes predominantly single nucleotides as they are displaced by the polymerase (Stodola and Burgers, 2016). Fen1 is encoded by the *rad27* gene in *S. cerevisiae* and is homologous to human FEN1 (Balakrishnan and Bambara, 2013). It has a PIP-box motif and binds to PCNA, which presumably localises it to the lagging strand with DNA polymerase δ (Chapados et al. 2004). In some situations, it is possible for strand displacement synthesis to form

longer flaps (e.g. in AT-rich regions of DNA), leading to an increase in catalytic activity by Fen1. This is thought to be another mechanism to ensure that the flaps displaced by the polymerase remain short (Burgers and Kunkel, 2017). Interestingly, Fen1 is not essential in *S. cerevisiae*, suggesting that other nucleases may be able to substitute for its role in Okazaki fragment maturation, albeit less efficiently, such as exonuclease 1 (Exo1) (Burgers, 2009; Balakrishnan and Bambara, 2013).

Sometimes, strand displacement can become uncoupled from the nuclease activity of Fen1. This is due to secondary structure formation or the binding of replication protein A (RPA), which is inhibitory to Fen1 (Burgers and Kunkel, 2017). In such situations, a second nuclease is required to process these flaps, which is the essential DNA synthesis defective 2 (Dna2) nuclease in *S. cerevisiae*. Dna2 is from a family of conserved proteins containing distinct helicase and nuclease domains (Budd et al. 1995) and it has a preference for cleaving long 5' nucleotide flaps (Bae et al. 1998; Bae and Seo, 2000; Bae et al. 2001; Kim et al. 2006; Masuda-Sasa et al. 2006; Zheng et al. 2008). However, Dna2 cleavage is not as precise as that of Fen1 and has been shown to leave behind short flaps of up to 5 nucleotides, with the remaining cleavage thought to be carried out by Fen1 (Kang et al. 2010; Levikova and Cejka, 2015). Recently, Dna2 was found to interact with Ctf4, which may play a role in its recruitment to the replication fork (Villa et al. 2016). In addition to its role in Okazaki fragment maturation, Dna2 has also been implicated in the DNA damage response given its role in activating the kinase mitosis entry checkpoint 1 (Mec1) (Wanrooij and Burgers, 2015).

Importantly, Dna2's nuclease activity is essential, unlike its helicase activity (Formosa and Nittis, 1999; Kang et al. 2000). Intriguingly, the lethality of Dna2 deletions is suppressed by conditions/mutations that limit strand displacement synthesis, such as overexpressing Fen1, deleting the Pol32 subunit of DNA polymerase δ, or deleting petite integration frequency 1 (Pif1) (Stith et al. 2008; Pike et al. 2009; Budd et al. 2006). Pif1 is a 5'-3' helicase conserved from yeast to humans and it has been shown to enhance strand

displacement synthesis by DNA polymerase δ (Bessler et al. 2001; Boule and Zakian, 2006; Rossi et al. 2008; Osmundson et al. 2017). In light of these results, it has been proposed that Pif1 may promote the formation of long flap substrates during Okazaki fragment maturation *in vivo* and is involved in the same pathway as Dna2 and DNA polymerase δ (Rossi et al. 2008). Recently, a crystal structure was published showing an interaction between PCNA and a non-canonical PIP-box motif in Pif1 (Buzovetsky et al. 2017). Mutations in this motif impaired the ability of Pif1 to enhance strand displacement synthesis by DNA polymerase δ *in vitro* (Buzovetsky et al. 2017). This interaction may explain how Pif1 is localised to replication forks, specifically the lagging strand DNA.

In addition to the nucleases Fen1 and Dna2, a third pathway for removing RNA primers involves ribonuclease H (RNaseH). These are a class of enzymes that are specifically able to remove RNA from hybrids containing RNA and DNA (Balakrishnan and Bambara, 2013). In eukaryotes, these include RNase H1 and RNase H2. *S. cerevisiae* without either of these enzymes are viable, suggesting that they are redundant for other RNA removal pathways during replication (Frank et al. 1998; Qiu et al. 1999). RNase H2 is thought to be the more important of the two for replication and has been shown to hydrolyse RNA primers during Okazaki fragment maturation by cleaving single 5' ribonucleotides (Murante et al. 1998). Importantly, RNase H2 is only able to cut up to the last ribonucleotide before the DNA, which must then be removed by Fen1 (Balakrishnan and Bambara, 2013; Murante et al. 1998; Eder et al. 1993).

1.2.3 Joining the fragments together: DNA ligase I

Iterative displacement and cleavage of nucleotides by DNA polymerase δ, Fen1 and/or Dna2 (i.e. 'nick translation') continues until the generation of a ligatable end, which then allows the two upstream and downstream Okazaki fragments to be joined together by a ligase, which is DNA ligase I in *S. cerevisiae* (Johnston and Nasmyth, 1978). Originally identified as a conditional cell cycle mutant, the *cdc9* gene was later shown to encode DNA

ligase I (Culotti and Hartwell, 1971; Johnston and Nasmyth, 1978). Ligation of all Okazaki fragments leads to the formation of a single, continuous lagging strand of DNA. The current model for Okazaki fragment maturation is depicted in Figure 1.3 (reproduced from Burgers and Kunkel, 2017).

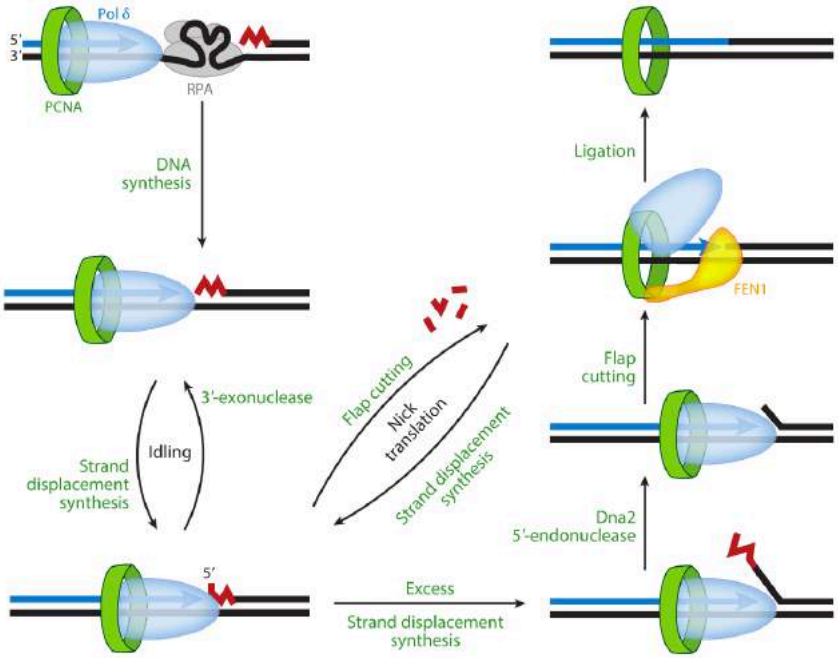

Figure 1.3 Model for Okazaki fragment maturation
Model for Okazaki fragment maturation showing strand displacement by DNA polymerase δ, cleavage of the displaced strands by Fen1 and/or Dna2, and ligation of the two Okazaki fragments by DNA ligase I (figure reproduced from Burgers and Kunkel, 2017).

Like DNA polymerase δ and Fen1, DNA ligase I contains a PIP-box motif that allows it to interact with PCNA (Vijayakumar et al. 2007). It has been proposed that all three of the core Okazaki fragment maturation proteins (DNA polymerase δ, Fen1, and DNA ligase I) simultaneously bind the homotrimeric PCNA; this has been referred to as the 'toolbelt' model (Indiani et al. 2005). Recently, this model was demonstrated in *S. cerevisiae* with DNA polymerase δ and Fen1 (Stodola and Burgers, 2016). However, it is not essential that these proteins bind simultaneously, as has been shown with PCNA mutants that can only bind either DNA polymerase δ or Fen1 (Dovrat et al. 2014).

1.3 Termination

When two replisomes approach one another, a number of processes are set in motion that result in the formation of two covalently closed daughter molecules of DNA. These include (though not necessarily in this order) replisome convergence, completion of synthesis (including processing of the final Okazaki fragment and ligation of adjacent lagging and leading strands), resolution (decatenation) of the nascent DNA, and disassembly of the CMG (Dewar and Walter, 2017). Compared to the early stages of replication, significantly less is known about the mechanisms of termination. Work in recent years has shed light on this process *in vivo* and *in vitro*. The current model of eukaryotic replication termination is depicted in Figure 1.4 (reproduced from Dewar and Walter, 2017).

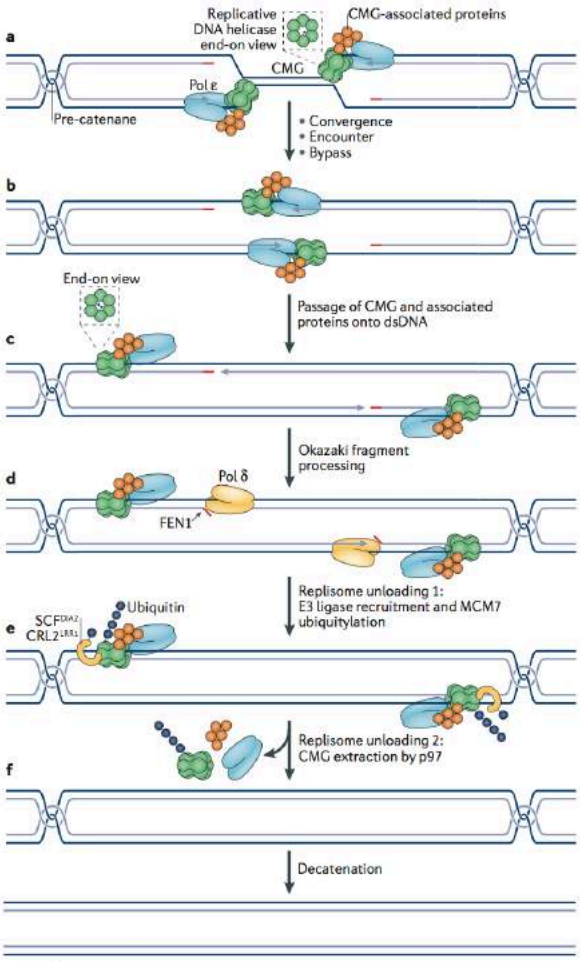

Figure 1.4 Eukaryotic DNA replication termination
(A-F) Replisome convergence, completion of synthesis, decatenation, and replisome disassembly (figure reproduced from Dewar and Walter, 2017).

1.3.1 Replisome convergence and completion of replication

The first step in eukaryotic replication termination involves the convergence of two CMGs. This requires the removal of any proteins that may be bound to the DNA in between the CMGs. In *Xenopus* extracts, it has been observed that converging replisomes do not slow down or stall as they approach one another, and that opposing leading strands are ligated to downstream Okazaki fragments prior to disassembly of the CMG (Dewar et al. 2015). Furthermore, the completion of synthesis and the final ligation step are not affected in the absence of a pathway for removing CMG (Dewar et al. 2015). This has led to the proposal that CMGs pass one another and are subsequently removed from dsDNA (Dewar et al. 2015).

During the elongation stage of replication, unwinding of the template DNA generates compensatory overwinding (positive supercoils) ahead of the CMG (Postow et al. 2001; Wang, 2002). The replisome is able to transmit this stress behind the replication fork by rotating and intertwining the daughter strands to form pre-catenanes, which become catenated daughter molecules following replication (Been and Champoux, 1980; Lucas et al. 2001; Zechiedrich and Cozzarelli, 1995). In *S. cerevisiae* it has been observed that pre-catenanes are restricted by a lack of fork rotation caused by Csm3 and Tof1 (Schalbetter et al. 2015). Thus, any supercoils that are generated at this stage can be resolved by either Topoisomerase I or Topoisomerase II (Wang, 2002; Yeeles et al. 2015). It remains unclear as to where these proteins are acting relative to the replication fork, although Topoisomerase I is part of the RPC (Gambus et al. 2006).

In addition, during termination the space between two replisomes becomes limiting for Topoisomerase I and Topoisomerase II to resolve any topological stress in the DNA (Sundin and Varshavsky, 1980). In this situation, fork rotation and pre-catenane formation are the primary ways through which the replisome transmits the torsional stress behind the replication fork (Gambus, 2017).

In addition to their role in Okazaki fragment maturation, the Pif1 family helicases – including Pif1 and rDNA recombination mutation (Rrm3) in *S. cerevisiae* – have been shown to promote replication through difficult regions of the genome (Paeschke et al. 2011; Paeschke et al. 2013; Boule et al. 2005; Koc et al. 2016). More recently Pif1 has been shown to promote the convergence of two replication forks *in vivo* (Steinacher et al. 2012). It is possible that these proteins (and/or others) are required to facilitate termination in addition to those already known to be present at the replication fork. This may help to explain why the recent reconstitution of termination with purified proteins was shown to be relatively inefficient *in vitro* (Devbhandari et al. 2017).

1.3.2 Decatenation of daughter DNA

Intertwined duplex DNA can only be resolved (decatenated) by Topoisomerase II. Thus, catenated replication products are only resolved when it is present, despite the fact that replication proceeds normally in its absence (presumably due to the presence of Topoisomerase I) (Dewar et al. 2015; Baxter and Diffley, 2008; DiNardo et al. 1984). This has also been demonstrated in a fully reconstituted replication system (Devbhandari et al. 2017). However, the inability to decatenate results in fatal problems downstream of replication for cells. In the complete absence of Topoisomerase II, for example, chromosomes are extensively missegregated *in vivo*; in the absence of catalytically active Topoisomerase II, cells arrest in G_2 (Baxter and Diffley, 2008). In either case, this leads to cell death (Baxter and Diffley, 2008; DiNardo et al. 1984; Holm et al. 1985; Uemura and Yanagida, 1984).

It is not clear when decatenation occurs in the sequence of events that constitute the end of replication, although it is not required for fork convergence and ligation (Dewar et al. 2015). It is often depicted as occurring after replisome convergence and replisome disassembly (though it may occur simultaneously with these other processes).

1.3.3 Replisome disassembly

Following the convergence of two replisomes and the completion of synthesis, the replisomes must then be removed from the DNA. This is an important step in order to ensure that the genome is replicated only once per cell cycle. In late S-phase in both *S. cerevisiae* and *Xenopus*, Mcm7 becomes polyubiquitylated with K48-linked ubiquitin chains (Moreno et al. 2014; Maric et al. 2014). This requires the SCF^{Dia2} (Skp, Cullin, F-box-containing complex associated with Dia2) E3 ubiquitin ligase in *S. cerevisiae* and the $CRL2^{LRR1}$ (Cullin RING ligase 2 associated with LRR1) E3 ubiquitin ligase in *Xenopus*. It is believed that SCF^{Dia2} remains constantly associated with the replisome, as opposed to specifically associating with terminating replisomes like $CRL2^{LRR1}$ (Gambus et al. 2006; Dewar et al. 2017). Once Mcm7 is ubiquitylated, the CMG is removed by the ATPase Cdc48 (along with a number of cofactors) in *S. cerevisiae* or p97 in *Xenopus* (Moreno et al. 2014; Maric et al. 2014; Franz et al. 2011; Meyer et al. 2012). It is not clear whether the CMG is degraded or de-ubiquitylated following removal from the DNA (Gambus et al. 2017). Recent experiments carried out in *Xenopus* suggest that it is de-ubiquitylated (Fullbright et al. 2016).

It is currently unclear how CMG disassembly is regulated to ensure that it only occurs following the end of replication, though one could speculate that it may have to do with the ability to access the ubiquitylation site on Mcm7.

Intriguingly, a backup mechanism for removing CMG has been identified in *C. elegans*. If $CRL2^{LRR1}$ is defective and the CMG is not removed during S-phase, then it can be removed in early mitosis (late prophase) by CDC-48 and its cofactor, UBXN-3 (Sonneville et al. 2017). However, *S. cerevisiae* lacking Dia2 retain CMGs on chromatin until the G1-phase of the next cell cycle (Maric et al. 2014). It remains to be see whether or not a similar pathway exists in humans.

1.4 Chromatin replication

In vivo, DNA in the nuclei of cells is packaged into a structure called chromatin. Thus, chromatin is the natural substrate for processes such as replication and transcription. The fundamental repeating unit of eukaryotic chromatin is the nucleosome, which is composed of two copies each of four (positively-charged) histone proteins: H2A, H2B, H3, and H4. These are wrapped around roughly 147 bp of DNA. The inherent stability of nucleosomes provides an opportunity to store information at specific positions in the genome in the form of covalent histone modifications. Importantly, the histone proteins and any modifications they contain must be replicated in each S-phase along with the DNA. The disruption of the chromatin landscape during replication provides an opportunity to change (or maintain) specific histone modifications. Such replication-induced alterations can change the transcriptional state of a cell (Burgess and Zhang, 2013). However, relatively little is known about how the replication machinery interacts with chromatin.

The coupling of DNA replication to nucleosome assembly is important as impaired nucleosome assembly in humans can destabilise replication forks, and eventually give rise to damage and genomic instability (Groth et al. 2007; Nabatiyan and Krude, 2004; Hoek and Stillman, 2003; Mejlvang et al. 2014; Ye et al. 2003). One mechanism that has been proposed in recent years involves nucleosome assembly on the lagging strand (Alabert et al. 2017; Kurat et al. 2017; Devbhandari et al. 2017; Smith and Whitehouse, 2012). In this model, nucleosomes are formed on Okazaki fragments as they are sufficiently elongated by DNA polymerase δ. Intriguingly, it has been pointed out that the size of an Okazaki fragment is roughly the size of a nucleosome repeat (approximately 200 bp in humans) (Alabert et al. 2017). It was demonstrated previously that Fen1 and DNA ligase I are able to function in a chromatin environment in *S. cerevisiae* (Chafin et al. 2000; Huggins et al. 2002). This has also been supported by the recent reconstitution of this process *in vitro*, although it did not appear that all of the fragments were matured to the same degree (Devbhandari et al. 2017). It may be the case that

additional factors are required for this process to be efficient in the context of chromatin, such as histone chaperones and nucleosome remodellers. In addition, the sequencing of Okazaki fragments from *S. cerevisiae* revealed that ligation sites between two fragments are close to nucleosome dyads (Smith and Whitehouse, 2012). Strand displacement synthesis by DNA polymerase δ (and thus the size of Okazaki fragments) is also restricted by nucleosome assembly on the nascent DNA (Devbhandari et al. 2017). Thus, the current model is that strand displacement occurs until DNA polymerase δ reaches a downstream nucleosome, at which point the adjacent Okazaki fragments are ligated together by DNA ligase I. This model also fits with the observation that PCNA is not unloaded from DNA until after Okazaki fragment ligation, and that impaired nucleosome assembly leads to impaired unloading of PCNA (Kubota et al. 2015; Mejlvang et al. 2014). How replication might be coupled to nucleosome assembly on the leading strand is less clear, and is discussed in the next section.

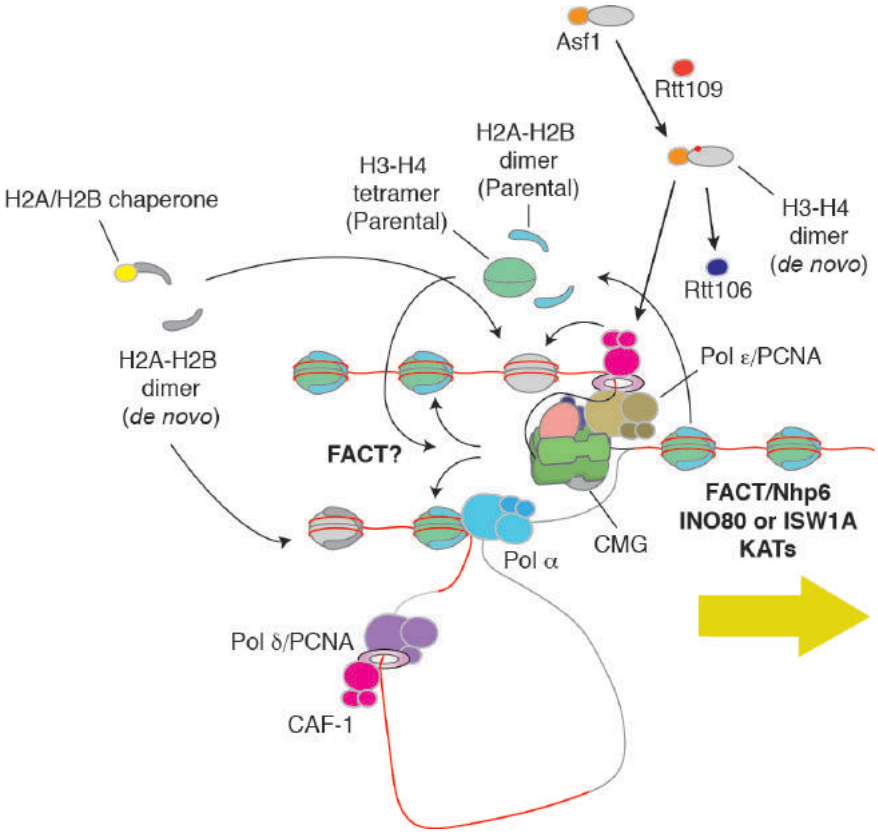

Figure 1.5 Model for chromatin replication
Current model for replication through chromatin (figure modified from Kurat et al. 2017).

1.4.1 Parental histone recycling

Early experiments using phage T4 replication proteins and SV40 minichromosomes in human cell extracts revealed that nucleosomes ahead of the replication fork do not dissociate from and remain bound to replicated DNA (Bonne-Andrea et al. 1990; Krude and Knippers 1991; Randall and Kelly, 1992). It was also shown that these nucleosomes are rapidly re-assembled and dispersed to both of the daughter strands *in vivo* (McKnight and Miller, 1977; Cusick et al. 1984; Sogo et al. 1986). However, it remained unclear as to how the replisome is able to progress through nucleosome-bound DNA.

Recent breakthroughs in the field have revealed that replication through chromatinised templates *in vitro* requires several proteins in addition to those needed to replicate naked DNA (Kurat et al. 2017). These minimally include the histone chaperones facilitates chromatin transcription (FACT) and non-histone protein 6 (Nhp6), though other proteins can enhance replication through chromatin, including acetyltransferases and ATP-dependent nucleosome spacing factors such as imitation switch subfamily 1a (ISW1a) and inositol requiring 80 (INO80) (Kurat et al. 2017). Together, these proteins allow the replisome to achieve *in vivo* replication rates through chromatin *in vitro* (Kurat et al. 2017). However, it remains unclear how these proteins promote replication in the context of chromatin. FACT is essential in *S. cerevisiae* and has been shown to be a part of the RPC (Gambus et al. 2006). It has also been shown to interact with both histones H3-H4 and H2A-H2B (Formosa, 2011; Winkler et al. 2011). It has been proposed to act either in front of the replisome, where it could play a role in disassembling nucleosomes ahead of the replication fork, or behind the replisome, where it could help to deposit parental nucleosomes on the nascent DNA (Kurat et al. 2017). It is possible that it acts in both capacities, and it may have other as yet undiscovered roles in chromatin replication. Nhp6 is required at much higher concentrations, suggesting that it may act distributivity as opposed to travelling with the replication fork (Kurat et al. 2017). INO80 has been shown to alter the position of nucleosomes around replication forks, though it is

unclear how (or if) it is targeted to replication forks during S-phase (Lee et al. 2015).

Furthermore, replication through chromatin in this *in vitro* system resulted in the recycling of parental nucleosomes on the nascent DNA (Kurat et al. 2017). It was previously demonstrated *in vivo* that parental $(H3\text{-}H4)_2$ tetramers generally remain intact and are segregated randomly to the newly synthesised DNA (Xu et al. 2010). Importantly, most of the parental $(H3\text{-}H4)_2$ tetramers have been found to be maintained in close vicinity to their original locus (Jackson and Chalkley, 1981; Radman-Livaja et al. 2011). It is not clear how (or if) (H2A-H2B) dimers are efficiently recycled on the nascent DNA.

Work in *S. cerevisiae* and humans has shed more light on the mechanisms through which parental nucleosomes are recycled by the replisome. Using newly-developed strand-specific sequencing techniques, it was revealed that parental $(H3\text{-}H4)_2$ tetramers are passed mostly symmetrically to both the leading and lagging strands during replication (Petryk et al. 2018; Yu et al. 2018). One group reported a slight leading strand bias in humans (Petryk et al. 2018) whereas another reported a slight lagging strand bias in *S. cerevisiae* (Yu et al. 2018). However, mutating the histone binding domains in DNA polymerase ε (Dpb3 and Dpb4) resulted in a complete lagging strand bias in *S. cerevisiae* (Yu et al. 2018) whereas mutating the histone binding domain of Mcm2 resulted in a significant increase in leading strand bias in humans (Petryk et al. 2018). Importantly, nucleosome partitioning between the daughter strands was affected whereas nucleosome recycling was unaffected in these experiments (Petryk et al. 2018). This data suggests that DNA polymerase ε and Mcm2 play important roles in transferring parental nucleosomes to the leading and lagging strands during replication, respectively, ensuring an equal distribution on the nascent DNA. It also hints at a mechanism for altering nucleosome distribution in response to various stimuli, allowing cells to both maintain and change epigenetic states (Yu et al. 2018). It was previously revealed that the Mcm2 histone binding domain is in its N-terminus with a preference for binding H3-H4 (Foltman et al. 2013;

Huang et al. 2015). In light of recent EM data, this places the histone binding domain at the front of the CMG (Douglas et al. 2018). This would make it ideally situated for binding nucleosomes ahead of the replisome. Other proteins in the replisome have been found to have histone binding domains, such as DNA polymerase α (which preferentially binds H2A-H2B) and RPA (which preferentially binds H3-H4) (Evrin et al. 2018; Liu et al. 2017). Given the viability of yeast cells with mutations in these histone binding motifs, it seems unlikely that these pathways represent the primary mechanism through which parental nucleosomes are transferred to nascent DNA (Petryk et al. 2018; Yu et al. 2018; Evrin et al. 2018). Instead, it is conceivable that a primary pathway exists that deposits the histones non-specifically to the leading and lagging strands (e.g. FACT). Mcm2, DNA polymerase ε, and other histone binding proteins in the replisome might then be important for ensuring that these nucleosomes are distributed evenly between the two strands of the nascent DNA.

1.4.2 *De novo* chromatin assembly

Even if all of the parental nucleosomes are recycled during replication, they will account for (at best) 50% of the nucleosomes on the nascent DNA. In order to establish fully-chromatinised products (which is important for maintaining chromatin states across multiple cell cycles) the remaining nucleosomes must come from a newly-synthesised (*de novo*) histone pool.

The mechanism through which new histones are incorporated into newly synthesised DNA was first discovered and characterised in SV40. Following the establishment of SV40 replication in cytosolic human cell extracts, it was shown that the replication products could be negatively supercoiled upon addition of an extract prepared from nuclei of the same cells (Stillman and Gluzman, 1985). The supercoiling was later shown to preferentially occur on the replicated products due to nucleosome deposition onto the DNA (Stillman, 1986). Chromatin assembly factor 1 (CAF-1) was revealed to be an essential factor for this process following fractionation of the nuclear extract (Smith and Stillman, 1989). CAF-1 is composed of three subunits: Cac1, Cac2,

and Cac3 in *S. cerevisiae* (Kim et al. 2016) and p150, p60, and RbAp48 in humans (Hammond et al. 2017); early experiments revealed that it co-localised with replication forks in human cells (Krude, 1995). It was later shown that CAF-1's ability to deposit nucleosomes onto replicated DNA required an interaction between a PIP-box motif in the p150 subunit and PCNA, effectively coupling chromatin assembly to replication (Shibahara and Stillman, 1999; Zhang et al. 2000).

Several other factors were later implicated in replication-coupled chromatin assembly *in vitro* and *in vivo*. Work in *Drosophila* embryo extracts identified replication-coupling assembly factor (RCAF), which is composed of histones H3 and H4 as well as the histone chaperone anti-silencing function 1 (Asf1) (Tyler et al. 1999). Asf1 has been shown to form a complex with Mcm2, suggesting that it may also play a role in recycling parental nucleosomes (Groth et al. 2007). Through extract fractionation it was revealed that RCAF is required for replication-coupled chromatin assembly in addition to CAF-1 (Tyler et al. 1999). However, it was not clear if any additional factors in the extract may be required for this process. Later studies found that Asf1 binds newly synthesised (H3-H4) dimers in the cytoplasm and recruits them into the nucleus, where they can be delivered to CAF-1 (Campos et al. 2010; Alvarez et al. 2011). To that end, Asf1 has been found to bind the p60 subunit of CAF-1 in humans (Cac2 in *S. cerevisiae*) (Mello et al. 2002; Tang et al. 2006). CAF-1 must then form $(H3\text{-}H4)_2$ tetramers to be deposited on the nascent DNA. Asf1 binding actively inhibits the formation of $(H3\text{-}H4)_2$ tetramers (English et al. 2006; Natsume et al. 2007). Recent evidence suggests that CAF-1 dimerises on DNA, with each CAF-1 associated with an (H3-H4) dimer; this dimerisation then leads to the formation of an $(H3\text{-}H4)_2$ tetramer on the DNA (Mattiroli et al. 2017; Sauer et al. 2017).

Furthermore, Asf1 has been shown to be required *in vivo* for acetylation of histone H3 lysine 56 (H3K56ac) by the acetyltransferase regulator of Ty1 transposition 109 (Rtt109) in *S. cerevisiae*. This modification marks newly-synthesised histones and is implicated in both DNA replication and repair

(Recht et al. 2006; Driscoll et al. 2007; Li et al. 2008; Chen et al. 2008). H3K56ac, as well as H3K27ac, have been shown to promote CAF-1 dependent chromatin assembly on replicated DNA in *S. cerevisiae* (Burgess and Zhang, 2010; Li et al. 2008). *In vitro* H3K56ac by Rtt109 is achieved in the presence of either Asf1 or the histone chaperone vacuolar protein sorting 75 (Vps75) (Selth and Svejstrup, 2007; Tsubota et al. 2007). Vps75 is a histone chaperone that preferentially binds histones H2A and H2B, and has been found to form a stable complex with Rtt109 *in vivo* (Selth and Svejstrup, 2007; Krogan et al. 2006). Interestingly, cells without Asf1 or Rtt109, or with H3K56 mutated to H3K56R are viable but show an increased sensitivity to genotoxic agents in *S. cerevisiae* (Clemente-Ruiz et al. 2011). H3K56ac is less abundant in humans, suggesting that this mark may not be as important in higher eukaryotes (Jasencakova et al. 2010; Annunziato, 2013; Das et al. 2009).

In addition to CAF-1 and Asf1, regulator of Ty1 transposition 106 (Rtt106) has also been implicated in replication-coupled chromatin assembly, and its function is partially redundant with CAF-1 (Li et al. 2008; Huang et al. 2005). Indeed, cells lacking both CAF-1 and Rtt106 are viable but defective in replication-coupled chromatin assembly and show signs of damage and checkpoint activation (Clemente-Ruiz et al. 2011). *In vitro* studies have revealed that Rtt106 preferentially binds (H3-H4) dimers in which H3 is acetylated at K56, as with CAF-1 (Li et al. 2008). Rtt106 has no known homologue in higher eukaryotes and it is not clear how it is recruited to sites of replication in *S. cerevisiae*. The viability of cells with individual deletions of Rtt106, CAF-1, Asf1, and Rtt109 in *S. cerevisiae* suggests that there are multiple redundant pathways for nucleosome assembly *in vivo* (Clemente-Ruiz et al. 2011). The consequences of depleting CAF-1 in human cells is much more severe, however, and leads to the accumulation of cells in S-phase as well as the activation of the checkpoint kinase Chk1 (Nabatiyan and Krude, 2004; Hoek and Stillman, 2003). Furthermore, replication-coupled chromatin assembly is completely defective in these cells, suggesting that (unlike in *S. cerevisiae*) this process requires CAF-1 (Nabatiyan and Krude, 2004; Hoek and Stillman, 2003). Interestingly, CAF-1 is not essential in *Arabidopsis*, but

mutants exhibit stem fasciation as well as disorganisation of the apical meristems (Reinholz 1966; Leyser and Furner, 1992; Kaya et al. 2001).

Both RPA and FACT (in addition to Rtt106, CAF-1, and Asf1) have been implicated in depositing new histones H3 and H4 on newly replicated DNA in *S. cerevisiae* (Liu et al. 2017; Yang et al. 2016). Moreover, Mcm2 has been shown to bind both new and old histones H3 and H4 and could thus play a role in new histone deposition with other chaperones such as Asf1 (Huang et al. 2015; Jasencakova et al. 2010). In the future it will be important to determine how these proteins coordinate with the full replisome to process both old and new histones during replication.

Furthermore, newly synthesised (H2A-H2B) dimers are transported from the cytoplasm to the nucleus with the assistance of nucleosome assembly protein 1 (Nap1) (D'Arcy et al. 2013; Straube et al. 2010). Nap1 and FACT have then been proposed to deliver (H2A-H2B) dimers to newly formed $(H3\text{-}H4)_2$ tetramers, thus completing the formation of nucleosomes on the nascent DNA (Alabert et al. 2017; Hammond et al. 2017). Importantly, new and old (H2A-H2B) dimers are deposited onto both new and old $(H3\text{-}H4)_2$ tetramers (Jackson, 1987; Xu et al. 2010).

1.5 Thesis summary

The work presented in this thesis attempts to shed some light on the mechanisms of Okazaki fragment maturation, termination, and chromatin replication using the model organism *S. cerevisiae*. Work in recent years has led to considerable progress in our understanding of the early stages of replication, including initiation and elongation. However, significantly less is known about the events that occur at end of replication, as well as the mechanisms through which replication occurs on chromatin. This is mostly due to difficulties studying these processes *in vivo*. The complete reconstitution of these processes with purified proteins *in vitro* will provide a powerful tool for studying how these complicated processes work *in vivo*. To that end, I adopted a biochemical approach and built upon the previously

reported reconstitution of replication initiation and elongation with purified proteins from *S. cerevisiae* (Yeeles et al. 2015; Yeeles et al. 2017). Initially, I developed purification protocols for the proteins involved in Okazaki fragment maturation and identified the minimal set of proteins required for both complete lagging strand synthesis and termination *in vitro* (Chapter 3). Interestingly, I obtained evidence showing that excess loaded Mcm2-7 double-hexamers are inhibitory to replication on chromatin, and identified a novel pathway for their removal involving Pif1 (Chapter 4). Later, I developed expression strains and purification protocols for the proteins implicated in *de novo* chromatin assembly: CAF-1, Asf1, Rtt106, Vps75, and Rtt109. I then identified the minimal set of proteins required for this process *in vitro*: histones, CAF-1 and Asf1 (Chapter 5). Finally, I determined the requirements for Okazaki fragment maturation and termination on chromatin, and established a fully-reconstituted system for studying complete chromatin replication, including both parental histone recycling and *de novo* chromatin assembly, *in vitro* (Chapter 6).

In addition to providing a powerful tool for future studies of these processes *in vitro*, this work provides significant insights into replication and chromatin assembly. To our knowledge, this is the first time Pif1 has been implicated in removing loaded Mcm2-7 from DNA. Indeed, it was previously unknown how (or when) excess Mcm2-7 loaded during G_1 are removed from DNA. Furthermore, this is the first reported reconstitution of *de novo* chromatin assembly in its entirety with purified proteins, and the first study to identify the minimal set of proteins required for this process *in vitro*: CAF-1 and Asf1.

Chapter 2. Materials and Methods

2.1 Enzymes and Reagents

2.1.1 Enzymes

Table 2-1 Enzymes used in this study

Enzyme	Source
Benzonase	Sigma-Aldrich
Ribonuclease A	Sigma-Aldrich
Restriction enzymes	New England Biolabs (NEB)
λ protein phosphatase	New England Biolabs (NEB)
Phusion DNA polymerase	New England Biolabs (NEB)
T4 DNA ligase	New England Biolabs (NEB)
Micrococcal nuclease	New England Biolabs (NEB)

2.1.2 Antibodies

Table 2-2 Primary polyclonal antibodies used in this study

Antibody	Source	Dilution
Anti-Histone H3	Abcam (ab1791)	1:2000
Anti-Histone H3K56ac	Active Motif (39281)	1:2500

Table 2-3 Secondary antibodies used in this study

Antibody	Source	Dilution
Anti-rabbit-HRP	Jackson ImmunoResearch	1:5000

2.1.3 General buffers

2.1.3.1 Buffers for general manipulation of DNA

50x TAE: 2 M Tris base, 2 M glacial acetic acid, 50 mM EDTA

6x Alkaline loading dye: 10% (w/v) sucrose, 0.1% (w/v) bromophenol blue, 300 mM NaOH

6x DNA Gel Loading Dye, Purple (NEB)

2.1.3.2 Buffers for general manipulation of proteins

Tris-HCl pH 7.2: Tris base dissolved in water to a final concentration of 1M and pH adjusted with concentrated HCl

TBS: 20 mM Tris-HCl pH 7.5, 150 mM NaCl

TBST: 20 mM Tris-HCl pH 7.5, 150 mM NaCl, 1 mM Tween-20

PBS: 137 mM NaCl, 2.7 mM KCl, 10 mM Na_2HPO_4, 1.8 mM KH_2PO_4

Transfer buffer for Westerns: 48 mM Trizma base, 39 mM glycine, 0.0375% (w/v) SDS, 20% methanol

Blocking buffer for Westerns: 5% (w/v) Marvel milk powder dissolved in TBST

2.2 Media

Ultra-pure Millipore water was used to make all media and solutions unless otherwise stated. Media was prepared by the Media Preparation Team at The Francis Crick Institute.

2.2.1 Media for *E. coli*

E. coli cells were grown in Luria Broth (LB) medium in suspension (0.5% bacto-tryptone, 0.25% bacto-yeast extract, 170 mM NaCl, pH 7). For growth on solid media, LB was supplemented with 2% agar and antibiotics as required at the following concentrations: ampicillin (50 μg/mL), chloramphenicol (35 μg/mL), kanamycin (50 μg/mL), streptinomycin (50 μg/mL). For transformations, *E. coli* cells were grown in SOC medium (0.5% bacto-yeast extract, 2% bacto-tryptone, 20 mM glucose, 10 mM NaCl, 2.5 mM KCl, 10 mM $MgCl_2$, 10 mM $MgSO_4$).

2.2.2 Media for *S. cerevisiae*

In suspension, *S. cerevisiae* cells were grown in Yeast Peptone (YP) medium (1% yeast extract, 2% peptone) with glucose, raffinose, or galactose to a final concentration of 2%. For growth on solid media, 2% agar was added to YPD. For selective growth on solid media, minimal drop-in media (2% agar, 2% glucose, and 1x yeast nitrogen base) was supplemented with amino acids as

required: adenine (5 mg/mL), histidine (10 mg/mL), leucine (10 mg/mL), tryptophan (2 mg/mL), and/or uracil (2 mg/mL).

2.3 Plasmids

Table 2-4 Plasmids used in this study

Name	Cloning vector	Insert	Use	Reference
pBluescript/ARS1 WTA	N/A	N/A	Template for *in vitro* DNA replication assay	(Marahrens and Stillman, 1992)
pJY22	pBS KS+	ARS1	Template for *in vitro* DNA replication assay	(Yeeles et al., 2017)
pET28a	N/A	N/A	Construction of expression strains in *E. coli*	Merck
pJY19	pET28a	PCNA	Expression of PCNA in *E. coli*	(Yeeles et al., 2017)
pAM3	pGEX-6p-1	CDC6	Expression of Cdc6 in *E. coli*	(Frigola et al., 2013)
pFJD5	pFJD12	6HIS-GINS	Expression of GINS in *E. coli*	(Gambus et al., 2009)
pMD132	pBP6	HIS-MCM10-FLAG	Expression of MCM10 in *E. coli*	(Douglas et al., 2018)

pCFK1	pGEX-6p-1	NAP1	Expression of NAP1 in *E. coli*	(Kurat et al., 2017)
N/A	pCDFDuet	Yeast histones H2A and H2B	Expression of yeast histones H2A and H2B in *E. coli*	(Kingston et al., 2011)
N/A	pETDuet	Yeast histones H3 and H4	Expression of yeast histones H3 and H4 in *E. coli*	(Kingston et al., 2011)
pRJ1228	pET28a	NHP6	Expression of Nhp6 in *E. coli*	(Ruone et al., 2003)
N/A	pRS303	FEN1-TEV-CBP	Galactose-inducible expression in yeast	Generated within the laboratory by Dr Anne Early
N/A	pRS303	CBP-TEV-DNA2	Galactose-inducible expression in yeast	Generated within the laboratory by Dr Anne Early
N/A	pRS303	Lig1-2XFLAG	Galactose-inducible expression in yeast	Generated within the laboratory by Dr Joe Yeeles

Table 2-5 Plasmids generated in this study

Name	Cloning vector	Insert	Generation of insert	5' cloning site	3' cloning site
pJHH1	N/A	CAC2	GeneArt Gene Synthesis	AscI	XhoI
pJHH2	N/A	CBP-CAC3	GeneArt Gene Synthesis	SgrAI	NotI
pJHH3	N/A	CBP-RTT106	GeneArt Gene Synthesis	SgrAI	NotI
pJHH4	N/A	CBP-VPS75	GeneArt Gene Synthesis	SgrAI	NotI
pJHH6	N/A	ASF1-CBP	GeneArt Gene Synthesis	SgrAI	NotI
pJHH7	N/A	CAC1	GeneArt Gene Synthesis	SgrAI	NotI
pJHH8	pRS306	CAC1 and CAC2	GeneArt Gene Synthesis	SgrAI (CAC1) AscI (CAC2)	NotI (CAC1) XhoI (CAC2)
pJHH9	pRS303	CBP-CAC3	GeneArt Gene Synthesis	SgrAI	NotI
pJHH10	pRS303	ASF1-CBP	GeneArt Gene Synthesis	SgrAI	NotI

pJHH11	pRS303	CBP-VPS75	GeneArt Gene Synthesis	SgrAI	NotI
pJHH12	pRS303	CBP-Rtt106	GeneArt Gene Synthesis	SgrAI	NotI
pJHH14	pET28a	6XHIS-Rtt109	PCR	NdeI	SalI
pJHH16	pET28a	6XHIS-Pif1	PCR	NheI	NotI
pJHH17	pETDuet	2XMyc-H3 and H4	JHH40 and JHH41 (Sigma)	NcoI	NcoI

2.4 DNA Oligonucleotides

Table 2-6 Oligonucleotides used in this study

Name	Sequence	Use	Purpose
JHH15	TCTTCAATAACATATGTCACTGAATGACTTCCTAAGTTCC	Forward primer (Rtt109)	Construction of pJHH14
JHH16	ATAAATATCAAGTCGACTCAAGTTTTAGGCAAGGCTTTAGC	Reverse primer (Rtt109)	Construction of pJHH14
JHH34	CTGCCAGGCGGCCGCCTATTATTCTAAGATGTGGTCTTC	Reverse primer (Pif1)	Construction of pJHH16
JHH36	TGACGTCGCTAGCATGAGTAGTCGTGGTTTCAGGT	Forward primer (Pif1)	Construction of pJHH16
JHH40	aactttaagaaggagatatacATGGAACAAAAACTCATCTCAGAAGAGGATCTGGAACAAAAACTCATCTCAGAAGAGGATCTGgcgcgtaccaaacagaccgcg	2x Myc insertion for H3	Construction of pJHH17
JHH41	cgcggtctgtttggtacgcgcCAGATCCTCTTCTGAGATGAGTTTTTGTTCCAGATCCTCTTCTGAGATGAGTTTTTGTTCCATgtatatctccttcttaaagtt	2x Myc insertion for H3	Construction of pJHH17

AM132	GAGGCTACTGCGCCAATT	Forward primer	Confirming integration of pRS306 at 5’
AM133	CTCAACCCTATCTCGGTCTATTCT	Reverse primer	Confirming integration of pRS303 and pRS306 at 5’
AM134	GTGCTGCAATGATACCGCGAG	Forward primer	Confirming integration of pRS303 and pRS306 at 3’
AM135	GTTACTTGGTTCTGGCGAGG	Reverse primer	Confirming integration of pRS306 at 3’
AM136	CACGACGCTTTGTCTTCATTC	Forward primer	Confirming integration of pRS303 at 5’
AM137	GTAGCCGCCGTTGTTGTTA	Reverse primer	Confirming integration of pRS303 at 3’

2.5 Strains

2.5.1 *E. coli* strains

Table 2-7 *E. coli* strains used in this study

Name	**Source**	**Use**	**Genotype**
NEB 5-alpha competent *E. coli*	NEB	Cloning	*E. coli fhuA2Δ(argF-lacZ)U169 phoA gInV44 ϕ80 Δ(lacZ)M15 gyrA96 recA1 relA1 endA1 thi-1 hsdR17*

BL21-CodonPlus (DE3)-RIL	Agilent	Protein expression	*E. coli* B F$^-$ *ompT hsdS($r_B^-m_B^-$) dcm$^+$ Tet^r gal λ(DE3) endA The [argU ileY BB leuW Cam^r]*
Rosetta (DE3) Competent Cells	Merck	Protein expression	*E. coli* B F$^-$ *ompT hsdS$_B$($r_B^-m_B^-$) gal dcm (DE3) pRARE (Cam^R)*

2.5.2 *S. cerevisiae* strains

Table 2-8 Yeast strains used in this study

Name	Genotype	Reference
yJF1	W303-1a pep4::KanMx4 bar1::Hph-NT1	(Frigola et al., 2013)
ySDORC	MAT**a** ade2-1 ura3-1 his3-11,15 trp1-1 leu2-3,112 can1-100, bar1::Hyg pep4::KanMX, his3::HIS3pRS303/ORC3$_{SUP}$, ORC4$_{SUP}$, trp1::TRP1pRS304/ORC5$_{SUP}$, ORC6$_{SUP}$, ura3::URA3pRS306/CBP-ORC1$_{SUP}$, ORC2$_{SUP}$	(Frigola et al., 2013)
yAM33	MAT**a** ade2-1 ura3-1 his3-11,15 trp1-1 leu2-3,112 can1-100, bar1::Hyg pep4::KanMX, his3::HIS3pRS303/CDT1, GAL4, trp1::TRP1pRS304/MCM4, MCM5, leu2::LEU2pRS305/MCM6, MCM7, ura3::URA3pRS306/MCM2, CBP-MCM3	(Frigola et al., 2013)
ySDK8	MAT**a** ade2-1 ura3-1 his3-11,15 trp1-1 leu2-3,112 can1-100, bar1::Hyg pep4::KanMX, trp1::TRP1pRS304/CDC7$_{SUP}$, CBP-DBF4$_{SUP}$	(On et al., 2014)

yKO3	MAT**a** ade2-1 ura3-1 his3-11,15 trp1-1 leu2-3,112 can1-100, cdc7-4, pep4:: Hyg, his3::HIS3pRS303/SLD3-13MYC, trp1::TRP1pRS304/SLD2, leu2::LEU2pRS305/SLD7, CDC45, ura3::URA3pRS306/DPB11	(On et al., 2014)
yTD6	MAT**a** ade2-1 ura3-1 his3-11,15 trp1-1 leu2-3,112 can1-100, bar1::Hyg pep4::KanMX, his3::HIS3pRS303/SLD3$_{SUP}$-TCP, GAL4, leu2::LEU2pRS305/ SLD7$_{SUP}$	(Yeeles et al., 2015)
yTD8	MAT**a** ade2-1 ura3-1 his3-11,15 trp1-1 leu2-3,112 can1-100, bar1::Hyg pep4::KanMX, his3::HIS3pRS303/SLD2$_{SUP}$-3XFLAG, GAL4	(Yeeles et al., 2015)
yJY13	MAT**a** ade2-1 ura3-1 his3-11,15 trp1-1 leu2-3,112 can1-100, bar1::Hyg pep4::KanMX, his3::HIS3pRS303/CDC45^{iflag2}, GAL4	(Yeeles et al., 2015)
pJY26	MAT**a** ade2-1 ura3-1 his3-11,15 trp1-1 leu2-3,112 can1-100, bar1::Hyg pep4::KanMX, his3::HIS3pRS303/DPB11-3XFLAG (Nat-NT2), GAL4	(Yeeles et al., 2015)
pJY31	MAT**a** ade2-1 ura3-1 his3-11,15 trp1-1 leu2-3,112 can1-100, bar1::Hyg pep4::KanMX, his3::HIS3pRS303/FEN1-3XFLAG (Nat-NT2), GAL4	Generated within the laboratory by Dr Joe Yeeles
pJY33	MAT**a** ade2-1 ura3-1 his3-11,15 trp1-1 leu2-3,112 can1-100, bar1::Hyg pep4::KanMX, his3::HIS3pRS303/LigI-2XFLAG, GAL4	Generated within the laboratory by Dr Joe Yeeles
yAJ2	MAT**a** ade2-1 ura3-1 his3-11,15 trp1-1 leu2-3,112 can1-100, bar1::Hyg pep4::KanMX, trp1::TRP1pRS304/POL2, DPB4-TEV-CBP, ura3::URA3pRS306/DPB2, DPB3	(Yeeles et al., 2015)
yCFK1	MAT**a** ade2-1 ura3-1 his3-11,15 trp1-1 leu2-3,112 can1-100, bar1::Hyg pep4::KanMX, IOC3-3XFLAG (Nat-NT2)	(Kurat et al., 2017)

yAE31	MAT**a** ade2-1 ura3-1 his3-11,15 trp1-1 leu2-3,112 can1-100, bar1::Hyg pep4::KanMX, his3::HIS3pRS303/CBP-TEV-RFA1, GAL4, ura3::URA3pRS306/RFA2, RFA3	(Yeeles et al., 2015)
yAE34	MAT**a** ade2-1 ura3-1 his3-11,15 trp1-1 leu2-3,112 can1-100, bar1::Hyg pep4::KanMX, his3::HIS3pRS303/POL32-CBP, GAL4, ura3::URA3pRS306/POL31, POL3	(Yeeles et al., 2017)
yAE40	MAT**a** ade2-1 ura3-1 his3-11,15 trp1-1 leu2-3,112 can1-100, bar1::Hyg pep4::KanMX, his3::HIS3pRS303/CBP-TEV-CTF4, GAL4	(Yeeles et al., 2015)
yAE41	MAT**a** ade2-1 ura3-1 his3-11,15 trp1-1 leu2-3,112 can1-100, bar1::Hyg pep4::KanMX, his3::HIS3pRS303/RFC1, GAL4, trp1::TRP1pRS304/RFC4, RFC5, ura3::URA3pRS306/RFC2, CBP-RFC3	(Yeeles et al., 2017)
yAE42	MAT**a** ade2-1 ura3-1 his3-11,15 trp1-1 leu2-3,112 can1-100, bar1::Hyg pep4::KanMX, his3::HIS3pRS303/CBP-TOP1, GAL4	(Yeeles et al., 2017)
yAE46	MAT**a** ade2-1 ura3-1 his3-11,15 trp1-1 leu2-3,112 can1-100, bar1::Hyg pep4::KanMX, trp1::TRP1pRS304/TOP2-TEV-CBP	(Yeeles et al., 2015)
yAE48	MAT**a** ade2-1 ura3-1 his3-11,15 trp1-1 leu2-3,112 can1-100, bar1::Hyg pep4::KanMX, ura3::URA3pRS306/CBP-CSM3, TOF1	(Yeeles et al., 2017)
yAE49	MAT**a** ade2-1 ura3-1 his3-11,15 trp1-1 leu2-3,112 can1-100, bar1::Hyg pep4::KanMX, his3::HIS3pRS303/CBP-DNA2, GAL4	Generated within the laboratory by Dr Anne Early
yAE71	MAT**a** ade2-1 ura3-1 his3-11,15 trp1-1 leu2-3,112 can1-100, bar1::Hyg pep4::KanMX, his3::HIS3pRS303/MRC1-TEV-3XFLAG (Nat-NT2), GAL4	Generated within the laboratory by Dr Anne Early

yAE86	MAT**a** ade2-1 ura3-1 his3-11,15 trp1-1 leu2-3,112 can1-100, bar1::Hyg pep4::KanMX, his3::HIS3pRS303/INO80-TEV-3XFLAG, NHP10, his3::HIS3pRS303/GAL4, TAF14, trp1::TRP1pRS304/LES3, LES4, trp1::TRP1pRS304/RVB1, RVB2, leu2::LEU2pRS305/LES5, LES6, leu2::LEU2pRS305/ARP5, ARP8 ura3::URA3pRS306/LES1, LES2 ura3::URA3pRS306/ACT1, ARP4	(Kurat et al., 2017)
yAE88	MAT**a** ade2-1 ura3-1 his3-11,15 trp1-1 leu2-3,112 can1-100, bar1::Hyg pep4::KanMX, his3::HIS3pRS303/CBP-TEV-CLB5 (Δ1-100), GAL4, ura3::URA3pRS306/CKS1, CDC28	Generated within the laboratory by Dr Anne Early
yAE89	MAT**a** ade2-1 ura3-1 his3-11,15 trp1-1 leu2-3,112 can1-100, bar1::Hyg pep4::KanMX, ura3::URA3pRS306/SPT16, 3XFLAG-TEV-POB3	Generated within the laboratory by Dr Anne Early
yAE95	MAT**a** ade2-1 ura3-1 his3-11,15 trp1-1 leu2-3,112 can1-100, bar1::Hyg pep4::KanMX, trp1::TRP1pRS304/POL1, POL12, ura3::URA3pRS306/CBP-TEV-PRI1, PRI2	Generated within the laboratory by Dr Anne Early

Table 2-9 Yeast strains generated in this study

Name	**Genotype**	**Use**
yJH1	MAT**a** ade2-1 ura3-1 his3-11,15 trp1-1 leu2-3,112 can1-100, bar1::Hyg pep4::KanMX, his3::HIS3pRS303/CBP-TEV-CAC3, GAL4, ura3::URA3pRS306/CAC1, CAC2	Expression of CAF-1 (Single integration of both vectors verified by PCR)
yJH2	MAT**a** ade2-1 ura3-1 his3-11,15 trp1-1 leu2-3,112 can1-100, bar1::Hyg pep4::KanMX, his3::HIS3pRS303/ASF1-TEV-CBP, GAL4	Expression of ASF1 (Single integration of both vectors verified by PCR)

yJH3	MAT**a** ade2-1 ura3-1 his3-11,15 trp1-1 leu2-3,112 can1-100, bar1::Hyg pep4::KanMX, his3::HIS3pRS303/CBP-TEV-VPS75, GAL4	Expression of VPS75 (Single integration of both vectors verified by PCR)
yJH4	MAT**a** ade2-1 ura3-1 his3-11,15 trp1-1 leu2-3,112 can1-100, bar1::Hyg pep4::KanMX, his3::HIS3pRS303/CBP-TEV-RTT106, GAL4	Expression of RTT106 (Single integration of both vectors verified by PCR)
yJH6	MAT**a** ade2-1 ura3-1 his3-11,15 trp1-1 leu2-3,112 can1-100, bar1::Hyg pep4::KanMX, his3::HIS3pRS303/CBP-TEV-CAC3, GAL4, ura3::URA3pRS306/CAC1, CAC2	Expression of CAF-1
yJH7	MAT**a** ade2-1 ura3-1 his3-11,15 trp1-1 leu2-3,112 can1-100, bar1::Hyg pep4::KanMX, his3::HIS3pRS303/ASF1-TEV-CBP, GAL4	Expression of ASF1
yJH8	MAT**a** ade2-1 ura3-1 his3-11,15 trp1-1 leu2-3,112 can1-100, bar1::Hyg pep4::KanMX, his3::HIS3pRS303/CBP-TEV-VPS75, GAL4	Expression of VPS75
yJH9	MAT**a** ade2-1 ura3-1 his3-11,15 trp1-1 leu2-3,112 can1-100, bar1::Hyg pep4::KanMX, his3::HIS3pRS303/CBP-TEV-RTT106, GAL4	Expression of RTT106

2.6 Molecular Biology Methods for *E. coli*

2.6.1 Transformation of *E. coli*

Chemically-competent DH5α cells (NEB) were thawed on ice (typically 25 μL per transformation). The plasmid DNA or ligation reaction to be transformed was then mixed with the cells and left on ice for 15 minutes. For ligation reactions, 5 μL of the reaction volume was used for the transformation; for plasmid DNA, approximately 50 ng of DNA. The cells were then incubated at 42°C for 45 seconds and then placed back on ice for 2-3 minutes. Following this, the cells were resuspended in 75 μL of SOC medium and incubated for an hour at 37°C. For transformations of ligation reactions, the entire transformation mixture was plated onto selective LB plates and grown

overnight at 37°C. For plasmid transformations, 1/10 of the reaction mixture was plated.

2.6.2 Isolation of plasmid DNA

Single *E. coli* colonies were used to inoculate 5 mL LB cultures, which were then grown shaking overnight at 250 rpm and 37°C. Plasmid DNA was isolated using the QIAprep Spin Miniprep Kit (QIAGEN) and DNA concentration was estimated using the Nanodrop (ND-1000 spectrophotometer, Thermo Scientific) as described in 2.8.2.

2.7 Molecular Biology Methods for *S. cerevisiae*

2.7.1 Transformation of *S. cerevisiae*

20 mL of yeast cells were grown in YPD overnight at 30°C. The next morning, cells were diluted to approximately 2 x 10^6 cells/mL in fresh medium and grown to a final concentration of 1 x 10^7 cells/mL. The cells were harvested via centrifugation at 3500 rpm for 2 minutes in an A-4-81 rotor (Eppendorf). The supernatant was removed and the cells were resuspended in 1 mL of sterile distilled water, then transferred to a microfuge tube and spun for 5 seconds at maximum speed in an FA-45-24-11 rotor (Eppendorf). The supernatant was removed and the cells were resuspended in 1 mL of sterile 0.1 M lithium acetate/TE buffer pH 7.5 and spun down at maximum speed as described previously. The resulting pellet was then resuspended in 0.1 M lithium acetate/TE buffer pH 7.5 to a final concentration of 2 x 10^9 cells/mL and mixed thoroughly with 300 μL of lithium acetate/PEG buffer pH 7.5, 5 μL 10 mg/mL salmon sperm DNA (Invitrogen), and 1-2 μg of linearised plasmid DNA. The mixture was then incubated (with gentle shaking) for 30 minutes at 30°C. Then, 100% DMSO was added to a final concentration of 10% and the cells were heat shocked for 15 minutes at 42°C. Following this, the cells were pelleted at maximum speed for 5 seconds in an FA-45-24-11 rotor and resuspended in 200 μL TE buffer pH 7.5. The cells were then plated on the appropriate selective media.

2.7.2 Isolation of yeast genomic DNA

Single colonies were used to inoculate 10 mL YPD cultures, which were grown with shaking (200 rpm) overnight at 30°C. The following morning, 1 mL of cells was pelleted via centrifugation at 3500 rpm for 2 minutes in an FA-45-24-11 rotor (Eppendorf). The supernatant was removed and the cells were resuspended in 200 μL of lysis buffer (100 mM NaCl, 10 mM Tris pH 8.0, 1 mM EDTA, and 0.1% SDS) and mixed with sterile glass beads. The mixture was vortexed at maximum for 1 minute, mixed with 200 μL of phenol, and then spun down for 2 minutes at maximum speed in a FA-45-24-11 rotor (Eppendorf). The aqueous layer was removed and extracted a second time with an equal volume of phenol (as above). Two volumes of ethanol was then added to the aqueous layer, which was mixed and left on dry ice to precipitate the DNA. The DNA was pelleted by spinning for 15 minutes (maximum speed) at 4°C in a FA-45-24-11 rotor (Eppendorf). The supernatant was removed and the pellet was left to dry at room temperature. Once dry, the pellet was resuspended in TE pH 8.0 and left to dissolve overnight at 4°C.

2.8 General Methods for Manipulation of DNA

2.8.1 DNA standards

Hyperladder I (Bioline), λ DNA-HindIII Digest (NEB), and 100 bp DNA Ladder (NEB) were all used in this study.

2.8.2 Determination of DNA concentration

The concentration of purified DNA was determined by measuring its absorbance at 260 nm with a Nanodrop ND-1000 spectrophotometer (Thermo Scientific). The calculations were based on a 50 μg/mL solution of double-stranded DNA giving an absorbance of 1 at 260 nm (A_{260}).

2.8.3 Agarose gel electrophoresis

2.8.3.1 One-dimensional agarose gel electrophoresis

For general molecular biology applications, 1% agarose gels were prepared with TAE and samples were mixed with 1/6 sample volume of 6x DNA Gel

Loading Dye (NEB). Mini gels (8 x 10 cm) were run in TAE buffer for 1 hour at 80 V (8 V/cm) in a commercially available electrophoresis apparatus from Bio-Rad. For visualising micrococcal nuclease digests (as described in 2.13.2), samples were separated through 1.3% agarose gels (8 x 10 cm) in TAE buffer for approximately 1 hour at 100 V.

For analysis of *in vitro* DNA replication assays, 0.6%-2% agarose gels (15 x 10 cm) were run for 16 hours at 24 V under native (TAE) or denaturing conditions (30 nM NaOH and 2 mM EDTA). Following electrophoresis, denaturing gels were immediately fixed in 5% TCA for 40 minutes (with gentle rotation) at 4°C. Native gels were stained with EtBr as described in 2.8.4 prior to fixation with 5% TCA. Gels were then dried onto 3MM CHR paper (GE) and exposed as described in 2.8.5.

2.8.3.2 Two-dimensional agarose gel electrophoresis

For two-dimensional gel electrophoresis in this study, samples were separated under native conditions in the first dimension followed by denaturing conditions in the second dimension. Prior to running in the second-dimension, relevant lanes from the native gels were excised and equilibrated in 1x alkaline running buffer for 30 minutes at 25°C. Both dimensions were run for 20 hours at 24V in 0.6% agarose gels (15 x 10 cm).

2.8.4 Visualisation of DNA

For cloning, DNA was visualised with Ethidium Bromide mixed into the agarose gel before solidifying (normally 0.5 μg/mL). For analysis of *in vitro* DNA replication assays, gels were stained after running by incubation in water and Ethidium Bromide (0.5 μg/mL) for 20 minutes and imaged on an Amerhsam Imager 600 (GE). For Micrococcal Nuclease digestions, 1.5 μg/mL of Ethidium Bromide was mixed into the agarose gel before solidifying in order to visualise the DNA.

2.8.5 Phosphorimager analysis

Dried gels were exposed for 1-16 hours to a phosphor screen (Sigma). The screens were analysed using an ImageQuant software on a Typhoon Trio (GE Healthcare).

2.9 General Methods for Protein Manipulation

2.9.1 Molecular weight standards

BenchMark Protein Ladder (Invitrogen) and PageRuler Plus Prestained Protein Ladder (Thermo Scientific) were used in this study.

2.9.2 SDS-PAGE

4-12% Criterion XT Bis-Tris, 12% Criterion XT Bis-Tris, 3-8% Criterion XT Tris-Acetate, and 4-15% Criterion TGX (Bio-Rad) gels were used in this study. Prior to loading gels, protein samples were supplemented with 4x NuPAGE LDS Sample Buffer (Life Technologies) and incubated for 5 minutes at 95°C. 4-12% Criterion gels were run in MOPS buffer (Invitrogen) for 1 hour at 200 V. 12% Criterion gels were run in MOPS buffer (Invitrogen) for 45 minutes at 200 V. 3-8% Criterion gels were run in XT-Tricine buffer (Bio-Rad) for 65 minutes at 150 V. 4-15% Criterion TGX gels were run in TGS buffer (Bio-Rad) for 20 minutes at 300V.

2.9.3 Determination of protein concentration

Protein concentration was measured by the method of Bradford (Bradford, 1976). Bradford Protein Reagent (Bio-Rad) was used according to the manufacturer's instructions and absorbance was measured at 595 nm in an Ultrospec 2100 (Amersham).

2.9.4 Coomassie blue staining

Following SDS-PAGE, gels were stained for approximately 30 minutes with InstantBlue Protein Stain (Expedeon).

2.9.5 Silver staining

Gels were silver stained with Silver Quest (Invitrogen) following the manufacturer's instructions after SDS-PAGE.

2.9.6 Western blotting

SDS-PAGE was performed as described in 2.9.2. Proteins were then transferred to a Hybond ECL nitrocellulose membrane (GE Healthcare) via wet transfer for 1 hour at 80 V and 4°C. The Criterion Blotter apparatus was used in this study (Bio-Rad). The membrane was then blocked at room temperature for 30 minutes with 5% milk +TBS. Incubations with primary antibodies were carried out over night with blocking buffer at 4°C. Following this, the membrane was washed at room temperature three times (10 minutes each) in TBST. The secondary antibodies were then applied and incubated with the membrane at room temperature for 1 hour in TBST. The membrane was washed again at room temperature three times (10 minutes each) in TBST. The TBST was removed and the membrane was applied with ECL chemiluminescence reagent (Pierce) and exposed to Amersham hyperfilm ECL (GE Healthcare) and developed with an X-ray film processor (JP-33 model, Jungwon Precision Industry).

2.10 Protein Purification

2.10.1 Reagents

Table 2-10 Protease inhibitor cocktail composition

Name	Concentration
AEBSF (Sigma)	0.5 mM
Pepstatin A (Sigma)	1 mM
Leupeptin (Sigma)	1 mM

2.10.2 Protein purification from *S. cerevisiae*

2.10.2.1 Protein expression in *S. cerevisiae*

Proteins were overexpressed from a bidirectional Gal1-10 promoter in *Saccharaomyces cerevisiae*. Unless otherwise stated, 8 L of cells were grown

(with shaking at 180 rpm) in YP with 2% raffinose at 30°C until cell density reached approximately 2-3 x 10^7 cells/mL. Cells expressing ORC, Mcm2-7/Cdt1, Dpb11, Sld2, Cdc45, Ctf4, RPA, and DNA Polymerase ε were then arrested in G1 phase with 100 ng/mL of the yeast mating pheromone alpha factor (CRUK) for 3 hours at 30°C. Cells expressing S-CDK were arrested in mitosis with 5 μg/mL Nocodazole (Sigma) for 3 hours at 30°C. All other expression strains used in this study were grown and induced asynchronously. Protein expression was induced by adding galactose to a final concentration of 2% for 3 hours at 30°C. Cells were harvested via centrifugation at 4700 rpm for 30 minutes (Sorvall RC12BP, Thermo Scientific). The pellets were washed and resuspended in 0.3-0.5 volumes of the appropriate lysis buffer with protease inhibitors (specified below for each protein), frozen drop-wise in liquid nitrogen, and then crushed in a freezer mill (SPEX CertiPrep 6850 Freezer/Mill) with 6 cycles of 2 minutes at a crushing rate of 15.

2.10.2.2 Purification of ORC (ySDORC)

Cell powder was resuspended in 25 mM HEPES-KOH pH 7.6, 10% glycerol, 0.05% v/v Nonidet P40 substitute (NP-40-S)(Roche), 2 mM βME, 100 mM KCl (buffer A + 100 mM KCl) + protease inhibitors (see Table 2-9). Insoluble material was cleared by centrifugation at 45,000 rpm for 45 minutes at 4°C. The clear phase was recovered, $CaCl_2$ was added to a final concentration of 2 mM, and the solution was rotated with 2 mL of calmodulin affinity resin (Agilent) for 1 hour at 4°C. The resin was collected and washed with 50 column volumes (CV) of buffer A + 300 mM KCl + 2 mM $CaCl_2$ and the protein was eluted with 10 CV of buffer A + 300 mM KCl + 2 mM EGTA + 2 mM EDTA. Peak fractions were pooled and concentrated with an Amicon Ultra 100,000 MWCO centrifugal filter (Millipore), then applied to a Superdex 200 16/60 PG column (GE Healthcare) pre-equilibrated in buffer A + 150 mM KCl. Following this, peak fractions were pooled, concentrated, and stored in aliquots at -80°C.

Buffer A: 25 mM HEPES-KOH pH 7.6, 10% glycerol, 0.05% v/v NP-40-S, 2 mM βME

2.10.2.3 Purification of Mcm2-7/Cdt1 (yAM33)

Cell powder was resuspended in 45 mM HEPES-KOH pH 7.6, 10% glycerol, βME (7.5 μL/50 mL), 0.02% v/v NP-40-S, 100 mM KOAc, 5 mM MgOAc (buffer B + βME) + protease inhibitors (see Table 2-9) and cell debris was cleared by centrifugation at 45,000 rpm for 45 minutes at 4°C. The clear phase was recovered, $CaCl_2$ was added to a final concentration of 2 mM, and the solution was rotated with 1 mL of calmodulin affinity resin (Agilent) for 2 hours at 4°C. The resin was collected and washed with 50 CV of buffer B + 2 mM $CaCl_2$ and the protein was eluted with 10 CV of buffer B + 2 mM EGTA + 1 mM EDTA. Peak fractions were pooled and concentrated with an Amicon Ultra 100,000 MWCO centrifugal filter (Millipore), then applied to a Superdex 200 16/60 PG column (GE Healthcare) pre-equilibrated in buffer B. Following this, peak fractions were pooled, concentrated, and stored in aliquots at -80°C.

Buffer B: 45 mM HEPES-KOH pH 7.6, 10% glycerol, βME (7.5 μL/50 mL), 0.02% v/v NP-40-S, 100 mM KOAc, 5 mM MgOAc

2.10.2.4 Purification of DDK (ySDK8)

Cell powder was resuspended in 25 mM HEPES-KOH pH 7.6, 10% glycerol, 2 mM βME, 0.05% v/v NP-40-S, 400 mM NaCl (buffer C + 400 mM NaCl + 2 mM βME + 0.05% v/v NP-40-S) + protease inhibitors (see Table 2-9). Insoluble material was cleared by centrifugation at 45,000 rpm for 45 minutes at 4°C. To the supernatant, $CaCl_2$ was added to a final concentration of 2 mM along with 1 mL of calmodulin affinity resin (Agilent) and the solution was rotated for 2 hours at 4°C. The resin was collected and washed with 50 CV of buffer C + 400 mM NaCl + 2 mM βME + 0.02% v/v NP-40-S + 2 mM $CaCl_2$ and then resuspended in 2 CV of buffer C + 400 mM NaCl + 2 mM βME + 0.02% v/v NP-40-S + 2 mM $CaCl_2$ + 1 mM $MnCl_2$ + 100 μL of lambda-phosphatase (2

mg/mL). Following a 1 hour incubation with gentle rotation at 4°C, the protein was eluted with 10 CV of buffer C + 400 mM NaCl + 2 mM βME + 0.02% v/v NP-40-S + 2 mM EGTA + 1 mM EDTA. Peak fractions were pooled and concentrated with an Amicon Ultra 30,000 MWCO centrifugal filter (Millipore), then applied to a Superdex 200 Increase 10/300 GL column (GE Healthcare) pre-equilibrated in buffer C + 200 mM K-Glutamate + 0.02% NP-40-S. Following this, peak fractions were pooled, concentrated, and stored in aliquots at -80°C.

Buffer C: 25 mM HEPES-KOH pH 7.6, 10% glycerol

2.10.2.5 Purification of Sld2 (yTD8)

Cell powder was resuspended in 25 mM HEPES-KOH pH 7.6, 10% glycerol, 1 mM DTT, 0.02% v/v NP-40-S, 500 mM KCl, 1 mM EDTA (buffer D + 500 mM KCl) + protease inhibitors (see Table 2-9). Cell debris was cleared by centrifugation at 45,000 rpm for 45 minutes at 4°C. Solid ammonium sulphate was added to the supernatant to 32% with gentle stirring at 4°C. Insoluble material was cleared by centrifugation at 15,000 rpm for 20 minutes and the ammonium sulphate concentration in the supernatant was increased to 48% with gentle stirring at 4°C. Precipitated protein was collected via centrifugation at 15,000 rpm for 20 minutes at 4°C. The pellet was then resuspended in 1/3 of the original volume of buffer D + 500 mM KCl + protease inhibitors and incubated with 4 mL of anti-Flag M2 affinity resin (Sigma) for 30 minutes at 4°C. The resin was collected and washed with 50 CV of buffer D + protease inhibitors and resuspended in 10 CV of buffer D + 500 mM KCl + 10 mM MgOAc + 1 mM ATP (without EDTA). Following a 10-minute incubation at 4°C, the flow-through was removed and the resin was washed with an additional 50 CV of buffer D + 500 mM KCl. The protein was eluted by incubating in 1 CV of buffer D + 0.5 mg/mL 3x FLAG peptide for 30 minutes at 4°C, followed by 4 CV of buffer D + 0.25 mg/mL 3x FLAG peptide at 4°C. The eluate was pooled and dialysed against buffer D + 280 mM KCl (2 x 1 L over 2 hours at 4°C) and applied to a HiTrap SP FF column (GE Healthcare)

equilibrated in buffer D + 250 mM KCl. The protein was eluted over a 10 CV gradient from 250 mM KCl to 1 M KCl in buffer D. Peak fractions were pooled and dialysed against buffer D + 350 mM + 40% v/v glycerol to reduce the volume and concentrate the protein (2 x 1 L over 2 hours at 4°C). The protein was then stored in aliquots at -80°C.

Buffer D: 25 mM HEPES-KOH pH 7.6, 10% glycerol, 1 mM DTT, 0.02% v/v NP-40-S, 1 mM EDTA

2.10.2.6 Purification of Sld3/7 (yTD6)

Cell powder was resuspended in buffer D + 500 mM KCl + protease inhibitors (see Table 2-9). Insoluble material was cleared by centrifugation at 45,000 rpm for 45 minutes at 4°C. IgG Sepharose 6 Fast Flow resin (GE Healthcare) was added to the supernatant (1 mL of resin per 10 mL of extract) and the solution was rotated for 40 minutes at 4°C. The resin was collected and washed with 50 CV of buffer D + 500 mM KCl. The protein was cleaved from the resin via a 2-hour incubation with 1 CV buffer D + 500 mM KCl + tobacco etch virus (TEV) protease (50 μg/mL) at 4°C. The eluate was concentrated with an Amicon Ultra 30,000 MWCO centrifugal filter (Millipore), then applied to a Superdex 200 Increase 10/300 GL column (GE Healthcare) pre-equilibrated in buffer D + 500 mM KCl. Following this, peak fractions were pooled, concentrated, and stored in aliquots at -80°C.

2.10.2.7 Purification of Cdc45 (yJY13)

Cell powder was resuspended in 25 mM HEPES-KOH pH 7.6, 10% glycerol, 1 mM DTT, 500 mM KOAc, 1 mM EDTA (buffer E + 500 mM KOAc) + protease inhibitors (see Table 2-9). Insoluble material was cleared by centrifugation at 45,000 rpm for 45 minutes at 4°C. Cdc45 was depleted from the soluble extract via incubation with 8 mL of anti-Flag M2 affinity resin (Sigma) for 2 hours at 4°C. The resin was collected and washed with 50 CV of buffer E + 500 mM KOAc, then 50 CV of buffer E + 300 mM KOAc. The protein was eluted by incubating in 1 CV of buffer E + 300 mM KOAc + 0.5 mg/mL 3x FLAG peptide for 30 minutes at 4°C, followed by 4 CV of buffer E + 300 mM

KOAc + 0.25 mg/mL 3x FLAG peptide at 4°C. The eluate was dialysed against 2 x 1 L of 20 mM K-phosphate pH 7.4, 150 mM KOAc, 0.5 mM DTT, and 10% Glycerol (buffer F + 20 mM K-phosphate pH 7.4) for 2 hours at 4°C. The sample was then applied to a 1.5 mL hydroxyapatite column (Bio-Rad) equilibrated in buffer F + 20 mM K-phosphate pH 7.4 and washed with buffer F + 80 mM K-phosphate pH 7.4 at 4°C. Cdc45 was eluted with buffer F + 250 mM K-phosphate pH 7.4 and dialysed in 2 x 1 L of buffer F + 300 mM KOAc for 2 hours at 4°C. The protein was concentrated with an Amicon Ultra 10,000 MWCO centrifugal filter (Millipore) and stored in aliquots at -80°C.

Buffer E: 25 mM HEPES-KOH pH 7.6, 10% glycerol, 1 mM DTT, 1 mM EDTA
Buffer F: 150 mM KOAc, 0.5 mM DTT, 10% Glycerol

2.10.2.8 Purification of Dpb11 (yJY26)

Cell powder was resuspended in buffer D + 500 mM KCl + protease inhibitors (see Table 2-9) and the debris was cleared by centrifugation at 45,000 rpm for 45 minutes at 4°C. The clear phase was incubated with 2 mL of anti-Flag M2 affinity resin (Sigma) for 90 minutes at 4°C. The resin was collected and washed with 50 CV of buffer D + 500 mM KCl. The protein was eluted by incubating in 1 CV of buffer D + 150 mM KCl + 0.5 mg/mL 3x FLAG peptide for 30 minutes at 4°C, followed by 4 CV of buffer D + 150 mM KCl + 0.25 mg/mL 3x FLAG peptide at 4°C. The eluate was applied to a 1 mL MonoS column (GE Healthcare) and Dpb11 was eluted over a 30 CV gradient from 150 mM KCl to 1 M KCl in buffer D. Peak fractions were then dialysed against buffer D + 300 mM KOAc and stored in aliquots at -80°C.

2.10.2.9 Purification of Fen1 (yJY31)

Cell powder was resuspended in 25 mM Tris-HCl pH 7.5, 150 mM NaCl, 0.01% NP-40-S, 10% glycerol (buffer G + 150 mM NaCl) + protease inhibitors (see Table 2-9) and cell debris was cleared by centrifugation at 45,000 rpm for 45 minutes at 4°C. The supernatant was incubated with 4 mL of anti-Flag M2 affinity resin (Sigma) for 1 hour at 4°C. The resin was collected and washed

with 50 CV of buffer G + 150 mM NaCl. The protein was eluted by incubating in 1 CV of buffer G + 150 mM NaCl + 0.5 mg/mL 3x FLAG peptide for 30 minutes at 4°C, followed by 4 CV of buffer G + 150 mM NaCl + 0.25 mg/mL 3x FLAG peptide at 4°C. The eluate was applied to a 1 mL HiTrap Heparin column (GE Healthcare) and the protein was eluted over a 30 CV gradient from 150 mM NaCl to 1 M NaCl in buffer G. Peak fractions were then dialysed against buffer G + 100 mM NaCl and stored in aliquots at -80°C.

Buffer G: 25 mM Tris-HCl pH 7.5, 0.01% NP-40-S, and 10% Glycerol

2.10.2.10 Purification of DNA Ligase I (yJY33)

Cell powder was resuspended in 50 mM Tris-HCl pH 7.5, 400 mM NaCl, 1 mM EDTA, 10 mM βME, 10% glycerol (buffer H + 400 mM NaCl) + protease inhibitors (see Table 2-9). Insoluble material was cleared via centrifugation at 45,000 rpm for 45 minutes at 4°C. The supernatant was incubated with 4 mL of anti-Flag M2 affinity resin (Sigma) for 30 minutes at 4°C. The resin was collected and washed with 50 CV of buffer H + 400 mM NaCl. LigI was eluted by incubating in 1 CV of buffer H + 400 mM NaCl + 0.5 mg/mL 3x FLAG peptide for 30 minutes at 4°C, followed by 4 CV of buffer H + 400 mM NaCl + 0.25 mg/mL 3x FLAG peptide at 4°C. The eluate was applied to a 1 mL MonoQ column (GE Healthcare) and the protein was eluted over a 30 CV gradient from 100 mM NaCl to 750 mM NaCl in buffer H. Peak fractions were then dialysed against buffer H + 100 mM NaCl and stored in aliquots at -80°C.

Buffer H: 50 mM Tris-HCl pH 7.5, 1 mM EDTA, 10 mM βME, 10% Glycerol

2.10.2.11 Purification of DNA Polymerase ε (yAJ2)

Cell powder was resuspended in buffer C + 100 mM KOAc + 5 mM DTT + protease inhibitors (see Table 2-9) and insoluble material was cleared by centrifugation at 45,000 rpm for 45 minutes at 4°C. The clear phase was recovered, $CaCl_2$ was added to a final concentration of 2 mM, and the solution was rotated with 2 mL of calmodulin affinity resin (Agilent) for 1 hour at 4°C.

The resin was collected and washed with 50 CV of buffer C + 500 mM KOAc + 2 mM DTT + 2 mM $CaCl_2$. DNA Polymerase ε was eluted with 10 CV of buffer C + 400 mM KOAc + 2 mM DTT + 2 mM EGTA + 2 mM EDTA. Peak fractions were pooled and loaded onto a HiTrap Heparin column (GE Healthcare) pre-equilibrated in buffer C + 400 mM KOAc + 1 mM DTT. The column was washed with 20 CV of buffer C + 450 mM KOAc + 1 mM DTT and the protein was eluted over a 12 CV gradient from 450 mM KOAc to 1 M KOAc in buffer C + 1 mM DTT. The eluate was concentrated with an Amicon Ultra 100,000 MWCO centrifugal filter (Millipore), then applied to a Superdex 200 Increase 10/300 GL column (GE Healthcare) pre-equilibrated in buffer C + 500 mM KOAc + 1 mM DTT. Following this, peak fractions were pooled, concentrated, and stored in aliquots at -80°C.

2.10.2.12 Purification of ISW1a (yCFK1)

Cell powder was resuspended in 25 mM HEPES-KOH pH 7.6, 300 mM KCl, 2 mM $MgCl_2$, 20% glycerol, 0.02% NP-40-S, 1 mM DTT, 0.1 mM EDTA (buffer I + 300 mM KCl) + protease inhibitors (see Table 2-9). Cell debris was cleared by centrifugation at 45,000 rpm for 45 minutes at 4°C. The supernatant was incubated with 2 mL of anti-Flag M2 affinity resin (Sigma) for 1 hour at 4°C and the resin was collected and washed with 50 CV of buffer I + 300 mM KCl. The protein was eluted by incubating the resin in 1 CV of buffer I + 300 mM KCl + 0.5 mg/mL 3x FLAG peptide for 30 minutes at 4°C, followed by 4 CV of buffer I + 300 mM KCl + 0.25 mg/mL 3x FLAG peptide at 4°C. The eluate was applied to a 1 mL MonoQ column (GE Healthcare) and the protein was eluted over a 15 CV gradient from 200 mM KCl to 600 mM NaCl in buffer I. Peak fractions were then concentrated with an Amicon Ultra 30,000 MWCO centrifugal filter (Millipore) and stored in aliquots at -80°C.

Buffer I: 25 mM HEPES-KOH pH 7.6, 2 mM $MgCl_2$, 20% glycerol, 0.02% NP-40-S, 1 mM DTT, 0.1 mM EDTA

2.10.2.13 Purification of RPA (yAE31)

Cell powder was resuspended in 25 mM Tris-HCl pH 7.6, 10% glycerol, 500 mM NaCl, 1 mM DTT (buffer J + 500 mM KCl) + protease inhibitors (see Table 2-9). Insoluble material was cleared by centrifugation at 45,000 rpm for 45 minutes at 4°C and the lysate conductivity was reduced to that of buffer J + 200 mM NaCl by diluting with buffer J + protease inhibitors (see Table 2-9). $CaCl_2$ was added to a final concentration of 2 mM along with 1 mL of calmodulin affinity resin (Agilent) and the solution was rotated for 90 minutes at 4°C. The resin was collected and washed with 50 CV of buffer J + 200 mM NaCl + 2 mM $CaCl_2$ and the protein was eluted with 10 CV of buffer J + 200 mM NaCl + 2 mM EGTA + 2 mM EDTA. Peak fractions were pooled and diluted to 50 mM NaCl with buffer J, then loaded onto a 1 mL HiTrap Heparin column (GE Healthcare) equilibrated in Buffer J + 50 mM NaCl + 1 mM EDTA. RPA was eluted over a 30 CV gradient from 50 mM NaCl to 1 M NaCl in buffer J + 1 mM EDTA. The eluate was concentrated with an Amicon Ultra 30,000 MWCO centrifugal filter (Millipore) and applied to a Superdex 200 Increase 10/300 GL column (GE Healthcare) pre-equilibrated in buffer J + 150 mM NaCl + 1 mM EDTA. Following this, peak fractions were pooled, concentrated, and stored in aliquots at -80°C.

Buffer J: 25 mM Tris-HCl pH 7.6, 10% glycerol, 1 mM DTT

2.10.2.14 Purification of DNA Polymerase δ (yAE34)

Cell powder was resuspended in 25 mM Tris-HCl pH 8.0, 10% glycerol, 400 mM NaCl, 1 mM DTT, 0.02% NP-40-S (buffer K + 400 mM NaCl + 0.02% NP-40-S) + protease inhibitors (see Table 2-9) and cell debris was cleared by centrifugation at 45,000 rpm for 45 minutes at 4°C. The clear phase was recovered, $CaCl_2$ was added to a final concentration of 2 mM, and the solution was rotated with 4 mL of calmodulin affinity resin (Agilent) for 2 hours at 4°C. The resin was collected and washed with 50 CV of buffer K + 300 mM NaCl + 0.02% NP-40-S + 2 mM $CaCl_2$ followed by 50 CV of buffer K + 200 mM NaCl + 2 mM $CaCl_2$. DNA Polymerase δ was eluted with 10 CV of buffer K + 200 mM NaCl + 2 mM EGTA + 2 mM EDTA. Peak fractions were pooled and

loaded onto a HiTrap Heparin column (GE Healthcare) pre-equilibrated in buffer K + 200 mM NaCl. The protein was eluted over 35 CV from 200 mM NaCl to 1 M NaCl in buffer K. Peak fractions were pooled and concentrated with an Amicon Ultra 30,000 MWCO centrifugal filter (Millipore), then applied to a Superdex 200 Increase 10/300 GL column (GE Healthcare) pre-equilibrated in buffer K + 150 mM NaCl + 0.02% NP-40-S. Following this, peak fractions were pooled, concentrated, and stored in aliquots at -80°C.

Buffer K: 25 mM Tris-HCl pH 8.0, 10% glycerol, 1 mM DTT

2.10.2.15 Purification of Ctf4 (yAE40)

Cell powder was resuspended in buffer J + 200 mM NaCl + protease inhibitors (see Table 2-9) and debris was cleared by centrifugation at 45,000 rpm for 45 minutes at 4°C. $CaCl_2$ was added to a final concentration of 2 mM together with 1 mL of calmodulin affinity resin (Agilent) and the extract was incubated for 90 minutes at 4°C. The resin was collected and washed with 50 CV of buffer J + 200 mM NaCl + 2 mM $CaCl_2$. The protein was eluted with 10 CV of buffer J + 200 mM NaCl + 2 mM EGTA + 1 mM EDTA. Peak fractions were pooled and the salt concentration was adjusted to 150 mM NaCl with buffer J. The sample was then applied to a MonoQ column (GE Healthcare) pre-equilibrated in buffer J + 150 mM NaCl + 1 mM EDTA. Ctf4 was eluted over a 30 CV gradient from 150 mM NaCl to 1 M NaCl in buffer J + 1 mM EDTA. Peak fractions were pooled and concentrated with an Amicon Ultra 30,000 MWCO centrifugal filter (Millipore), then applied to a Superdex 200 Increase 10/300 GL column (GE Healthcare) pre-equilibrated in buffer J + 150 mM NaCl + 1 mM EDTA. Following this, peak fractions were pooled, concentrated, and stored in aliquots at -80°C.

2.10.2.16 Purification of RFC (yAE41)

Cell powder was resuspended in buffer C + 1 mM DTT + 400 mM NaCl + protease inhibitors (see Table 2-9). Insoluble material was cleared via centrifugation at 45,000 rpm for 45 minutes at 4°C. To the supernatant, $CaCl_2$ was added to a final concentration of 2 mM along with 1.5 mL of calmodulin

affinity resin (Agilent) and the solution was rotated for 90 minutes at 4°C. The resin was collected and washed with 50 CV of buffer C + 1 mM DTT + 400 mM NaCl + 2 mM $CaCl_2$. RFC was eluted with 10 CV of buffer C + 1 mM DTT + 400 mM NaCl + 2 mM EGTA + 2 mM EDTA. The eluate was diluted 2-fold in buffer C + 1 mM DTT and then applied to a MonoS column (GE Healthcare) pre-equilibrated in buffer C + 1 mM DTT + 200 mM NaCl + 1 mM EDTA. The protein was eluted over a 30 CV gradient from 200 mM NaCl to 1 M NaCl in buffer C + 1 mM DTT + 1 mM EDTA. Peak fractions were pooled and concentrated with an Amicon Ultra 30,000 MWCO centrifugal filter (Millipore), then applied to a Superdex 200 Increase 10/300 GL column (GE Healthcare) pre-equilibrated in buffer C + 1 mM DTT + 150 mM NaCl + 1 mM EDTA. Following this, peak fractions were pooled, concentrated, and stored in aliquots at -80°C.

2.10.2.17 Purification of Topoisomerase I (yAE42)

Cell powder was resuspended in 50 mM Tris-HCl pH 7.6, 20% glycerol, 0.04% NP-40-S, 300 mM NaCl + 1 mM DTT (buffer L + 300 mM NaCl + 1 mM DTT + 0.04% NP-40-S) + protease inhibitors (see Table 2-9) and insoluble material was cleared via centrifugation at 45,000 rpm for 45 minutes at 4°C. $CaCl_2$ was added to a final concentration of 2 mM together with 1 mL of calmodulin affinity resin (Agilent) and the extract was incubated for 2 hours at 4°C. The resin was collected and washed with 50 CV of buffer L + 300 mM NaCl + 1 mM DTT + 0.04% NP-40-S + 2 mM $CaCl_2$ and then 50 CV of buffer L + 300 mM NaCl + 1 mM DTT + 2 mM $CaCl_2$. The protein was eluted with 10 CV of buffer L + 1 mM DTT + 300 mM NaCl + 2 mM EGTA + 2 mM EDTA and the eluate was pooled and concentrated with an Amicon Ultra 10,000 MWCO centrifugal filter (Millipore). The sample was then applied to a Superdex 200 Increase 10/300 GL column (GE Healthcare) pre-equilibrated in buffer L + 1 mM DTT + 150 mM NaCl + 0.02% NP-40-S. Following this, peak fractions were pooled, concentrated, and stored in aliquots at -80°C.

Buffer L: 50 mM Tris-HCl pH 7.6, 20% glycerol, 0.04% NP-40-S

2.10.2.18 Purification of Topoisomerase II (yAE46)

Cell powder was resuspended in buffer J + 300 mM NaCl + 0.02% NP-40-S + protease inhibitors (see Table 2-9) and cell debris was cleared by centrifugation at 45,000 rpm for 45 minutes at 4°C. The clear phase was recovered, $CaCl_2$ was added to a final concentration of 2 mM, and the solution was rotated with 4 mL of calmodulin affinity resin (Agilent) for 1 hour at 4°C. The resin was collected and washed with 50 CV of buffer J + 300 mM NaCl + 0.02% NP-40-S + 2 mM $CaCl_2$. Topoisomerase II was eluted with 10 CV of buffer J + 300 mM NaCl + 0.02% NP-40-S + 2 mM EGTA + 2 mM EDTA and the eluate was concentrated with an Amicon Ultra 30,000 MWCO centrifugal filter (Millipore). The sample was then applied to a Superdex 200 Increase 10/300 GL column (GE Healthcare) pre-equilibrated in buffer J + 150 mM NaCl + 0.02% NP-40-S. Peak fractions were pooled and the salt concentration was adjusted to 100 mM in buffer J + 0.02% NP-40-S. The sample was then applied to a MonoQ column (GE Healthcare) pre-equilibrated in buffer J + 100 mM NaCl + 0.02% NP-40-S. The protein was eluted over a 25 CV gradient from 100 mM NaCl to 800 mM NaCl in buffer J + 0.02% NP-40-S. Following this, peak fractions were pooled and dialysed in 1 x 2 L of buffer J + 150 mM NaCl + 0.02% NP-40-S for 2 hours at 4°C. Topoisomerase II was then concentrated and stored in aliquots at -80°C.

2.10.2.19 Purification of Csm3/Tof1 (yAE48)

Cell powder was resuspended in buffer J + 200 mM NaCl + 0.02% NP-40-S + protease inhibitors (see Table 2-9). Debris was cleared by centrifugation at 45,000 rpm for 45 minutes at 4°C. To the supernatant, $CaCl_2$ was added to a final concentration of 2 mM along with 4 mL of calmodulin affinity resin (Agilent) and the solution was rotated for 1 hour at 4°C. The resin was collected and washed with 50 CV of buffer J + 200 mM NaCl + 0.02% NP-40-S + 2 mM $CaCl_2$ and Csm3/Tof1 was eluted via incubation with buffer J + 200 mM NaCl + 2 mM $CaCl_2$ + 0.02% NP-40-S + 100 μg/mL TEV protease for 16 hours at 4°C. The protein was collected in the flow-through, concentrated with an Amicon Ultra 30,000 MWCO centrifugal filter (Millipore), and applied to a Superdex 200 Increase 10/300 GL column (GE Healthcare) pre-

equilibrated in buffer J + 150 mM NaCl + 0.02% NP-40-S. Following this, peak fractions were pooled, concentrated, and stored in aliquots at -80°C.

2.10.2.20 Purification of Dna2 (yAE49)

Cell powder was resuspended in 25 mM Tris-HCl pH 7.5, 10% glycerol, 150 mM NaCl, 0.5 mM βME (buffer M + 0.5 mM βME + 150 mM NaCl) + protease inhibitors (see Table 2-9). Insoluble material was cleared via centrifugation at 45,000 rpm for 45 minutes at 4°C. $CaCl_2$ was added to a final concentration of 2 mM together with 4 mL of calmodulin affinity resin (Agilent) and the extract was incubated for 2 hours at 4°C. The resin was collected and washed with 50 CV of buffer M + 150 mM NaCl + 1 mM βME + 2 mM $CaCl_2$. The protein was eluted with 10 CV of buffer M + 150 mM NaCl + 1 mM βME + 2 mM EGTA + 2 mM EDTA. The eluate was diluted to 100 mM NaCl in buffer M + 1 mM βME and then applied to a HiTrap Heparin column (GE Healthcare) pre-equilibrated in buffer M + 100 mM NaCl + 1 mM βME. Dna2 was eluted over a 30 CV gradient from 100 mM NaCl to 600 mM NaCl in buffer M + 1 mM βME. Peak fractions were pooled and then applied to a MonoQ column (GE Healthcare) pre-equilibrated in buffer M + 100 mM NaCl + 5 mM βME. The protein was eluted over a 30 CV gradient from 100 mM NaCl to 600 mM NaCl in buffer M + 5 mM βME. Peak fractions were pooled and dialysed against buffer M + 150 mM NaCl + 5 mM βME (2 x 1 L over 2 hours at 4°C). Dna2 was then concentrated with an Amicon Ultra 30,000 MWCO centrifugal filter (Millipore) and stored in aliquots at -80°C.

Buffer M: 25 mM Tris-HCl pH 7.5, 10% glycerol

2.10.2.21 Purification of Mrc1 (yAE71)

Cell powder was resuspended in buffer L + 400 mM NaCl + 1 mM DTT + 1 mM EDTA + protease inhibitors (see Table 2-9) and cell debris was cleared by centrifugation at 45,000 rpm for 45 minutes at 4°C. The supernatant was incubated with 2 mL of anti-Flag M2 affinity resin (Sigma) for 2 hours at 4°C. The resin was collected and washed with 50 CV of buffer L + 400 mM NaCl + 1

mM DTT + 1 mM EDTA and Mrc1 was eluted by incubating in 1 CV of buffer L + 400 mM NaCl + 1 mM DTT + 1 mM EDTA + 0.5 mg/mL 3x FLAG peptide for 30 minutes at 4°C, followed by 4 CV of buffer L + 400 mM NaCl + 1 mM DTT + 1 mM EDTA + 0.25 mg/mL 3x FLAG peptide at 4°C. The eluate was applied to a 1 mL MonoQ column (GE Healthcare) pre-equilibrated in buffer L + 150 mM NaCl + 1 mM DTT + 1 mM EDTA and the protein was eluted over a 30 CV gradient from 150 mM NaCl to 1 M NaCl in buffer L + 1 mM DTT + 1 mM EDTA. Peak fractions were then dialysed against 25 mM Tris-HCl pH 7.5, 150 mM NaCl, 40% glycerol v/v (to reduce the volume and concentrate the protein), 1 mM EDTA, 1 mM DTT, 0.02% NP-40-S (2 x 1 L for 2 hours at 4°C). The protein was then stored in aliquots at -80°C.

2.10.2.22 Purification of Ino80 (yAE86)

Cell powder was resuspended in 25 mM HEPES-KOH pH 7.6, 500 mM KCl, 4 mM $MgCl_2$, 1 mM DTT, 1 mM EDTA, 0.05% NP-40-S, 10% glycerol (buffer N + 500 mM KCl) + protease inhibitors (see Table 2-9). Cell debris was cleared by centrifugation at 45,000 rpm for 45 minutes at 4°C. The supernatant was incubated with 1 mL of anti-Flag M2 affinity resin (Sigma) for 1 hour at 4°C. The resin was collected and washed with 50 CV of buffer N + 200 mM KCl and Ino80 was eluted by incubating in 1 CV of 25 mM Tris-HCl pH 7.2, 200 mM KOAc, 4 mM $MgCl_2$, 1 mM DTT, 0.05% NP-40-S, 10% glycerol (buffer O + 200 mM KOAc + 4 mM $MgCl_2$ + 0.05% NP-40-S) + 0.5 mg/mL 3x FLAG peptide for 30 minutes at 4°C, followed by 4 CV of buffer O + 200 mM KOAc + 4 mM $MgCl_2$ + 0.05% NP-40-S + 0.25 mg/mL 3x FLAG peptide at 4°C. The eluate was applied to a 1 mL MonoQ column (GE Healthcare) pre-equilibrated in buffer O + 100 mM KCl + 4 mM $MgCl_2$ + 0.05% NP-40-S and the column was washed with a 10 CV gradient from 100 mM KCl to 300 mM KCl in buffer O + 4 mM $MgCl_2$ + 0.05% NP-40-S. Ino80 was then eluted with a gradient from 300 mM KCl to 1 M KCl in buffer O + 4 mM $MgCl_2$ + 0.05% NP-40-S. Peak fractions were then dialysed against buffer O + 100 mM NaCl + 1 mM EDTA (2 x 1 L for 2 hours at 4°C). Following this, the protein was concentrated with a Vivaspin 100,000 MWCO centrifugal filter (Sartorius) and stored in aliquots at -80°C.

Buffer N: 25 mM HEPES-KOH pH 7.6, 4 mM $MgCl_2$, 1 mM DTT, 1 mM EDTA, 0.05% NP-40-S, 10% glycerol
Buffer O: 25 mM Tris-HCl pH 7.2, 1 mM DTT, 10% glycerol

2.10.2.23 Purification of S-CDK (yAE88)

Cell powder was resuspended in 40 mM HEPES-KOH pH 7.6, 300 mM KOAc, 0.02% NP-40-S, 10% glycerol (buffer P + 300 mM KOAc) + protease inhibitors (see Table 2-9) and insoluble material was cleared by centrifugation at 45,000 rpm for 45 minutes at 4°C. The clear phase was recovered, $CaCl_2$ was added to a final concentration of 2 mM, and the solution was rotated with 4 mL of calmodulin affinity resin (Agilent) for 1 hour at 4°C. The resin was collected and washed with 50 CV of buffer P + 300 mM KOAc + 2 mM $CaCl_2$ and S-CDK was eluted via incubation with buffer P + 300 mM KOAc + 1 mM DTT + 2 mM $CaCl_2$ + 100 μg/mL TEV protease for 16 hours at 4°C. The protein was collected in the flow-through, concentrated with an Amicon Ultra 10,000 MWCO centrifugal filter (Millipore), and applied to a Superdex 200 Increase 10/300 GL column (GE Healthcare) pre-equilibrated in buffer P + 300 mM KOAc. Following this, peak fractions were pooled, concentrated, and stored in aliquots at -80°C.

Buffer P: 40 mM HEPES-KOH pH 7.6, 0.02% NP-40-S, 10% glycerol

2.10.2.24 Purification of FACT (yAE89)

Cell powder was resuspended in 20 mM Tris-HCl pH 8.0, 500 mM NaCl, 10% glycerol (buffer Q + 500 mM NaCl) + protease inhibitors (see Table 2-9) and the debris was cleared by centrifugation at 45,000 rpm for 45 minutes at 4°C. The clear phase was incubated with 2 mL of anti-Flag M2 affinity resin (Sigma) for 90 minutes at 4°C. The resin was collected and washed with 50 CV of buffer Q + 500 mM NaCl. The protein was eluted by incubating in 1 CV of buffer Q + 500 mM NaCl + 0.5 mg/mL 3x FLAG peptide for 30 minutes at 4°C, followed by 4 CV of buffer Q + 500 mM NaCl + 0.25 mg/mL 3x FLAG peptide at 4°C. The eluate was concentrated with an Amicon Ultra 10,000

MWCO centrifugal filter (Millipore) and applied to a Superdex 200 Increase 10/300 GL column (GE Healthcare) pre-equilibrated in buffer Q + 200 mM NaCl. Peak fractions were then pooled, concentrated, and stored in aliquots at -80°C.

Buffer Q: 20 mM Tris-HCl pH 8.0, 500 mM NaCl, 10% glycerol

2.10.2.25 Purification of DNA Polymerase α (yAE95)

Cell powder was resuspended in buffer J + 400 mM NaCl + 0.02% NP-40-S + protease inhibitors (see Table 2-9) and insoluble material was cleared by centrifugation at 45,000 rpm for 45 minutes at 4°C. The clear phase was recovered and the salt concentration was reduced to 300 mM NaCl by diluting in buffer J + 0.02% NP-40-S. $CaCl_2$ was added to a final concentration of 2 mM and the solution was rotated with 1 mL of calmodulin affinity resin (Agilent) for 90 minutes at 4°C. The resin was collected and washed with 50 CV of buffer J + 300 mM NaCl + 0.02% NP-40-S + 2 mM $CaCl_2$ and the protein was eluted with 10 CV of buffer J + 300 mM NaCl + 0.02% NP-40-S + 2 mM EGTA + 2 mM EDTA. The eluate was pooled and diluted to 150 mM NaCl in buffer J + 0.02% NP-40-S, then applied to a 1 mL MonoQ column (GE Healthcare). DNA Polymerase α was eluted over a 30 CV gradient from 120 mM NaCl to 1 M NaCl in buffer J + 0.02% NP-40-S. Peak fractions were pooled, concentrated with an Amicon Ultra 30,000 MWCO centrifugal filter (Millipore), and applied to a Superdex 200 Increase 10/300 GL column (GE Healthcare) pre-equilibrated in buffer J + 150 mM NaCl + 0.02% NP-40-S + 1 mM EDTA. Peak fractions were then pooled, concentrated, and stored in aliquots at -80°C.

2.10.2.26 Purification of CAF-1 (yJH1)

Cell powder was resuspended in buffer K + 100 mM NaCl + 10 mM $MgCl_2$ + 0.01% NP-40 + protease inhibitors (see Table 2-9). Insoluble material was cleared by centrifugation at 45,000 rpm for 45 minutes at 4°C and $CaCl_2$ was added to the extract at a final concentration of 2 mM along with 1 mL of calmodulin affinity resin (Agilent) and the solution was rotated for 90 minutes at 4°C. The resin was collected and washed with 50 CV of buffer K +

100 mM NaCl + 10 mM $MgCl_2$ + 0.01% NP-40 + 2 mM $CaCl_2$ and the protein was eluted with 10 CV of buffer K + 100 mM NaCl + 10 mM $MgCl_2$ + 0.01% NP-40 + 2 mM EGTA + 2 mM EDTA. The eluate was pooled and loaded onto a 1 mL MonoQ column (GE Healthcare) equilibrated in buffer K + 100 mM NaCl + 0.5 mM EDTA. CAF-1 was eluted over a 30 CV gradient from 100 mM NaCl to 1 M NaCl in buffer K + 0.5 mM EDTA. Peak fractions were pooled, concentrated with an Amicon Ultra 30,000 MWCO centrifugal filter (Millipore), and applied to a Superdex 200 Increase 10/300 GL column (GE Healthcare) pre-equilibrated in buffer K + 100 mM NaCl + 10 mM $MgCl_2$ + 1 mM EDTA + 0.01% NP-40. Fractions containing CAF-1 were then pooled, concentrated, and stored in aliquots at -80°C.

2.10.2.27 Purification of Asf1 (yJH2)

Cell powder was resuspended in 30 mM HEPES-KOH pH 7.5, 100 mM KCl, 5 mM DTT, 0.1% NP-40-S, 10% glycerol (buffer R + 100 mM KCl + 5 mM DTT + 0.1% NP-40) + protease inhibitors (see Table 2-9) and debris was cleared by centrifugation at 45,000 rpm for 45 minutes at 4°C. The clear phase was recovered, $CaCl_2$ was added to a final concentration of 2 mM, and the solution was rotated with 1 mL of calmodulin affinity resin (Agilent) for 1 hour at 4°C. The resin was collected and washed with 50 CV of buffer R + 100 mM KCl + 100 mM KCl + 5 mM DTT + 0.1% NP-40-S + 2 mM $CaCl_2$ and the protein was eluted with 10 CV of buffer R + 100 mM KCl + 5 mM DTT + 0.1% NP-40-S + 2 mM EGTA + 2 mM EDTA. The eluate was pooled and loaded onto a 1 mL MonoQ column (GE Healthcare) equilibrated in buffer R + 100 mM KCl + 1 mM DTT + 0.5 mM EDTA. Asf1 was eluted over a 30 CV gradient from 100 mM KCl to 1 M KCl in buffer R + 1 mM DTT + 0.5 mM EDTA. Peak fractions were collected, re-applied to the same column, and eluted under the conditions described previously. Fractions containing Asf1 were then pooled and dialysed against 2 x 1 L of buffer R + 100 mM KCl + 5 mM DTT + 0.1% NP-40-S. Dialysed Asf1 was concentrated with an Amicon Ultra 10,000 MWCO centrifugal filter (Millipore) and stored in aliquots at -80°C.

Buffer R: 30 mM HEPES-KOH pH 7.5, 10% glycerol

2.10.2.28 Purification of Vps75 (yJH3)

Cell powder was resuspended in 25 mM Tris-HCl pH 7.5, 250 mM KOAc, 5 mM DTT, 0.1% NP-40-S, 20% glycerol (buffer S + 250 mM KOAc + 5 mM DTT + 0.1% NP-40) + protease inhibitors (see Table 2-9). Debris was cleared by centrifugation at 45,000 rpm for 45 minutes at 4°C and $CaCl_2$ was added to the extract at a final concentration of 2 mM along with 1 mL of calmodulin affinity resin (Agilent) and the solution was rotated for 90 minutes at 4°C. The resin was collected and washed with 50 CV of buffer S + 250 mM KOAc + 5 mM DTT + 0.1% NP-40 + 2 mM $CaCl_2$ and the protein was eluted with 10 CV of buffer S + 250 mM KOAc + 5 mM DTT + 0.1% NP-40 + 2 mM EGTA + 2 mM EDTA. The eluate was pooled and loaded onto a 1 mL MonoQ column (GE Healthcare) equilibrated in buffer S + 250 mM KOAc + 1 mM DTT + 0.5 mM EDTA. Vps75 was eluted over a 30 CV gradient from 250 mM KOAc to 2 M KOAc in buffer S + 1 mM DTT + 0.5 mM EDTA + 10% glycerol. Peak fractions were pooled and dialysed against 2 x 1 L of buffer S + 250 mM KOAc + 5 mM DTT + 0.1% NP-40-S. The dialysed protein was then concentrated with an Amicon Ultra 10,000 MWCO centrifugal filter (Millipore) and stored in aliquots at -80°C.

Buffer S: 25 mM Tris-HCl pH 7.5, 20% glycerol

2.10.2.29 Purification of Rtt106 (yJH4)

With two key exceptions, Rtt106 was purified using the same protocol and buffers as CAF-1 in 2.10.2.26. One difference was that yJH4 was used instead of yJH1. The other difference was that Rtt106 was dialysed after elution from the MonoQ column in 2 x 1 L of buffer K + 100 mM NaCl + 10 mM $MgCl_2$ + 1 mM EDTA + 0.01% NP-40. Dialysed Rtt106 was then concentrated with an Amicon Ultra 30,000 MWCO centrifugal filter (Millipore) and stored in aliquots at -80°C.

2.10.3 Protein purification from *E. coli*

2.10.3.1 Purification of PCNA (pJY19)

The pET28a/PCNA plasmid was transformed into BL21 (DE3) Rosetta cells (Millipore). The resultant colonies were then used to inoculate 2 x 1 L of LB with 100 μg/mL ampicillin and 34 μg/mL chloramphenicol at 37°C. The cultures were grown to an OD_{600} of 0.5 and protein expression was induced by the addition of IPTG to 0.5 mM and growth continued for a further 2.5 hours at 37°C. Cells were then harvested via centrifugation, washed once with 50 mM Tris-HCl pH 7.5 and 10% w/v sucrose and the pellet was resuspended in 50 mM Tris-HCl pH 7.2, 10% w/v sucrose, and protease inhibitors (see Table 2-9). Cells were lysed with sonication (1 minute, 5 seconds on/5 seconds off, 40%) and insoluble material was cleared by centrifugation at 50,000 rpm for 30 minutes (unless otherwise stated, all steps were carried out at 4°C). Ammonium sulphate was added to 150 mM, followed by the (drop-wise) addition of polymin P to 0.4% (from a stock of 10%). Following 10 minutes of stirring, cell debris was cleared by centrifugation at 15,000 rpm for 15 minutes and 0.24 g/mL of ammonium sulphate was added to the recovered supernatant. The solution was stirred for 10 minutes and then subjected to centrifugation (as before). The pellet was resusupended in 25 mM Tris-HCl pH 7.2, 10% glycerol, 1 mM EDTA, 100 mM NaCl (buffer T + 100 mM NaCl) and diluted to a conductivity corresponding to buffer T + 100 mM NaCl with buffer T. The sample was then applied to a 1 mL HiTrap SP FF column (GE Healthcare), 1 mL HiTrap Heparin (GE Healthcare), and 1 mL DEAE column (GE Healthcare) assembled in tandem and pre-equilibrated in buffer T + 100 mM NaCl. Once the sample was applied, the first two columns were removed and the protein was eluted from the 1 mL DEAE column over 30 CV from 100 mM NaCl to 600 mM NaCl in buffer T. Peak fractions were pooled, diluted two-fold in buffer T (no salt), and loaded onto a 1 mL MonoQ column (GE Healthcare) pre-equilibrated in buffer T. PCNA was eluted over a 30 CV gradient from 0 mM NaCl to 600 mM NaCl in buffer T. Fractions containing PCNA were pooled, concentrated with an Amicon Ultra 3,000 MWCO centrifugal filter (Millipore), and applied to a Superdex 200 Increase

10/300 GL column (GE Healthcare) pre-equilibrated in buffer T + 150 mM NaCl. Peak fractions were then pooled and stored in aliquots at -80°C.

Buffer T: 25 mM Tris-HCl pH 7.2, 10% glycerol, 1 mM EDTA

2.10.3.2 Purification of Cdc6 (pAM3)

The Cdc6/pGEX-6p-1 plasmid was transformed into BL21-CodonPlus (DE3) cells (Agilent). Resultant colonies were used to inoculate 2 x 1 L of LB with 100 μg/mL of ampicillin and 34 μg/mL chloramphenicol at 37°C. Once the cultures reached an OD_{600} of 0.5 they were cooled on ice for 10 minutes, and then protein expression was induced with 1 mM IPTG for 5 hours at 18°C. Cells were then harvested by centrifugation for 10 minutes at 6,000 rpm in a SLA-3000 rotor (Thermo Scientific) and the pellet was resuspended in 50 mM $KXPO_4$ pH 7.6, 150 mM KOAc, 5 mM $MgCl_2$, 2 mM ATP, 1% Triton, 1 mM DTT (buffer U + 150 mM KOAc + 2 mM ATP + 1% Triton) + protease inhibitors (see Table 2-9). Cells were lysed via sonication (1 minute, 5 seconds on/5 seconds off, 40%) and insoluble material was cleared by centrifugation at 15,000 rpm for 30 minutes (SS34 rotor; Thermo Scientific). The supernatant was then recovered and rotated with 2 mL glutathione agarose pre-equilibrated in buffer U + 150 mM KOAc + 2 mM ATP + 1% Triton for 2 hours at 4°C. The resin was collected and washed with 20 mL of buffer U + 150 mM KOAc + 2 mM ATP + 1% Triton + protease inhibitors followed by 20 mL of buffer U + 150 mM KOAc + 2 mM ATP + 1% Triton (no protease inhibitors) and then resuspended in a 50% slurry with buffer U + 150 mM KOAc + 2 mM ATP + 1% Triton. The solution was then rotated with 50 μL of PreScission Protease (GE Healthcare) for 2 hours at 4°C. The flow-through was collected and diluted in buffer U + 2 mM ATP + 0.1% Triton and then applied to a 1.5 mL hydroxyapatite column (Bio-Rad) equilibrated in buffer U + 75 mM KOAc + 2 mM ATP + 0.1% Triton. The solution was rotated for 15 minutes at 4°C. The flow-through was collected and reapplied to the hydroxyapatite column, which was then washed with 5 x 1 mL of buffer U + 75 mM KOAc + 2 mM ATP + 0.1% Triton. The resin was washed further with 5 x 800 μL of buffer U + 150 mM KOAc + 15% glycerol + 0.1% Triton and Cdc6 was eluted with 8 x

800 μL of buffer U + 400 mM KOAc + 15% glycerol + 0.1% Triton. Following this, the protein was dialysed against 25 mM HEPES-KOH pH 7.6, 10 mM MgOAc, 0.02% NP-40-S, 10% glycerol, 100 mM KOAc (2 x 1 L for 2 hours at 4°C), concentrated with an Amicon Ultra 3,000 MWCO centrifugal filter (Millipore) and stored in aliquots at -80°C.

Buffer U: 50 mM $KXPO_4$ pH 7.6, 5 mM $MgCl_2$, 1 mM DTT

2.10.3.3 Purification of GINS (pFJD5)

The pFJD12/GINS plasmid was transformed into BL21 (DE3) Rosetta cells (Millipore) and the resultant colonies were used to inoculate 2 x 1 L of LB with 50 μg/mL kanamycin and 34 μg/mL chloramphenicol at 37°C. Protein expression was induced once the cultures reached an OD_{600} of 0.5 with 1 mM IPTG for 3 hours at 37°C. Cells were then harvested by centrifugation for 10 minutes at 6,000 rpm in a SLA-3000 rotor (Thermo Scientific) and the pellet was resuspended in 50 mM HEPES-KOH pH 7.6, 200 mM KCl, βME (7 μL/50 mL), 10 mM MgOAc, 10% glycerol, 1 mM EDTA, 1 mM EGTA, 0.05% NP-40-S (buffer V + 200 mM KCl + βME) + protease inhibitors (see Table 2-9). Lysozyme (100 μg/mL) was added and the solution was incubated for 30 minutes at 4°C. Cells were then sonicated (1 minute, 5 seconds on/5 seconds off, 40%) and insoluble material was cleared by centrifugation at 15,000 rpm for 30 minutes (SS34 rotor; Thermo Scientific). The supernatant was recovered and rotated with 5 mL Ni-NTA agarose (Thermo Scientific) pre-equilibrated in buffer V + 200 mM KCl for 1 hour at 4°C. The resin was then collected and washed with 50 CV of buffer V + 200 mM KCl + 50 mM imidazole followed by elution of GINS with 10 x 1 mL of buffer V + 200 mM imidazole + 200 mM KCl. Following this, the eluate was pooled and dialysed against 2 x 1 L buffer V + 50 mM KCl for 2 hours at 4°C. The dialysed sample was then loaded onto a 1 mL MonoQ column (GE Healthcare) equilibrated in buffer V + 50 mM KCl and the protein was eluted over a 20 CV gradient from 50 mM KCl to 500 mM KCl in buffer V. Peak fractions were pooled, concentrated with an Amicon Ultra 30,000 MWCO centrifugal filter

(Millipore), and applied to a Superdex 200 Increase 10/300 GL column (GE Healthcare) pre-equilibrated in 25 mM HEPES-KOH pH 7.6, 200 mM KOAc, 1 mM EDTA, 0.02% NP-40-S, 10% glycerol, 1 mM DTT. Fractions containing GINS were then pooled, concentrated, and stored in aliquots at -80°C.

Buffer V: 50 mM HEPES-KOH pH 7.6, 10 mM MgOAc, 10% glycerol, 1 mM EDTA, 1 mM EGTA, 0.05% NP-40-S

2.10.3.4 Purification of Mcm10 (pMD132)

The pBP6/Mcm10 plasmid was transformed into BL21-CodonPlus (DE3) cells (Agilent) and the resultant colonies were used to inoculate 2 x 1 L of LB with 50 μg/mL kanamycin and 34 μg/mL chloramphenicol at 37°C. Protein expression was induced once the cultures reached an OD_{600} of 0.5 with 1 mM IPTG for 3 hours at 37°C. Cells were then harvested by centrifugation for 10 minutes at 6,000 rpm in a SLA-3000 rotor (Thermo Scientific) and the pellet was resuspended in 25 mM HEPES-KOH pH 7.6, 500 mM NaCl, 10% glycerol, 0.05% NP-40-S (buffer W + 500 mM NaCl) + protease inhibitors (see Table 2-9). Lysozyme (100 μg/mL) was added and the solution was incubated for 30 minutes at 4°C. Cells were then sonicated (1 minute, 5 seconds on/5 seconds off, 40%) and insoluble material was cleared by centrifugation at 15,000 rpm for 30 minutes (SS34 rotor; Thermo Scientific). The supernatant was incubated with 3 mL of anti-Flag M2 affinity resin (Sigma) for 90 minutes at 4°C. The resin was collected and washed with 50 CV of buffer W + 500 mM NaCl followed by 50 CV of buffer W + 300 mM NaCl. The protein was then eluted by incubating in 1 CV of buffer W + 300 mM NaCl + 0.5 mg/mL 3x FLAG peptide for 30 minutes at 4°C, followed by 4 CV of buffer W + 300 mM NaCl + 0.25 mg/mL 3x FLAG peptide at 4°C. The eluate was rotated with 2 mL Ni-NTA agarose (Thermo Scientific) pre-equilibrated in buffer W + 500 mM NaCl + 10 mM imidazole for 1 hour at 4°C. The resin was then collected and washed with 50 CV of buffer W + 500 mM NaCl + 10 mM imidazole followed by elution of Mcm10 with 10 x 1 mL of buffer W + 200 mM imidazole + 500 mM NaCl. Peak fractions were pooled, concentrated with an Amicon Ultra

10,000 MWCO centrifugal filter (Millipore), and applied to a Superdex 200 Increase 10/300 GL column (GE Healthcare) pre-equilibrated in buffer W + 200 mM NaCl + 1 mM EDTA. Fractions containing Mcm10 were then pooled, concentrated, and stored in aliquots at -80°C.

Buffer W: 25 mM HEPES-KOH pH 7.6, 10% glycerol, 0.05% NP-40-S

2.10.3.5 Purification of Nap1 (pCFK1)

The pGEX-6p-1/Nap1 plasmid was transformed into BL21-CodonPlus (DE3) cells (Agilent) and the resultant colonies were used to inoculate 2 x 1 L of LB with 100 μg/mL ampicillin at 37°C. Protein expression was induced once the cultures reached an OD_{600} of 0.6 with 0.5 mM IPTG for 4 hours at 37°C. Cells were then harvested by centrifugation for 10 minutes at 6,000 rpm in a SLA-3000 rotor (Thermo Scientific) and the pellet was resuspended in 50 mM $KXPO_4$ pH 7.6, 150 mM KOAc, 5 mM $MgCl_2$, 2 mM ATP, 1% Triton, 1 mM DTT (buffer U + 150 mM KOAc + 2 mM ATP + 1% Triton) + protease inhibitors (see Table 2-9). Cells were lysed via sonication (1 minute, 5 seconds on/5 seconds off, 40%) and insoluble material was cleared by centrifugation at 15,000 rpm for 30 minutes (SS34 rotor; Thermo Scientific). The supernatant was then recovered and rotated with 2 mL glutathione agarose pre-equilibrated in buffer U + 150 mM KOAc + 2 mM ATP + 1% Triton for 2 hours at 4°C. The resin was collected and washed with 40 mL of buffer U + 150 mM KOAc + 2 mM ATP + 1% Triton + protease inhibitors followed by 40 mL of buffer U + 150 mM KOAc + 2 mM ATP + 1% Triton (no protease inhibitors) and then resuspended in a 50% slurry with buffer U + 150 mM KOAc + 2 mM ATP + 1% Triton. The solution was then rotated with 50 μL of PreScission Protease (GE Healthcare) for 2 hours at 4°C. The flow-through was collected and dialysed against 2 x 1 L of 20 mM Tris-HCl pH 7.5, 100 mM NaCl, 0.5 mM EDTA, 1 mM DTT, 10% glycerol (buffer X + 100 mM NaCl) for 2 hours at 4°C. Following this, the eluate was loaded onto a 1 mL MonoQ column (GE Healthcare) equilibrated in buffer X + 100 mM NaCl and the protein was eluted over a 60 CV gradient from 100 mM NaCl to 1 M NaCl in buffer X.

Fractions containing Nap1 were pooled, concentrated with an Amicon Ultra 3,000 MWCO centrifugal filter (Millipore), and stored in aliquots at -80°C.

Buffer X: 20 mM Tris-HCl pH 7.5, 0.5 mM EDTA, 1 mM DTT, 10% glycerol

2.10.3.6 Purification of yeast histones H2A, H2B, H3, and H4

The glycerol stock for this purification was provided by Dr Christoph Kurat. Cells were grown in 2 x 1 L of LB with 100 μg/mL ampicillin, 34 μg/mL chloramphenicol, and 50 μg/mL spectinomycin at 37°C. Protein expression was induced once the cultures reached an OD_{600} of 0.6 with 0.5 mM IPTG for 4 hours at 37°C. Cells were then harvested by centrifugation for 10 minutes at 6,000 rpm in a SLA-3000 rotor (Thermo Scientific) and the pellet was resuspended in 20 mM Tris-HCl pH 8, 500 mM NaCl, 5 mM EDTA, 10 mM βME (buffer Y + 500 mM NaCl) + protease inhibitors (see Table 2-9). Cells were lysed via sonication (1 minute, 5 seconds on/5 seconds off, 40%) and insoluble material was cleared by centrifugation at 15,000 rpm for 30 minutes (SS34 rotor; Thermo Scientific). The supernatant was then recovered and applied to a 5 mL HiTrap Heparin column (GE Healthcare) pre-equilibrated in buffer Y. The histone octamer was eluted over a 30 CV gradient from 0 M NaCl to 1 M NaCl in buffer Y. Peak fractions were then applied to a Superdex 200 16/60 PG column (GE Healthcare) pre-equilibrated in buffer Y + 2 M NaCl. Following this, fractions containing the histone octamer were pooled and stored in aliquots at -80°C. This protocol was used for both tagged and untagged histones.

Buffer Y: 20 mM Tris-HCl pH 8, 5 mM EDTA, 10 mM βME

2.10.3.7 Purification of Nhp6 (pRJ1228)

The glycerol stock for this purification was provided by Dr Christoph Kurat. Cells were grown in 2 x 1 L of LB with 100 μg/mL ampicillin at 37°C. Protein expression was induced once the cultures reached an OD_{600} of 0.6 with 1 mM IPTG for 3 hours at 37°C. Cells were then harvested by centrifugation for 10

minutes at 6,000 rpm in a SLA-3000 rotor (Thermo Scientific) and the pellet was resuspended in 20 mM Tris-HCl pH 7.5, 500 mM NaCl, 2 mM EDTA, 10% glycerol, 1 mM βME (buffer Z + 500 mM NaCl) + protease inhibitors (see Table 2-9). Cells were lysed via sonication (1 minute, 5 seconds on/5 seconds off, 40%) and insoluble material was cleared by centrifugation at 15,000 rpm for 30 minutes (SS34 rotor; Thermo Scientific). Trichloroacetic acid (TCA) was added slowly to the supernatant to a final concentration of 2% (the volume of 50% TCA to add was determined by multiplying the volume of the supernatant by 0.0417) and the solution was stirred for 30 minutes at 4°C. Insoluble material was cleared by centrifugation at 15,000 rpm for 30 minutes and the TCA concentration in the supernatant was increased to 10% (the volume of 50% TCA to add was calculated by multiplying the volume of the supernatant by 0.19) with stirring for 30 minutes at 4°C. Precipitated protein was collected via centrifugation at 15,000 rpm for 30 minutes at 4°C. The pellet was washed with acetone, vortexed, and centrifuged at 15,000 rpm for 5 minutes and then dried under vacuum (at 30°C). It was then resuspended in and dialysed against buffer Z + 300 mM NaCl (3 x 1 L for 2 hours at 4°C). The dialysed sample was filtered through a 0.2 μm Millex-GP Sterile Syringe Filter (Thermo Scientific) and applied to a 1 mL MonoS column (GE Healthcare) pre-equilibrated in buffer Z + 300 mM NaCl. Nhp6 was eluted over a 35 CV gradient from 300 mM NaCl to 1400 mM NaCl in buffer Z. Peak fractions were pooled, dialysed against 600 mL of buffer containing 25 mM HEPES-KOH pH 7.6, 200 mM KOAc, 10% glycerol, 1 mM βME, concentrated with an Amicon Ultra 3,000 MWCO centrifugal filter (Millipore), and stored in aliquots at -80°C.

Buffer Z: 20 mM Tris-HCl pH 7.5, 2 mM EDTA, 10% glycerol, 1 mM βME

2.10.3.8 Purification of Rtt109 (pJHH14)

The pJHH14 plasmid was transformed into BL21-CodonPlus (DE3) cells (Agilent) and the resultant colonies were used to inoculate 2 x 1 L of LB with 50 μg/mL kanamycin and 34 μg/mL chloramphenicol at 37°C. Protein

expression was induced once the cultures reached an OD_{600} of 0.6 with 0.5 mM IPTG for 4 hours at 37°C. Cells were then harvested by centrifugation for 10 minutes at 6,000 rpm in a SLA-3000 rotor (Thermo Scientific) and the pellet was resuspended in 25 mM Tris-HCl pH 7.5, 150 mM NaCl, 1% Triton, 5 mM Imidazole, 10% glycerol (buffer AA + 5 mM Imidazole + 1% Triton) + protease inhibitors (see Table 2-9). Cells were lysed via sonication (1 minute, 5 seconds on/5 seconds off, 40%) and insoluble material was cleared by centrifugation at 15,000 rpm for 30 minutes (SS34 rotor; Thermo Scientific). The supernatant was then applied to a 1 mL HisTrap column (GE) pre-equilibrated in buffer AA + 20 mM Imidazole. Rtt109 was eluted over a 60 CV gradient from 20 mM Imidazole to 500 mM Imidazole in buffer AA. Peak fractions were pooled, concentrated with an Amicon Ultra 30,000 MWCO centrifugal filter (Millipore), and applied to a Superdex 200 Increase 10/300 GL column (GE Healthcare) pre-equilibrated in buffer AA. Following this, peak fractions were pooled, concentrated with an Amicon Ultra 10,000 MWCO centrifugal filter (Millipore), and stored in aliquots at -80°C.

Buffer AA: 25 mM Tris-HCl pH 7.5, 150 mM NaCl, 10% glycerol

2.10.3.9 Purification of Pif1 (pJHH16)

The pJHH16 plasmid was transformed into Rosetta (DE3) Competent Cells (Merck) and the resultant colonies were used to inoculate 10 x 1 L of LB with 100 μg/mL ampicillin and 34 μg/mL chloramphenicol at 37°C. Protein expression was induced once the cultures reached an OD_{600} of 0.3-0.5 with 0.1 mM IPTG for 20 hours at 16°C. Cells were then harvested by centrifugation for 10 minutes at 6,000 rpm in a SLA-3000 rotor (Thermo Scientific) and the pellet was resuspended in 40 mM $KXPO_4$ pH 7.0, 100 mM NaCl, 8 mM $MgCl_2$, 0.01% NP-40-S, 1 mM DTT, 10% glycerol (buffer BB + 100 mM NaCl + 1 mM DTT) + protease inhibitors (see Table 2-9). Cells were lysed via sonication (1 minute, 5 seconds on/5 seconds off, 40%) and insoluble material was cleared by centrifugation at 15,000 rpm for 30 minutes (SS34 rotor; Thermo Scientific). The supernatant was then recovered and rotated with 2 mL Ni-NTA agarose (Thermo Scientific) pre-equilibrated in buffer BB +

100 mM NaCl + 1 mM DTT for 2 hours at 4°C. The resin was collected and washed with 100 mL of buffer BB + 300 mM NaCl + 1 mM DTT + 2 mM ATP + 20 mM Imidazole and the protein was eluted in 10 x 1 mL of buffer BB + 150 mM NaCl + 1 mM DTT + 200 mM Imidazole. The eluate was diluted two-fold in buffer BB + 1 mM DTT + 150 mM NaCl and applied to a MonoS column (GE Healthcare) pre-equilibrated in buffer BB + 150 mM NaCl + 1 mM DTT + 0.5 mM EDTA. Pif1 was eluted over a 30 CV gradient from 150 mM NaCl to 1 M NaCl in buffer BB. Peak fractions were pooled, concentrated with an Amicon Ultra 30,000 MWCO centrifugal filter (Millipore), and applied to a Superdex 200 Increase 10/300 GL column (GE Healthcare) pre-equilibrated in buffer BB + 150 mM NaCl + 1 mM DTT + 0.5 mM EDTA. Following this, peak fractions were pooled, concentrated, and stored in aliquots at -80°C.

Buffer BB: 40 mM $KXPO_4$ pH 7.0, 8 mM $MgCl_2$, 0.01% NP-40-S, 10% glycerol

2.11 Preparation of S-Phase Whole Cell Extract

6 L of *Saccharomyces cerevisiae* (yKO3) were grown in YP + 2% raffinose at 25°C until cell density reached approximately 0.6 x 10^7 cells/mL. Expression of Cdc45, Dpb11, Sld2, Sld3, and Sld7 was induced with galactose to a final concentration of 2% for 2 hours at 25°C. Cells were then shifted to 37°C in order to arrest them in S-phase and grown for a further 5 hours at 25°C. The cells were harvested via centrifugation at 4700 rpm for 30 minutes (Sorvall RC12BP, Thermo Scientific). The pellets were washed with 50 mM HEPES-KOH pH 7.6, 0.3 M K-Glutamate, 2 mM EDTA, 0.8 M sorbitol, 3 mM DTT (buffer AA) and then resuspended in 0.3 V of 100 mM HEPES-KOH pH 7.6, 10 mM MgOAc, 0.8 M sorbitol, 1.5 M K-Glutamate, 5 mM DTT (buffer BB) + protease inhibitors (see Table 2-9). The cells were then frozen drop-wise in liquid nitrogen and crushed in a freezer mill (SPEX CertiPrep 6850 Freezer/Mill) with 4 cycles of 2 minutes at a crushing rate of 15. Frozen cell powder (no less than 16.5 g) was transferred to a Type 70 Ti rotor ultracentrifuge tube (Beckman Coulter) and thawed completely at 4°C. The lysate was then centrifuged for 60 minutes at 50,000 rpm and 4°C. The

supernatant was recovered and dialysed for 3 hours against 3 x 1 L of 50 mM HEPES-KOH, pH7.6, 5 mM MgOAc, 0.3 M K-Glutamate, 1 mM EDTA, 1 mM EGTA, 10% glycerol, 3 mM DTT (buffer CC) + protease inhibitors (see Table 2-9). Following this, the dialysed extract was centrifuged for 30 minutes at 90,000 rpm and 4°C in a TLA 100.3 rotor (Beckman Coulter). The supernatant was aliquoted, frozen in liquid nitrogen, and stored at -80°C.

Buffer AA: 50 mM HEPES-KOH pH 7.6, 0.3 M K-Glutamate, 2 mM EDTA, 0.8 M Sorbitol, 3 mM DTT
Buffer BB: 100 mM HEPES-KOH pH 7.6, 10 mM MgOAc, 0.8 M Sorbitol, 1.5 M K-Glutamate, 5 mM DTT
Buffer CC: 50 mM HEPES-KOH, pH7.6, 5 mM MgOAc, 0.3 M K-Glutamate, 1 mM EDTA, 1 mM EGTA, 10% glycerol, 3 mM DTT

2.12 Histone Acetylation Assay

100 nM yeast histones, 50 nM Rtt109, 200 nM Asf1, and 200 nM Vps75 (purified as described in 2.10) were incubated in 100 mM Tris-HCl pH 8.0, 2 mM DTT, 20 mM acetyl-CoA (buffer DD) for 45 minutes with shaking at 30°C. The total volume was 50 μL. Finally, 12.5 μL of 4x NuPAGE LDS Sample Buffer (Life Technologies) was added and the reaction incubated for 5 minutes at 95°C. The products were analysed via SDS-PAGE followed by Western Blotting (as described in 2.9.2 and 2.9.6) in order to detect H3K56ac and H3 (see Table 2-2 and Table 2-3).

Buffer DD: 100 mM Tris-HCl pH 8, 2 mM DTT, 20 mM acetyl-CoA

2.13 Preparation and Manipulation of Chromatinised DNA

2.13.1 Chromatin assembly on soluble plasmid DNA

Saturated chromatin was assembled in 60 μL containing 10 mM HEPES-KOH pH 7.6, 50 mM KCl, 5 mM $MgCl_2$, 0.5 mM EDTA, 10% glycerol (buffer EE). 3.5 μM Nap1, 7 nM ISW1a, and 2.7 (variable) μg of yeast histones were added (in that order) to buffer EE and ultra-pure millipore water and the mixture was

incubated for 30 minutes on ice. Then, 40 mM creatine phosphate, 3 mM ATP, creatine phosphokinase (0.6 μL per reaction from a stock of 14 mg/mL), and 500 ng of circular template DNA (unless otherwise stated, pJY22) were added and the reaction incubated for 4 hours with shaking (1250 rpm) at 30°C. Free yeast histones were then removed using Illustra MicroSpin S-400 HR columns (GE Healthcare) pre-equilibrated in 25 mM HEPES-KOH pH 7.5, 100 mM K-Glutamate, 10 mM MgOAc, 1 mM DTT, 0.01% NP-40-S.

Buffer EE: 10 mM HEPES-KOH pH 7.6, 50 mM KCl, 5 mM $MgCl_2$, 0.5 mM EDTA, 10% glycerol

2.13.2 Micrococcal nuclease digest of chromatinised DNA

Chromatin was assembled as described in 2.13.1. Then, $CaCl_2$ was added to 5 nM followed by micrococcal nuclease (NEB; 1 μL of a 1:20 dilution per 60 μL of chromatinised DNA) and the reaction was incubated for 5 minutes at 37°C. The digested DNA was purified with a High Pure PCR Product Purification Kit (Roche) after quenching the reaction with 300 μL of Binding Buffer.

2.14 *In Vitro* DNA Replication Assays

2.14.1 5'-^{32}P-labelling of HindIII-digested lambda DNA

36 μL of HindIII-digested lambda DNA (NEB; 500 mg/mL) was de-phosphorylated with 2 μL of Calf Intestinal Phosphatase (NEB) in the appropriate buffer for 1 hour with shaking (1250 rpm) at 37°C. The samples were then purified with a High Pure PCR Product Purification Kit (Roche). Following this, the de-phosphorylated DNA (8 μL) was incubated with T4 Polynucleotide Kinase (2 μL) in the appropriate buffer, along with γ^{32}P-dATP (3 μL) and H_2O (5 μL) for 1 hour with shaking (1250 rpm) at 37°C. Unincorporated nucleotides were removed by passing the sample over two Illustra MicroSpin G-50 columns (GE Healthcare) and EDTA was added to a final concentration of 5 mM. The sample was stored at -20°C.

2.14.2 Extract-based replication assays on soluble DNA

MCM loading was performed in a buffer containing 25 mM HEPES-KOH pH 7.5, 100 mM K-Glutamate, 10 mM MgOAc, 0.02% NP-40-S, 5 mM ATP. Purified ORC (25 nM), Cdc6 (50 nM), and Mcm2-7/Cdt1 (100 nM) were added (in that order) to this mixture along with 250 ng (per reaction) of circular template DNA (pBluescript/ARS1 WTA) to give a final volume of 36 μL. Reactions were incubated for 30 minutes with shaking (1250 rpm) at 30°C. In a separate tube, 25 mM HEPES-KOH pH 7.5, 100 mM K-Glutamate, 10 mM MgOAc, 0.02% NP-40-S, 5 mM ATP, 2 mM DTT, and 100 nM DDK were prepared in a total volume of 72 μL (as well as a separate mix without DDK). 8 μL of the DDK (or –DDK) mix was combined with 4 μL of the MCM loading reaction so that the total volume of each individual reaction was 12 μL. The reactions were continued with shaking (1250 rpm) for a further 20 minutes at 25°C. The volume was then increased with 8 μL of 200 mM HEPES-KOH pH 7.5, 40 mM $MgCl_2$, 10 mM DTT, 20 mM ATP, 200 mM creatine phosphate, creatine phosphokinase (0.5 μL per reaction from a stock of 14 mg/mL); 1 mM CTP, GTP, and UTP; 500 μM dATP, dGTP, dTTP; 125 μM dCTP, and 33 nM α^{32}P-dCTP. Replication was initiated by the addition of 20 μL of S-phase extract (prepared as described in 2.11), giving a total volume (per reaction) of 40 μL. For supercoiling assays, CAF-1 was added to 2.5 nM – 40 nM. Reactions were also supplemented with 150 nM of purified yeast histones H2A, H2B, H3, and H4. For running samples under denaturing conditions, reactions were ended with 30 mM EDTA and unincorporated nucleotides were removed using Illustra MicroSpin G-50 columns (GE Healthcare). Samples were then separated through alkaline agarose gels, dried, and exposed as described in 2.8. For running samples under native conditions, reactions were ended with 30 mM EDTA and incubated with 0.5% SDS and 16 μg of Proteinase K (Millipore) for 30 minutes at 37°C. Unincorporated nucleotides were then removed using Illustra MicroSpin G-50 columns (GE Healthcare) and the DNA isolated via phenol-chloroform extraction with Phase Lock Gel Tubes as per the manufacturer's instructions (5PRIME). The DNA was purified and resuspended in a convenient volume by ethanol precipitation and the

samples separated through native agarose gels, dried, and exposed as described in 2.8.

2.14.3 Fully-reconstituted replication assays on soluble DNA

Unless otherwise stated, replication reactions were carried out with shaking (1250 rpm) at 30°C. MCM loading was performed in a buffer containing 25 mM HEPES-KOH pH 7.5, 100 mM K-Glutamate, 10 mM MgOAc, 1 mM DTT, 0.01% NP-40-S, 5 mM ATP. Purified ORC (10 nM), Cdc6 (50 nM), and Mcm2-7/Cdt1 (5 – 400 nM) were added (in that order) to this mixture along with 5 nM circular template DNA (unless otherwise stated, pJY22). Reactions were incubated for 20 minutes (for train experiments, this step was lengthened to sixty minutes), at which point DDK (or buffer without DDK) was added to 25 nM and CDK to 20 nM. The reaction was continued for a further 20 minutes and the reaction volume increased two-fold with buffer and proteins to give a final reaction buffer of 25 mM HEPES-KOH pH 7.5, 250 mM K-Glutamate, 10 mM MgOAc, 1 mM DTT, 0.01% NP-40-S, 3 mM ATP; 200 μM CTP, GTP, and UTP; 80 μM dATP, dCTP, dGTP, dTTP; and 33 nM α^{32}P-dCTP. Replication was initiated by the addition of a master-mix of proteins containing (unless otherwise stated) 100 nM RPA, 30 nM Dpb11, 40 nM Cdc45, 20 nM Topoisomerase II, 10 nM Topoisomerase I, 20 nM Ctf4, 20 nM DNA Polymerase ε, 5 nM Mcm10, 210 nM GINS, 20 nM S-CDK, 20 nM Csm3/Tof1, 20 nM Mrc1, 20 nM RFC, 20 nM PCNA, 10 nM DNA Polymerase δ, 25 nM Sld3/7, 50 nM Sld2, and 20 nM DNA Polymerase α. For experiments requiring Okazaki fragment maturation and termination, Dna2, DNA Ligase I, and Fen1 were added (as specified) to 40 nM. Where indicated, Pif1 was added to 1-50 nM. Samples were then processed and separated under denaturing or native conditions as described in 2.14.2.

2.14.4 Fully-reconstituted replication assays on soluble chromatinised DNA

Reactions were performed as described in 2.14.3, with the addition (as required) of 40-80 nM FACT, 400-800 nM Nhp6, 50 nM INO80, and 50 nM ISW1a. Chromatinised DNA templates were prepared as described in 2.13.

For MNase digest of replication products, 5 nM $CaCl_2$ was added after replication followed by MNase (1 μL of a 1:20 dilution per 20 μL reaction) and the mixture was incubated for 1 – 10 minutes with shaking (1250 rpm) at 37°C. The reaction was quenched with EGTA and the samples were processed and separated under denaturing or native conditions (1.3% agarose gels) as described in 2.14.2.

2.14.5 Reconstitution of replication-coupled nucleosome assembly on soluble DNA

Reactions were performed as described in 2.14.3 (including DNA Ligase I and Fen1), with the addition (as required) of 60 nM yeast histones, 75-150 nM CAF-1, 120-240 nM Asf1, 120 nM Nap1, 75 nM Rtt106, 15 nM Rtt109, 30 nM Vps75, and 50 nM ISW1a. For reactions containing Rtt109, acetyl-CoA was added to 20 nM. The chromatin assembly factors were pre-incubated for thirty minutes and added along with the master-mix of proteins required to initiate replication as described in 2.14.3. The DNA template used in these assays was pBluescript/ARS1 WTA. For supercoiling assays, samples were processed and separated under native conditions (1.5% agarose gels) as described in 2.14.2. For MNase digests of replication products, samples were processed as described in 2.14.4.

2.15 Electron Microscopy Methods

EM experiments were performed in collaboration with Patrik Eickhoff in Dr Alessandro Costa's lab at The Francis Crick Institute. Patrik stained the samples, prepared grids, then collected and analysed the data.

2.15.1 Negative stain grid preparation

Commercially available grids (EM resolutions C300Cu100) were glow discharged for 30 seconds at 45 mA with a 100x glow discharger (Electron Microscopy Sciences). In all EM Mcm2-7 train experiments, samples were diluted 1:4 in replication buffer without NP-40, DTT, or ATP. A 4 μL drop of this dilution was then applied to a glow discharged grid for 1 minute prior to

staining with 2% uranyl acetate solution for 5, 10, 15, and 20 seconds. The excess stain was then removed via blotting and the grids were stored before imaging at room temperature.

2.15.2 EM data collection

For all samples, images were collected on a Tecnai G2 Spirit transmission electron microscope (FEI) operated at 120 kV (Electron Microscopy Science Technology Platform, The Francis Crick Institute). They were recorded using a 2k x 2k Gatan Ultrascan 100 camera at a magnification of 30,000x (3.45 Å). Several hundred micrographs were collected for each data set.

2.15.3 EM image processing

Mcm2-7 train particles were picked manually and surrounding particles were picked semi-automatically in EMAN-2.07 (Tang et al. 2007). Contrast transfer function parameters were estimated using Gctf-v1.18. Further image processing was performed in RELION-2.1 including several rounds of 2D classification. Classification was performed on extracted particles with a box size of 98 or 128 pixels. To visualise repeated Mcm2-7 hexamers of the trains the particle box size of one class was expanded to 254 pixels and averaged.

Chapter 3. Results I

3.1 Introduction

The concept of 'replication licensing' emerged when it was found that passage through mitosis allowed replicated sperm chromatin to become re-competent for replication, and the key step in mitosis that allowed this to happen was nuclear envelope permeabilisation (Blow and Laskey, 1988). This led to the proposal of a model for how replication is regulated in the cell cycle in which a 'licensing factor' is required to initiate replication (Blow and Laskey, 1988). This factor marks the unreplicated sites from the replicated sites, thus preventing re-replication of the DNA.

It was later found that the 'licensing factor' is Mcm2-7, which is loaded onto origins of replication during G1-phase of the cell cycle as an inactive double hexamer, a process that has been reconstituted with purified proteins *in vitro* (Chong et al. 1995; Remus et al. 2009; Evrin et al. 2009). The Mcm2-7 double hexamer is activated during S-phase following DDK phosphorylation of Mcm4 and Mcm6, which leads to the recruitment of a number of firing factors including CDK, Sld3/7, Cdc45, Sld2, Dpb11, DNA polymerase ε, GINS, and Mcm10 (Zegerman and Diffley, 2007; Tanaka et al. 2007; Yeeles et al. 2015; Deegan et al. 2016). These factors form two active CMG helicases to which a number of other proteins are recruited, including DNA polymerase α, Ctf4, Mrc1, Csm3, Tof1, and Topoisomerase I. Other proteins localised to the replication fork include PCNA, RFC, DNA polymerase δ, and Topoisomerase II (Yu et al. 2014). However, these proteins are not known to associate stably with the RPC. The initiation of replication was recently reconstituted *in vitro*, first in cell-free extracts and then with purified proteins from *S. cerevisiae* (Heller et al. 2011; On et al. 2014; Gros et al. 2014; Yeeles et al. 2015; Devbhandari et al. 2017).

Following initiation, replication proceeds continuously on the leading strand and discontinuously on the lagging strand. During lagging strand synthesis,

replication occurs via the synthesis of Okazaki fragments, which must then be processed in order to form a single, continuous strand of DNA (Okazaki et al. 1968). Processing of these fragments involves the coordinated actions of DNA polymerase δ, Fen1, Dna2, and DNA ligase I.

The end of eukaryotic DNA replication involves the convergence of two replication forks, completion of DNA synthesis, disassembly of the replisomes, and decatenation of the daughter DNA (Dewar and Walter, 2017). Compared to initiation and elongation, significantly less is known about these processes *in vivo*. In order to gain more insight into the late stages of replication, I built upon the purified replication system established previously (Yeeles et al. 2015; Yeeles et al. 2017). In this chapter I describe the purification of proteins involved in Okazaki fragment maturation, including Fen1, Dna2, and DNA ligase I. I then go on to describe the reconstitution of Okazaki fragment maturation and termination of replication with purified proteins, leading to the generation of covalently-closed daughter DNA.

3.2 Results

3.2.1 Purification of Fen1

Fen1 was tagged with a 3X-FLAG tag on its C-terminus and codon-optimised for expression in *S. cerevisiae*. I then purified it to homogeneity via anti-FLAG immunoprecipitation (Figure 3.1B), followed by heparin chromatography (Figure 3.1C). Heparin resin is composed of sulfate (a polyanion, like DNA) and can mimic the interaction with the sugar-phosphate backbone of the double-helix (Bromfield and Smith, 2015). It is often used to purify proteins that bind to DNA. Fen1 eluted from the column in a defined peak and appeared to be pure of any contaminants visible by Coomassie staining. I then dialysed the protein into a buffer more suitable for use in downstream assays, containing a lower concentration of NaCl. For a detailed purification protocol, see 2.10.2.9.

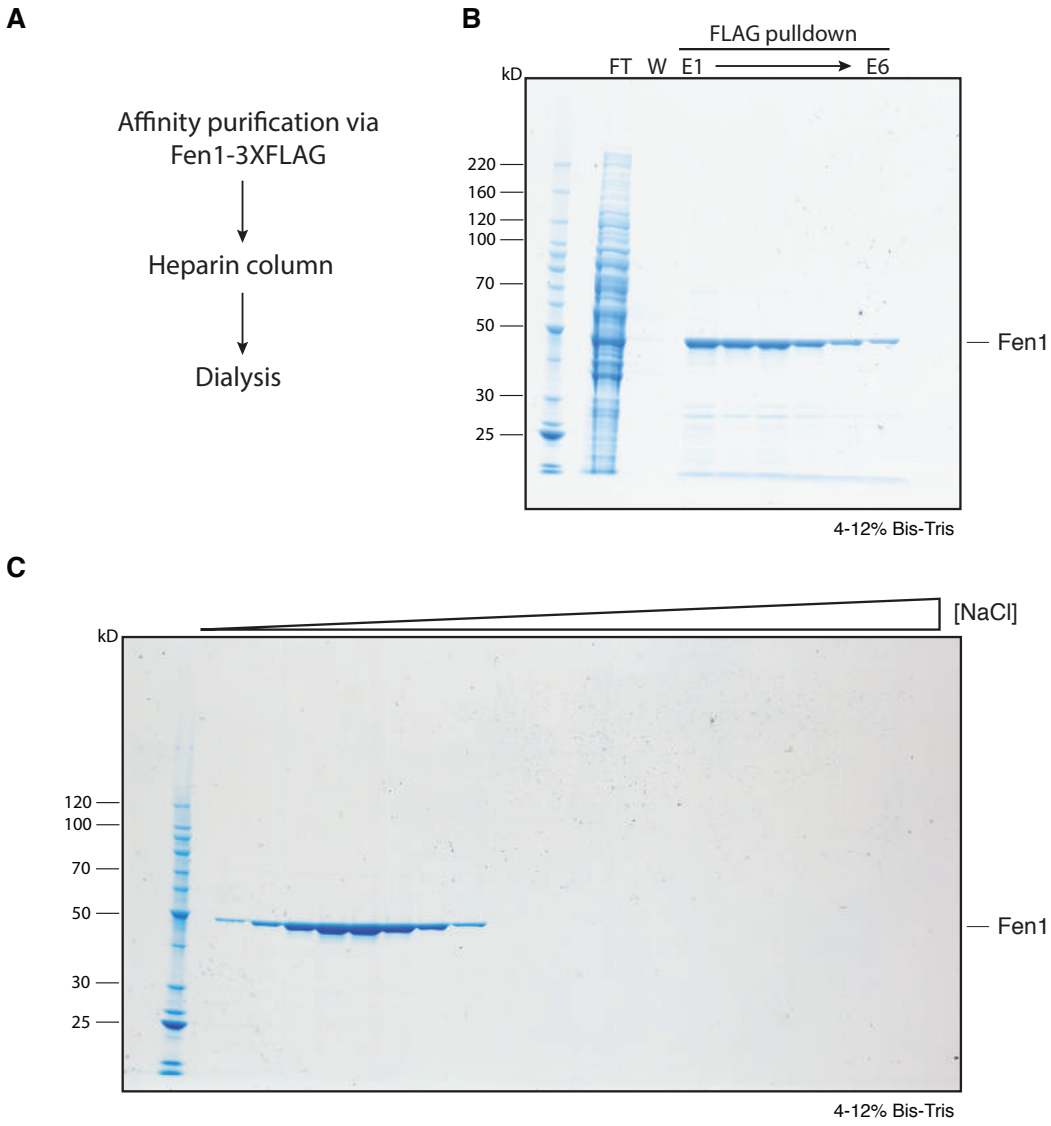

Figure 3.1 Purification of Fen1
The purification scheme for Fen1 is depicted in **(A)**. Flow-through (FT), wash (W), and eluate (E) fractions following anti-FLAG immunoprecipitation **(B)**. The final heparin chromatography step of the purification is shown in **(C)**. Protein analysed by SDS-PAGE with Coomassie staining.

3.2.2 Purification of Dna2

Dna2 was tagged with a CBP tag on its C-terminus and codon-optimised for expression in *S. cerevisiae*. I then purified it to homogeneity by calmodulin affinity chromatography (Figure 3.2B), followed by heparin chromatography (Figure 3.2C), and ion-exchange chromatography (Figure 3.2D). Due to its overall negative charge, I used a MonoQ column to purify Dna2. The protein eluted from the heparin and ion-exchange columns in defined peaks and appeared to be relatively pure. I then dialysed the protein into a buffer

containing a lower concentration of NaCl. For a detailed purification protocol, see 2.10.2.20.

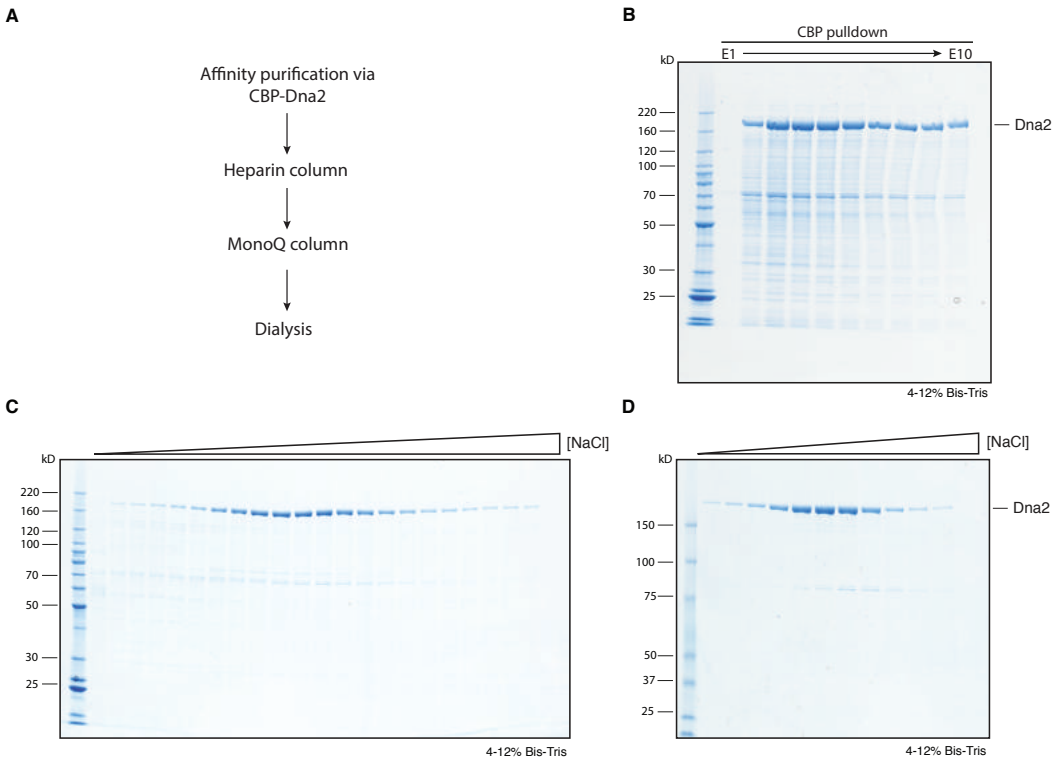

Figure 3.2 Purification of Dna2
The purification scheme for Dna2 is depicted in **(A)**. Eluate (E) fractions following calmodulin affinity chromatography **(B)**. The heparin chromatography step is shown in **(C)** and the final ion-exchange chromatography (MonoQ) step of the purification is shown in **(D)**. Protein analysed by SDS-PAGE with Coomassie staining.

3.2.3 Purification of Dna ligase I

DNA ligase I was tagged with a 2X-FLAG tag on its C-terminus and codon-optimised for expression in *S. cerevisiae*. I then purified it to homogeneity via anti-FLAG immunoprecipitation (Figure 3.3B) and ion-exchange chromatography (Figure 3.3C). Due to its overall negative charge, I used a MonoQ column to purify DNA ligase I. The protein eluted from the ion-exchange column in a defined peak and appeared to be relatively pure. I then dialysed the protein into a buffer containing a lower concentration of NaCl. For a detailed purification protocol, see 2.10.2.10.

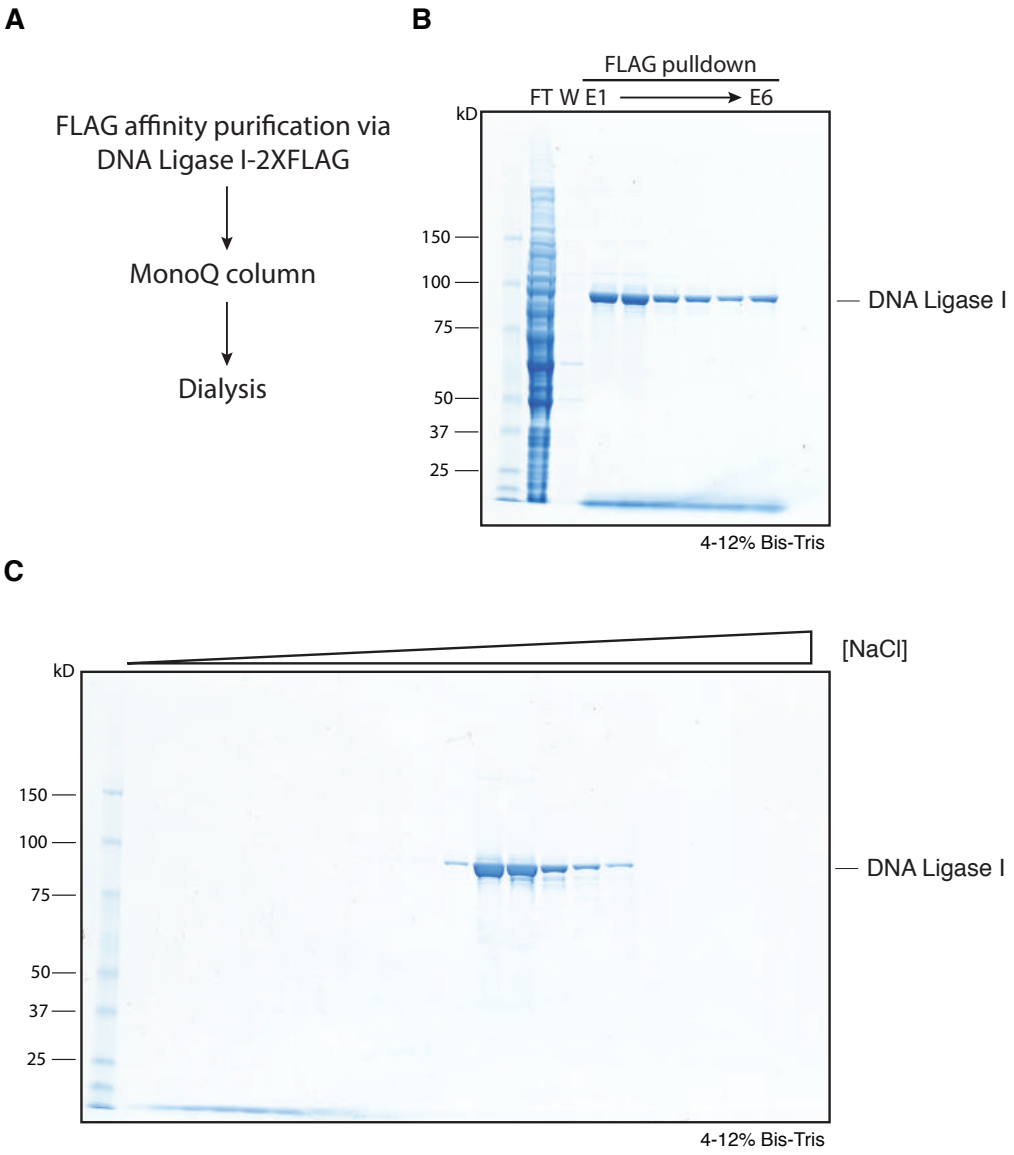

Figure 3.3 Purification of DNA ligase I
The purification scheme for DNA ligase I is depicted in **(A)**. Flow-through (FT), wash (W), and eluate (E) fractions following anti-FLAG immunoprecipitation **(B)**. The final ion-exchange chromatography step (MonoQ) is depicted in **(C)**. Protein analysed by SDS-PAGE with Coomassie staining.

3.2.4 Reconstitution of Okazaki fragment maturation *in vitro*

In order to reconstitute Okazaki fragment maturation, I added purified Fen1, Dna2, and DNA ligase I to the soluble DNA replication reaction described by Yeeles et al. 2017. I purified all of the proteins required for these replication reactions, and they are shown in Figure 3.4 (for detailed purification protocols, see section 2.10).

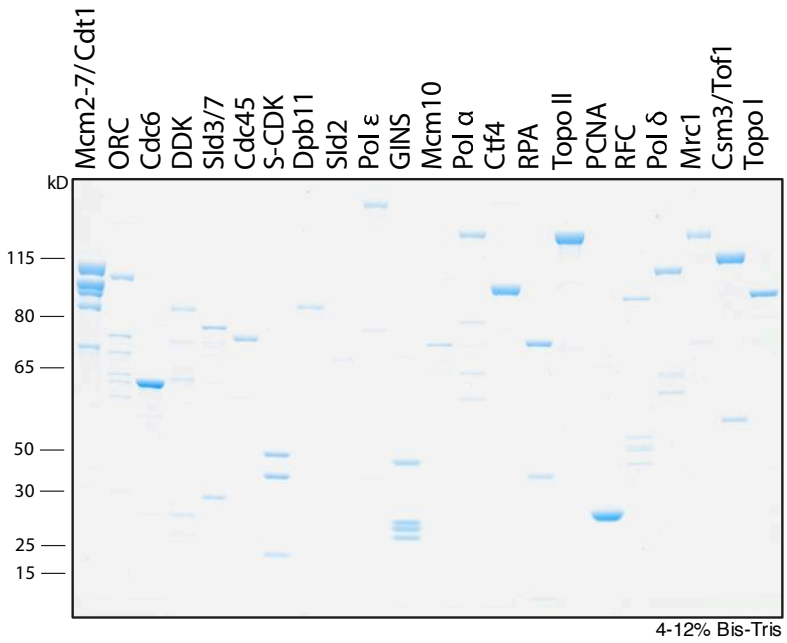

Figure 3.4 Purified proteins required for replication initiation and elongation
Purified loading and firing factors, as well as additional proteins required for replicating DNA. Proteins analysed by SDS-PAGE with Coomassie staining.

The reactions were performed according to the scheme in Figure 3.5A so that the three additional proteins were added along with the firing factors (Yeeles et al. 2017). The radiolabelled replication products were then separated on an alkaline agarose gel, dried, and subjected to autoradiography. The two distinct classes of DDK-dependent replication products - leading and lagging strands - identified by Yeeles et al. 2017 disappeared in the presence of Fen1, Dna2, and DNA ligase I (Figure 3.5B, lanes 3 and 5). Instead, I observed two discrete products, one of which was approximately the same size as the input plasmid DNA whilst the other was slightly smaller (Figure 3.5B, lane 5). I also observed a smear of products running below these two bands, presumably due to incomplete replication. The products in Figure 3.5B, lane 5 are only present in reactions containing Fen1 and DNA ligase I, as evidenced by the change in product distributions when these proteins were absent (Figure 3.5B, lanes 7 and 9). The appearance of these products, as well as the lengthening of lagging strands, suggests that the replisome machinery is able to process Okazaki fragments into a single, continuous strand in the presence of Fen1 and DNA ligase I. Dna2 was not required to form these products, nor

could it substitute for Fen1 (Figure 3.5B, compare lanes 9 and 11). Given that purified Dna2 has proven difficult to work with previously, it is a possibility that the protein was not completely active (Levikova et al. 2013). Nonetheless, the lagging strands are slightly longer in Figure 3.5B, lane 9, suggesting that some Okazaki fragments are able to be processed by Dna2. This was somewhat surprising as Dna2 - not Fen1 - is required for cell viability *in vivo* (Budd and Campbell, 1995; Reagan et al. 1995). It is likely that this system does not generate many of the long RPA-coated flaps that escape cleavage by Fen1 and instead require cleavage by both Dna2 and Fen1. Rather, it seems that DNA polymerase δ generates the short flap substrates that can be cleaved by Fen1. There are a number of nucleases that may substitute for Fen1 *in vivo* (such as Exonuclease 1) which may explain why it is dispensable *in vivo* but required in this *in vitro* system (Tishkoff et al. 1997; Sun et al. 2003). Since it had no apparent role in this system, future experiments (unless otherwise stated) were carried out without Dna2.

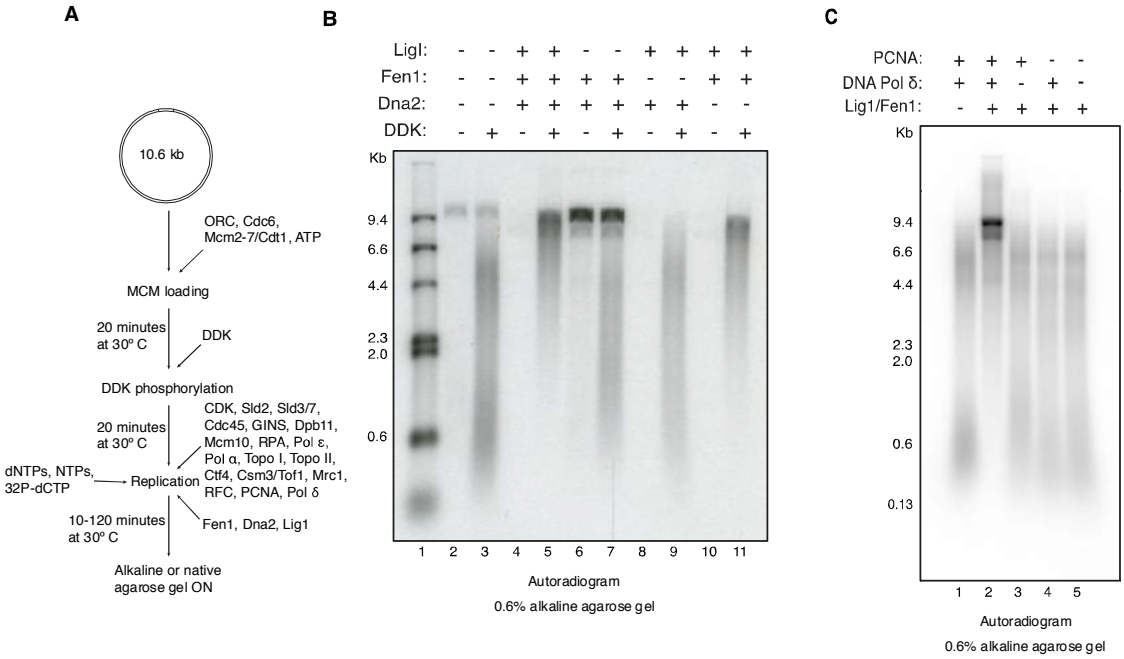

Figure 3.5 Reconstitution of Okazaki fragment maturation *in vitro*
(A) General scheme for replication reactions. The template used in these experiments was pJY22. **(B)** Fen1, Dna2, and DNA ligase I drop-out experiment performed for 30-minutes as in (A). **(C)** PCNA and DNA polymerase δ drop-out experiment performed for 30-minutes as in (A). Products in (B) and (C) were separated over alkaline agarose gels (0.6%). These experiments were performed twice, and the results are reproducible.

We observed replication-independent products in Figure 3.5B, lanes 2, 3, 6 and 7. These are formed in the absence of Fen1, Dna2, and Lig1, but are very prominent when the reaction is carried out with Fen1 and Dna2 in the absence of Lig1. We suspect this may be due to nicks in the DNA, which are then 'labelled' by a polymerase incorporating α^{32}P-dCTP.

Further experiments revealed that the products in Figure 3.5B, lane 5 required both DNA polymerase δ and the processivity factor PCNA (Figure 3.5C). This was expected as DNA polymerase δ is required for strand displacement synthesis, creating the substrate for cleavage by Fen1. PCNA acts as a binding platform, tethering these proteins to the replication fork via their PIP-box motifs (Dovrat et al. 2014). Without this binding, these proteins may not be able to process the lagging strand effectively. Indeed, I see shorter and much more apparent lagging strands in the absence of either DNA polymerase δ or PCNA (Figure 3.5D, compare lanes 2-5). These results provide further evidence that this system recapitulates Okazaki fragment maturation, dependent upon DNA ligase I, Fen1, DNA polymerase δ, and PCNA.

3.2.5 Generation of full-length products requires Fen1 and DNA ligase I

In order to further characterise the products in Figure 3.5B, lane 5, I linearised them after replication with XhoI. This led to the observation of a prominent band of approximately unit length, as well as a smear of lower molecular weight products (Figure 3.6A, lane 4). This is also seen graphically in Figure 3.6C, which is composed of lane profiles from Figure 3.6A (lanes 2 and 4). Considering the placement of the linearisation site with respect to the origin, a band of unit length suggests that in most cases, the lagging strand is being ligated to the leading strand (Figure 3.6B). If this were not the case, one would not expect a full-length product upon linearisation with XhoI. The smear of products below the linear band are likely intermediates that have not completed replication (Figure 3.6A, lane 4). Intriguingly, these results suggested that this assay was capable of termination.

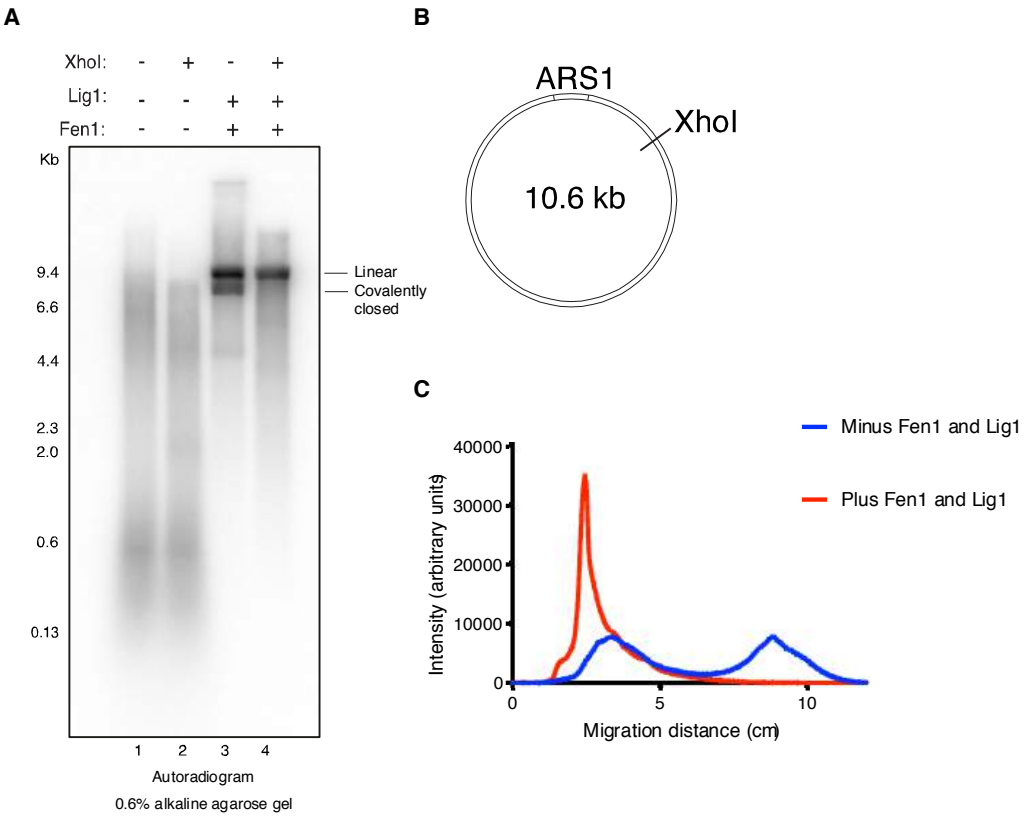

Figure 3.6 Full-length products require Fen1 and DNA ligase I
(A) 60-minute reaction performed as in Figure 3.5A, with or without Fen1 and DNA ligase I, followed by linearisation of replication products by XhoI. Products were separated over an alkaline agarose gel (0.6%). **(B)** Schematic depicting the plasmid origin (ARS1) relative to the cut site (XhoI). **(C)** Lane profiles of the data in lanes 2 and 4 of (A). This experiment was performed twice, and the result is reproducible.

3.2.6 Reconstitution of DNA replication termination *in vitro*

To address whether or not termination was occurring in this *in vitro* reaction with Fen1 and DNA ligase I, I separated the replication products overnight by native agarose gel electrophoresis. Total DNA was visualised with ethidium bromide (Figure 3.7A, left panel, lanes 1-3), then the gel was dried and subjected to autoradiography to detect the replicated DNA (Figure 3.7A, right panel, lanes 1-3). The products, which were DDK-dependent, consisted of a high molecular weight population as well as a population of relaxed, covalently closed daughter molecules (Figure 3.7A, right panel, lane 2). The presence of these covalently-closed topoisomers among the replicated products was evidence that this assay is capable of termination. Just above

these I observed a population of products that might have replicated but are nicked or 'gapped' in some way, causing them to run slower. Furthermore, I predicted that the high molecular weight products in this lane were comprised of molecules that were not able to complete replication (perhaps due to an inability to terminate), and/or that they had completely replicated but were topologically linked and unable to decatenate. In order to assess the composition of these products I linearised them after replication with XhoI. I observed a product of approximately unit length as well as larger replication intermediates, RIs (Figure 3.7A, right panel, lane 3). The full-length product was presumably composed of relaxed, covalently-closed topoisomers as well as previously catenated products. This accounted for approximately 40% of the products in Figure 3.7A, right panel, lane 3. This was quantified by calculating the amount of radioactive signal in the terminated (linear) product and dividing by the total radioactive signal in the lane. The high molecular weight products in this lane were likely RIs that had been unable to terminate, migrating slower upon linearisation with XhoI. These made up roughly 60% of the products in Figure 3.7A, right panel, lane 3. A time-course of replication followed by linearisation with XhoI revealed that the amount of terminated product increased over time, with 40% of the products terminated after an hour and nearly 60% of the products terminated over two hours (Figures 3.7B and 3.7C). This suggests that termination is a relatively slow and inefficient process compared to the rest of replication, based on the observation that elongation rates in this system are 1.5-2 kb/min (Yeeles et al. 2017). It is possible that some protein (or proteins) might enhance the rate of termination.

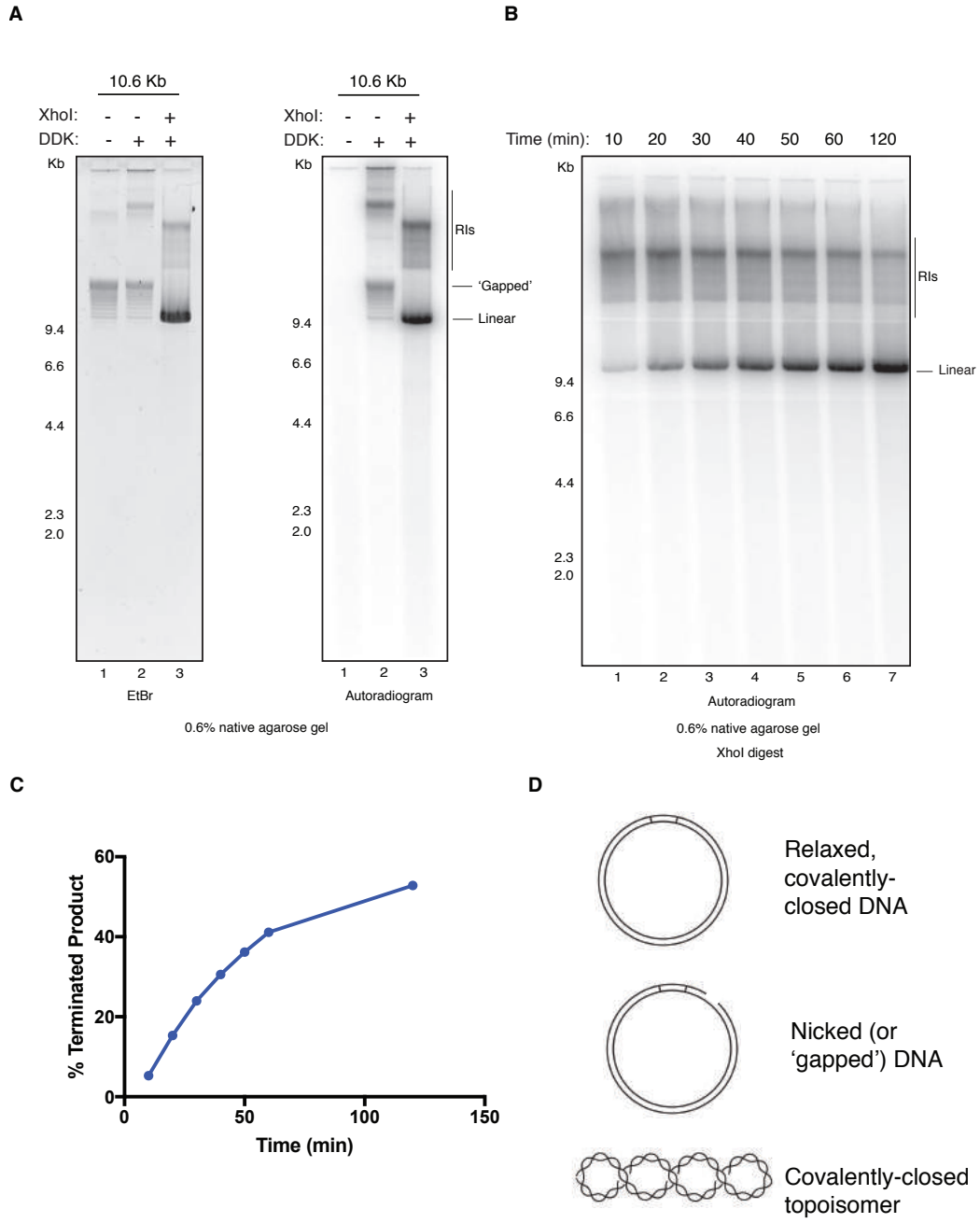

Figure 3.7 Reconstitution of DNA replication termination *in vitro*
(A) 60-minute reaction performed as in Figure 3.5A, with Fen1 and DNA ligase I, with or without linearisation by XhoI. **(B)** Time-course performed under same experimental conditions as in (A) with linearisation by XhoI. Products in (A) and (B) were separated over native agarose gels (0.6%). **(C)** Percent terminated (linearised) product as a function of time from (B). These experiments were performed twice, and the results are reproducible. **(D)** Representative images of different forms of DNA.

3.2.7 Decatenation of daughter molecules requires Topoisomerase II

Following replication, the nascent DNA is decatenated by Topoisomerase II. However, Topoisomerase II (unlike Topoisomerase I) is also capable of catenating DNA. It is not clear what drives the process of decatenation rather than catenation and it seems that many of the products in the purified replication reaction are unresolved catenanes. In order to test if either Topoisomerase I or II is limiting in this system, I titrated both to see if the product distribution changed (Figure 3.8). The replication products were separated overnight by native gel electrophoresis and analysed as described in section 3.2.6.

I observed some decatenation only in the presence of Topoisomerase II (see Figure 3.8A, right panel, lanes 1 and 3), consistent with previous *in vitro* data showing that this process is supported by Topoisomerase II, but not Topoisomerase I (Devbhandari et al. 2017). Titrating Topoisomerases I and II did not significantly change the distribution of the replication products, suggesting that additional factors are required for further decatenation and termination to occur (see Figures 3.8A and 3.8B). Interestingly, it seems that higher concentrations of Topoisomerase II may even be driving catenation of the daughter DNA. This is suggested by the appearance of more products in the well in Figure 3.8A, lane 7. Additionally, replication is inhibited at the highest concentrations of both Topoisomerases I and II (Figure 3.8A and Figure 3.8B, lanes 9 and 10), which is expected as these proteins have strong affinities for DNA. It is also possible that some of the products of the reaction are terminal protein-DNA intermediates resulting from aborted action by Topoisomerases I and II. This may explain why less DNA is recovered at the highest concentrations of both enzymes (Figure 3.8A and B, lanes 9 and 10).

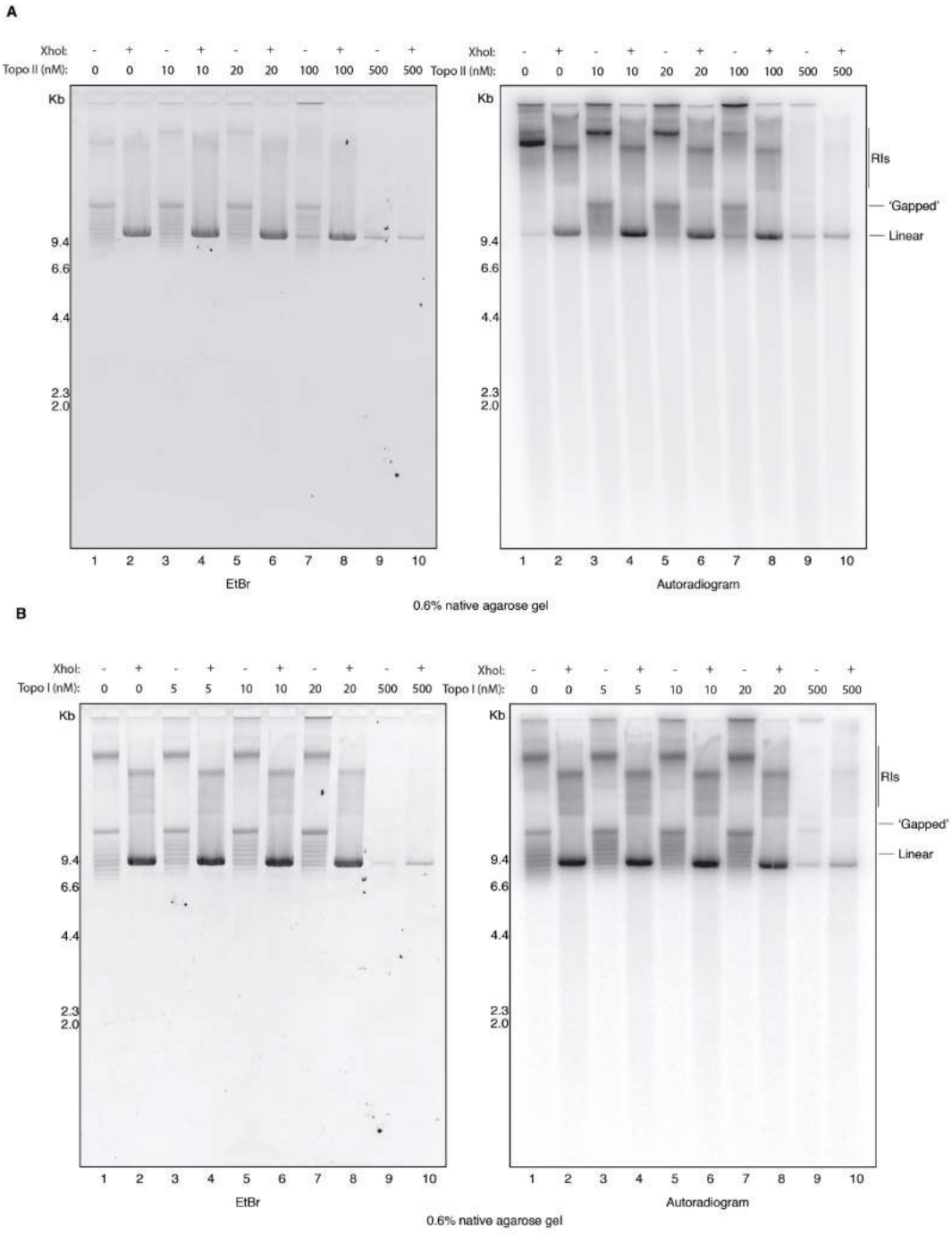

Figure 3.8 Decatenation of daughter DNA requires Topoisomerase II
(A) 60-minute reaction performed as in Figure 3.5A, with Fen1, DNA ligase I, and varying concentrations of TopoII, followed by linearisation with XhoI. **(B)** 60-minute reaction performed as in (A), with varying concentrations of TopoI, followed by linearisation with XhoI. Products in (A) and (B) were separated over native agarose gels (0.6%). This experiments were performed three times, and the results are reproducible.

3.2.8 Replication intermediates exhibit defects in termination

To better understand the nature of the products in Figure 3.7A, I performed further analysis via two-dimensional gel electrophoresis using native conditions in the first dimension and alkaline conditions in the second dimension. Initially, I took the products of the unlinearised replication reaction and the results can be seen in Figure 3.9A. This revealed that the lower band on the alkaline gel (Figure 3.9A, panel A) seen previously represented the relaxed, covalently closed replication products seen on the native gel (Figure 3.9A, panel B). These products migrated slightly faster than unit length, which would be expected of a covalently-closed plasmid migrating under denaturing conditions. The upper band on the alkaline gel (Figure 3.9A, panel A) represents the high molecular weight RIs from the native gel (Figure 3.9A, panel B). Moreover, the majority of the population of gapped molecules on the native gel as well as some covalently-closed products migrated to this position in the alkaline gel. This suggests that these species also contain RIs as well as some fully replicated, covalently-closed products. The smear of products seen on the alkaline gel (Figure 3.9A, panel A) is mostly comprised of RIs.

I was interested in understanding the nature of the RIs seen after linearisation of the replication reaction in Figure 3.9A. I performed two-dimensional gel analysis of the linearised products (Figure 3.9B). As expected, most of the linear band (Figure 3.9B, panel E) migrated as full-length in the second dimension. These account for approximately 50% of the products in this lane (Figure 3.9B, panel F). However, the remaining 50% of products migrated as a faster smear suggesting that there are other species present in the linearised product. These might include terminated products in which not all of the Okazaki fragments were ligated together, or perhaps not all of ribonucleoside monophosphates were removed from the primers synthesised by DNA polymerase α. These would be degraded in an alkaline gel, leaving gaps in the DNA. Furthermore, the RIs resolved into a 'C'-shaped curve migrating the length of the alkaline gel with a bifurcated tail (Figure 3.9B, panel F). In the absence of origin-specific conditions, the curve most

likely comprises X-shaped molecules where the centre of the x is shifted to different positions along the molecule. The most symmetric molecules would be most impeded; these are represented by the products at the peak of the curve on the two-dimensional gel (Figure 3.9B, panel F). For a diagrammatic representation see Figure 3.9C. Products in which the centre of the X is shifted to either end of the molecule would migrate faster in the native gel as they are more linear-like. However, under denaturing conditions, these products migrate as a smear dependent on their length. Each of these molecules is comprised of long and short arms emanating from the centre of the X. The longer labelled nascent strands will migrate slower than their shorter counterparts (Figure 3.9C). Together, these give rise to the 'C'-shaped curve in the second dimension as depicted in Figure 3.9B, panel F.

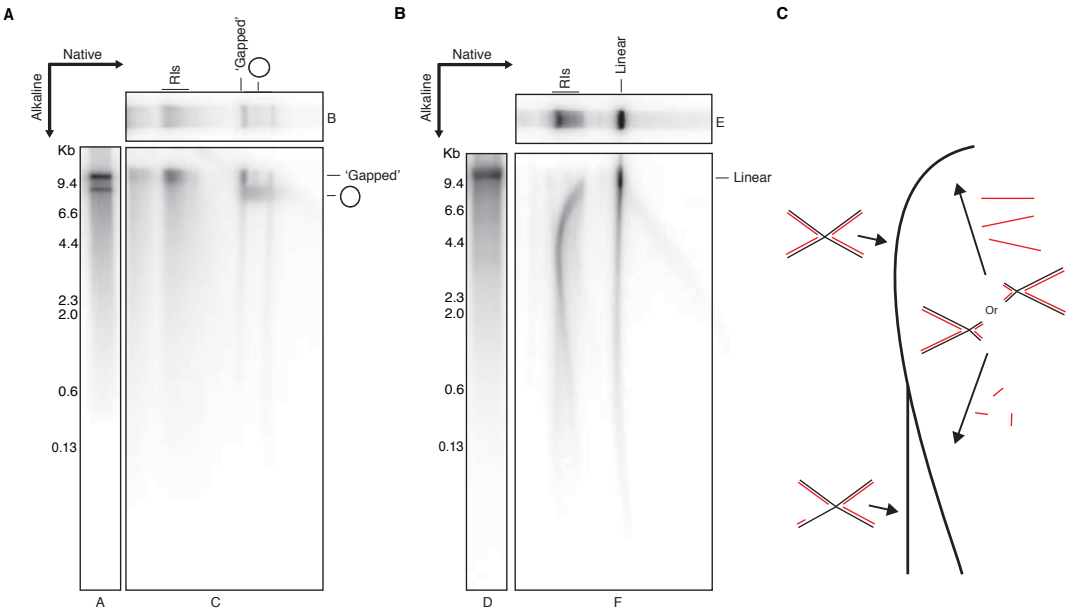

Figure 3.9 Replication intermediates exhibit defects in termination **(A)** Two-dimensional analysis of 60-minute reaction performed as in Figure 3.5A, with Fen1 and DNA ligase I and without linearisation by XhoI. **(B)** Reaction carried out as in (A), with linearisation by XhoI. **(C)** Diagrammatic representation of the RIs in Figure 3.9B, panel F. Panels A and D are one-dimensional alkaline gels and panels B and E are one-dimensional native gels. Panels C and F are two-dimensional gels. All panels are autoradiograms. These experiments were performed twice, and the results are reproducible.

The bifurcated tail at the bottom of the curve suggests that a population of leading and/or lagging strands are shorter than the rest, presumably due to a defect in replicating the final stretch of DNA between two converging CMGs.

Together, these results support the idea that some of the high molecular weight products I observed on the native gel are fully replicated but unable to decatenate. The rest are not capable of completing replication, and exhibit defects that are consistent with an inability to terminate.

3.3 Discussion

3.3.1 Reconstitution of Okazaki fragment maturation *in vitro*

Early work in this chapter detailed the purification of proteins previously implicated in Okazaki fragment maturation, including the nucleases Fen1 and Dna2, and DNA ligase I. With the aim of studying Okazaki fragment maturation *in vitro*, I purified the proteins required to recapitulate replication initiation and elongation as described previously (Yeeles et al. 2015; Yeeles et al. 2017). I was then able to reconstitute Okazaki fragment maturation by adding Fen1, Dna2 and DNA ligase I to these purified replication proteins (Figure 3.5). In addition to the proteins required for initiation and elongation, I found that this process minimally requires Fen1 and DNA ligase I. Furthermore, I showed that DNA polymerase δ and PCNA are essential for Okazaki fragment maturation (Figure 3.5C). This was not too surprising and further confirms that this reconstituted system recapitulates what occurs *in vivo*.

Importantly, Dna2 does not substitute for Fen1 as the sole nuclease during Okazaki fragment maturation in this system (Figure 3.5B). Multiple pathways have been proposed for Okazaki fragment maturation involving both Fen1 and Dna2. It seems likely that this system predominantly recapitulates the pathway in which Fen1 cleaves a short flap created when the 5'-end of a downstream Okazaki fragment is displaced by DNA polymerase δ (Stodola and Burgers, 2016). In another pathway, these flaps are displaced by DNA

polymerase δ to such an extent that they can become bound by RPA. Fen1 cannot cleave these long RPA-coated flaps alone, which instead require both Dna2 and Fen1. It is not clear what drives the formation of these long flaps and how often they form *in vivo*. Pif1 has been shown to promote strand displacement by DNA polymerase δ, suggesting that it could play a role in creating these long flap substrates (Rossi et al. 2008). In fact, Pif1 mutants have been shown to rescue the lethality of Dna2 mutants in *S. cerevisiae* (Budd et al. 2006). If Dna2 is the only nuclease capable of cleaving these long flaps, that may explain why it is essential for cell viability *in vivo* but is dispensable in this system, where there is no Pif1.

3.3.2 Reconstitution of DNA replication termination *in vitro*

In section 3.2.5 of this chapter I showed that the products of the purified replication reaction with Fen1 and DNA ligase I were unit length upon linearisation with XhoI (Figure 3.6). This suggested that the products were terminated at the end of replication. I later showed this to be the case after observing covalently-closed molecules on native gels (Figure 3.7). The terminated product accumulated over time, with almost 60% of the products terminated after two hours (Figure 3.7B). This suggests that while the purified proteins in this reaction are sufficient to generate covalently-closed molecules, termination is a relatively slow and inefficient process compared to initiation and elongation. Work carried out in *Xenopus* egg extracts revealed that two converging replisomes do not slow down or stall during termination (Dewar et al. 2015). Thus, it might be the case that additional factors are required to promote rapid and efficient termination. Rrm3 and Pif1 are two candidates as they have both been shown to promote replisome progression through difficult to replicate regions of the genome *in vivo* (Ivessa et al. 2003; Fachinetti et al. 2010; Sabouri et al. 2012; Steinacher et al. 2012).

I observed some decatenation of the replicated products in the presence of Topoisomerase II (Figure 3.8). Titrating more Topoisomerase II into our reaction did not change the product distribution, however, and leaving it out

resulted in the accumulation of fully-replicated but catenated intermediates in the presence of Topoisomerase I. It is likely that additional factors are required for complete decatenation. One candidate is condensin, which has been shown *in vivo* and *in vitro* to promote decatenation with Topoisomerase II (Bhat et al. 1996; Charbin et al. 2014). The Sgs1-Top3-Rmi1 complex is another possibility as it has been shown to promote the resolution of late replication intermediates and decatenation of DNA *in vitro* (Suski and Marians, 2008; Cejka et al. 2012). Topoisomerase II has also been shown to be regulated by post-translational modifications *in vivo*, and these may be important for its function (Bedez et al. 2018).

Furthermore, CMG removal at the end of replication has been shown to be mediated by a number of proteins, including Cdc48 and SCF^{DIA2} in *S. cerevisiae* (Maric et al. 2014). These are not present in this system and it is not clear if the covalently-closed products are still bound by CMG. In any case, the data reveal that termination and some decatenation can occur efficiently in the absence of this pathway for removing CMG. This supports the model proposed previously in which CMG removal does not occur until after the leading strands are ligated to the lagging strands on the opposing forks at the end of replication (Dewar et al. 2015).

3.3.3 Replication intermediates exhibit defects in termination

I found that roughly 60% of the replication products were intermediates after an hour, though the ratio of intermediates to terminated products was reduced over time (Figure 3.7). Two-dimensional gel analysis of the linearised replication products revealed that these intermediates were x-shaped molecules (Figure 3.9B, panel F). This suggested that the replisomes on these molecules had progressed mostly unimpeded but were unable to converge and complete replication. It was not clear as to whether this termination defect was due to a topological constraint during convergence or some other problem, such as a protein-DNA barrier or an inability to unwind the last bit of DNA between the two converging CMGs. In any case, an

additional factor (or factors) may be required to resolve these intermediates, such as Rrm3, Pif1 or Sgs1-Top3-Rmi1.

Chapter 4. Results II

4.1 Introduction

The Pif1 family helicases are conserved from yeast to humans (Bessler et al. 2001). In *S. cerevisiae* these include Pif1 and Rrm3. These helicases have a 5'-3' polarity and are implicated in facilitating replication fork progression through difficult to replicate regions of the genome. For example, Pif1 promotes replication and suppresses genome instability through G-quadruplex motifs (Paeschke et al. 2011; Paeschke et al. 2013). It has also been shown to remove protein barriers on DNA, such as telomerase and Rap1 bound to telomeric DNA (Boule et al. 2005; Koc et al. 2016). Similarly, Rrm3 has been called a 'sweepase' for its ability to remove nonhistone proteins bound to DNA (Mohanty et al. 2006).

Furthermore, Pif1 has been implicated in Okazaki fragment maturation in *S. cerevisiae*. Pif1 has been shown to promote strand displacement by DNA polymerase δ, which could help to create the long-flap substrates requiring cleavage by Dna2 during Okazaki fragment maturation (Rossi et al. 2008; Pike et al. 2009; Wilson et al. 2013). Dna2 is an essential gene but the lethality of Dna2 mutants is rescued in strains that are lacking both Pif1 and Dna2 (Budd et al. 2006). Importantly, Dna2 has nuclease and helicase activities but it is the loss of the nuclease activity that is lethal (Formosa and Nittis, 1999; Kang et al. 2000). Together, these data suggest that Dna2 and Pif1 function in the same pathway during Okazaki fragment maturation, an alternative to the pathway in which the sole nuclease required is Fen1. While it has been shown that Pif1 promotes this Dna2 pathway using pre-formed substrates *in vitro*, it has never been tested in a fully-reconstituted system as described in Chapter 3 (Rossi et al. 2008; Pike et al. 2009).

Recently, Pif1 has been found to promote replication fork convergence during termination (Steinacher et al. 2012). In addition, fork stalling and increases in X-shaped termination intermediates have also been reported in Pfh1-

depleted cells, Pfh1 being the Pif1 homologue in *S. pombe* (Sabouri et al. 2012; Steinacher et al. 2012). These phenotypes match those of the RIs described in Chapter 3, where replication was carried out in the absence of Pif1. Unpublished data also suggests that Pif1 is able to enhance termination at the end of replication *in vitro* (Tom Deegan). Given the similarities in the phenotypes in cells lacking Pfh1 and the RIs described in Chapter 3 resulting from replication in the absence of Pif1, I also wanted to know whether or not Pif1 could promote resolution of these RIs and enhance termination in the fully-reconstituted replication system described in Chapter 3.

4.2 Results

4.2.1 Purification of Pif1

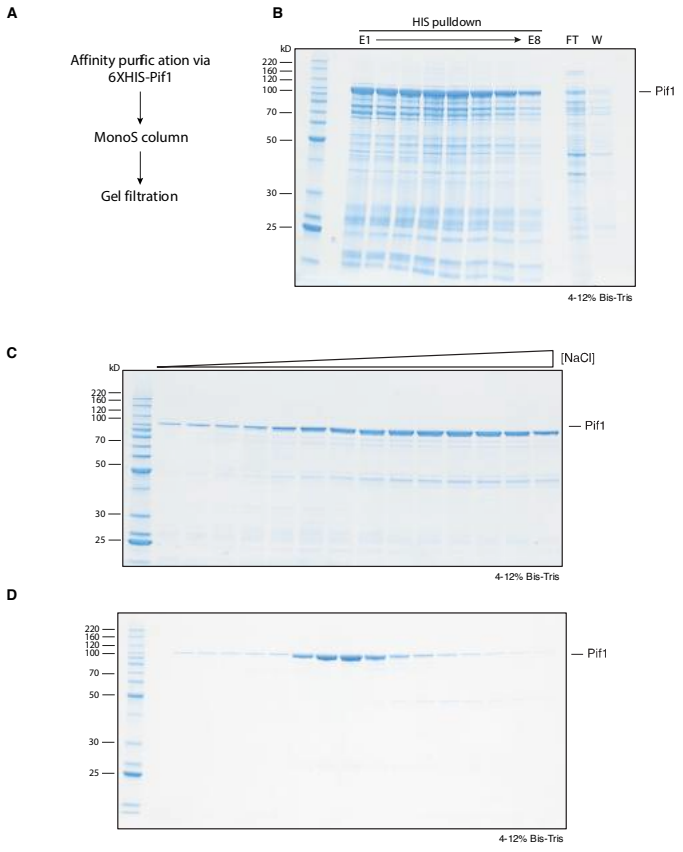

Figure 4.1 Purification of Pif1
The purification scheme for Pif1 is depicted in **(A)**. Eluate (E) fractions following nickel affinity chromatography **(B)**. The ion-exchange chromatography (MonoS) step is shown in **(C)** and the final size-exclusion chromatography step of the purification is shown in **(D)**. Protein analysed by SDS-PAGE with Coomassie staining.

Following previously established protocols, I amplified the nuclear isoform of Pif1 (amino acids 40-859) from genomic *S. cerevisiae* DNA via PCR (Boule et al. 2005). I then cloned it into the pET28a expression vector, which provided a 6X-Histidine tag on its N-terminus, and then optimised it for expression in *E. coli*. I purified the protein to homogeneity by nickel affinity chromatography (Figure 4.1B), followed by ion-exchange chromatography (Figure 4.1C), and size-exclusion chromatography (Figure 4.1D). Due to its overall positive charge, I used a MonoS column to purify Pif1. The protein eluted from the ion-exchange column in a broad peak, with a prominent contaminant around 50 kDa. It then eluted in a defined peak following the final size-exclusion chromatography step and appeared to be pure.

4.2.2 Dna2 alone or with Pif1 does not substitute for Fen1

I wanted to address whether or not Pif1 could enhance strand displacement by DNA polymerase δ, creating a long RPA-coated flap substrate during Okazaki fragment maturation for Dna2. In order to test this, I added purified Pif1 to the soluble replication reaction described in Chapter 3 with the addition of DNA ligase I (but no Fen1). The radiolabelled replication products were then separated on an alkaline agarose gel, dried, and subjected to autoradiography as described previously (Figure 4.2A). Two distinct classes of replication products – leading and lagging strands – were observed in the absence of Dna2 and Pif1 (Figure 4.2A, lane 1). The lagging strands were much longer in the sample with Pif1 but no Dna2, suggesting that Pif1 can indeed promote strand displacement by DNA polymerase δ (Figure 4.2, lane 5). Further supporting this idea was the observation that the overall ^{32}P signal is higher, implying more synthesis, in the presence of Pif1 (Figure 4.2, lanes 1 and 5).

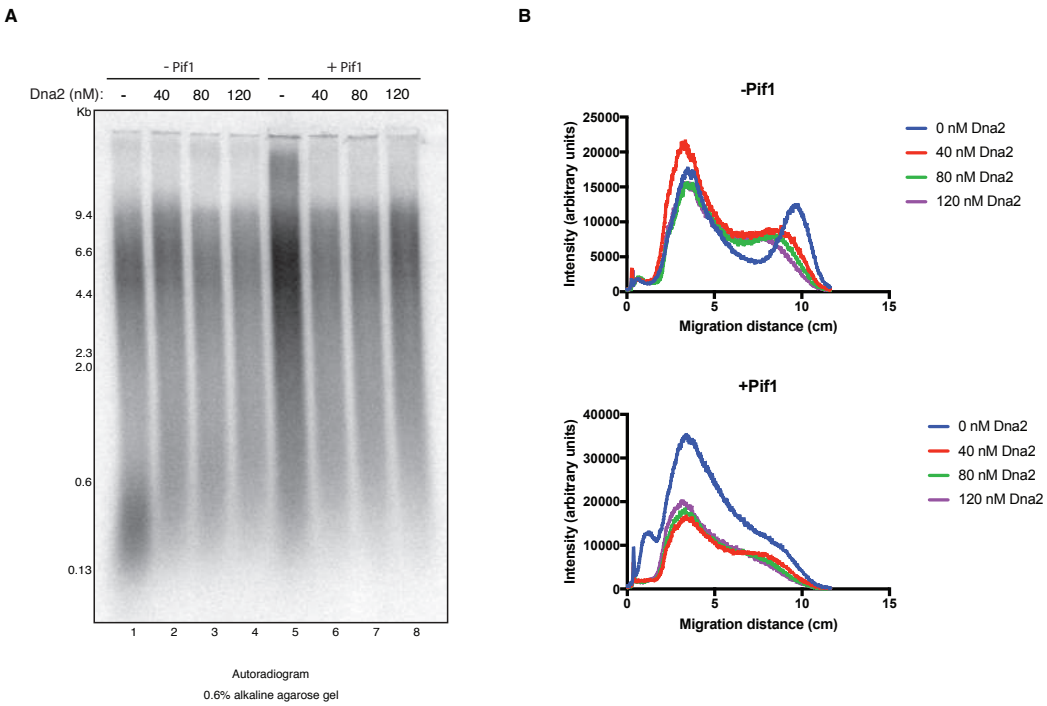

Figure 4.2 Dna2 does not substitute for Fen1 during Okazaki fragment maturation, with or without Pif1
(A) Dna2 and Pif1 drop-out experiment performed for 30-minutes as in Figure 3.5A with DNA ligase I (no Fen1). Products were separated over an alkaline agarose gel (0.6%). **(B)** Lane profiles of the data in lanes 1-8 of (A). This experiment was performed twice, and the result is reproducible.

In addition, the lagging strands became longer in the presence of Dna2 without Pif1 (Figure 4.1, lanes 1-4). This can be visualised graphically in Figure 4.2B, top panel, which is composed of lane profiles from Figure 4.2A (lanes 1-4). This observation suggests that some, but not all, of the Okazaki fragments can be processed by Dna2. Interestingly, Pif1 did not enhance this effect (Figure 4.2A, lanes 5-8). If anything, Dna2 seems to suppress Pif1's ability to enhance strand displacement by DNA polymerase δ. This can be visualised graphically in Figure 4.2B, bottom panel, which is composed of lane profiles from Figure 4.2A (lanes 5-8). In contrast with previous *in vitro* and *in vivo* data, the data presented here suggests that Dna2 and Pif1 are not acting in the same pathway during Okazaki fragment maturation (Budd et al. 2006; Rossi et al. 2008; Pike et al. 2009).

4.2.3 Pif1 promotes the resolution of RIs

In order to assess the effect(s) of Pif1 on termination, I titrated Pif1 in the replication reaction described in Chapter 3 with the addition of Fen1 and DNA ligase I. To distinguish RIs from terminated products, the products were linearised with XhoI prior to overnight separation by native agarose gel electrophoresis (Figure 4.3).

Without Pif1, approximately 35% of the products were terminated (linear) after 60 minutes of replication, as seen in Figure 4.3A, lane 9. Consistent with the data presented in Chapter 3, these products accumulated slowly over the course of an hour (Figure 4.3A, lanes 1 and 9). The addition of 1 nM of Pif1 enhances termination so that roughly 30% of the products are terminated after 15 minutes of replication (Figure 4.3A, lane 2). Increasing the concentration of Pif1 to 5 nM slightly improves this number to around 35% (Figure 4.3A, lane 3). The increase in terminated product comes at the expense of the RIs, suggesting that these RIs are being resolved by Pif1. However, the amount of terminated product seems to level off after about 30 minutes of replication, reaching a maximum of 40% with either 1 nM or 5 nM of Pif1 (Figure 4.3A, lanes 2, 3, 6, 7, 10, 11). The percent of terminated product over time can be visualised graphically in Figure 4.3B. Interestingly, the amount of terminated product does not appear to increase with the addition of more Pif1. Roughly 30% of the products are terminated after 15 minutes of replication with 50 nM of Pif1, and this does not increase even after 30 or 60 minutes of replication (Figure 4.3A, lanes 4, 8, 12). This suggests that termination may be inhibited at high concentrations of Pif1. It also appears that Pif1 is inhibitory to overall replication at high concentrations, based on a decrease in ^{32}P signal in Figure 4.3A, lanes 4, 8, and 12. Furthermore, the products in the wells of the gel appear more prominent with increasing concentrations of Pif1 (Figure 4.3A). This may be due to increased strand displacement activity and rolling circle replication by DNA polymerase δ in the presence of Pif1. Together, the data presented in this section indicates that the lag in termination seen previously is removed

by Pif1. There is no difference in terms of the total amount of terminated product, with or without Pif1.

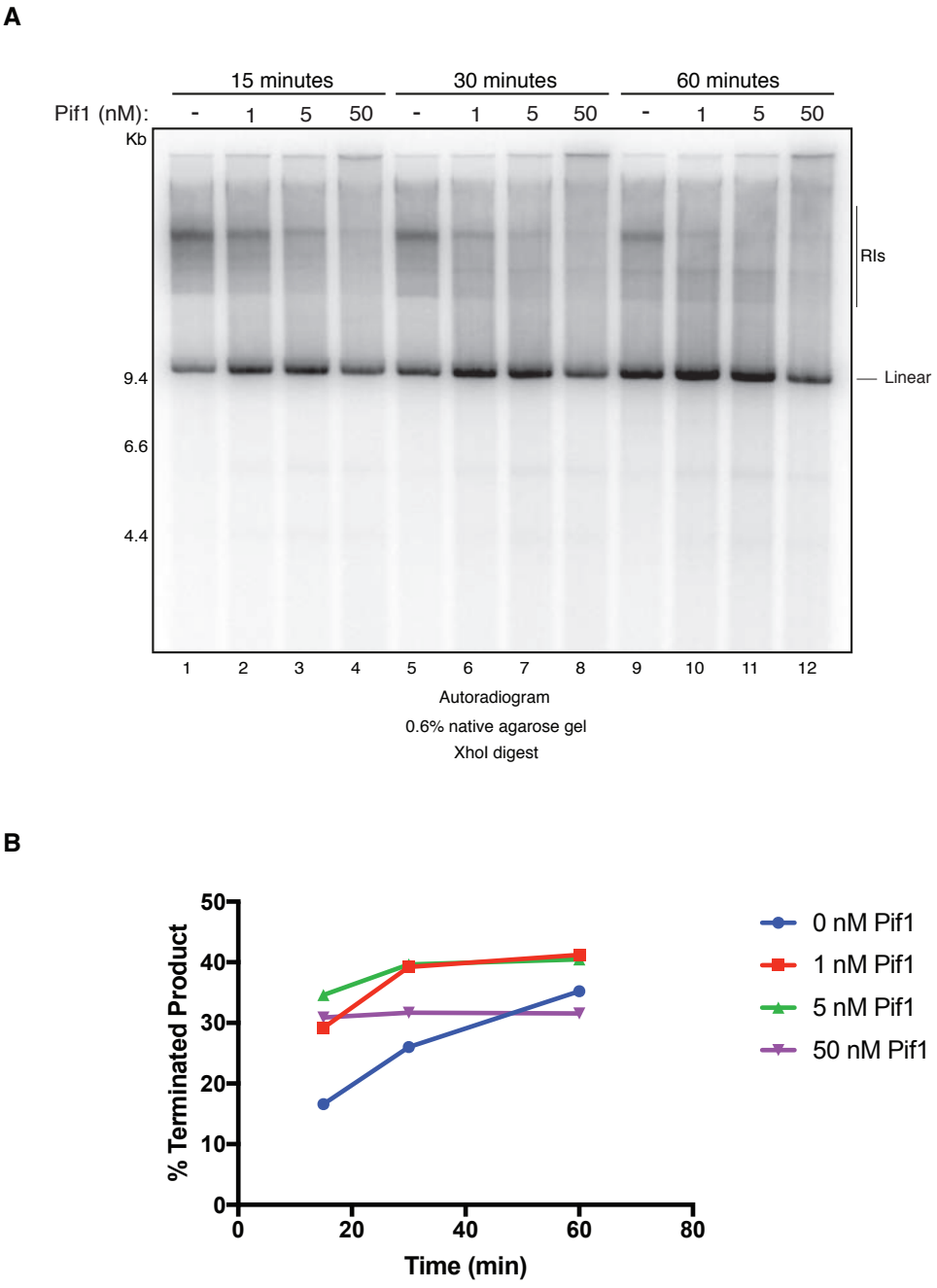

Figure 4.3 Pif1 promotes the resolution of RIs
(A) Pif1 titration and time-course experiment performed for up to 60-minutes as in Figure 3.5A with Fen1 and DNA ligase I. Products were linearised with XhoI and separated over a native agarose gel (0.6%). **(B)** Lane profiles of the data in lanes 1-12 of (A). This experiment was performed twice, and the result is reproducible.

4.2.4 Termination is inhibited by an excess of loaded Mcm2-7

Whilst looking for factors that could influence the efficiency of termination, it was shown that inactive Mcm2-7 double hexamers could be pushed along DNA by an active CMG (Douglas et al. 2018). In this case, they were using a linear template with covalent protein roadblocks to determine the directionality of CMG (Douglas et al. 2018). In light of this new data, I began to wonder if an excess of loaded inactive Mcm2-7 double hexamers could inhibit termination by physically blocking the convergence of two CMGs. This is important as Mcm2-7 are loaded in excess over ORC and origins of replication during G1 phase of the cell cycle (Burkhart et al. 1995; Lei et al. 1996; Donovan et al. 1997; Mahbubani et al. 1997; Edwards et al. 2002). If they are inhibitory to termination, then a mechanism must exist to remove them during replication. In order to test this I titrated Mcm2-7 in the loading reaction prior to replication, as described in section Chapter 3.

I found that increasing the concentration of Mcm2-7 has an inhibitory effect on termination as the amount of terminated product decreases with increasing concentrations of Mcm2-7. While the amount of terminated product decreases, the RIs can be seen to increase (Figure 4.4A, lanes 1-4). Titrating Mcm2-7 below 30 nM did not seem to make a difference, however, as the overall product distribution remained the same (Figure 4.4B, lanes 1-3). Importantly, the total ^{32}P signal is mostly unchanged regardless of whether the Mcm2-7 concentration is 30 nM or 400 nM, suggesting that initiation and elongation are not affected and the defect is specific to termination (Figure 4.4A and 4.4E). Below 30 nM, the total ^{32}P signal decreases as there are fewer origins firing and thus less replication. In all prior experiments presented in this thesis, the loading reaction was carried out with 30 nM Mcm2-7.

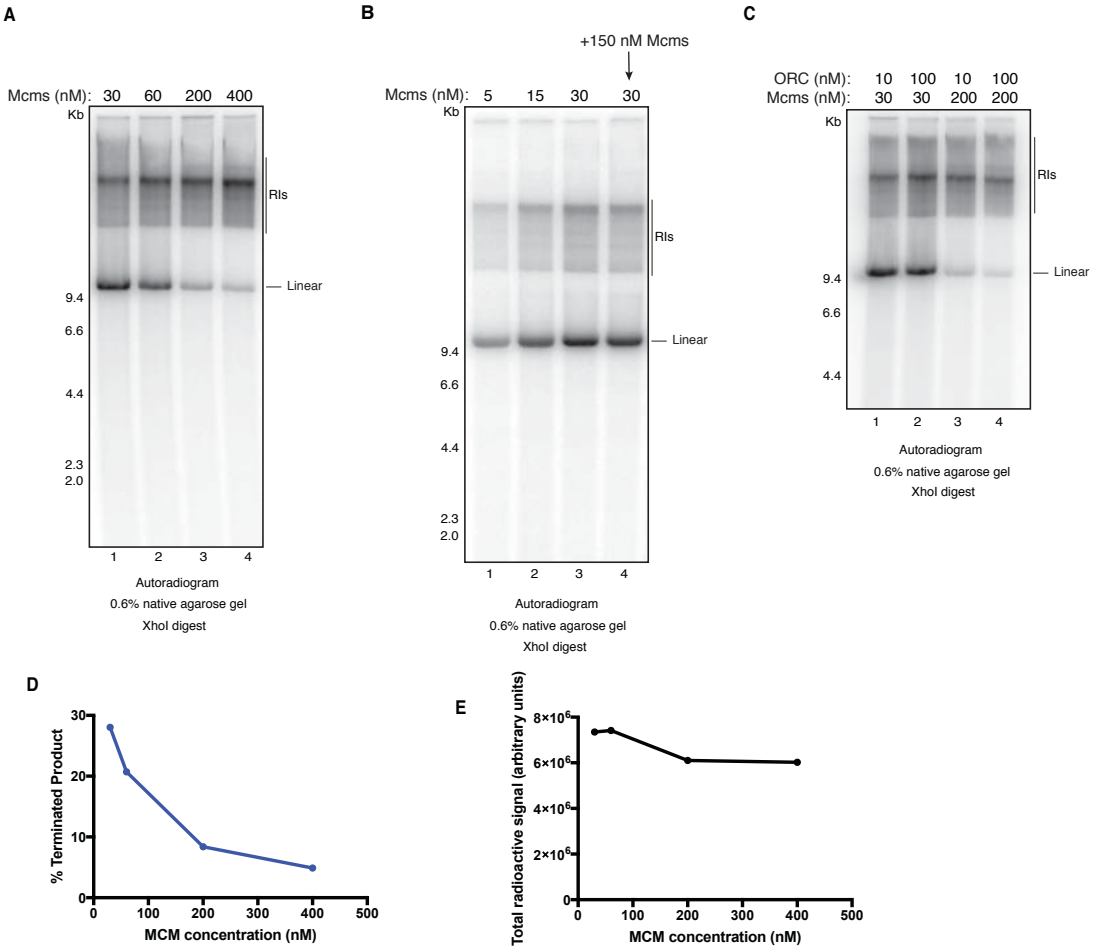

Figure 4.4 Termination is inhibited by an excess of loaded Mcm2-7
(A) Mcm2-7 titration experiment performed for 60-minutes as in Figure 3.5A with Fen1 and DNA ligase I. Products were linearised with XhoI. **(B)** Mcm2-7 titration and addback experiment performed for 60-minutes as in (A). **(C)** ORC and Mcm2-7 titration experiment performed for 60-minutes as in (A). Products in (A), (B), and (C) were separated over a native agarose gel (0.6%). **(D)** Quantification of the terminated product in (A). **(E)** Quantification of the total radioactive signal in (A). These experiments were performed twice, and the results are reproducible.

In order to test whether or not the defect was specific to loaded Mcm2-7 and not due to having free Mcm2-7 in solution during replication, I added excess Mcm2-7 to the reaction after loading under low Mcm2-7 conditions (30 nM). The effect is clearly specific to loaded Mcm2-7 as adding 150 nM Mcm2-7 during the replication step did not have any effect on termination (Figure 4.4B, lanes 3 and 4). Furthermore, the inhibitory effect of excess loaded Mcm2-7 on termination appears to be independent of ORC concentration (Figure 4.4C). This suggests that multiple loading events can be orchestrated by a single molecule of ORC.

4.2.5 Visualisation of Mcm2-7 trains on DNA via EM

To determine the nature of the termination defect I observed in section 4.2.4, I collaborated with Patrik Eickhoff in Dr Alessandro Costa's lab at the Francis Crick Institute. For these experiments, I loaded an excess of Mcm2-7 (200 nM) on DNA and performed replication as described in Chapter 3 with the addition of Fen1 and DNA ligase I (EM experiments were carried out without ^{32}P-dCTP). The samples were then analysed by electron microscopy after negative staining.

Interestingly, we observed Mcm2-7 double hexamer trains under conditions where an excess of Mcm2-7 was loaded onto DNA, similar to what was seen by Douglas et al. 2018. This time, however, the trains were found between two converging CMGs (Figure 4.5A, green panels). Because the N-termini of the CMGs were observed pushing the double hexamers, we knew that the two CMGs were converging (Figure 4.5A, green panels). We could also observe other replisome components, such as DNA polymerase ε and Ctf4. Statistical analysis of 772 micrographs revealed that approximately 20.8% of trains were not capped at either end by CMG, 48% of trains were capped at one end by CMG, and 31.2% of trains were capped at both ends by CMG (Table 4-1). These numbers are likely skewed by the ability to average both ends of the trains.

Together, along with the revelation that the linearised RIs were x-shaped molecules (Figure 3.9), these results suggested that replication had proceeded around most of the plasmid unimpeded, and that active CMGs could push inactive Mcm2-7 double hexamers ahead of the replication fork, although they would need to be removed in order for termination to occur at the end of replication, hence the inhibition of termination under these conditions. Notably, no trains were observed in samples where loading was carried out under a low concentration (30 nM) of Mcm2-7. Particles not part of the trains were found to be a combination of double hexamers and single Mcm2-7/Cdt1 molecules (Figure 4.5B, red panels).

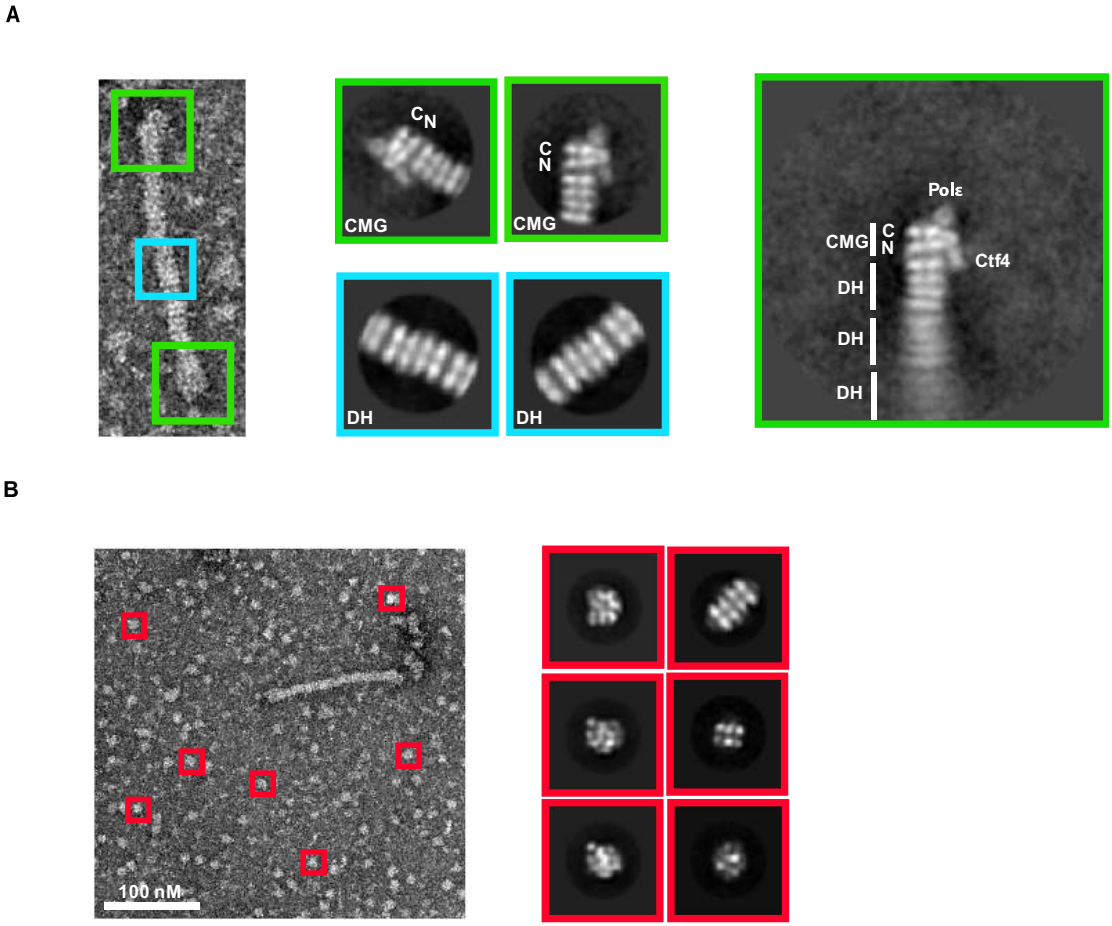

Figure 4.5 Visualisation of Mcm2-7 trains on DNA via EM
(A) Representative micrographs (negative stain) of replication products under conditions of excess loaded Mcm2-7. Panels in green are annotated 2D class averages of train ends (CMGs). Panels in blue are 2D class averages of the particles (double hexamers) between converging CMGs. **(B)** Representative micrograph and 2D class averages of particles not included in trains (i.e. double hexamers and single Mcm2-7/Cdt1).

Table 4-1 Statistical analysis of Mcm2-7 train data collected via EM*

		Low Mcm + Mcm10	High Mcm + Mcm10	High Mcm + Mcm10
Processing	Total micrographs	20	772	200
	Total surrounding particles	-	-	93,213
	Total Mcm particles	-	-	57,790 (62.0%)
	Surrounding Mcm-Cdt1	-	-	46,940 (50.3%)
	Surrounding single Mcm	-	-	7,892 (8.5%)
	Surrounding double Mcm	-	-	2,958 (3.2%)
	Surrounding CMG	-	-	0 (0%)
	Total unidentified particles	-	-	35,423 (38.0%)
	Total trains	0 / grid square	769 (75 / grid square)	75 / grid square
	Total picked train termini	-	1,538	-
	Terminal CMG	-	849 (55.2%)	-
	Terminal non-CMG	-	689 (44.8%)	-
	Trains without CMG	-	160 (20.8%)	-
	Trains with one CMG	-	369 (48.0%)	-
	Trains with double CMG	-	240 (31.2%)	-
Staining	Grids	EM resolutions C300Cu100	EM resolutions C300Cu100	EM resolutions C300Cu100
	Glow discharging	30 sec (45 mA)	30 sec (45 mA)	30 sec (45 mA)
	Sample volume	4 μl	4 μl	4 μl
	Incubation time	1 min	1 min	1 min
	Stain	2% uranyl acetate	2% uranyl acetate	2% uranyl acetate
	Staining time	5 / 10 / 15 / 20 sec	5 / 10 / 15 / 20 sec	5 / 10 / 15 / 20 sec
Data collection	Microscope	FEI Tecnai G2 Sprit	FEI Tecnai G2 Sprit	FEI Tecnai G2 Sprit
	Detector	2k x 2k Gatan Ultrascan 100	2k x 2k Gatan Ultrascan 100	2k x 2k Gatan Ultrascan 100
	Filament	LaB6	LaB6	LaB6
	Voltage	120 kV	120 kV	120 kV
	Defocus range	-0.5 / -2.5 μm	-0.5 / -2.5 μm	-0.5 / -2.5 μm
	Magnification	x30,000	x30,000	x30,000
	Pixel size	3.45 Å	3.45 Å	3.45 Å
	CTF estimation	Gctf-v1.18	Gctf-v1.18	Gctf-v1.18
	Picking	EMAN-2.07	EMAN-2.07	EMAN-2.07

***Data collected and analysed by Patrik Eickhoff**

4.2.6 Mcm2-7 trains are removed in the presence of Pif1

Given Pif1's ability to enhance termination (as described in section 4.2.3), I wanted to know if Pif1 could play a role in removing excess Mcm2-7 double hexamers from DNA. In order to test this idea, I added Pif1 to the replication reaction described in Chapter 3 with Fen1 and DNA ligase I.

Under conditions where Mcm2-7 was loaded in excess, I observed a significant inhibition of termination (as seen in 4.2.4). However, this inhibition was completely rescued by the addition of Pif1 (Figure 4.6, left

panel, lanes 6 and 7). This suggested that Pif1 was playing a role in removing excess Mcm2-7 double hexamers between two converging CMGs. Under conditions where Mcm2-7 was not loaded in excess, Pif1 only slightly enhanced the amount of terminated product (Figure 4.6, left panel, lanes 1 and 2). This was expected as the amount of terminated product is roughly the same after an hour of replication with or without Pif1 (Figure 4.3).

Consistent with my previous result (Figure 4.3), I observed a Pif1-dependent accumulation of products in the well which then disappeared in the presence of Dna2, regardless of whether or not Mcm2-7 was loaded in excess (Figure 4.6, left panel, lanes 2, 3, 7, 8). However, Dna2 appears unable to remove the excess Mcm2-7 double hexamers (Figure 4.6, left panel, lane 9), a role that seems to be specific to Pif1. Furthermore, analysis by electron microscopy after negative staining revealed a significant reduction in the amount of trains observed in samples with an excess of loaded Mcm2-7 in which replication was carried out with Pif1 (Patrik Eickhoff, personal communication). This further confirms a role for Pif1 in removing excess Mcm2-7 from DNA.

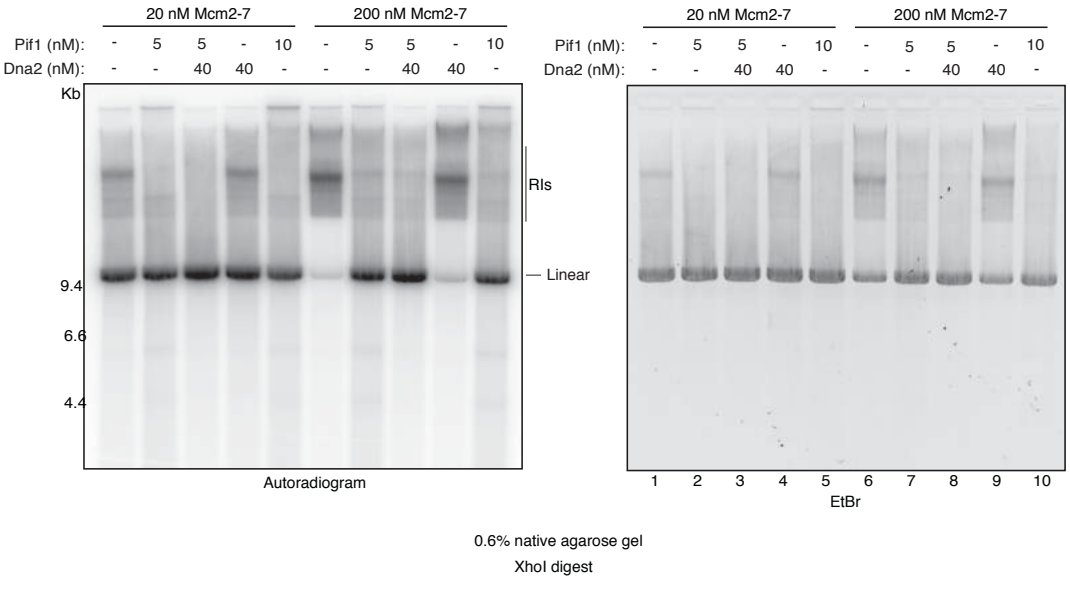

Figure 4.6 Mcm2-7 trains are removed in the presence of Pif1
Pif1 and Dna2 addback experiment performed under both high and low Mcm2-7 loading conditions for 60-minutes as in Figure 3.5A with Fen1 and DNA ligase I. Products were linearised with XhoI and separated over a native agarose gel (0.6%). This experiment was performed twice, and the result is reproducible.

In order to assess the kinetics of Mcm2-7 double hexamer removal by Pif1, I modified the assay described earlier in this section. Following replication for an hour (in the absence of Pif1) with an excess of loaded Mcm2-7, I added Pif1 back and took 10 minute time-points for up to an hour (Figure 4.7). Roughly 15% of products were terminated after an hour of replication without Pif1, but after 10 minutes with Pif1 this increased to about 40% (Figure 4.7A, lanes 1 and 5). By 20 minutes this number had levelled off at approximately 50% (Figure 4.7A, lane 6). Thus, the majority of termination occurred in the first 10 minutes and the reaction appeared to be mostly finished by 20 minutes (Figure 4.7A, lanes 1, 5, 6). It remains to be seen if Pif1 can remove Mcm2-7 double hexamers during replication, or if this role is only applicable at the end of replication in the context of trains.

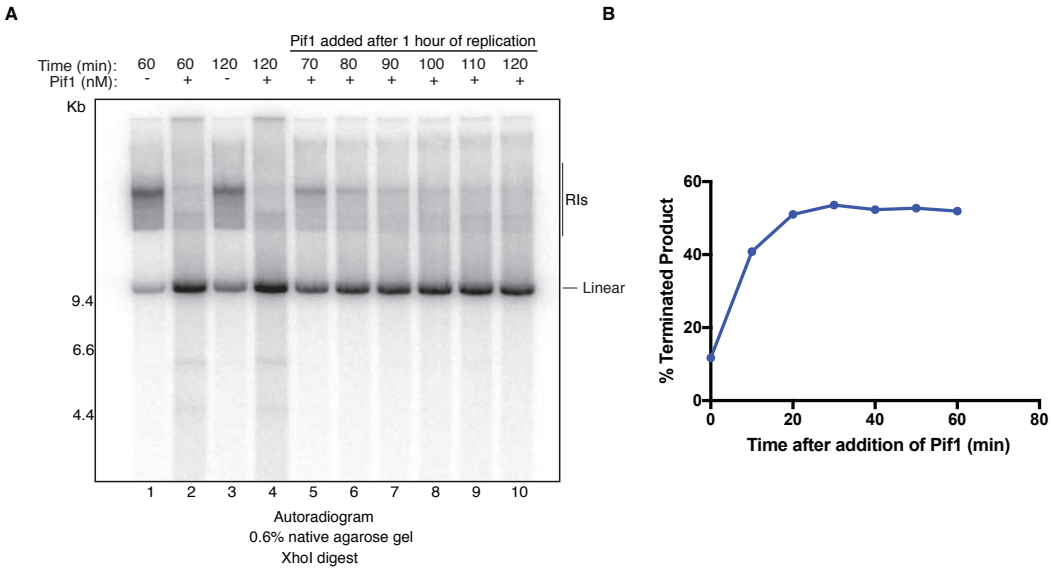

Figure 4.7 Kinetics of Mcm2-7 removal by Pif1
(A) Pif1 addback experiment in which 5 nM Pif1 was added after an hour of replication, carried out as in Figure 3.5A with the addition of Fen1 and DNA ligase I. Products were linearised with XhoI and separated over a native agarose gel (0.6%). **(B)** Percent terminated (linearised) product as a function of time from (A). This experiment was performed twice, and the result is reproducible.

4.2.7 Pif1 alone does not remove loaded Mcm2-7 from DNA

Following the observation that Pif1 could remove Mcm2-7 double hexamers from DNA, I wanted to know whether or not this only happens in the context

of replication or if Pif1 can generally remove Mcm2-7 double hexamers from DNA. In order to test this I modified the loading assay described by Coster et al. 2014. I first loaded an excess of Mcm2-7 (200 nM) onto an immobilised 10.6 kb template in the presence of ORC, Cdc6, Cdt1, and ATP, then incubated with or without Pif1 for up to an hour at 30° C. I washed the DNA with 0.5 M NaCl and checked to see if Mcm2-7 remained bound via SDS-PAGE and silver staining (Figure 4.8). The high salt wash ensures that only topologically bound proteins remain associated with the DNA, in this case the loaded Mcm2-7. I found that 95% of the loaded Mcm2-7 remains bound to the DNA, even after incubation for an hour with Pif1. This was quantified by taking the total signal in each lane and dividing it by the signal in the control sample without Pif1. This suggests that Pif1 requires the context of replication in order to remove loaded Mcm2-7.

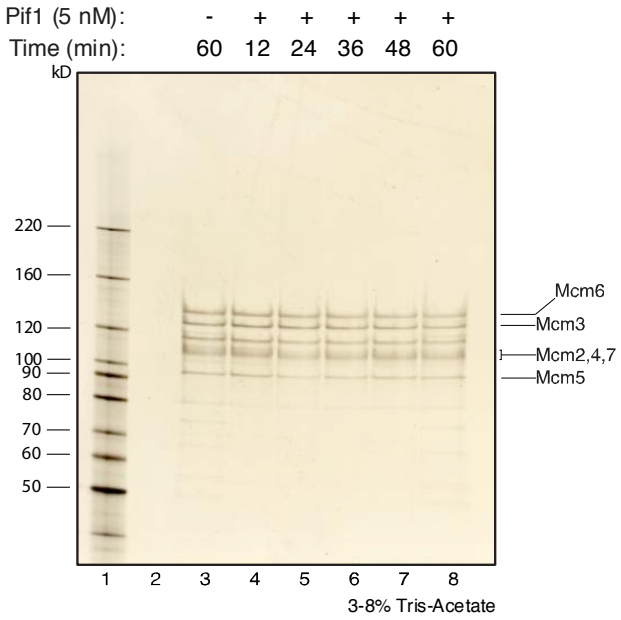

Figure 4.8 Pif1 removal of Mcm2-7 from DNA is replication dependent
Loading assay in which Mcm2-7 was loaded onto immobilised DNA and incubated for up to an hour with or without Pif1. Protein was analysed via SDS-PAGE and silver staining. This experiment was performed twice, and the result is reproducible.

4.2.8 Excess double hexamers are inhibitory to replication through chromatin

In vivo, DNA in the nuclei of cells is packaged into chromatin. Replication through chromatin requires additional proteins on top of those described in Chapter 3 needed to replicate naked DNA. This minimally includes the histone chaperone FACT, though other proteins can enhance replication through chromatin, including the chaperone Nhp6, acetyltransferases, and ATP-dependent spacing factors such as ISW1a and INO80 (Kurat et al. 2017). Given Pif1's ability to remove excess inactive Mcm2-7 double hexamers from naked DNA, I wanted to know whether or not Pif1 is required to remove excess double hexamers as they encounter nucleosomes or if the replisome can push double hexamers past nucleosomes. Although my previous data clearly pointed to a role for Pif1 in removing these double hexamers, it was not clear if this was happening at the end of replication in the context of trains or if they were being removed during replication as they were encountered by the replisome (Figure 4.6 and Figure 4.7). In order to test this I prepared chromatinised DNA using a modification of the protocol described by Kurat et al. 2017. I first loaded varying amounts of Mcm2-7 on plasmid template DNA (10.6 kb) in a volume of 20 μL. This was carried out using standard loading buffer conditions used throughout this chapter and described previously (see 2.14.3). I then added purified Nap1, ISW1a, and unmodified histone proteins from *S. cerevisiae* to assemble the DNA into chromatin in a total volume of 60 μL (for more detail, see 2.13.1). This step was carried out for 4 hours at 30° C .

Following chromatin assembly, free histones and other proteins were removed and the samples were replicated as described in Chapter 3 with Fen1 and DNA ligase I, along with various combinations of FACT/Nhp6 and Pif1. Replication on chromatin without an excess of loaded Mcm2-7 seemed to proceed without issue as the products reached full-length by at least twenty minutes of replication (Figure 4.9A, lane 7). Replication in this sample was also stimulated by FACT/Nhp6, INO80, and Pif1, suggesting that the input chromatin was saturated with nucleosomes (Figure 4.9A, lane 6). The

saturation of input chromatin can be visualised by the DNA ladder after Micrococcal nuclease digest in Figure 4.9B, lane 1. Interestingly, replication was inhibited on chromatin with an excess of loaded Mcm2-7. This is indicated by the short products in Figure 4.9A, lane 2. This suggests that excess double hexamers can block replication fork progression at nucleosomes if they are not removed. Pif1 appears to rescue this defect as the products appear to be approaching full-length in Figure 4.9A, lane 3. The chromatin remodeller INO80 does not substitute for Pif1, though it appears to be promoting replication as the overall ^{32}P signal is stronger in the presence of INO80 (Figure 4.9A, lanes 4 and 5). Presumably, Pif1 is removing the excess double hexamers from ahead of the fork, as seen previously on naked DNA. The FACT/Nhp6-dependence was not as striking in this sample, ostensibly because the input DNA was less saturated with nucleosomes due to the presence of excess Mcm2-7 (Figure 4.9A, lane 1). This can also be visualised by the short DNA ladder after Micrococcal nuclease digest of the input DNA in Figure 4.9B, lane 2.

It is not clear how FACT and Nhp6 enhance replication on chromatin, so it is difficult to say what role they are playing in the context of trains on chromatin. What is clear is that FACT and Nhp6 promote replication *in vivo* replication rates on chromatin in the absence of trains (Kurat et al. 2017). The twenty-minute reactions in Figure 4.9A, lanes 1-7 were carried out for a further forty-minutes (Figure 4.9A, lanes 9-15). While the products were overall longer and more abundant, the trends in product distributions remain essentially the same.

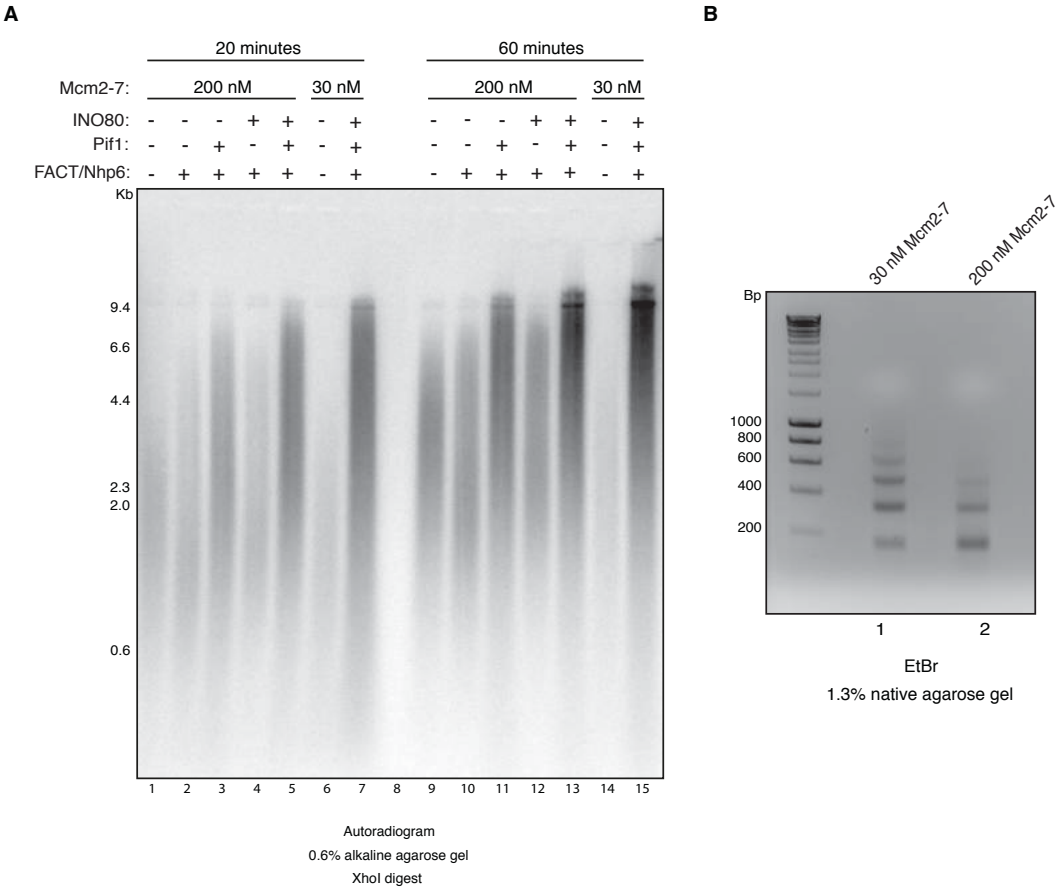

Figure 4.9 Excess Mcm2-7 is inhibitory to replication on chromatin, but is rescued by Pif1
(A) Replication of chromatin with or without an excess of loaded Mcm2-7, with various combinations of FACT/Nhp6 and Pif1. The reaction was carried out as in Figure 3.5A for 20 minutes with the addition of Fen1 and DNA ligase I. Products were linearised with XhoI and separated over an alkaline agarose gel (0.6%). **(B)** Micrococcal nuclease digest of input chromatinised DNA from (A). This experiment was performed three times, and the result is reproducible.

In order to ensure that Pif1 was promoting termination of replication on chromatin with an excess of loaded Mcm2-7, I performed a time-course experiment using the same protein components from the reaction in Figure 4.9A, lane 3. The products were linearised following replication with XhoI. I found that termination was indeed occurring in the presence of Pif1 (Figure 4.10). The terminated (linear) product was slow to accumulate, so it might be the case that other factors are required in order to promote this process *in vivo*.

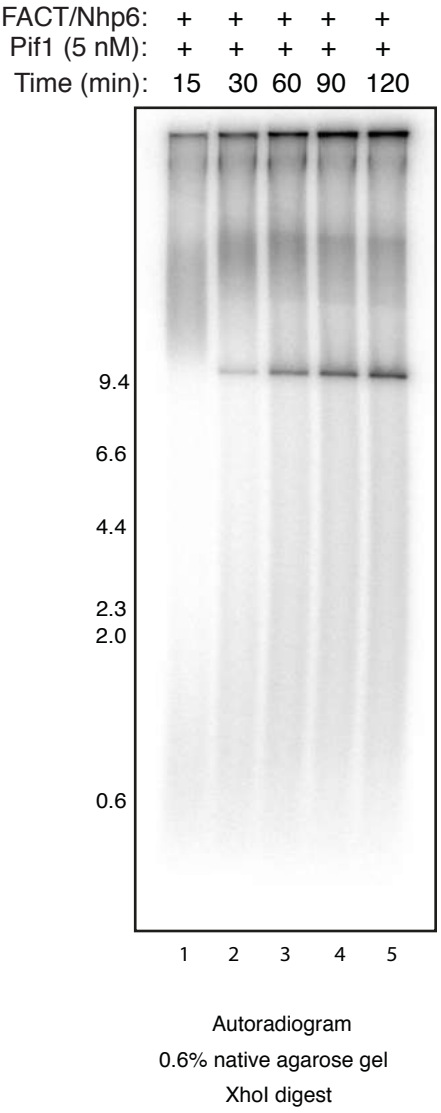

Figure 4.10 Pif1 promotes termination on chromatin with excess Mcm2-7
Pif1 time-course experiment performed for up to 120-minutes as in Figure 3.5A with Fen1 and DNA ligase I. Products were linearised with XhoI and separated over a native agarose gel (0.6%). This experiment was performed twice, and the result is reproducible.

4.3 Discussion

4.3.1 Pif1 enhances DNA replication termination *in vitro*

Early work in this chapter detailed the purification of the *S. cerevisiae* Pif1 helicase from *E. coli*. I then checked to see whether it had any effect on replication using the purified replication system developed by Yeeles et al. 2017 and expanded upon in Chapter 3. There was unpublished evidence at the time showing that Pif1 could enhance termination in a similar purified

replication system established by Dr Tom Deegan whilst working in Dr Karim Labib's lab at the University of Dundee.

I found that Pif1 enhances the strand displacement activity of DNA polymerase δ but does not promote Dna2 as the sole nuclease during Okazaki fragment maturation in the absence of Fen1 (Figure 4.2). However, Dna2 is functional and appears to be capable of processing some fragments (even in the absence of Pif1) as the lagging strands are lengthened in the presence of Dna2 and DNA ligase I (Figure 4.2A, lane 2). Thus, it seems that Okazaki fragment maturation in this minimal system absolutely requires Fen1, though a small population fragments are processed by Dna2. These results suggest that Pif1, at least on its own, is not able to promote the formation of substrates during Okazaki fragment maturation that require cleavage by Dna2.

I then showed that DNA replication termination is enhanced in two ways by Pif1. Firstly, I found that Pif1 is able to resolve the RIs observed in Chapter 3. Work detailed in Chapter 3 revealed that these RIs were unable to complete replication due to a defect in termination (Figure 3.9). However, the nature of these RIs and how they form was not known at this point, so it was not clear how they were being resolved by Pif1. Secondly, I observed that the rate of termination is increased in the presence of Pif1 (Figure 4.3). Other Pif1 family helicases, such as Rrm3 (*S. cerevisiae*) and Pfh1 (*S. pombe*), have been shown to promote replisome progression when the replication fork slows, encounters a barrier, or during termination when two replication forks converge (Sabouri et al. 2012; Steinacher et al. 2012). Pif1 translocates on the opposite strand to CMG (which has a polarity of 3'-5') and may be providing extra unwinding support to the CMG at the very end of replication, as is thought to happen in *E. coli* with Rep and UvrD supporting the main helicase, DnaB (Guy et al. 2009). Interestingly, the percent of terminated products never exceeds 40-60%, even in the presence of Pif1. This may be due to a limiting factor in the reaction, or perhaps additional proteins are required to help promote termination *in vivo*.

4.3.2 Excess loaded Mcm2-7 double hexamers block termination but are removed by Pif1

Later in the chapter, I showed that an excess of loaded Mcm2-7 double hexamers was able to inhibit termination at the end of replication (Figure 4.4). Further analysis by electron microscopy after negative staining of the replication products allowed for the visualisation of multiple adjacent Mcm2-7 double hexamers between two converging CMGs (Figure 4.5). Thus, it seemed possible that the termination defect observed in the RIs previously may have been partly due to Mcm2-7 double hexamers physically blocking the convergence of two CMGs.

I then found that Pif1 was able to remove the excess loaded Mcm2-7 double hexamers, allowing for convergence of the two CMGs (Figure 4.6). Pif1 and Pif1 family helicases have been shown to facilitate replisome progression through protein barriers on DNA, including Pif1's role in removing Rap1 on telomeric DNA (Koc et al. 2016). However, this is the first time Pif1 has been implicated in the replication-dependent removal of loaded Mcm2-7 from DNA. It is not clear how this might work, but Pif1's interaction with PCNA through its non-canonical PIP box motif provides a means for its localisation to the replication fork (Buzovetsky et al. 2017).

4.3.3 Excess loaded Mcm2-7 double hexamers are removed during replication

Lastly, I showed in this chapter that excess loaded Mcm2-7 double hexamers must be removed during replication through chromatinised DNA. Replication was severely inhibited on chromatin that had an excess of loaded Mcm2-7, indicating that the replisome is unable to push double hexamers through nucleosomes (Figure 4.9A), even in the presence of proteins such as FACT and Nhp6 that are known to enhance replication through chromatin (Kurat et al. 2017). Interestingly, Pif1 appears to rescue this effect, indicating a pathway for how these double hexamers are removed ahead of the fork during replication. It may be the case that other factors are required for this

process to occur more efficiently *in vivo*, though minimally this process only seems to require Pif1.

In *S. cerevisiae* and humans, it has been observed *in vivo* that Mcm2-7 is loaded in approximately 20-fold excess over both replication origins and ORC (Burkhart et al. 1995; Lei et al. 1996; Donovan et al. 1997; Mahbubani et al. 1997; Edwards et al. 2002). It has never been shown how or when these excess double hexamers are removed, either during or after replication. The data presented in this chapter suggests that they must be removed during replication in order to allow for the replisome's unimpeded progression through chromatin and proper termination.

Chapter 5. Results III

5.1 Introduction

The current model for replication-coupled chromatin assembly is that Asf1 imports newly-synthesised histones H3 and H4 into the nucleus, where they are acetylated at H3K56 by Rtt109 (Burgess and Zhang, 2013). H3K56ac promotes the transfer of H3-H4 from Asf1 to downstream chaperones, including CAF-1 (Li et al. 2008; Burgess and Zhang, 2013). Recently, dimerisation of CAF-1 has been shown to be important for $(H3\text{-}H4)_2$ assembly prior to deposition onto replicated DNA (Mattiroli et al. 2017). The histone octamer is then completed by the deposition of two dimers composed of histones H2A and H2B (Burgess and Zhang, 2013). The histone chaperone Rtt106 has an affinity for H3K56ac and is thought to deposit histones onto DNA in a manner similar to CAF-1, though its role in this process is unclear (Li et al. 2008; Su et al. 2012).

Building on the purified replication system described in Chapters 3 and 4, I set out to reconstitute replication-coupled chromatin assembly, first in extracts and ultimately with purified proteins *in vitro*. Such a system would allow me to determine the absolute requirements for this process and to answer outstanding questions in the field that are difficult to answer *in vivo*, such as how chromatin assembly is coupled to replication on both the leading and lagging strands.

5.2 Results

5.2.1 Strain construction

The DNA sequences encoding the three subunits of CAF-1 (Cac1, Cac2, and Cac3), as well as those encoding Asf1, Rtt106, and Vps75 were chemically synthesised (GeneArt) following codon-optimisation for expression in *S. cerevisiae*. I then cloned the sequences into pRS vectors for inducible expression under the control of a bidirectional inducible GAL1/GAL10 promoter (Sikorski and Hieter, 1989). For a schematic of the vectors used for

expression (pRS303 and pRS306), see Figure 5.1. I then linearised the vectors with a restriction enzyme at a site within the auxotrophic marker (in this case, either URA or HIS) and transformed them into yJF1 (Frigola et al. 2013). For the yeast transformation protocol used to construct these strains, see section 2.7.1. I PCR amplified the gene encoding Rtt109 from genomic *S. cerevisiae* DNA. I then cloned it into the pET28a expression vector, which provided a 6X-Histidine tag on its N-terminus, and optimised it for expression in *E. coli*.

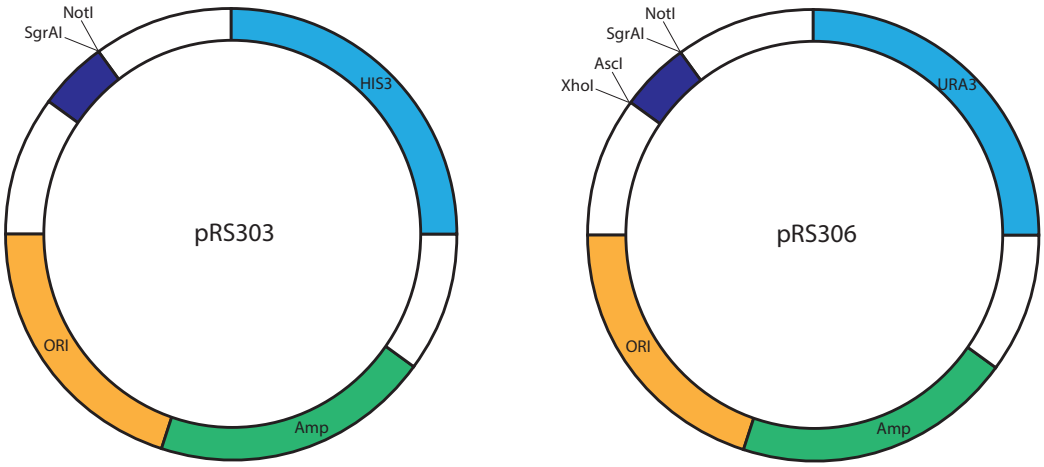

Figure 5.1 Schematic of the vectors used for expression in *S. cerevisiae*
The sequences for Cac3, Asf1, Rtt106, and Vps75 were cloned between the SgrAI and NotI sites in pRS303. The sequences for Cac1 and Cac2 were cloned between the SgrAI and NotI (Cac1) and AscI and XhoI (Cac2) sites in pRS306.

5.2.2 Purification of CAF-1

I tagged CAF-1 with a CBP tag on the N-terminus of Cac3. I then purified it to homogeneity by calmodulin affinity chromatography (Figure 5.2B), followed by ion-exchange chromatography (Figure 5.2C), and size-exclusion chromatography (Figure 5.2D). Due to its overall negative charge, I chose to use a MonoQ column to purify CAF-1. The protein eluted in defined peaks following ion-exchange and size-exclusion chromatography, and appeared to be relatively pure. I found that Cac3 (47 kDa) with a CBP tag (4 kDa) is approximately the same size as Cac2 (52 kDa). In order to look at all three subunits, I took advantage of a TEV protease site in between the CBP tag and Cac3. Following cleavage, I found that the purified CAF-1 was indeed

composed of all three subunits: Cac1, Cac2, and Cac3 (Figure 5.2E). For a detailed purification protocol, see 2.10.2.26.

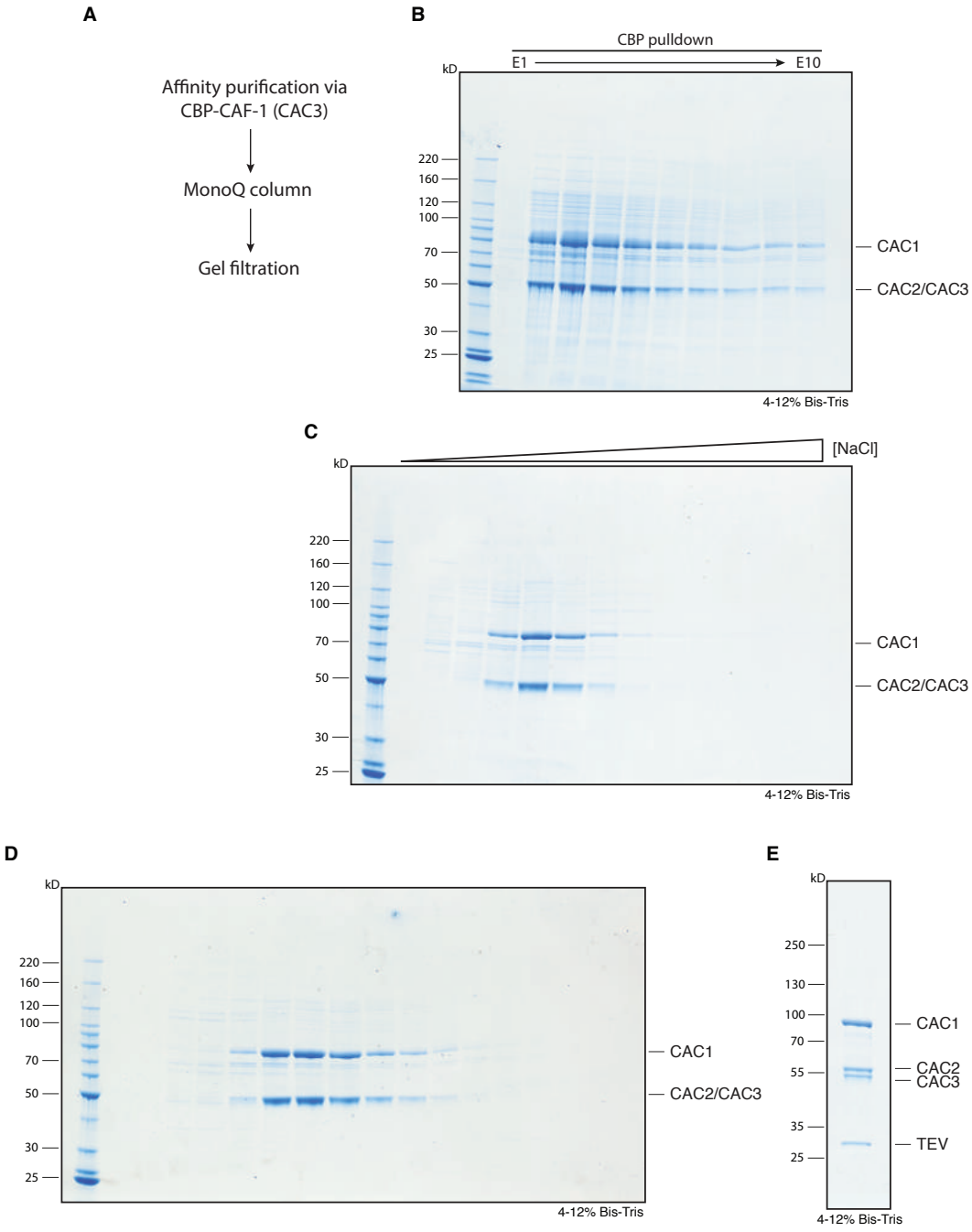

Figure 5.2 Purification of CAF-1
The purification scheme for CAF-1 is depicted in **(A)**. Eluate (E) fractions following calmodulin affinity chromatography **(B)**. The ion-exchange chromatography (MonoQ) step is shown in **(C)** and the final size-exclusion chromatography step of the purification is shown in **(D)**. TEV cleavage of the CBP tag from Cac3 is depicted in **(E)**. Protein analysed by SDS-PAGE with Coomassie staining.

5.2.3 Purification of Asf1

I tagged Asf1 with a CBP tag on its C-terminus. I purified it to homogeneity by calmodulin affinity chromatography (Figure 5.3B), followed by ion-exchange chromatography (Figure 5.3C and Figure 5.3D). Due to its overall negative charge, I used a MonoQ column to purify Asf1. The protein eluted in defined peaks following two ion-exchange chromatography steps, and appeared to be pure after the second step (Figure 5.3D). I then dialysed the protein into a buffer containing a lower concentration of NaCl. For a detailed purification protocol, see 2.10.2.27.

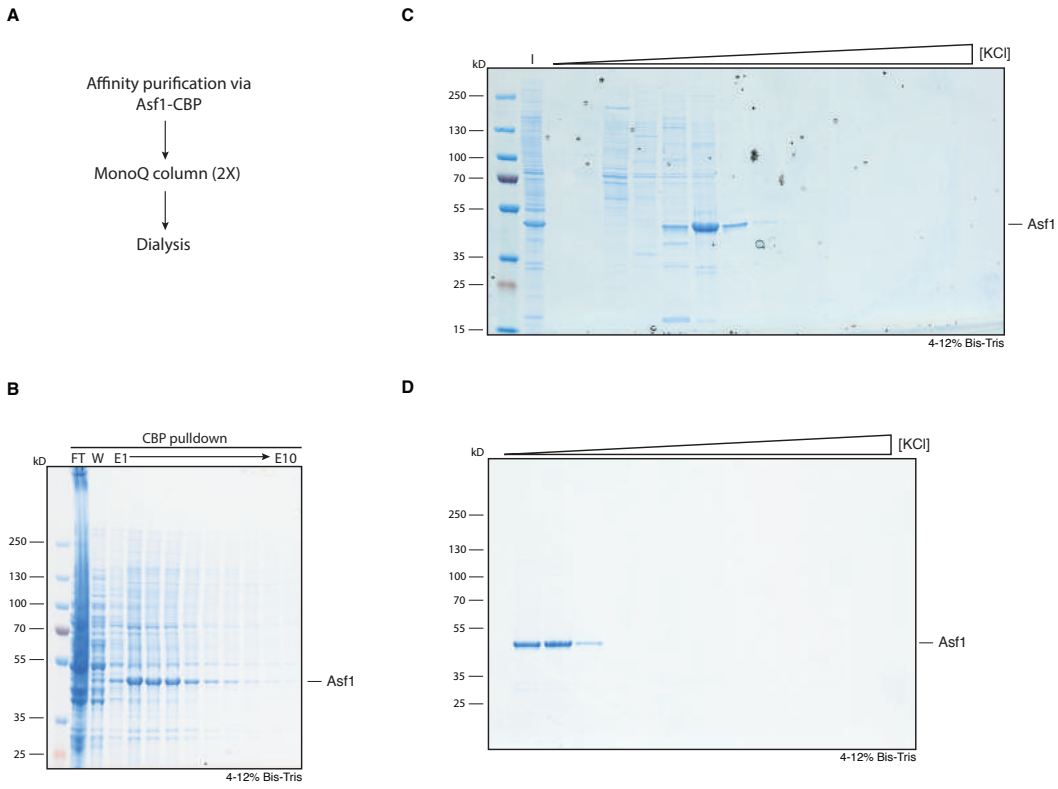

Figure 5.3 Purification of Asf1
The purification scheme for Asf1 is depicted in **(A)**. Eluate (E) fractions following calmodulin affinity chromatography **(B)**. The first ion-exchange chromatography (MonoQ) step is shown in **(C)** and the second is shown in **(D)**. Protein analysed by SDS-PAGE with Coomassie staining.

5.2.4 Purification of Rtt106

I tagged Rtt106 with a CBP tag on its N-terminus. I then purified it to homogeneity by calmodulin affinity chromatography (Figure 5.4B) and ion-exchange chromatography (Figure 5.4C). Due to its overall negative charge, I

used a MonoQ column to purify Rtt106. The protein eluted in a defined peak following ion-exchange chromatography and appeared to be pure (Figure 5.4C). I then dialysed the protein into a buffer containing a lower concentration of NaCl. For a detailed purification protocol, see 2.10.2.29.

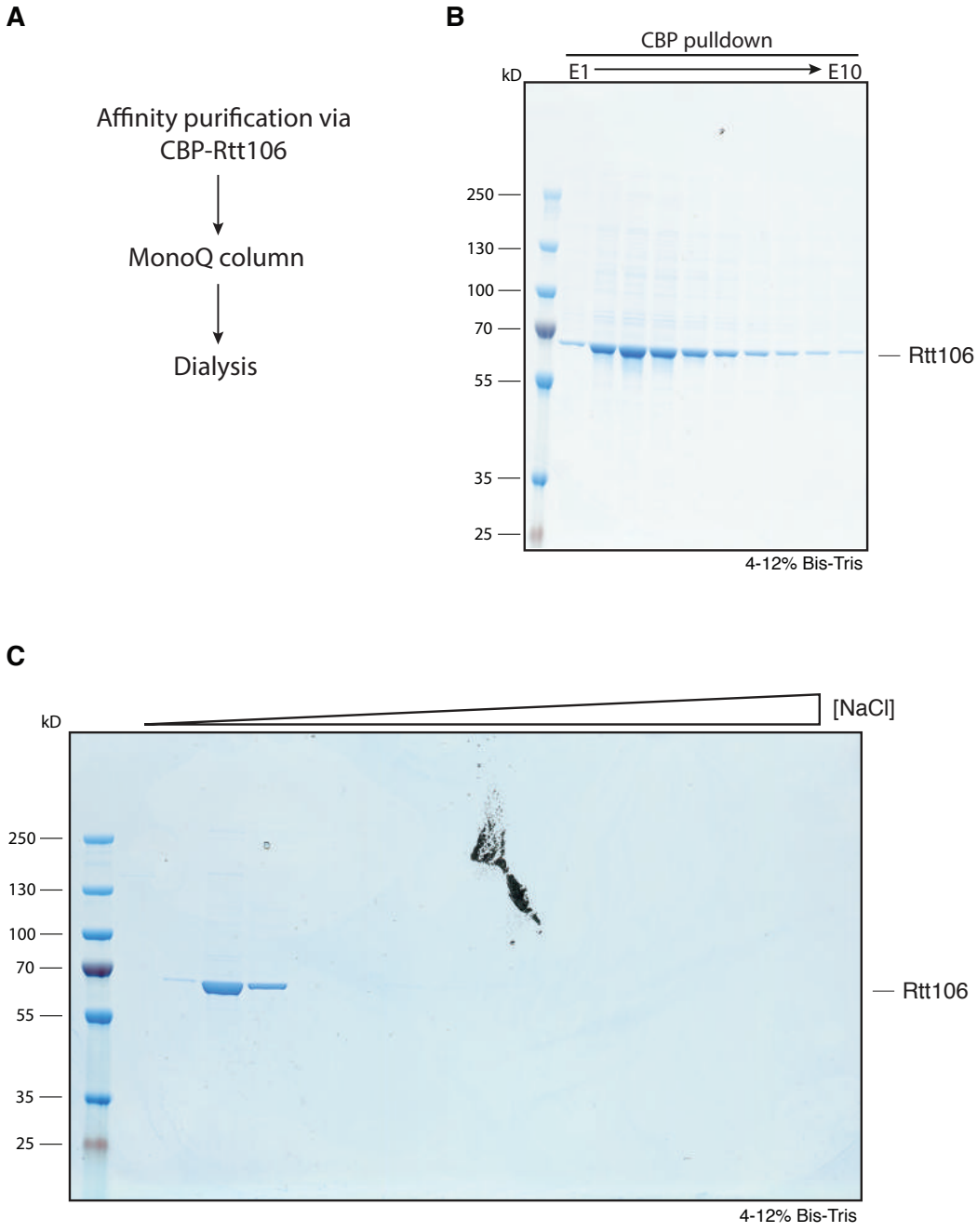

Figure 5.4 Purification of Rtt106
The purification scheme for Rtt106 is depicted in **(A)**. Eluate (E) fractions following calmodulin affinity chromatography **(B)**. The ion-exchange chromatography (MonoQ) step is shown in **(C)**. Protein analysed by SDS-PAGE with Coomassie staining.

5.2.5 Purification of Vps75

I tagged Vps75 with a CBP tag on its N-terminus. I then purified it to homogeneity by calmodulin affinity chromatography (Figure 5.5B) and ion-exchange chromatography (Figure 5.5C). Due to its overall negative charge, I used a MonoQ column to purify Vps75. The protein eluted in a defined peak following ion-exchange chromatography and appeared to be pure (Figure 5.5C). I then dialysed the protein into a buffer containing a lower concentration of KOAc. For a detailed purification protocol, see 2.10.2.28.

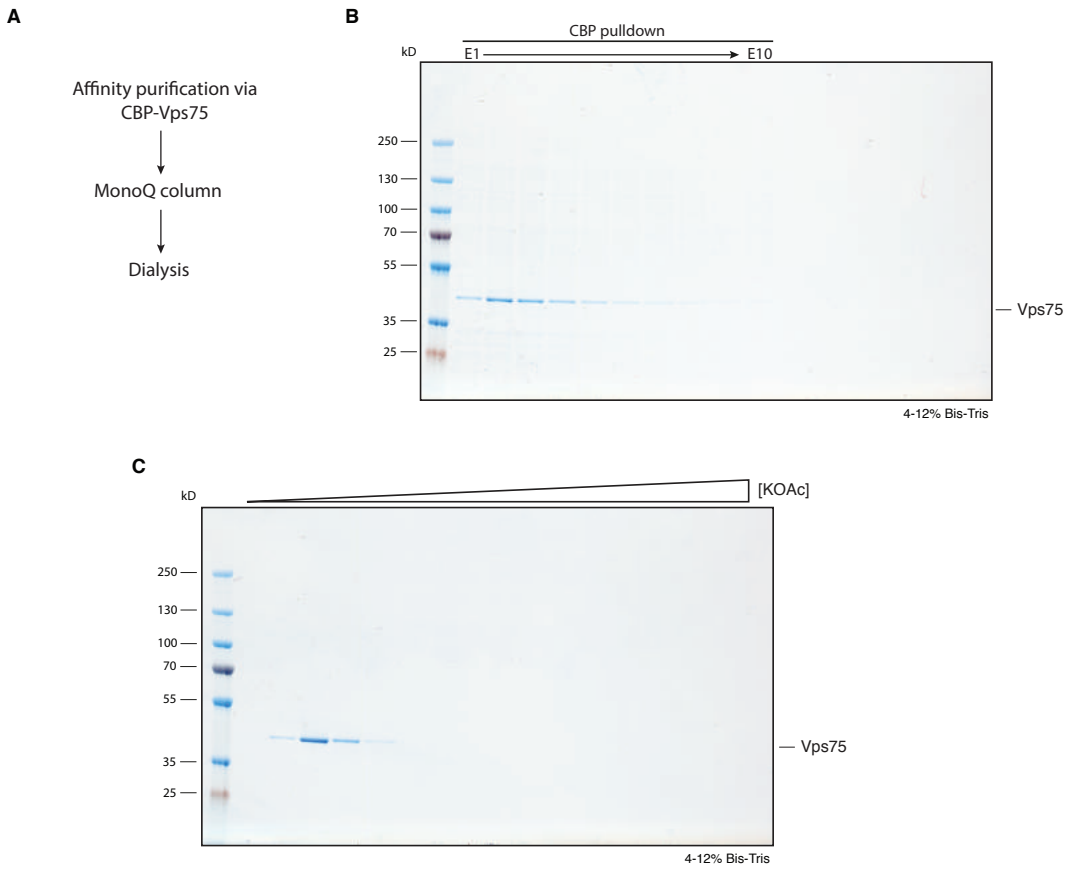

Figure 5.5 Purification of Vps75
The purification scheme for Vps75 is depicted in **(A)**. Eluate (E) fractions following calmodulin affinity chromatography **(B)**. The ion-exchange chromatography (MonoQ) step is shown in **(C)**. Protein analysed by SDS-PAGE with Coomassie staining.

5.2.6 Purification of Rtt109

I purified Rtt109 to homogeneity by nickel affinity chromatography (Figure 5.6B) and size-exclusion chromatography (Figure 5.6C). The protein eluted from the HisTrap (GE) column in a broad peak, with a number of prominent

contaminants (Figure 5.6B). Following the final size-exclusion chromatography step, however, Rtt109 eluted in a defined peak and appeared to be pure (Figure 5.6C). For a detailed purification protocol, see 2.10.3.8.

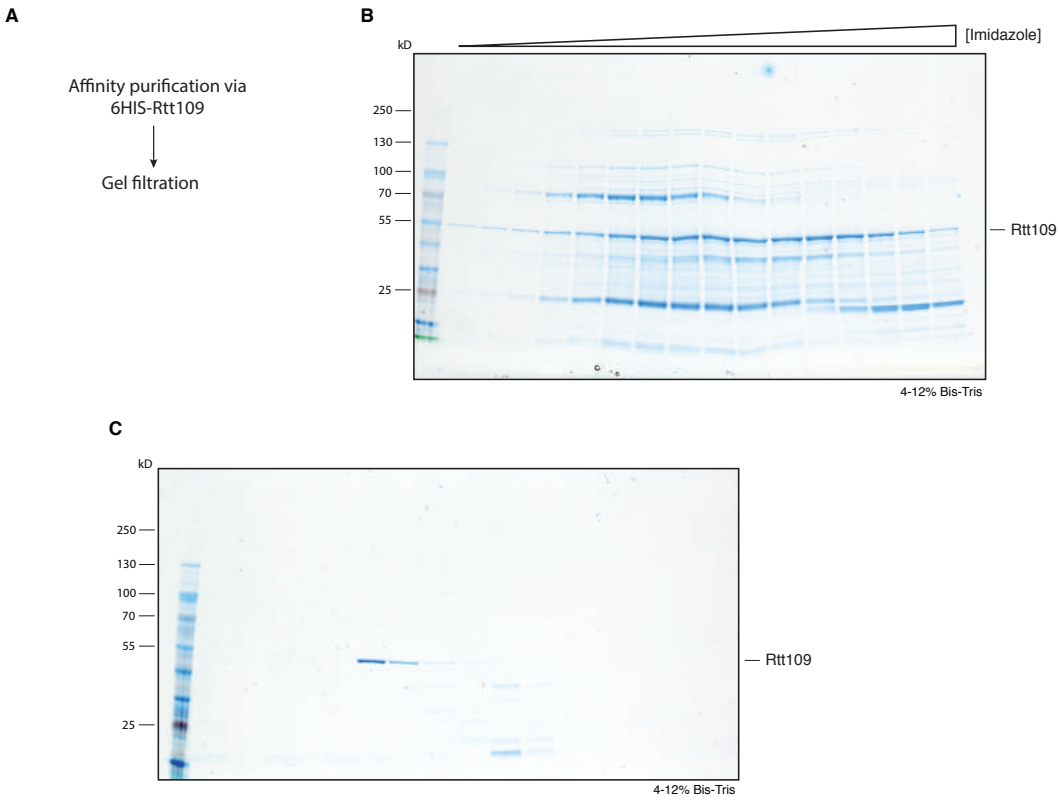

Figure 5.6 Purification of Rtt109
The purification scheme for Rtt109 is depicted in **(A)**. Eluate (E) fractions following nickel affinity chromatography **(B)**. The size-exclusion chromatography step is shown in **(C)**. Protein analysed by SDS-PAGE with Coomassie staining.

5.2.7 CAF-1 promotes replication-dependent chromatin assembly

In order to test the activity of the CAF-1 purified in 5.2.2, I established a supercoiling assay similar to work that had previously been done in SV40 (Stillman and Gluzman, 1985; Stillman, 1986). It was shown that cytosolic extracts from human cells supplemented with SV40 T antigen were capable of replicating SV40 DNA, or plasmids with the origin of replication from SV40 (Li and Kelly, 1985; Stillman et al. 1985; Stillman and Gluzman, 1985). The products of this reaction were mostly relaxed and covalently-closed plasmid DNA. It was later shown that the addition of an extract prepared from cell

nuclei on top of the cytosolic extract promoted negative supercoiling of the replication products (Stillman and Gluzman, 1985). This supercoiling was then shown to be due to the deposition of nucleosomes onto DNA, a process that is uniquely coupled to replication by the histone chaperone CAF-1 (Stillman, 1986; Smith and Stillman, 1989). The supercoiling assay relies on the premise that the binding of a nucleosome introduces one net negative supercoil on a plasmid following deproteinization of the DNA.

In these experiments I used a cell-free S-phase extract from *S. cerevisiae* established by On et al. 2014. This extract is depleted of DDK and overexpresses the replication firing factors Sld2, Sld3, Sld7, Cdc45, and Dpb11. This extract and similar ones have been shown to support replication of DNA with loaded Mcm2-7 following phosphorylation by DDK (On et al. 2014; Gros et al. 2014). I supplemented the S-phase extract with purified *S. cerevisiae* histone proteins to ensure that they were not limiting. For a detailed reaction scheme, see Figure 5.7A.

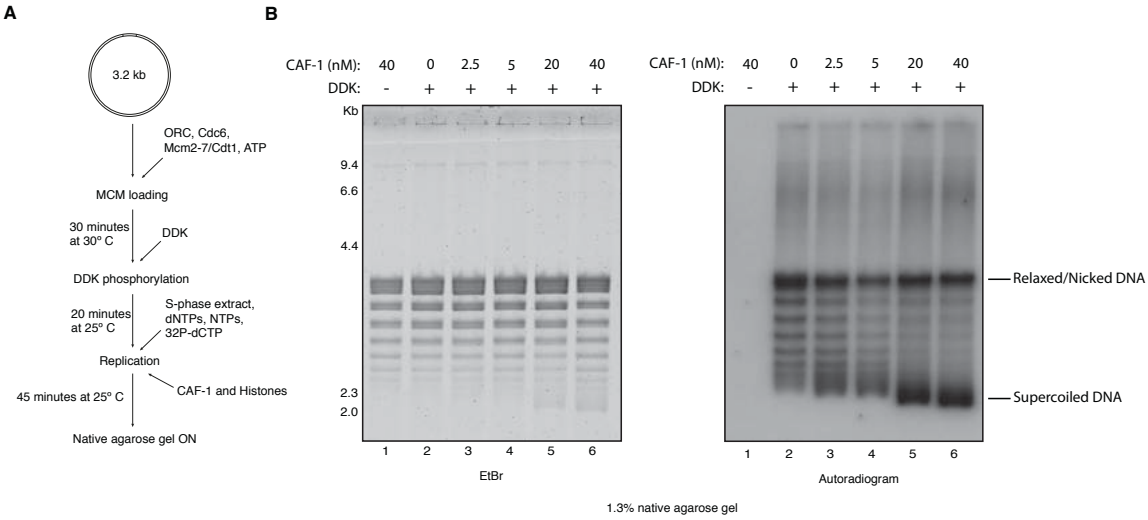

Figure 5.7 CAF-1 promotes replication-dependent supercoiling of DNA
(A) General scheme for extract-based replication reactions. The template used in these reactions was pBluescript/ARS1 WTA. **(B)** CAF-1 titration experiment performed for 45 minutes as in (A). Products in (B) were separated over native agarose gels (1.3% and 1%, respectively). This experiment was performed twice, and the result is reproducible.

Using this system, I was able to show that replicated DNA became more negatively supercoiled with increasing concentrations of CAF-1 (Figure 5.7B). EtBr staining of the products, following separation over a native agarose gel, revealed that the bulk of the DNA remains relaxed after replication (Figure 5.7B, left panel). This represents both the unreplicated as well as the replicated DNA. Importantly, the majority of the replicated DNA is negatively supercoiled following replication with CAF-1 as indicated in the autoradiogram (Figure 5.7B, right panel). Some of the DNA might be nicked by factors in the extract, which could explain why a population of the replication products is not supercoiled, even at the highest concentrations of CAF-1 (Figure 5.7B, right panel).

Following the observation that CAF-1 could promote replication-dependent negative supercoiling of DNA in extracts from *S. cerevisiae*, I wanted to know whether or not this was due to the deposition of nucleosomes onto the DNA. In order to test this, I digested the reaction products with Micrococcal nuclease following replication with and without CAF-1 (Figure 5.8). The presence of a DNA ladder in the samples with CAF-1 suggested that the replication-dependent supercoiling was in fact due to the deposition of nucleosomes onto replicated DNA (Figure 5.8, lanes 4-6). The ladder also suggested that the nucleosomes were evenly spaced in arrays of up to at least three nucleosomes, as indicated by the distinct mono-, di-, and tri-nucleosomal bands. While CAF-1 is clearly active and able to deposit nucleosomes onto DNA, it is possible that other factors that facilitate replication-dependent chromatin assembly are limiting in the extract, including the histone chaperones Asf1, Rtt106, Vps75, and the acetyltransferase Rtt109. Unexpectedly, I observed a mononucleosomal band in the samples without CAF-1 (Figure 5.8, lanes 10-12). This is likely due to endogenous proteins, as the extract was not depleted of CAF-1. However, the endogenous protein in the extract was not sufficient to supercoil the DNA – at least not to the extent that it was supercoiled in the presence of CAF-1 (Figure 5.8, lanes 1 and 7).

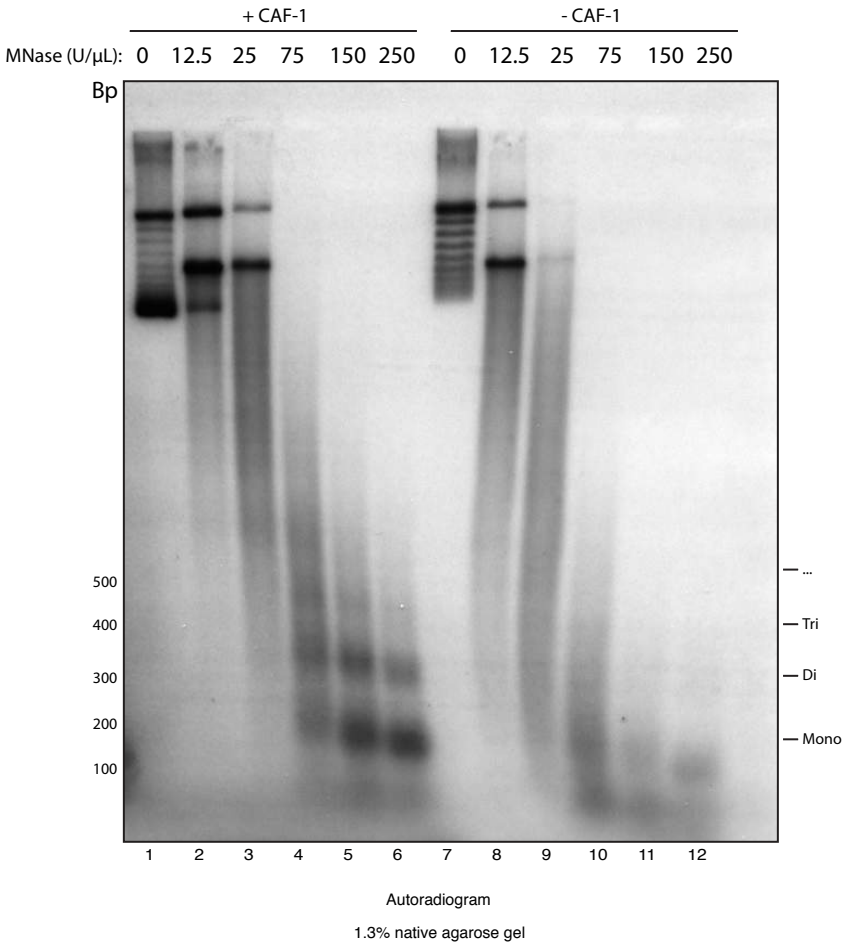

Figure 5.8 CAF-1 promotes replication-dependent chromatin assembly
Micrococcal nuclease digestion of DNA replicated in extracts with or without CAF-1. Experiment performed for 45 minutes as in Figure 5.7A. Products were separated over a native agarose gel (1.3%). This experiment was performed twice, and the result is reproducible.

5.2.8 Reconstitution of H3K56 acetylation *in vitro*

In order to test the activities of the purified histone chaperones Asf1 and Vps75, as well as the acetyltransferase Rtt109, I reconstituted the acetylation of H3K56 as described previously by Tsubota et al. 2007. I found that H3K56 acetylation (H3K56ac) required either Asf1 or Vps75 in addition to the histones and Rtt109 (Figure 5.9A). Surprisingly, I observed H3K56ac in the presence of Vps75 and histones without Rtt109. Due to previously observed interactions between Vps75 and Rtt109 *in vivo*, I suspected that my purified Vps75 may have been contaminated with Rtt109 (Krogan et al. 2006; Fillingham et al. 2008). Indeed, mass spectrometry of my purified Vps75 protein revealed a slight contamination with Rtt109 (data not shown).

Titrating the concentration of Vps75 suggested that very little of the chaperone/enzyme complex is required for acetylation of H3K56 (Figure 5.9B).

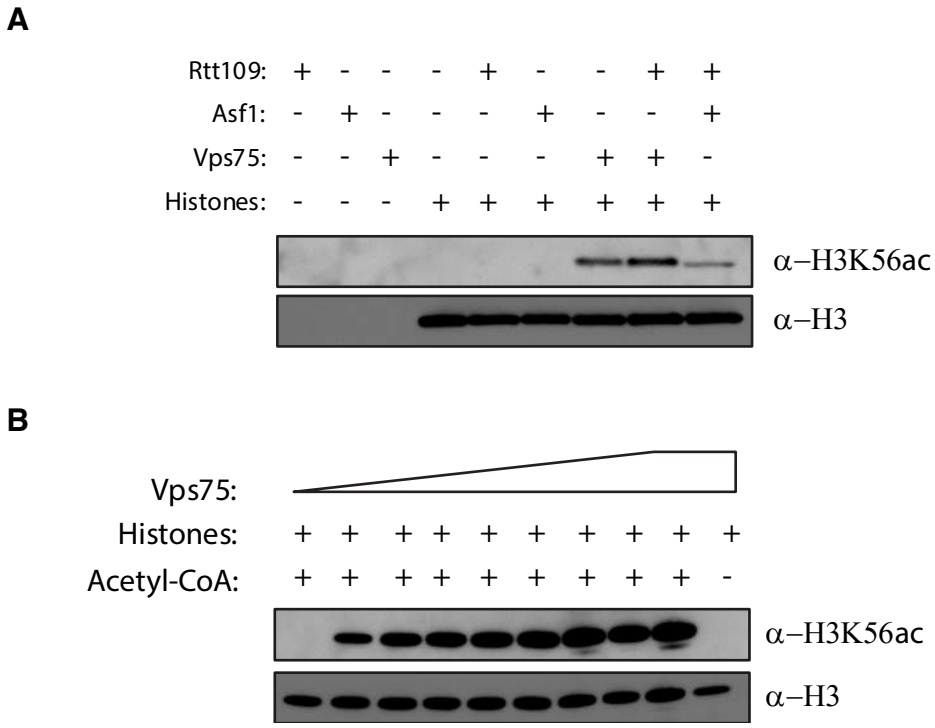

Figure 5.9 Reconstitution of H3K56ac *in vitro*
(A) H3K56ac *in vitro* with acetyl-CoA, purified *S. cerevisiae* histones, Asf1, Vps75, and Rtt109. Experiment performed for 30-minutes as described in section 2.12. **(B)** Vps75/Rtt109 titration experiment. Products were analysed by SDS-PAGE and western blotting using commercially available antibodies against H3 and H3K56ac. These experiments were performed three times, and the results are reproducible.

5.2.9 Reconstitution of replication-dependent chromatin assembly with purified proteins *in vitro*

In Chapter 3, I detailed the establishment of an *in vitro* replication assay that recapitulates initiation, elongation, and termination with purified proteins. This chapter has detailed the purification of proteins that are implicated in replication-coupled chromatin assembly *in vitro* and *in vivo*. I was now in a position to reconstitute replication-coupled chromatin assembly with purified proteins *in vitro*. In order to do this, I set up a supercoiling assay using a modified version of the replication assay described in Chapter 3 (Figure 3.5A). Following phosphorylation of loaded Mcm2-7 with DDK (or a

buffer control), I added a mixture of histone chaperones and histone proteins purified from *S. cerevisiae* along with the firing factors and other replication proteins, including Fen1 and DNA ligase I. The templates used in this reaction were the same as those used in the extract-based replication-dependent chromatin assembly experiments (pBluescript/ARS1 WTA). Importantly, the templates for these assays did not contain nucleosomes (i.e. naked DNA). Initially, the mixture of histone chaperones included CAF-1, Asf1, Rtt106, Vps75, and the acetyltransferase Rtt109. I was not sure if an H2A-H2B-binding histone chaperone would be required, so I also included Nap1 (for a detailed purification protocol, see 2.10.3.5). In the end, I found that Nap1 was not required for replication-dependent supercoiling of DNA (Figure 5.10, lanes 7 and 8). If anything, it promoted replication-independent supercoiling at the expense of replication-dependent supercoiling of the DNA. In all of the reactions containing Nap1, a significant amount of the bulk DNA was supercoiled, even in the absence of DDK (Figure 5.10, bottom panel, lanes 1-6 and 9-10). However, this was not the case for the replicated DNA (Figure 5.10, top panel, lanes 1-6 and 9-10). Only in the absence of Nap1 was there supercoiling of the replicated DNA but not the bulk of the DNA (Figure 5.10, lanes 7 and 8). This result suggested that Nap1 was not required for replication-dependent chromatin assembly, but it was not clear which of the other proteins was required: CAF-1, Asf1, Rtt106, Vps75, and/or Rtt109.

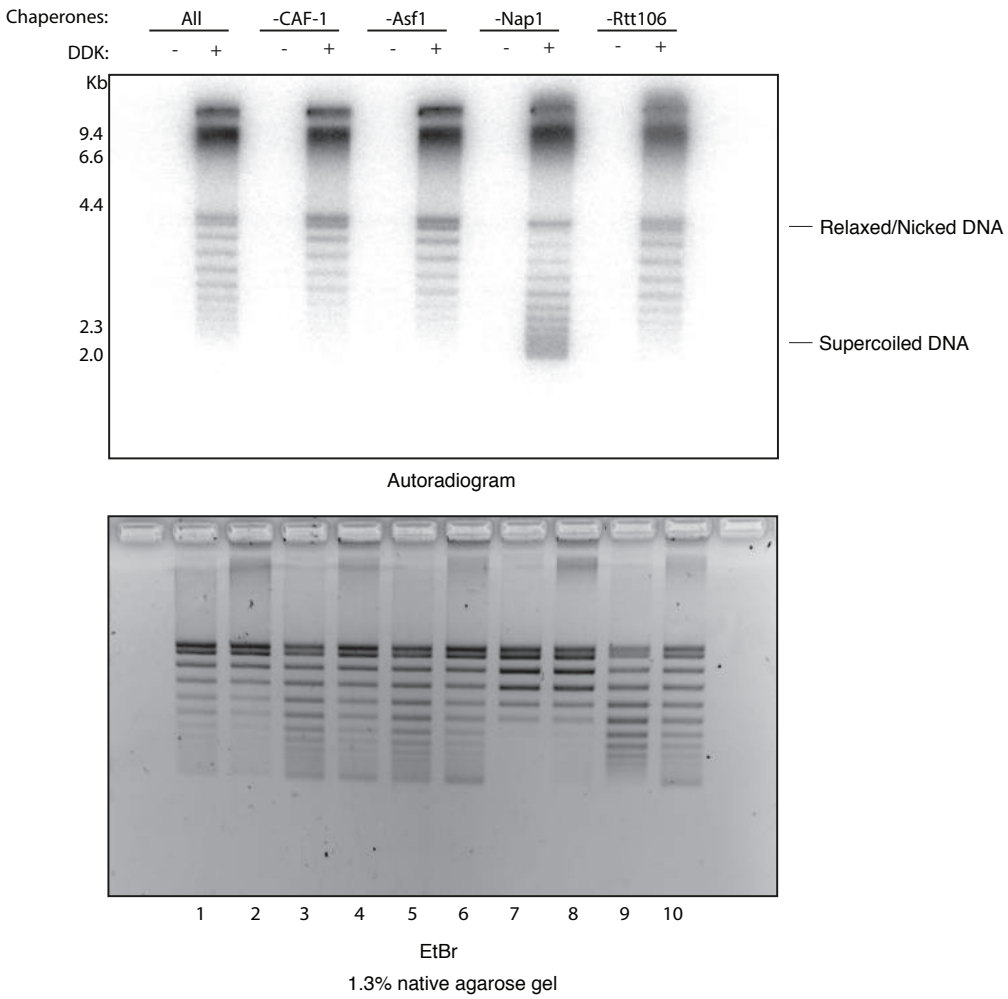

Figure 5.10 Reconstitution of replication-dependent chromatin assembly (1)
Histone chaperone dropout experiment performed for 20 minutes as described in section 2.14.5. Products were separated over a native agarose gel (1.3%). This experiment was performed twice, and the result is reproducible.

5.2.10 Replication-dependent chromatin assembly requires CAF-1 and Asf1

In order to determine which of the remaining chaperones were required for replication-dependent chromatin assembly, I repeated the experiment from 5.2.9 in the absence of Nap1. I found that CAF-1 and Asf1 both seem to be necessary as I did not observe any significant supercoiling of the replicated DNA in the absence of either CAF-1 or Asf1 (Figure 5.11, lanes 1-4). Rtt106 and the combination of Vps75/Rtt109 are dispensable for supercoiling of the replicated DNA and thus are not required for replication-dependent chromatin assembly, at least in this minimal *in vitro* system (Figure 5.11,

lanes 5-10). However, these proteins might be playing subtle roles in these reactions as there appears to be more replication-independent supercoiling of the DNA when they are left out of the reaction, especially Rtt106. This is indicated by an increase in supercoiling of the bulk DNA in Figure 5.11, lower panel, lanes 5 and 6.

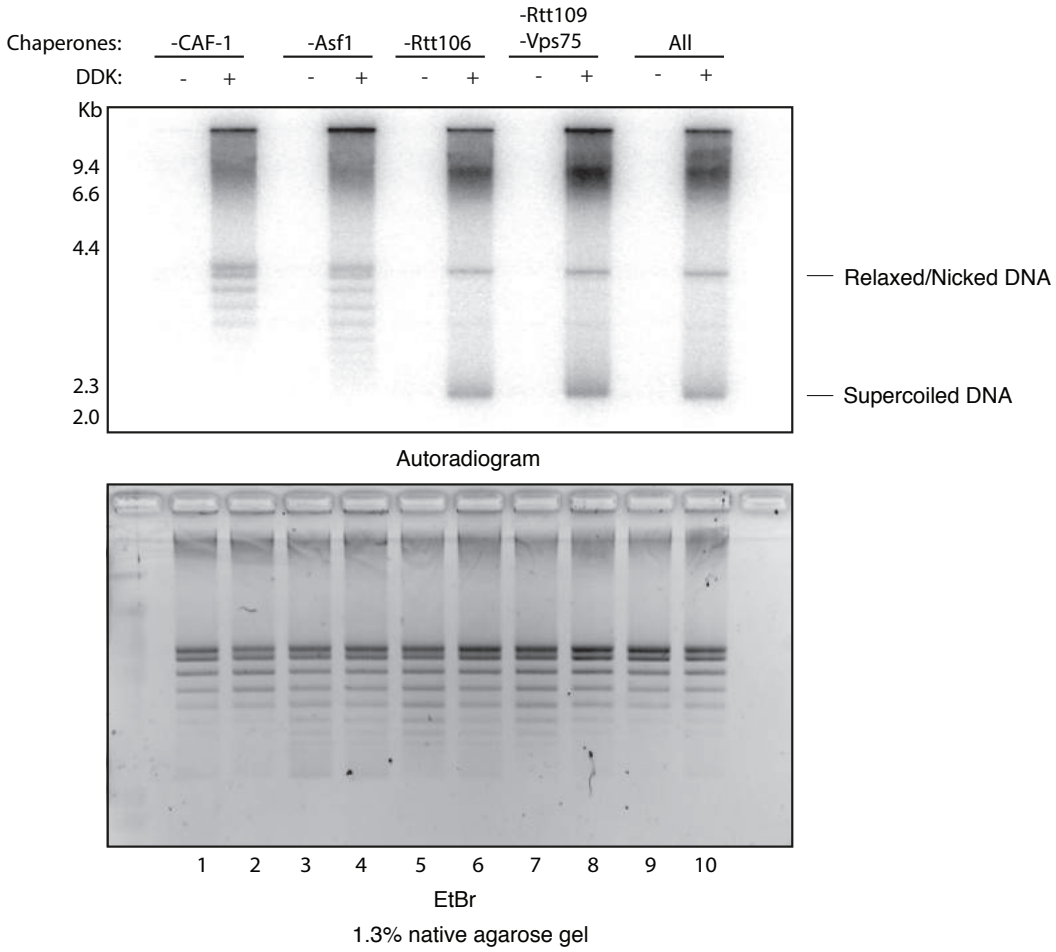

Figure 5.11 Reconstitution of replication-dependent chromatin assembly (2)
Histone chaperone dropout experiment performed for 20 minutes as described in section 2.14.5. Products were separated over a native agarose gel (1.3%). This experiment was performed three times, and the result is reproducible.

I then wanted to know whether or not Asf1 was absolutely required for replication-dependent chromatin assembly in addition to CAF-1. To do this, I titrated both chaperones in the absence of the other to see if doubling their concentrations was enough to promote supercoiling of the replicated DNA (Figure 5.12). In the end, I found that doubling the concentrations of either

chaperone in the absence of the other had no effect on the amount (or lack of) supercoiled replication product (Figure 5.12, lanes 7-10). Thus, CAF-1 and Asf1 are the minimal histone chaperone requirements for this replication-dependent chromatin assembly reaction.

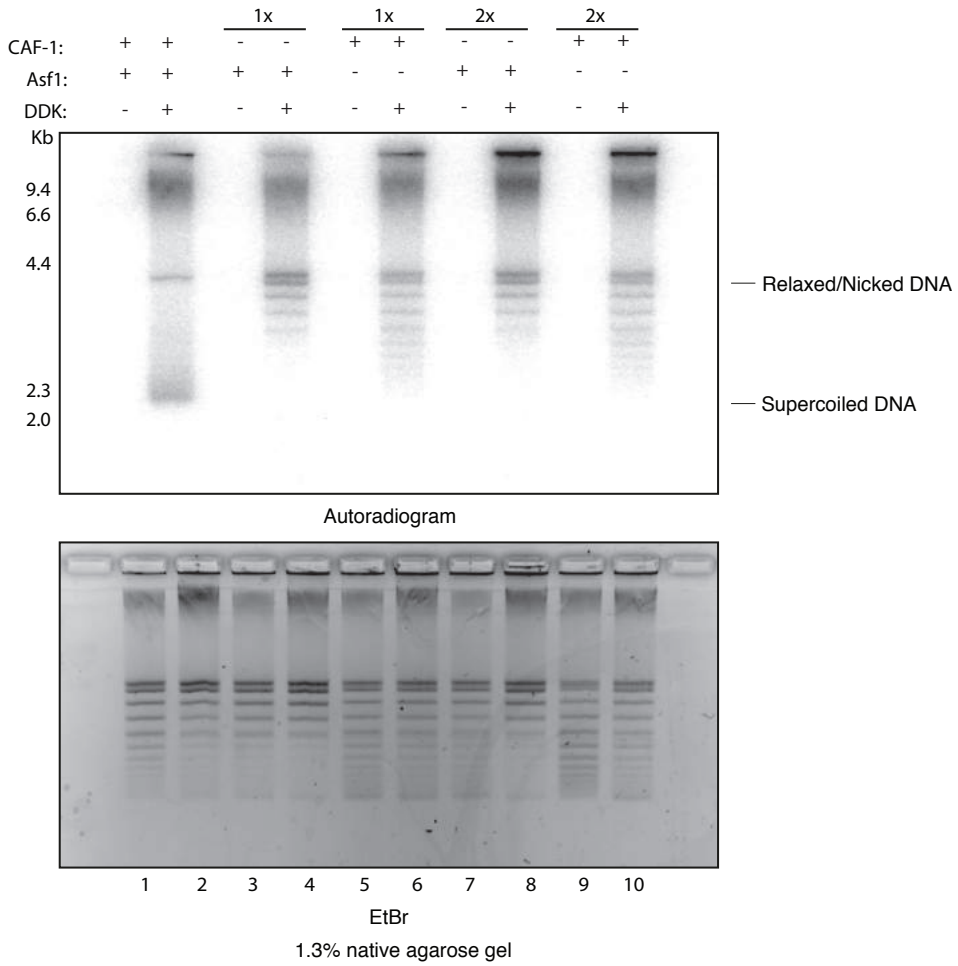

Figure 5.12 Reconstitution of replication-dependent chromatin assembly (3)

CAF-1 and Asf1 dropout/titration experiment performed for 20 minutes as described in section 2.14.5. Products were separated over a native agarose gel (1.3%). This experiment was performed three times, and the result is reproducible.

In this experiment, as well as in the previous one, I observed an increase in supercoiling of the bulk DNA in the absence of Asf1 (Figure 5.12, lower panel, lanes 5, 6, 9, and 10). Loss of CAF-1 does not have the same effect, suggesting that Asf1 might be playing a role in suppressing replication-independent deposition of nucleosomes on DNA.

5.2.11 Rtt106 and Asf1 do not substitute for CAF-1

Rtt106 has been implicated in replication-coupled chromatin assembly *in vivo* and has been proposed to deposit newly-synthesised $(H3\text{-}H4)_2$ tetramers on replicated DNA downstream of Asf1, similar to CAF-1 (Burgess and Zhang, 2013). Using purified proteins, I previously showed that Rtt106 could not promote replication-dependent chromatin assembly in lieu of CAF-1 (Figure 5.11). However, this did not exclude the possibility that the reaction simply did not contain enough Rtt106. In order to test this possibility, I titrated Rtt106 with Asf1 in the absence of CAF-1 (Figure 5.13).

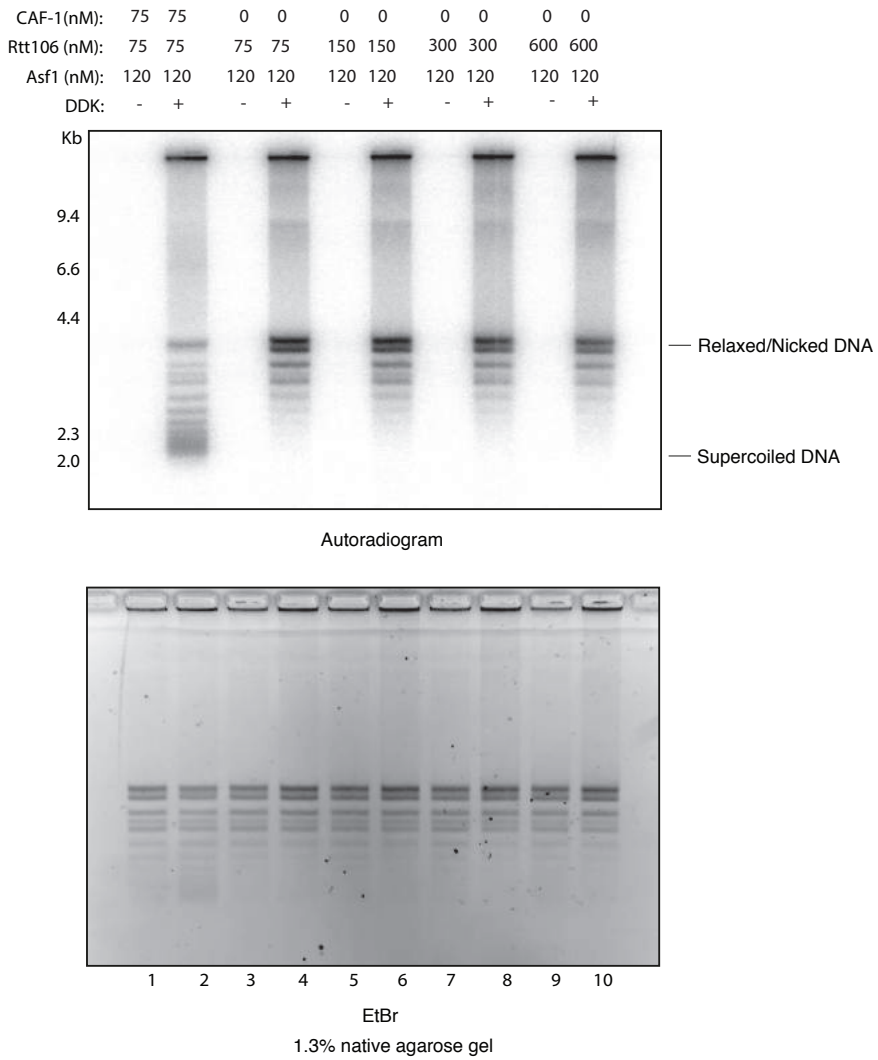

Figure 5.13 Rtt106 and Asf1 do not substitute for CAF-1
Rtt106 titration experiment performed for 20-minutes as described in section 2.14.5. Products were separated over a native agarose gel (1.3%). This experiment was performed twice, and the result is reproducible.

I found that Rtt106 could not promote supercoiling of replicated DNA, even if added in significant excess (Figure 5.14, lanes 9 and 10). Interestingly, while Rtt106 does not promote supercoiling of replicated DNA, it seems to restrict the amount of supercoiling on the bulk DNA (Figure 5.13, lower panel). This is consistent with observations made in Figure 5.11.

5.2.12 ISW1a promotes regular nucleosome spacing on replicated DNA

I wanted to confirm that the replication-dependent supercoiling observed in the previous two sections was due to the deposition of nucleosomes onto DNA. In order to test this, I digested the reaction products with Micrococcal nuclease following replication with and without the ATP-dependent nucleosome spacing factor ISW1a (Figure 5.14). ISW1a spaces nucleosomes on DNA and I purified it from yeast as described in section 2.10.2.12. I included it in this reaction to see whether or not it was necessary to promote extensive nucleosome arrays on the replicated DNA, as implicated *in vivo* (Yadav and Whitehouse, 2016). Following separation under native conditions, the gel was stained with EtBr as a control to show that the products not treated with Micrococcal nuclease were supercoiled and that this supercoiling was replication-dependent (Figure 5.14A, both panels, lanes 1 and 7). Following this, the gel was dried and subjected to autoradiography (as with all previous replication experiments in this thesis).

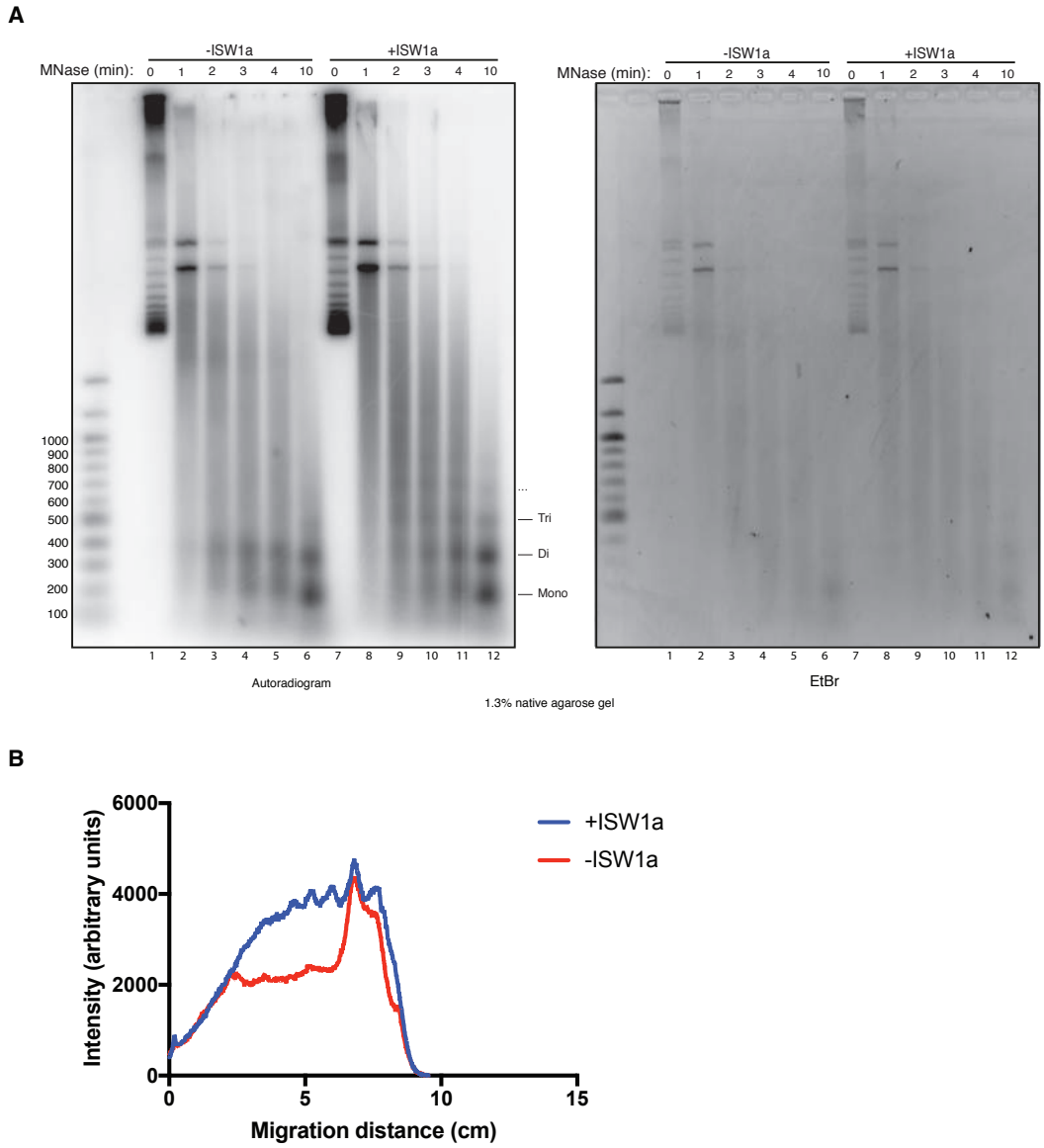

Figure 5.14 ISW1a promotes regular nucleosome spacing on replicated DNA

(A) Micrococcal nuclease digest of replication-dependent chromatin assembly reaction with and without ISW1a. Experiment performed for 20-minutes as described in section 2.14.5. Products were digested with Micrococcal nuclease and separated over a native agarose gel (1.3%). **(B)** Lane profiles of the data in lanes 5 and 11 of the autoradiogram in (A). This experiment was performed three times, and the result is reproducible.

The presence of a DNA ladder in the autoradiogram following digestion suggested that the replication-dependent supercoiling was indeed due to the deposition of nucleosomes onto replicated DNA (Figure 5.14A, left panel). The ladder in the sample containing ISW1a further revealed that the nucleosomes were evenly spaced in arrays of up to at least four or five nucleosomes, as indicated by distinct mono-, di-, tri-, etc nucleosomal bands

(Figure 5.14A, left panel, lanes 8-12). The ladder in the sample without ISW1a was much less extensive and composed of only mono- and di- nucleosomal bands (Figure 5.14A, left panel, lanes 2-6). Comparing lane profiles from the samples with and without ISW1a revealed that the products are much more resistant to Micrococcal nuclease in the presence of ISW1a (Figure 5.14B). Together, these results suggest that nucleosomes are being arranged into dense nucleosomal arrays during or shortly after replication in the presence of ISW1a. Interestingly, the overall replication-dependent supercoiling reaction seems to be enhanced by ISW1a (Figure 5.14A, left panel, lanes 1 and 7).

5.2.13 Replication-coupled chromatin assembly requires PCNA

It has been shown that CAF-1 interacts with PCNA, and it is through this interaction that chromatin assembly is coupled to replication (Shibahara and Stillman, 1999; Zhang et al. 2000; Moggs et al. 2000). Given that PCNA is enriched on the lagging strand during replication, it is unclear how (or if) chromatin assembly is coupled to replication on the leading strand (Yu et al. 2014). In order to test this, I modified the replication-dependent chromatin assembly reaction with CAF-1 and Asf1 described earlier in section 5.2.9. To look specifically at leading strand synthesis, the reactions were performed in the absence of the lagging strand polymerase, DNA polymerase δ, as well as DNA ligase I and the nuclease Fen1. I also increased the concentration of DNA polymerase α, which has been shown to increase the frequency of priming (Yeeles et al. 2017). This ensured that any lagging strands that could potentially form would be too short to form extensive nucleosomal arrays. Following replication, I digested the products with Micrococcal nuclease and analysed the products as described in section 5.2.12.

In the absence of PCNA and DNA polymerase δ, I observed a very short DNA ladder, comprised of no more than a mono- and a faint di-nucleosomal band (Figure 5.15, lanes 1-6). Expectedly, no supercoiling was observed in the absence of Okazaki fragment maturation and termination (Figure 5.15, lanes 1, 7, and 13). In the presence of PCNA, however, the DNA ladder was much

more extensive, with up to tetra- and penta-nucleosomal bands, suggesting that PCNA is required for replication-dependent chromatin assembly on both the leading and the lagging strands (Figure 5.15, lanes 7-12). Importantly, this result also suggests that chromatin assembly is replication-coupled in this system via PCNA.

In this experiment (and in the previous one) I observed a discrete Micrococcal nuclease-resistant band that is smaller than a mononucleosome (Figure 5.15, lanes 6, 12, and 18). This band likely represents a subnucleosomal particle composed of $(H3/H4)_2$ bound to DNA.

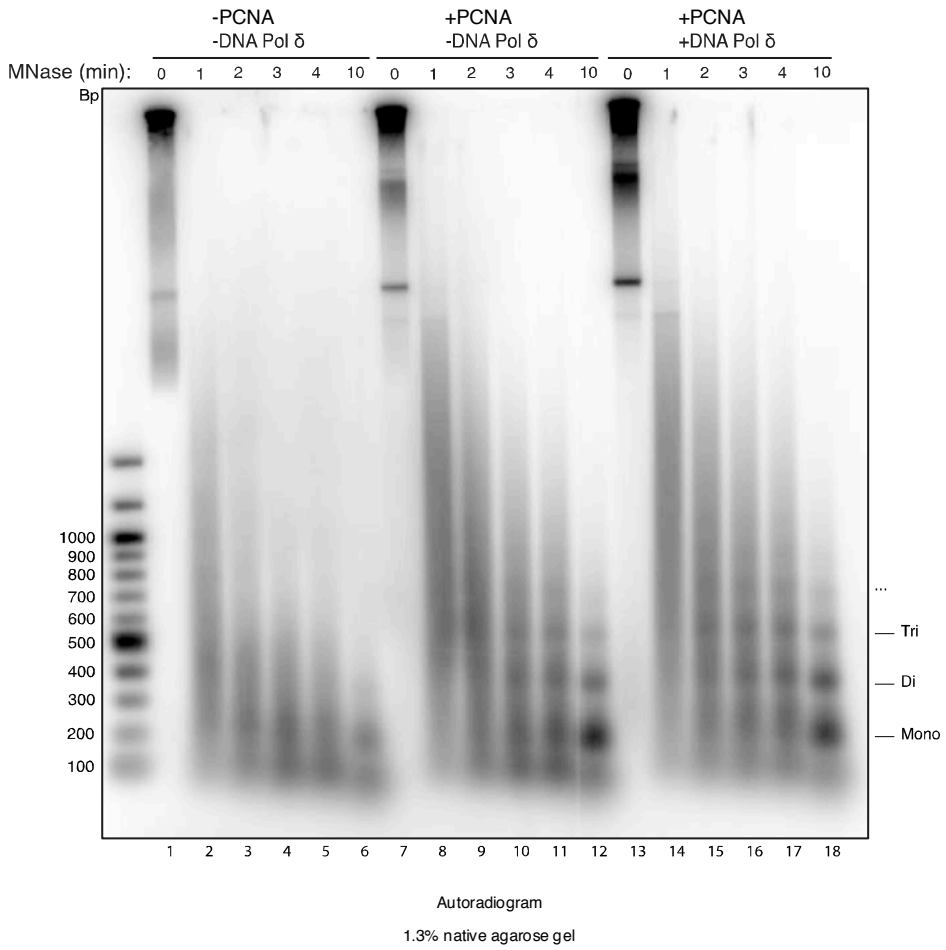

Figure 5.15 Replication-coupled chromatin assembly requires PCNA
(A) Micrococcal nuclease digest of replication-dependent chromatin assembly reaction with and without DNA polymerase δ and PCNA. Experiment performed for 20 minutes as described in section 2.14.5. Products were digested with Micrococcal nuclease and separated over a native agarose gel (1.3%). This experiment was performed twice, and the result is reproducible.

5.3 Discussion

5.3.1 Towards the reconstitution of replication-coupled chromatin assembly with purified proteins *in vitro*

Early in this chapter, I described the expression and purification of proteins that have been implicated in replication-coupled chromatin assembly both *in vitro* and *in vivo*. These included the histone chaperones CAF-1, Asf1, Rtt106, Vps75, and the acetyltransferase Rtt109. I then established supercoiling and Micrococcal nuclease assays using purified CAF-1 and an S-phase extract derived from *S. cerevisiae*. This revealed that CAF-1 was active and sufficient for promoting nucleosome deposition onto newly replicated DNA (Figure 5.7 and Figure 5.8). Presumably the extract contained sufficient amounts of any other proteins that may be required for replication-coupled chromatin assembly, such as Asf1, Rtt106, Vps75, and Rtt109. Having an extract-based assay would be useful in establishing a completely purified system as it could provide a means for identifying additional factors required if the proteins purified earlier in this chapter were not sufficient to reconstitute replication-coupled chromatin assembly. Following this, I reconstituted H3K56ac *in vitro* with Rtt109, Asf1, and Vps75 as was previously described by Tsubota et al. 2007. This confirmed that these proteins were active and able to promote H3K56ac. These were the first steps in recapitulating the entirety of replication-coupled chromatin assembly with purified proteins *in vitro*.

5.3.2 Reconstitution of replication-coupled chromatin assembly with purified proteins *in vitro*

In the end I was able to reconstitute replication-coupled chromatin assembly with purified proteins, building on the replication assay described in Chapters 3 and 4. Initially, I did this with purified CAF-1, Asf1, Rtt106, Vps75, and Rtt109. The H2A and H2B-binding chaperone Nap1 was not required and was even inhibitory to the replication-coupled chromatin assembly reaction (Figure 5.10). This suggested that an additional H2A and H2B chaperone was not required for this reaction beyond the proteins that make up the replisome, some of which may be able to bind histones H2A and H2B. Several replisome components included in this assay have previously been shown to

bind histones, including RPA, DNA polymerase ε, DNA polymerase α, and Mcm2 (Foltman et al. 2013; Liu et al. 2017). It is also possible that this function is carried out by one of the other chaperones in the reaction, including CAF-1, Asf1, Rtt106, Vps75, and/or Rtt109.

Later, I found that Rtt106, Vps75, and Rtt109 were dispensable for replication-coupled chromatin assembly in this *in vitro* system. This suggests that H3K56ac is not required for – nor does it enhance – the deposition of histones onto newly replicated DNA. This is somewhat surprising, given that *in vivo* and *in vitro* data has shown this histone modification plays a role in a number of processes, including replication in *S. cerevisiae*. Importantly, H3K56ac has been observed to increase during S phase of the cell cycle and mostly disappear by G2/M in the absence of DNA damage (Masumoto et al. 2005; Zhou et al. 2006). In addition to enhancing the affinities of both CAF-1 and Rtt106 for H3-H4 dimers, cells lacking either Rtt109 or expressing histone H3 with lysine 56 mutated to R exhibit sensitivity to genotoxic agents and an increased frequency of spontaneous chromosome breaks (Driscoll et al. 2007; Han et al. 2007; Li et al. 2008). Furthermore, cells with mutations in Rtt109 have synthetic lethal or slow-growth phenotypes when coupled with mutations in genes encoding DNA replication and double-strand break repair proteins (Han et al. 2007; Collins et al. 2007). However, given the observation that H3K56ac is not required to reconstitute replication-coupled chromatin assembly *in vitro*, it may be the case that this histone modification is important for specific *in vivo* contexts, such as during the DNA damage response (Masumoto et al. 2005).

The inability of Rtt106 to promote replication-coupled chromatin assembly *in vitro* was surprising given its previous implication in studies both *in vivo* and *in vitro* (Li et al. 2008; Fazly et al. 2012; Su et al. 2012). Recently, Rtt106 has been shown to physically interact with the histone chaperone FACT, which is not present in the *in vitro* assays described in this chapter (Yang et al. 2016). It is possible that this interaction is important to promote Rtt106-dependent deposition of nucleosomes onto DNA.

I went on to show that CAF-1 and Asf1 are the minimal set of histone chaperones required for replication-coupled chromatin assembly *in vitro* (Figure 5.12). This confirms previous observations in extracts suggesting that both of these proteins are required (Tyler et al. 1999). Whilst the role of CAF-1 in this process has been extensively characterised, significantly less is known about Asf1. Reconstituting replication-coupled chromatin assembly with purified proteins has provided a powerful tool with which to study these proteins and how they interact with histones and the replisome *in vitro*.

5.3.3 Replication-coupled chromatin assembly requires PCNA

Furthermore, I found that replication-coupled chromatin assembly requires PCNA (Figure 5.15). This was expected as CAF-1 has been shown to deposit nucleosomes onto DNA via an interaction with PCNA (Shibahara et al. 1999; Zhang et al. 2000). However, it was unknown whether or not this interaction was required for chromatin assembly on both the leading and lagging strands given that the lagging strand (and not the leading strand) is enriched with PCNA (Yu et al. 2014). Intriguingly, the results presented in this chapter pointed to the fact that chromatin assembly on both the leading and lagging strands requires PCNA (Figure 5.15). Further experiments will be required to definitely prove this observation, using a CAF-1 mutant that is unable to bind PCNA.

Chapter 6. Results IV

6.1 Introduction

In eukaryotes, chromatin is the physiological substrate for cellular processes such as replication and transcription. Previously, I detailed the reconstitution of Okazaki fragment maturation and termination of DNA replication on naked DNA (Chapter 3). Building on the work by Yeeles et al. 2015 and Yeeles et al. 2017, it was recently shown with purified proteins *in vitro* that replication through chromatin minimally requires the histone chaperone FACT. Other proteins can enhance replication in this context, including additional histone chaperones, acetyltransferases, and ATP-dependent nucleosome spacing factors (Kurat et al. 2017; Devbhandari et al. 2017; Azmi et al. 2017). However, significantly less is known about the molecular requirements for Okazaki fragment maturation and termination of DNA replication on chromatin, and how (or if) they differ from naked DNA. For example, it is not clear if the nuclease Fen1 and DNA ligase I are sufficient to mature Okazaki fragments on chromatin as they are able to on naked DNA. In order to study this and other questions, I built upon the systems established previously in Chapter 3 and Chapter 4.

During each cell cycle, the genome is replicated once to produce two identical copies of DNA. In addition, other factors must also be duplicated if they are associated with DNA. This includes the histone proteins, which carry modifications that can be used to store information at specific locations in the genome. This information can then be propagated over time following multiple cellular divisions, providing a means through which to regulate gene expression even after the factors that originally established these modifications are gone (Bonasio et al. 2010; Ptashne 2007; Hathaway et al. 2012; Alabert and Groth, 2012; Almouzni and Cedar, 2016). However, even if all of these modified – or parental – histones are passed to the daughter molecules, they will account for only half of the histone content on the nascent DNA. The other half must then be contributed from a newly-

synthesised (*de novo*) pool of histones which are thought to be deposited on the replicated DNA by chaperones such as CAF-1, Asf1, and Rtt106. Reconstitution of this *de novo* pathway with purified proteins *in vitro* was described in Chapter 5.

Whilst significant progress has been made in identifying the factors responsible for replicating chromatin both *in vitro* and *in vivo*, significantly less is known about how nucleosomes and their modifications are actually inherited during replication (Campos and Reinberg, 2009; Swygert and Peterson, 2014). This is due in large part to difficulties in unpicking such complex processes *in vivo*, and a lack of sophisticated systems for studying them *in vitro*. Following the work of Kurat et al. 2017 and the reconstitution of replication-coupled chromatin assembly (Chapter 5), it was now possible to establish assays for studying complete chromatin replication with purified proteins *in vitro.* Such a system would make it possible to address a number of outstanding questions in the field, including how the parental and *de novo* pathways coordinate to assemble nucleosomes on replicated DNA. Furthermore, it would provide a powerful *in vitro* approach to begin studying the mechanisms through which histone modifications are inherited through multiple cell cycles *in vivo*.

6.2 Results

6.2.1 Reconstitution of Okazaki fragment maturation *in vitro* on chromatin

In order to determine the requirements for Okazaki fragment maturation and termination on chromatin, I assembled nucleosomes onto a 10.6 kb template plasmid DNA (pJY22) as described by Kurat et al. 2017 (Figure 6.1A). Consistent with their data, I observed a smear of leading and lagging strand products after replication in the presence of the histone chaperones FACT and Nhp6 (Figure 6.1C, lanes 1 and 2). However, instead of a smear of products - leading and lagging strands - I observed discrete products in the presence of Fen1, Dna2, and DNA ligase I. The largest of these was approximately full-length; these products are likely to be completely

replicated whilst the rest of the products are faster migrating RIs (Figure 6.1C, lane 2).

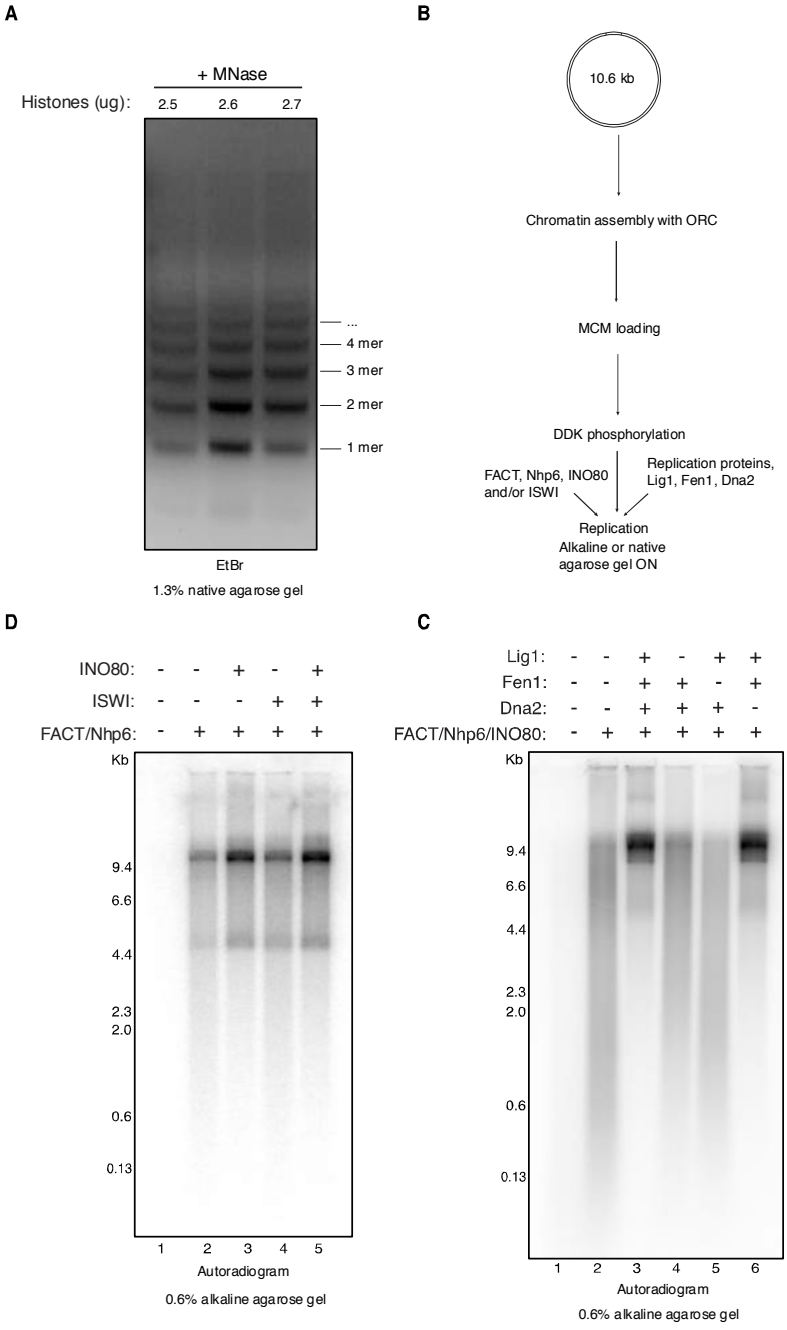

Figure 6.1 Okazaki fragment maturation on chromatin
(A) Input chromatinised DNA following digestion with Micrococcal nuclease **(B)** General scheme for purified replication reactions on chromatin. Unless otherwise stated, the template used in these reactions was pJY22. **(C)** Fen1, Dna2, and DNA ligase I drop-out experiment performed for 30-minutes as in (B). **(D)** ISW1a and INO80 drop-out experiment performed for 30-minutes with Fen1 and DNA ligase I as in (B). Products in (C) and (D) were separated over alkaline agarose gels (0.6%). These experiments were performed three times each, and the results are reproducible.

Drop-out experiments revealed that the product in Figure 6.1C, lane 3 is dependent on Fen1 and DNA ligase I. This is evidenced by the presence of a smear consisting of leading and lagging strands in lanes 4 and 5 of Figure 6.1C. Dna2 does not appear to play a significant role in this system, as with naked DNA (compare Figure 6.1C, lanes 3 and 6).

Furthermore, the addition of the ATP-dependent nucleosome spacing factor INO80 seemed to promote this process, as evidenced by the stronger ^{32}P signal and slightly longer products in Figure 6.1D, lane 3. ISW1a, another ATP-dependent nucleosome spacing factor, appeared to have no obvious effect on replication (Figure 6.1D, lanes 4-5). Given the stimulatory effect of INO80, it is included in all future experiments involving the replication of chromatinised DNA. Together, the results presented in this section suggest that this assay recapitulates Okazaki fragment maturation on chromatinised DNA.

6.2.2 Reconstitution of DNA replication termination *in vitro* on chromatin

I next wanted to determine whether or not termination was occurring in this *in vitro* system on chromatinised DNA. In order to do this, I first separated the replication products via native agarose gel electrophoresis. Total DNA, both replicated and unreplicated, was visualised with ethidium bromide (Figure 6.2, left panel). The gel was then subjected to autoradiography in order to detect the replicated DNA (Figure 6.2, right panel). The replicated products exhibited a profile similar to that of naked DNA (compare Figure 6.2, right panel, lane 2 to Figure 3.7A, right panel, lane 2); I observed what appeared to be negatively-supercoiled, covalently-closed topoisomers as well as a high molecular weight population (Figure 6.2, lane 2). It may be the case that the smear of non-discrete 'topoisomers' may in fact be early replication intermediates. Importantly, these reactions did not contain soluble (free) nucleosomes.

Furthermore, termination was not enhanced when CAF-1, Asf1, and INO80 were added in addition to FACT and Nhp6 (Figure 6.2, lanes 3, 4, and 5). Together, these results indicate that I have recapitulated termination in the context of chromatin; as with naked DNA, this process only minimally requires Fen1 and DNA ligase I in addition to the proteins described by Kurat et al. 2017 and Yeeles et al. 2017.

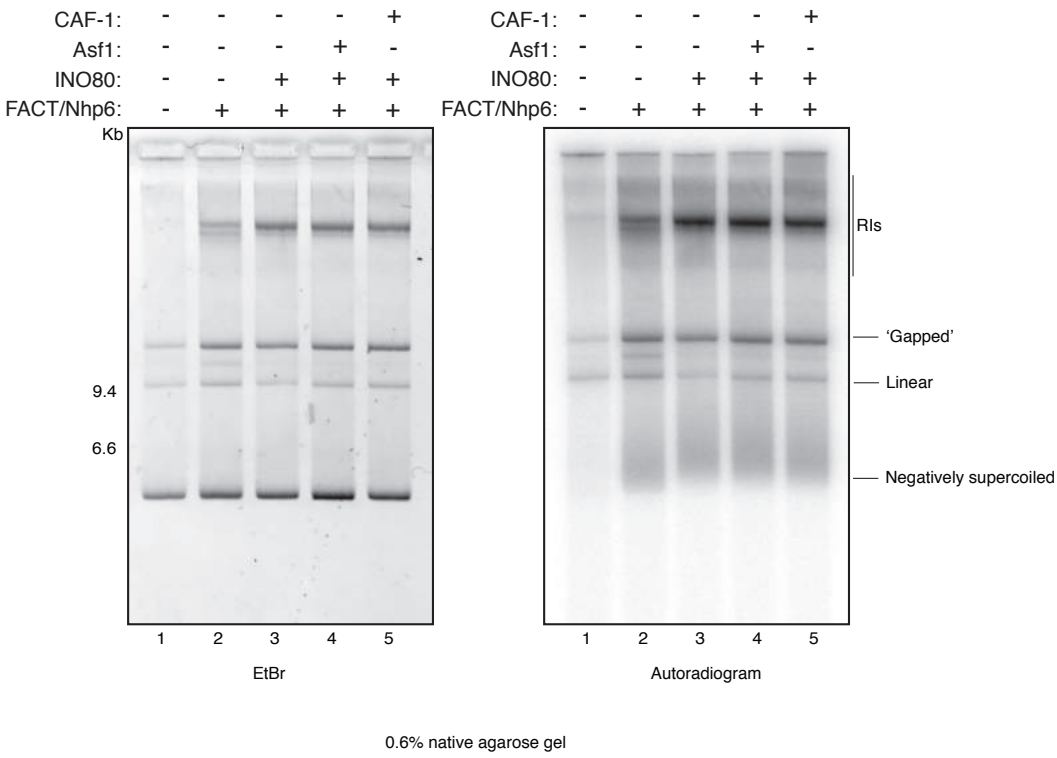

Figure 6.2 Termination of DNA replication on chromatin (1)
60-minute chromatin replication reaction performed with Fen1 and DNA ligase I as in Figure 6.1B. Products were separated over a native agarose gel (0.6%). This experiment was performed twice, and the result is reproducible.

A time-course of replication followed by linearisation with XhoI revealed that the amount of terminated product increased over time, with approximately 10% of the products terminated after ten minutes and up to 30% of the products terminated after two hours (Figure 6.3). This suggests that termination is a relatively slow and inefficient process compared to the rest of replication, based on the observation that elongation rates in this system are 1.5-2 kb/min (Kurat et al. 2017). It is possible that I am missing a protein

(or proteins), such as Pif1, which may be able to enhance termination on chromatin as with naked DNA (Chapter 4).

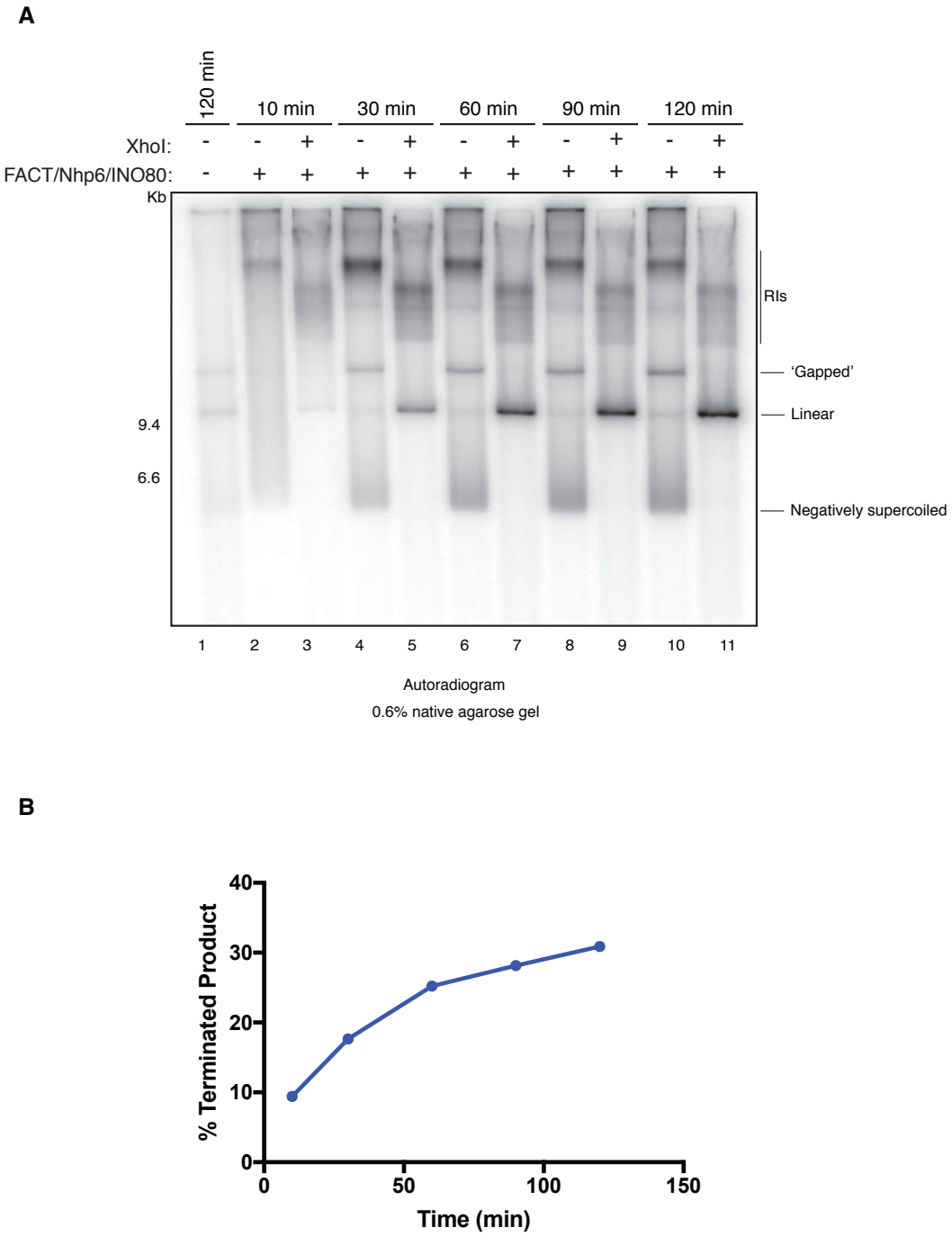

Figure 6.3 Termination of DNA replication on chromatin (2)
(A) Time-course performed under the same experimental conditions as in Figure 6.2 with linearisation by XhoI. Products in (A) were separated over a native agarose gel (0.6%). **(B)** Percent terminated (linearised) product as a function of time from (A). This experiment was performed twice, and the result is reproducible.

6.2.3 Pif1 enhances termination on chromatinised DNA

In order to test whether or not Pif1 could enhance termination on chromatin, I added purified Pif1 to the reaction described in section 6.2.2 along with FACT, Nhp6, and INO80. For this experiment, half of each reaction was linearised with XhoI in order to quantify the amount of terminated replication product (Figure 6.4).

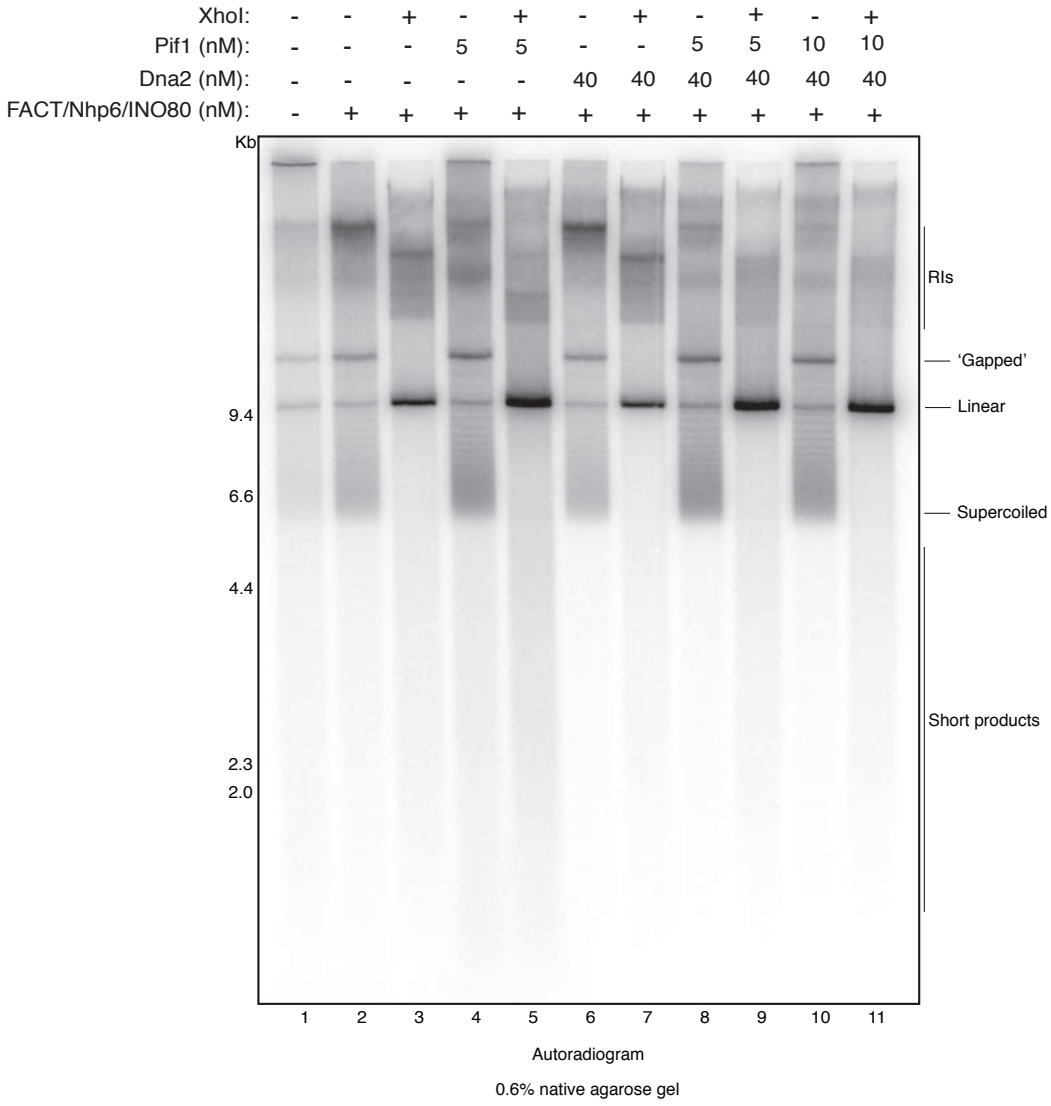

Figure 6.4 Termination of DNA replication on chromatin (3)
Pif1 and Dna2 dropout experiment (60-minutes) performed under the same experimental conditions as in Figure 6.2, with and without linearisation by XhoI. Products were separated over a native agarose gel (0.6%). This experiment was performed twice, and the result is reproducible.

Without Pif1, some of the products were terminated (Figure 6.4, lanes 2 and 3). With Pif1, the number of terminated products appeared to increase (Figure 6.4, lanes 4 and 5). The addition of Pif1 also appeared to promote the resolution of RIs, similar to what was observed on naked DNA in Chapter 4. However, Pif1 appeared to enhance the appearance of short products running faster than the supercoiled DNA, as seen in Figure 6.4, lanes 4 and 5. Given the ability of Dna2 to suppress Pif1's enhancement of strand displacement by DNA polymerase δ (Chapter 4), I wanted to see if these short products could be reduced in number by Dna2.

It turns out that Dna2 does indeed help to reduce the number of these products (Figure 6.4, lanes 6-11), and it may also enhance termination on chromatin with Pif1 (Figure 6.4, lanes 8 and 9). Increasing the concentration of Pif1 did not improve this further (Figure 6.4, lanes 10 and 11) and termination was not enhanced with Dna2 alone in the absence of Pif1 (Figure 6.4, lanes 6 and 7).

Together, these data suggest that Pif1 promotes termination on chromatin, an effect that may be enhanced by Dna2.

6.2.4 CAF-1, Asf1, and Rtt106 do not substitute for FACT/Nhp6

The experiment in Figure 6.2 revealed that CAF-1 and Asf1 could not enhance the amount of terminated replication products on chromatin on top of Fact and Nhp6. In light of this data, I wanted to know if CAF-1, Asf1, and/or Rtt106 could substitute for FACT and Nhp6 for replicating chromatinised DNA. In the end, I found that CAF-1, Asf1, and Rtt106 could not substitute for FACT and Nhp6, either alone or in combination (Figure 6.5). Replication in this experiment was dependent upon FACT and Nhp6, as evidenced by the lack of ^{32}P signal in Figure 6.5, lane 1. In the presence of FACT and Nhp6, the ^{32}P signal was strong and the products were composed of both leading and lagging strands on a denaturing gel in the absence of Fen1 and DNA ligase I (Figure 6.5, lane 2). Both Asf1 and Rtt106 appeared to support some replication either alone or in combination, but the ^{32}P signal in these samples

was significantly less compared to the sample replicated with FACT and Nhp6 (Figure 6.5, lanes 4, 5, and 8). CAF-1 did not support replication alone and even appeared to be inhibitory when combined with Asf1 and Rtt106 (Figure 6.5, lanes 3, 6, 7, and 9). Together, these data suggest that FACT and Nhp6 are required to replicate chromatin and cannot be replaced in this role by CAF-1, Asf1, and/or Rtt106. This is consistent with previous *in vitro* data (Kurat et al. 2017).

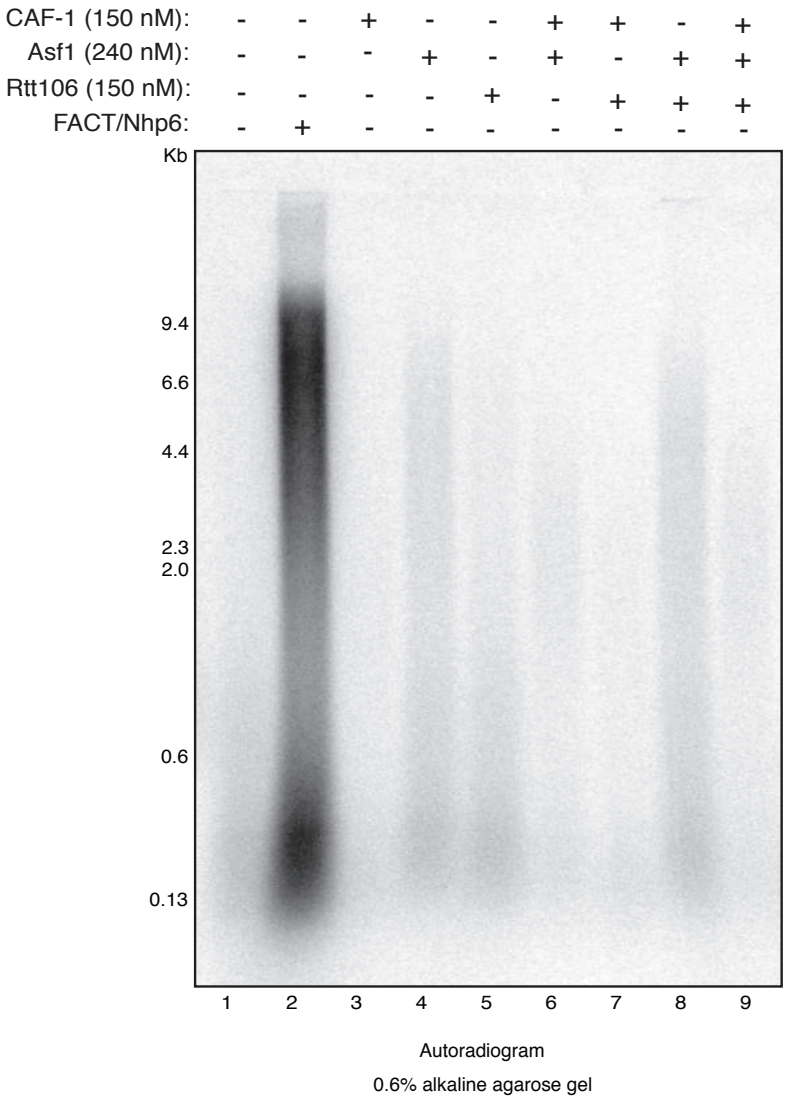

Figure 6.5 CAF-1, Asf1, and Rtt106 do not substitute for FACT/Nhp6
FACT/Nhp6, CAF-1, Asf1, and Rtt106 dropout experiment performed under the same experimental conditions as in Figure 6.2, without Fen1 and DNA ligase I. Products were separated over an alkaline agarose gel (0.6%). This experiment was performed twice, and the result is reproducible.

6.2.5 Reconstitution of complete chromatin replication

Having reconstituted both replication-coupled chromatin assembly (Chapter 5) and termination of replication on chromatinised DNA (Chapter 6), I was in a position to combine these systems and establish assays for studying complete chromatin replication. This would involve re-deposition of parental histones behind the replication fork as well as the deposition of histones from a soluble pool, ensuring the full chromatinisation of the nascent DNA. *In vivo,* the histones in the soluble pool have been newly synthesised and transported into the nucleus.

Initially, I set up three reactions and digested the products with Micrococcal nuclease following replication for twenty minutes (Figure 6.6). In the first reaction, I assessed replication of a naked DNA template (pBluescript/ARS1 WTA) in the presence of soluble histones, Asf1, and CAF-1 (Figure 6.6, 'De novo'). This was a control for the *de novo* pathway in the absence of parental histone re-deposition behind the replication fork. In the second reaction, I replicated a chromatinised DNA template (pBluescript/ARS1 WTA) in the presence of FACT, Nhp6, and INO80 (Figure 6.6, 'Parental'). This was a control to assess the re-deposition of parental histones behind the replication fork in the absence of the *de novo* pathway. Importantly, no soluble histones were added to this reaction. In the third reaction I replicated a chromatinised DNA template in the presence of all of the proteins used in the previous two reactions, both 'De novo' and 'Parental' (Figure 6.6, 'Both'). In order to generate extensive nucleosome arrays, all of the reactions contained ISW1a. Furthermore, the input chromatinised DNA used in both the 'Parental' and 'Both' reactions was digested with Micrococcal nuclease in order to ensure the DNA was saturated with nucleosomes (Figure 6.6, right panel). It was important for the input DNA to be fully saturated in order to accurately assess the contribution of both the *de novo* and parental pathways.

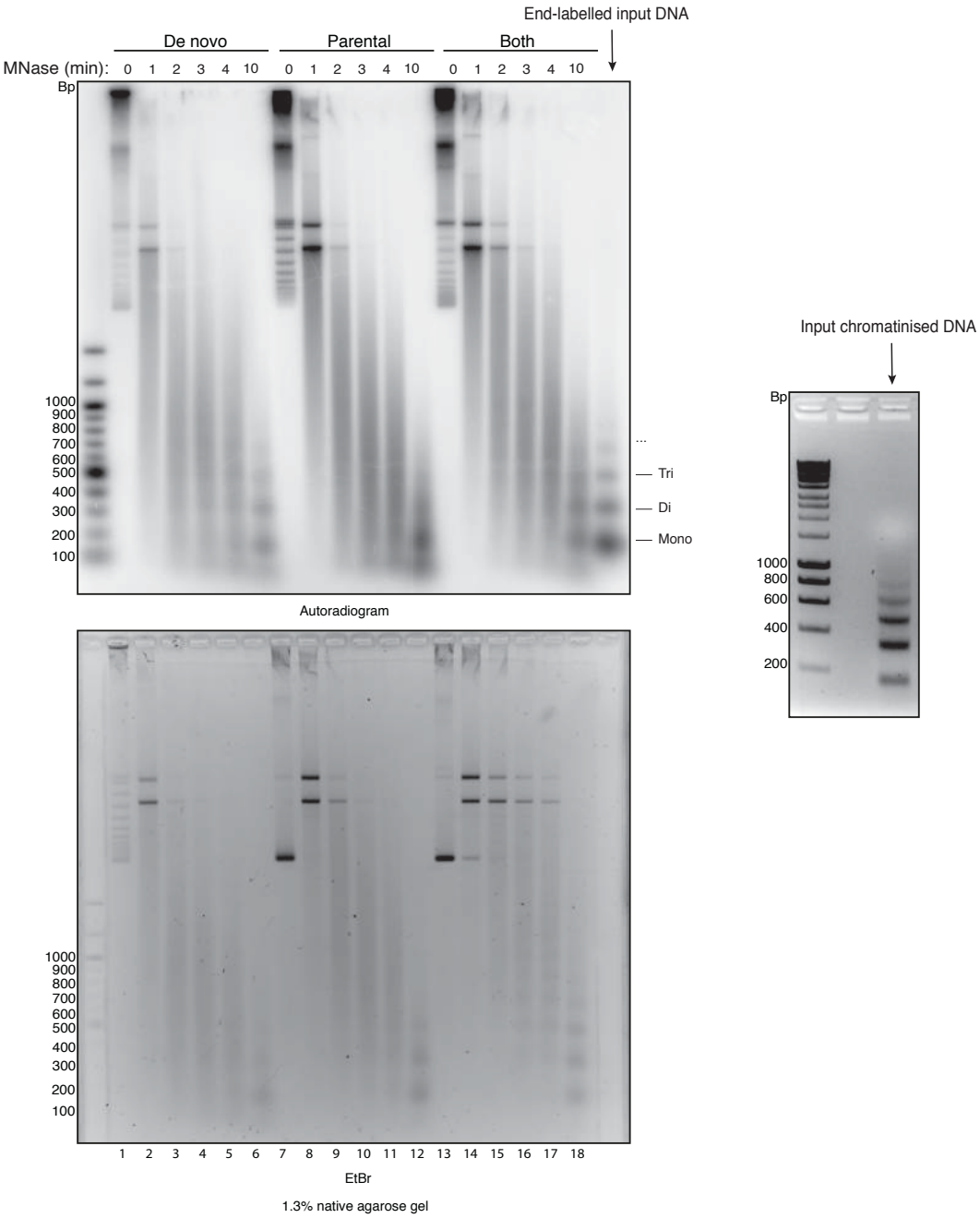

Figure 6.6 Reconstitution of complete chromatin replication
Replication reactions performed for 20-minutes under the same experimental conditions as in Figure 6.2, with Fen1 and DNA ligase I. The 'De novo' reaction contained CAF-1, Asf1, and soluble histones. The 'Parental' reaction contained FACT, Nhp6, and INO80. The 'Both' reaction contained all of the proteins in the 'De novo' and 'Parental' reactions. All reactions contained ISW1a. Products were digested with Micrococcal nuclease and separated over a native agarose gel (1.3%). The right panel shows the Micrococcal nuclease digested input chromatinised DNA used in the 'Parental' and 'Both' reactions. This experiment was performed twice, and the result is reproducible.

Firstly, it was clear that the *de novo* reaction was quite efficient as evidenced by the extensive nucleosome ladder following Micrococcal nuclease digestion of the products (Figure 6.6, 'De novo'). EtBr staining showed that the products not treated with Micrococcal nuclease were supercoiled and that this supercoiling was replication-dependent (Figure 6.6, lane 1). Secondly, the parental reaction revealed that histones were indeed being re-deposited behind the replication fork, though the ladder was much less extensive than in the *de novo* reaction (Figure 6.6, 'Parental'). This was not surprising as the histone content is expected to be diluted between the two nascent strands of DNA. In the combined reaction, the products were more resistant to Micrococcal nuclease and the ladder was much more extensive than in the parental reaction (Figure 6.6, 'Both'). It was not much better than in the *de novo* reaction, however, and it was not clear if the replicated molecules in the combined reaction contained histones from both the *de novo* and parental pathways.

Following digestion with Micrococcal nuclease, some of the input chromatinised DNA was end-labelled with ^{32}P-dATP. This was run alongside the products from all three reactions described earlier in this section as a control to determine the histone content of the nucleosomes on the replicated DNA. The nucleosomes in the input contain the full histone octamer: two copies each of histones H2A, H2B, H3, and H4. Previously, it was not clear if the products of the reconstituted *de novo* pathway contained all of these histones or a smaller subset, such as $(H3\text{-}H4)_2$ without H2A and H2B. The $(H3\text{-}H4)_2$ subset migrates slightly faster than the full histone octamer through an agarose gel. Because the products in each of the three reactions migrate the same distance in the gel as the end-labelled ladder of input DNA, it seems that the nucleosomes in these reactions are likely composed of the full histone octamer following replication (Figure 6.6, 'End-labelled input DNA').

6.3 Discussion

6.3.1 Reconstitution of Okazaki fragment maturation and termination on chromatin

Early work in this chapter described the reconstitution of Okazaki fragment maturation on chromatinised DNA. This process minimally requires the nuclease Fen1 and DNA ligase I in addition to the proteins needed for replication initiation and elongation described previously (Yeeles et al. 2015; Yeeles et al. 2017; Kurat et al. 2017). This process had previously only been reconstituted on naked DNA (Chapter 3), so it was not clear if additional proteins would be required on chromatinised DNA. However, the data presented in this chapter suggest that additional proteins are not required to promote Okazaki fragment maturation beyond those needed for naked DNA. Furthermore, the ATP-dependent nucleosome spacing factor INO80 may enhance Okazaki fragment maturation in the context of chromatin as there appears to be more full-length products after replication in the presence of INO80 (Figure 6.1D). ISW1a appears to have no effect on the accumulation of these products, either alone or in addition to INO80. Together, these data suggest that Okazaki fragment maturation is sensitive to nucleosome positioning on DNA. This is consistent with previous work showing that lagging strand synthesis is coupled to chromatin assembly, with important implications for the regulation of gene expression and epigenetic inheritance *in vivo* (Smith and Whitehouse, 2012; Yadav and Whitehouse, 2016).

The products of the replication reaction on chromatin were later shown to be terminated and covalently-closed when replication was carried out with Fen1 and DNA ligase I (Figure 6.2). Compared with naked DNA, this process is relatively slow and the terminated products were found to accumulate over time; roughly 30% of the products were terminated after two hours of replication on chromatin whereas on naked DNA this figure was nearly 60% (Figure 3.7 and Figure 6.3). I then found that termination on chromatin is enhanced by Pif1, as with naked DNA (Figure 6.4). Roughly 40% of the products were terminated after one hour of replication in the presence of Pif1 and the addition of Dna2 slightly improved this figure to 45%.

The data presented in this chapter reveal that Pif1 can resolve RIs as well as enhance the rate of termination on chromatin, similar to what was observed on naked DNA in Chapter 4. Previously, I also showed that Pif1 could remove excess Mcm2-7 double hexamers from chromatin during replication (Chapter 4). It seems likely that Pif1 is able to enhance termination on chromatin in part by removing excess double hexamers from DNA, allowing unimpeded progression and convergence of CMGs. This would be consistent with the *in vivo* observation that Pif1 and Pif1 family helicases are able to promote replisome progression through difficult to replicate regions of the genome (Sabouri et al. 2012; Steinacher et al. 2012).

6.3.2 Reconstitution of complete chromatin replication

Later in this chapter I showed that the combination of histone chaperones FACT and Nhp6 are required in order to replicate chromatinised DNA, consistent with the findings of Kurat et al. 2017. Other chaperones do not substitute for them in this role, including CAF-1, Asf1, and Rtt106 (Figure 6.5). This suggests that the re-deposition of parental histones behind the replication fork is a separate and distinct pathway from *de novo* histone deposition by CAF-1 and Asf1 as presented in Chapter 5. It is unclear how these two pathways are regulated and contribute to the full chromatinisation of newly-replicated DNA.

In order to begin studying this process, I replicated chromatinised DNA in the presence of FACT, Nhp6, and INO80, as well as the proteins involved in *de novo* chromatin assembly, including purified histones, Asf1, and CAF-1 (Figure 6.6). Following digestion of the replication products with Micrococcal nuclease, I observed a nucleosome ladder with up to tetra- and penta-nucleosomal bands. This was more extensive than the ladder following digestion of products from a similar reaction that did not contain the proteins involved in *de novo* chromatin assembly. The resultant di- and tri-nucleosomal bands in this reaction confirmed that parental histones were indeed being re-deposited behind the replication fork, similar to what was

observed by Kurat et al. 2017. In a separate reaction, naked DNA was replicated in the presence of proteins required for *de novo* chromatin assembly including purified histones, Asf1, and CAF-1. This reaction did not contain FACT, Nhp6, or INO80. The ladder in this reaction was extensive and included up to tetra- and penta- nucleosomal bands following digestion with Micrococcal nuclease (Figure 6.6). Intriguingly, this ladder was similar to the ladder produced following digestion of the products replicated in the combined reaction, which in theory included both parental histone re-deposition and *de novo* chromatin assembly (Figure 6.6, 'Both'). The similarities in the products from these two reactions made it difficult to interpret the contribution of parental histone re-deposition and *de novo* chromatin assembly on the replicated DNA. One possibility is that the efficient *de novo* chromatin assembly pathway is out-competing parental histone re-deposition in this reaction. Even if this were the case, the previous experiment revealed that the combination of histone chaperones FACT and Nhp6 are required to replicate chromatinised DNA. The other possibility is that parental histones are being re-deposited behind the fork alongside the deposition of histones from the *de novo* chromatin assembly pathway. Further experiments will be required to address how these processes are coordinated. For example, one approach would be to tag the histones, with one tag for the histones involved the *de novo* chromatin assembly pathway and another for the histones used to chromatinise the input DNA. This would then allow me to determine if the parental histones are being re-deposited behind the replication fork in this assay. If necessary, I can titrate the proteins involved in the *de novo* chromatin assembly pathway in order to determine the conditions in which parental histones are efficiently re-deposited on the replicated DNA.

Furthermore, work *in vivo* has suggested that parental heterotetramers of histones H3 and H4 generally remain intact when nucleosomes are disrupted during replication, though there is mixing of old and new histones H2A and H2B (Xu et al. 2010; Katan-Khaykovich and Struhl, 2011; Prior et al. 1980;

Annunziato 2005). The work described in this chapter has provided a powerful *in vitro* tool for understanding how these processes work *in vivo*.

Chapter 7. Discussion

7.1 Introduction

Discontinuous synthesis on the lagging strand during replication leads to the generation of discrete Okazaki fragments, which are then processed to form a single, continuous strand of DNA (Okazaki et al. 1968). Following this, the end of replication involves a number of sequential processes that must occur in order to generate two identical copies of DNA (Gambus, 2017; Dewar et al. 2017). Termination events mostly occur asynchronously and without sequence specificity, making these processes difficult to study *in vivo*. Finally, DNA is rapidly re-assembled into chromatin following replication. This involves the transfer of parental histones from the template DNA to the daughter DNA, as well as the deposition of newly-synthesised histones by chaperones such as CAF-1 (Smith and Stillman, 1989). The mechanisms underlying these complex processes have proved difficult to study both *in vivo* and *in vitro*. Following the recent reconstitution of replication initiation and elongation with purified proteins *in vitro*, it has become possible to reconstitute and study Okazaki fragment maturation, termination, and replication-coupled chromatin assembly as they occur *in vivo* (Yeeles et al. 2015; Yeeles et al. 2017; Kurat et al. 2017; Devbhandari et al. 2017).

7.2 Okazaki fragment maturation *in vitro*

In this study, I initially set out to determine the requirements for Okazaki fragment maturation on naked DNA, building upon a system that reconstituted replication initiation and elongation with purified proteins *in vitro* (Yeeles et al. 2015; Yeeles et al. 2017). Consistent with previous *in vitro* and *in vivo* studies, I found that this process minimally requires the nuclease Fen1, DNA ligase I, DNA polymerase δ, and PCNA (Maga et al. 2001; Ayyagari et al. 2002; Rossi and Bambara, 2006; Stodola and Burgers, 2016). However, this was one of the first studies to examine this process in the context of fully reconstituted replication with purified proteins. It was also reconstituted in another recently established *in vitro* replication system (Devbhandari et al.

2017). However, they observed short products even in the presence of Fen1 and DNA ligase I, despite having the same protein components in their reactions as those described in Chapter 3. I could not exclude the possibility that one or more of my purified proteins contained a contaminant that could potentially enhance lagging strand synthesis. In order to determine whether or not this was the case, I analysed a master mix of my replication proteins by mass spectrometry (data not shown). Whilst there were a number of low-level contaminants, including ribosomal components and heat-shock proteins, none of them are known to be involved in lagging strand synthesis. Thus, it seems that the discrepancies between our reactions could be due to differences in reaction conditions or protein concentration/activity.

The nuclease Dna2 was not required for Okazaki fragment maturation nor could it substitute for Fen1. This was surprising as Dna2 is essential for cell viability *in vivo*, unlike Fen1 (Budd and Campbell, 1995; Reagan et al. 1995). Perhaps Dna2 is the only nuclease *in vivo* that is able to process long-flaps generated by DNA polymerase δ, whereas there are other nucleases that can substitute for Fen1, such as Exonuclease 1 (Burgers, 2009; Balakrishnan and Bambara, 2013). This would be consistent with the finding that the nuclease activity of Dna2 is its essential function (Formosa and Nittis, 1999; Kang et al. 2000). Of course, the protein used for the experiments in this thesis may not have been completely active. Dna2 has been found to be difficult to work with *in vitro* (Levikova et al. 2013). In any case, the subtle lengthening of Okazaki fragments observed in the absence of Fen1 suggests that a small fraction of the fragments are processed by Dna2 and DNA ligase I (Chapter 3 and Chapter 4). It was later proposed in Chapter 3 that the helicase Pif1 may be necessary to generate the long-flap substrates for Dna2 during Okazaki fragment maturation, based on previous *in vitro* and *in vivo* data (Rossi et al. 2008; Budd et al. 2006). Whilst I found that Dna2 is able to suppress Pif1's ability to enhance strand displacement synthesis by DNA polymerase δ, it seems that Dna2 is only able to process a small fraction of Okazaki fragments in the absence of Fen1, with or without Pif1 (Chapter 4). It may be that only a small number of long flaps are generated *in vivo*, but the inability to process

them may be lethal to the cell. It has been predicted that the majority of flaps generated during strand displacement synthesis are short enough to be processed by Fen1 (Burgers and Kunkel, 2017). It will be interesting in the future to use this assay to study the mechanism of Okazaki fragment maturation, including the coordination of the nucleases Fen1 and Dna2.

Chromatin is the physiological substrate for replication *in vivo*. Thus, it is important to understand how processes like Okazaki fragment maturation work not only on naked DNA, but ultimately on chromatinised DNA. Replication initiation and elongation were both recently reconstituted on chromatin with purified proteins *in vitro* (Kurat et al. 2017). Building upon this system, I found that Okazaki fragment maturation in this context requires Fen1 and DNA ligase I (and presumably PCNA and DNA polymerase δ), as with naked DNA (Chapter 6). Dna2 is dispensable for Okazaki fragment maturation on chromatin in this minimal *in vitro* system, as it is on naked DNA. Furthermore, this process seems to be slightly enhanced by the ATP-dependent nucleosome spacing factor INO80. This suggests that lagging strand synthesis is linked to chromatin assembly, as previously suggested *in vitro* and *in vivo* (Smith and Whitehouse, 2012; Kurat et al. 2017; Devbhandari et al. 2017). ISW1a, another nucleosome remodeller, had no effect on the distribution of replication products. It may be that INO80 optimally positions nucleosomes for downstream processes, such as strand displacement by DNA polymerase δ and flap cleavage by Fen1 and/or Dna2. In any case, these results have important implications given the role of chromatin in gene expression and the inheritance of epigenetic states. It is plausible that INO80 could remove nucleosomes around the replication fork, as it has been shown to do around double-strand breaks (van Attikum et al. 2007; Tsukuda et al. 2005). Furthermore, *S. cerevisiae* lacking INO80 have been found to progress more slowly through S-phase, and the replication fork is significantly delayed in human cells lacking INO80 (Papamichos-Chronakis and Peterson, 2008; Vassileva et al. 2014). More experiments will be necessary to determine the precise roles of these remodellers in chromatin replication, as well as the effects they have on downstream processes *in vivo*.

In summary, Okazaki fragment maturation requires Fen1 and DNA ligase I on both naked and chromatinised DNA. This is in addition to the proteins needed for replication initiation and elongation described previously (Yeeles et al. 2015; Yeeles et al. 2017; Kurat et al. 2017). Dna2 does not substitute for Fen1, nor is its ability to process Okazaki fragments enhanced in the presence of Pif1. Moreover, the idea that lagging strand synthesis and chromatin assembly are linked is supported by the observation that Okazaki fragment maturation is somewhat enhanced in the presence of INO80.

7.3 Termination of DNA replication *in vitro*

Following the establishment of Okazaki fragment maturation, the *in vitro* replication system described previously was now recapitulating initiation as well as complete leading and lagging strand synthesis (Yeeles et al. 2015; Yeeles et al. 2017; Kurat et al. 2017). Next, I wanted to determine the requirements for termination *in vitro*. Reconstitution of this process would provide greater understanding of the mechanisms through which this process occurs at the end of replication. Intriguingly, linearisation of the products replicated in the presence of Fen1 and DNA ligase I resulted in a single band of unit-length on an alkaline gel (Chapter 3). The linearisation site (XhoI) was spaced approximately four-thousand base-pairs away from the origin (but not directly across from the origin), so the appearance of a unit-length band suggested that the lagging strand was being ligated to the leading strand. Previous work had revealed that converging CMGs pass each other on opposite leading strands, allowing for the rapid ligation of these strands to downstream Okazaki fragments and completion of DNA synthesis (Dewar et al. 2015). Indeed, I found that termination was occurring in the minimal *in vitro* system described in Chapter 3. This process did not require additional proteins beyond those already described. The terminated products accumulated slowly over time, with 40% of the products terminated after one hour of replication and nearly 60% after two hours (Chapter 3). This was also the case on chromatin, though the amount of terminated product accounted for only 30% of the total products after two hours (Chapter 6). These results

suggested that termination is less efficient than initiation and elongation as replication rates in this system have been measured at 1.5-2 kb/min on naked DNA (Yeeles et al. 2017). Given that converging replisomes do not slow down or stall at the end of replication in *Xenopus* extracts, it seemed that a factor (or factors) may have been missing that facilitate termination *in vivo* (Dewar et al. 2015). Pif1 was a likely candidate as it has been shown to promote replisome progression through protein barriers and difficult to replicate regions of the genome; its homologue in *S. pombe* has also been shown to promote fork convergence during termination *in vivo* (Steinacher et al. 2012; Paeschke et al. 2011; Paeschke et al. 2013; Boule et al. 2005; Koc et al. 2016).

I found that termination is promoted in two ways by Pif1: it promotes the resolution of replication intermediates and increases the rate of termination (Chapter 4). This has also been shown in a similar *in vitro* system by Dr Tom Deegan at the University of Dundee (unpublished data). Furthermore, I found this to be the case on chromatin as well as naked DNA. The differences in termination efficiencies between chromatin and naked DNA were resolved in the presence of Pif1 (and to a lesser extent, Dna2). The decreased termination efficiency observed on chromatin may have been due to increased stalling of the replisome at nucleosomes, which pose a barrier to replication. It is conceivable that this block could then be overcome with the help of Pif1. In any case, the end of replication must occur without issue *in vivo* as any unreplicated DNA can lead to the formation of anaphase bridges and ultimately genomic instability (Chan et al. 2009; Sofueva et al. 2011; Steinacher et al. 2012).

Whilst looking for factors that influence the efficiency of termination, I found that increasing the concentration of loaded Mcm2-7 double hexamers was inhibitory to termination on naked DNA (Chapter 4). Intriguingly, these excess loaded double hexamers were removed in the presence of Pif1. This suggested that part of Pif1's role in enhancing termination was through its removal of topologically bound Mcm2-7 between two converging CMGs. It

seemed plausible that this could be a second pathway for removing Mcm2-7 at the end of replication, similar to the one involving polyubiquitylation of Mcm7 by SCF^{Dia2} in *S. cerevisiae* and $CRL2^{Lrr1}$ in vertebrates (Maric et al. 2014; Dewar et al. 2017).

I then went on to find that excess loaded double hexamers are severely inhibitory to replication generally (not only termination) on chromatinised DNA. This suggested that these excess (unfired) double hexamers need to be removed during replication as they block the replisome's progression through nucleosomes. Furthermore, I showed that this inhibitory effect on replication is rescued by Pif1. Thus, it seems that excess double hexamers probably do not accumulate as trains *in vivo*. Instead, they are likely removed as they are encountered by the replisome, allowing replication to proceed unimpeded through chromatin. This has important implications given that *in vivo* Mcm2-7 has been shown to load in roughly 20-fold excess relative to replication origins and ORC in both *S. cerevisiae* and humans, leading to the licensing of many more origins than are needed to replicate the genome (Burkhart et al. 1995; Lei et al. 1996; Donovan et al. 1997; Mahbubani et al. 1997; Edwards et al. 2002). It has never been clear when or how these unused double hexamers are removed from dormant origins during the cell cycle, and it was possible (and still is) that they could be pushed ahead of the replisome and become activated in the event of a stalled or collapsed replication fork. However, the results presented in this thesis provide the first indication that these excess double hexamers must be removed during replication, and that a pathway for this removal involves Pif1. This is effectively a replication-dependent mechanism for the de-licensing of dormant origins, and is a novel role for Pif1. It is also a possibility that in *S. cerevisiae*, Rrm3 may be the more relevant of the two Pif1-family helicases in terms of removing loaded MCMs. However, humans only have one copy of Pif1. The human MCM-binding protein (MCM-BP) has also been implicated in the removal of loaded MCMs from chromatin (Nishiyama et al. 2011). It will now be important to determine how (or if) these proteins are involved in removing MCMs *in vivo*.

7.4 Complete chromatin replication *in vitro*

Following the reconstitution of replication initiation, elongation, and termination, it was now possible to build upon the *in vitro* replication system established earlier in this thesis in order to understand the requirements for complete chromatin replication as it occurs *in vivo*. This would involve the replication of a chromatin template and then reassembly of the products into fully chromatinised daughter DNA. In order for this to occur, nucleosomes are recycled and transferred from the template to the daughter DNA. These make up (at best) 50% of the nucleosomes on the nascent DNA. The rest come from a newly-synthesised pool and are deposited in a replication-coupled manner. One pathway in which parental histones are re-deposited behind the fork had been reconstituted previously (Kurat et al. 2017), so I began by establishing several assays for studying replication-coupled chromatin assembly, first in extracts and then using purified proteins in the *in vitro* replication system. I found that this process minimally requires histone proteins H2A, H2B, H3, and H4 as well as the histone chaperones CAF-1 and Asf1 (Chapter 5). This is in addition to the proteins described previously for the reconstitution of replication initiation, elongation, and termination (Chapter 3). The need for CAF-1 and Asf1 confirms early studies of SV40 replication in human cell extracts during the 1980s and 1990s (Smith and Stillman, 1989; Tyler et al. 1999). It has been a long standing question as to whether other factors in the extracts used in these early experiments were also required for replication-coupled chromatin assembly. Furthermore, the mechanism of replication in eukaryotes is different than it is in SV40. For example the SV40 system does not contain DNA Polymerase ε and relies on T antigen instead of a helicase like the CMG. Despite its early usefulness, SV40 is not an ideal system in which to study how chromatin assembly is coupled to replication. The system described in this thesis provides a means to study this process in the context of a completely reconstituted eukaryotic replisome.

Recent work has shed light on the mechanism through which CAF-1 forms $(H3\text{-}H4)_2$ tetramers prior to deposition on replicated DNA (Mattiroli et al. 2017). The role of Asf1 is less clear, though it has been shown to interact

directly with CAF-1 in *D. melanogaster* and humans (Tyler et al. 2001; Mello et al. 2002). However, the extent to which CAF-1 and Asf1 interact to deposit newly-synthesised histones on nascent DNA is not known.

I also found that the ATP-dependent nucleosome spacing factor, ISW1a, is required to generate periodic nucleosome arrays following nucleosome deposition by CAF-1 and Asf1. Given the relatively short time in which the reaction was carried out, this suggests that the nucleosomes are deposited and then quickly positioned on the nascent DNA. This is similar to what has been observed *in vivo*, where deleting chromatin remodellers such as ISW1a results in the loss of an extensive Micrococcal nuclease ladder following digestion of replicated DNA (Yadav and Whitehouse, 2016). Furthermore, a number of other proteins that have been implicated in replication-coupled chromatin assembly *in vivo* were found to be dispensable in this system, such as the histone chaperones Rtt106 and Vps75, as well as the histone acetyl-transferase Rtt109. However, this does not rule out the possibility that they are needed under specific conditions *in vivo*, such as in the presence of replication stress (Masumoto et al. 2005). Indeed, H3K56ac has been shown to promote chromatin reassembly following double strand break repair (Chen et al. 2008).

It has been shown previously that CAF-1 couples chromatin assembly to replication through an interaction with PCNA (Shibahara and Stillman, 1999; Zhang et al. 2000; Moggs et al. 2000). This coupling is important in part to ensure that histones and their modifications are preserved at specific loci in the genome. Moreover, it has been recently observed that (1) processive synthesis on the leading strand is largely independent of PCNA and (2) the lagging strand is enriched with PCNA (Georgescu et al. 2014; Yu et al. 2014). This raised the question of whether chromatin assembly on both the leading and lagging strands is coupled to replication via PCNA. Using the *in vitro* replication system I found that chromatin assembly on both strands likely requires the interaction between CAF-1 and PCNA (Chapter 5). This implies that the mechanism of *de novo* chromatin assembly is probably similar on the

two strands, with both being mediated by CAF-1. However, future experiments will be required to understand the mechanisms of chromatin assembly on the leading and lagging strands during replication. It should also be noted that PCNA has many interactors *in vivo*, and the absence of these interactors may change the dynamics of processes such as replication-coupled chromatin assembly in the *in vitro* system described in this thesis.

Having reconstituted *de novo* chromatin assembly, I wanted to combine this process with FACT/Nhp6-dependent replication of chromatinised DNA to begin looking at how the re-deposition of parental nucleosomes is coordinated with *de novo* chromatin assembly by CAF-1 and Asf1 (Kurat et al. 2017). Due to the efficiency of the *de novo* chromatin assembly reaction (as evidenced by an extensive ladder following digestion with Micrococcal nuclease), I was unable to determine whether or not the two pathways were contributing nucleosomes equally to the daughter DNA. However, a previous result revealed that CAF-1 and Asf1 do not substitute for FACT/Nhp6 during the replication of chromatinised DNA. Future experiments will be required to determine how these pathways are coordinated with each other and with the replisome. One useful approach will be to tag two sets of histones, one used for the *de novo* chromatin assembly reaction and the other used to chromatinise the template DNA. These could then be used to isolate the parental and *de novo* nucleosomes assembled onto the nascent DNA. Furthermore, coupling this approach with new strand-specific sequencing techniques, such as eSPAN and SCAR-seq, will provide a powerful method for studying these processes in this *in vitro* system (Petryk et al. 2018; Yu et al. 2018; Yu et al. 2014). These techniques have already been used *in vivo* to show how Mcm2 and DNA polymerase ε ensure that parental $(H3\text{-}H4)_2$ tetramers are passed symmetrically to the nascent DNA (Petryk et al. 2018; Yu et al. 2018). It was previously known that $(H3\text{-}H4)_2$ tetramers generally remain intact and are segregated randomly to the newly synthesised DNA (Xu et al. 2010). The power of a fully reconstituted system is that one has complete control over all components of the reaction. Such a system can thus be exploited to unpick the mechanism of histone transfer to each of the

daughter strands in ways that are not possible *in vivo*. Ultimately, this system could be used to study how histone modifiers are recruited to the replisome, and the mechanisms through which histone modifications are inherited during and after replication. This has the potential to provide significant insights into how epigenetic states are inherited *in vivo.*

In conclusion, the results presented here reveal the minimal set of proteins required for complete lagging strand synthesis, termination, and replication-coupled chromatin assembly *in vitro*. In addition, I have presented evidence showing that unused dormant origins must be de-licensed during replication, and that the licensing factor, Mcm2-7, can be removed in the presence of the helicase Pif1. In the future, the *in vitro* replication system described in this thesis will be a powerful tool for studying the mechanisms of replication as well as those of other replication-coupled processes.

Reference List

Acharya, N., Klassen, R., Johnson, R. E., Prakash, L., & Prakash, S. (2011). PCNA binding domains in all three subunits of yeast DNA polymerase delta modulate its function in DNA replication. Proc Natl Acad Sci U S A, 108(44), 17927-17932. doi:10.1073/pnas.1109981108

Alabert, C., & Groth, A. (2012). Chromatin replication and epigenome maintenance. Nat Rev Mol Cell Biol, 13(3), 153-167. doi:10.1038/nrm3288

Alabert, C., Jasencakova, Z., & Groth, A. (2017). Chromatin Replication and Histone Dynamics. Adv Exp Med Biol, 1042, 311-333. doi:10.1007/978-981-10-6955-0_15

Almouzni, G., & Cedar, H. (2016). Maintenance of Epigenetic Information. Cold Spring Harb Perspect Biol, 8(5). doi:10.1101/cshperspect.a019372

Alvarez, F., Munoz, F., Schilcher, P., Imhof, A., Almouzni, G., & Loyola, A. (2011). Sequential establishment of marks on soluble histones H3 and H4. J Biol Chem, 286(20), 17714-17721. doi:10.1074/jbc.M111.223453

Annunziato, A. T. (2005). Split decision: what happens to nucleosomes during DNA replication? J Biol Chem, 280(13), 12065-12068. doi:10.1074/jbc.R400039200

Annunziato, A. T. (2013). Assembling chromatin: the long and winding road. Biochim Biophys Acta, 1819(3-4), 196-210. doi:10.1016/j.bbagrm.2011.07.005

Arias, E. E., & Walter, J. C. (2007). Strength in numbers: preventing rereplication via multiple mechanisms in eukaryotic cells. Genes Dev, 21(5), 497-518.

Ayyagari, R., Gomes, X. V., Gordenin, D. A., & Burgers, P. M. (2003). Okazaki fragment maturation in yeast. I. Distribution of functions between FEN1 AND DNA2. J Biol Chem, 278(3), 1618-1625. doi:10.1074/jbc.M209801200

Azmi, I. F., Watanabe, S., Maloney, M. F., Kang, S., Belsky, J. A., MacAlpine, D. M., . . . Bell, S. P. (2017). Nucleosomes influence multiple steps during replication initiation. Elife, 6. doi:10.7554/eLife.22512

Bae, S. H., Bae, K. H., Kim, J. A., & Seo, Y. S. (2001). RPA governs endonuclease switching during processing of Okazaki fragments in eukaryotes. Nature, 412(6845), 456-461.

Bae, S. H., Choi, E., Lee, K. H., Park, J. S., Lee, S. H., & Seo, Y. S. (1998). Dna2 of Saccharomyces cerevisiae possesses a single-stranded DNA- specific endonuclease activity that is able to act on double-stranded DNA in the presence of ATP. J Biol Chem, 273(41), 26880-26890.

Bae, S. H., & Seo, Y. S. (2000). Characterization of the enzymatic properties of the yeast dna2 Helicase/endonuclease suggests a new model for Okazaki fragment processing. J Biol Chem, 275(48), 38022-38031. doi:10.1074/jbc.M006513200

Balakrishnan, L., & Bambara, R. A. (2011). Eukaryotic lagging strand DNA replication employs a multi-pathway mechanism that protects genome integrity. J Biol Chem, 286(9), 6865-6870. doi:10.1074/jbc.R110.209502

Balakrishnan, L., & Bambara, R. A. (2013). Okazaki fragment metabolism. Cold Spring Harb Perspect Biol, 5(2). doi:10.1101/cshperspect.a010173

Balakrishnan, L., & Bambara, R. A. (2013). Flap endonuclease 1. Annu Rev Biochem, 82, 119-138. doi:10.1146/annurev-biochem-072511-122603

Bambara, R. A., Murante, R. S., & Henricksen, L. A. (1997). Enzymes and reactions at the eukaryotic DNA replication fork. J Biol Chem, 272(8), 4647-4650.

Baxter, J., & Diffley, J. F. X. (2008). Topoisomerase II inactivation prevents the completion of DNA replication in budding yeast. Mol Cell, 30(6), 790-802.

Been, M. D., & Champoux, J. J. (1980). Breakage of single-stranded DNA by rat liver nicking-closing enzyme with the formation of a DNA-enzyme complex. Nucleic Acids Res, 8(24), 6129-6142.

Bell, S. P., & Dutta, A. (2002). DNA replication in eukaryotic cells. Annu Rev Biochem, 71, 333-374.

Bessler, J. B., Torres, J. Z., & Zakian, V. A. (2001). The Pif1p subfamily of helicases: region-specific DNA helicases? Trends Cell Biol, 11(2), 60-65.

Bhat, M. A., Philp, A. V., Glover, D. M., & Bellen, H. J. (1996). Chromatid segregation at anaphase requires the barren product, a novel chromosome-associated protein that interacts with Topoisomerase II. Cell, 87(6), 1103-1114.

Blow, J. J. (1993). Preventing re-replication of DNA in a single cell cycle: evidence for a replication licensing factor. J Cell Biol, 122(5), 993-1002.

Blow, J. J., & Gillespie, P. J. (2008). Replication licensing and cancer--a fatal entanglement? Nat Rev Cancer, 8(10), 799-806.

Blow, J. J., & Laskey, R. A. (1988). A role for the nuclear envelope in controlling DNA replication within the cell cycle. Nature, 332(6164), 546-548. doi:10.1038/332546a0

Bonasio, R., Tu, S., & Reinberg, D. (2010). Molecular signals of epigenetic states. Science, 330(6004), 612-616. doi:10.1126/science.1191078

Bonne-Andrea, C., Wong, M. L., & Alberts, B. M. (1990). In vitro replication through nucleosomes without histone displacement. *Nature, 343*(6260), 719-726. doi:10.1038/343719a0

Boule, J. B., Vega, L. R., & Zakian, V. A. (2005). The yeast Pif1p helicase removes telomerase from telomeric DNA. Nature, 438(7064), 57-61. doi:10.1038/nature04091

Boule, J. B., & Zakian, V. A. (2006). Roles of Pif1-like helicases in the maintenance of genomic stability. Nucleic Acids Res, 34(15), 4147-4153. doi:10.1093/nar/gkl561

Bousset, K., & Diffley, J. F. X. (1998). The Cdc7 protein kinase is required for origin firing during S phase. Genes Dev, 12(4), 480-490.

Budd, M. E., & Campbell, J. L. (1995). A yeast gene required for DNA replication encodes a protein with homology to DNA helicases. Proc Natl Acad Sci U S A, 92(17), 7642-7646.

Budd, M. E., Choe, W. C., & Campbell, J. L. (1995). DNA2 encodes a DNA helicase essential for replication of eukaryotic chromosomes. J Biol Chem, 270(45), 26766-26769.

Budd, M. E., Reis, C. C., Smith, S., Myung, K., & Campbell, J. L. (2006). Evidence suggesting that Pif1 helicase functions in DNA replication with the Dna2 helicase/nuclease and DNA polymerase delta. Mol Cell Biol, 26(7), 2490-2500. doi:10.1128/MCB.26.7.2490-2500.2006

Burgers, P. M. (2009). Polymerase dynamics at the eukaryotic DNA replication fork. J Biol Chem, 284(7), 4041-4045. doi:10.1074/jbc.R800062200

Burgers, P. M. J., & Kunkel, T. A. (2017). Eukaryotic DNA Replication Fork. Annu Rev Biochem, 86, 417-438. doi:10.1146/annurev-biochem-061516-044709

Burgess, R. J., & Zhang, Z. (2010). Roles for Gcn5 in promoting nucleosome assembly and maintaining genome integrity. Cell Cycle, 9(15), 2979-2985. doi:10.4161/cc.9.15.12498

Burgess, R. J., & Zhang, Z. (2013). Histone chaperones in nucleosome assembly and human disease. Nat Struct Mol Biol, 20(1), 14-22. doi:10.1038/nsmb.2461

Burkhart, R., Schulte, D., Hu, D., Musahl, C., Gohring, F., & Knippers, R. (1995). Interactions of human nuclear proteins P1Mcm3 and P1Cdc46. Eur J Biochem, 228(2), 431-438.

Buzovetsky, O., Kwon, Y., Pham, N. T., Kim, C., Ira, G., Sung, P., & Xiong, Y. (2017). Role of the Pif1-PCNA Complex in Pol delta-Dependent Strand Displacement DNA Synthesis and Break-Induced Replication. Cell Rep, 21(7), 1707-1714. doi:10.1016/j.celrep.2017.10.079

Calzada, A., Hodgson, B., Kanemaki, M., Bueno, A., & Labib, K. (2005). Molecular anatomy and regulation of a stable replisome at a paused eukaryotic DNA replication fork. Genes Dev, 19(16), 1905-1919. doi:10.1101/gad.337205

Cusick, M. E., DePamphilis, M. L., & Wassarman, P. M. (1984). Dispersive segregation of nucleosomes during replication of simian virus 40 chromosomes. *J Mol Biol, 178*(2), 249-271 Issn: 0022-2836.

Campos, E. I., Fillingham, J., Li, G., Zheng, H., Voigt, P., Kuo, W. H., . . . Reinberg, D. (2010). The program for processing newly synthesized histones H3.1 and H4. Nat Struct Mol Biol, 17(11), 1343-1351. doi:10.1038/nsmb.1911

Campos, E. I., & Reinberg, D. (2009). Histones: annotating chromatin. Annu Rev Genet, 43, 559-599. doi:10.1146/annurev.genet.032608.103928

Cejka, P., Plank, J. L., Dombrowski, C. C., & Kowalczykowski, S. C. (2012). Decatenation of DNA by the S. cerevisiae Sgs1-Top3-Rmi1 and RPA complex: a mechanism for disentangling chromosomes. Mol Cell, 47(6), 886-896. doi:10.1016/j.molcel.2012.06.032

Chafin, D. R., Vitolo, J. M., Henricksen, L. A., Bambara, R. A., & Hayes, J. J. (2000). Human DNA ligase I efficiently seals nicks in nucleosomes. EMBO J, 19(20), 5492-5501. doi:10.1093/emboj/19.20.5492

Chan, K. L., Palmai-Pallag, T., Ying, S., & Hickson, I. D. (2009). Replication stress induces sister-chromatid bridging at fragile site loci in mitosis. Nat Cell Biol, 11(6), 753-760. doi:10.1038/ncb1882

Chapados, B. R., Hosfield, D. J., Han, S., Qiu, J., Yelent, B., Shen, B., & Tainer, J. A. (2004). Structural basis for FEN-1 substrate specificity and PCNA-mediated activation in DNA replication and repair. Cell, 116(1), 39-50.

Charbin, A., Bouchoux, C., & Uhlmann, F. (2014). Condensin aids sister chromatid decatenation by topoisomerase II. Nucleic Acids Res, 42(1), 340-348. doi:10.1093/nar/gkt882

Chen, C. C., Carson, J. J., Feser, J., Tamburini, B., Zabaronick, S., Linger, J., & Tyler, J. K. (2008). Acetylated lysine 56 on histone H3 drives chromatin assembly after repair and signals for the completion of repair. Cell, 134(2), 231-243. doi:10.1016/j.cell.2008.06.035

Chilkova, O., Stenlund, P., Isoz, I., Stith, C. M., Grabowski, P., Lundstrom, E. B., . . . Johansson, E. (2007). The eukaryotic leading and lagging strand DNA polymerases are loaded onto primer-ends via separate mechanisms but have comparable processivity in the presence of PCNA. Nucleic Acids Res, 35(19), 6588-6597. doi:10.1093/nar/gkm741

Clemente-Ruiz, M., Gonzalez-Prieto, R., & Prado, F. (2011). Histone H3K56 acetylation, CAF1, and Rtt106 coordinate nucleosome assembly and stability of advancing replication forks. PLoS Genet, 7(11), e1002376. doi:10.1371/journal.pgen.1002376

Collins, S. R., Miller, K. M., Maas, N. L., Roguev, A., Fillingham, J., Chu, C. S., . . . Krogan, N. J. (2007). Functional dissection of protein complexes involved in yeast chromosome biology using a genetic interaction map. Nature, 446(7137), 806-810. doi:10.1038/nature05649

Cortez, D., Glick, G., & Elledge, S. J. (2004). Minichromosome maintenance proteins are direct targets of the ATM and ATR checkpoint kinases. Proc Natl Acad Sci U S A, 101(27), 10078-10083.

Culotti, J., & Hartwell, L. H. (1971). Genetic control of the cell division cycle in yeast. 3. Seven genes controlling nuclear division. Exp Cell Res, 67(2), 389-401.

D'Arcy, S., Martin, K. W., Panchenko, T., Chen, X., Bergeron, S., Stargell, L. A., . . . Luger, K. (2013). Chaperone Nap1 shields histone surfaces used in a nucleosome and can put H2A-H2B in an unconventional tetrameric form. Mol Cell, 51(5), 662-677. doi:10.1016/j.molcel.2013.07.015

Daigaku, Y., Keszthelyi, A., Muller, C. A., Miyabe, I., Brooks, T., Retkute, R., . . . Carr, A. M. (2015). A global profile of replicative polymerase usage. Nat Struct Mol Biol, 22(3), 192-198. doi:10.1038/nsmb.2962

Das, C., Lucia, M. S., Hansen, K. C., & Tyler, J. K. (2009). CBP/p300-mediated acetylation of histone H3 on lysine 56. Nature, 459(7243), 113-117. doi:10.1038/nature07861

Deegan, T. D., Yeeles, J. T., & Diffley, J. F. X. (2016). Phosphopeptide binding by Sld3 links Dbf4-dependent kinase to MCM replicative helicase activation. EMBO J, 35(9), 961-973. doi:10.15252/embj.201593552

Devbhandari, S., Jiang, J., Kumar, C., Whitehouse, I., & Remus, D. (2017). Chromatin Constrains the Initiation and Elongation of DNA Replication. Mol Cell, 65(1), 131-141. doi:10.1016/j.molcel.2016.10.035

Dewar, J. M., Budzowska, M., & Walter, J. C. (2015). The mechanism of DNA replication termination in vertebrates. Nature, 525(7569), 345-350. doi:10.1038/nature14887

Dewar, J. M., Low, E., Mann, M., Raschle, M., & Walter, J. C. (2017). CRL2(Lrr1) promotes unloading of the vertebrate replisome from chromatin during replication termination. Genes Dev, 31(3), 275-290. doi:10.1101/gad.291799.116

Dewar, J. M., & Walter, J. C. (2017). Mechanisms of DNA replication termination. Nat Rev Mol Cell Biol, 18(8), 507-516. doi:10.1038/nrm.2017.42

Diffley, J. F. X., Cocker, J. H., Dowell, S. J., & Rowley, A. (1994). Two steps in the assembly of complexes at yeast replication origins in vivo. Cell, 78(2), 303-316.

Diller, J. D., & Raghuraman, M. K. (1994). Eukaryotic replication origins: control in space and time. Trends Biochem Sci, 19(8), 320-325.

Dimitrova, D. S., Todorov, I. T., Melendy, T., & Gilbert, D. M. (1999). Mcm2, but not RPA, is a component of the mammalian early G1-phase prereplication complex. J Cell Biol, 146(4), 709-722.

DiNardo, S., Voelkel, K., & Sternglanz, R. (1984). DNA topoisomerase II mutant of Saccharomyces cerevisiae: topoisomerase II is required for segregation of daughter molecules at the termination of DNA replication. Proc Natl Acad Sci U S A, 81(9), 2616-2620.

Donaldson, A. D., Fangman, W. L., & Brewer, B. J. (1998). Cdc7 is required throughout the yeast S phase to activate replication origins. Genes Dev., 12(4), 491-501.

Donovan, S., Harwood, J., Drury, L. S., & Diffley, J. F. X. (1997). Cdc6p-dependent loading of Mcm proteins onto pre-replicative chromatin in budding yeast. Proc Natl Acad Sci U S A, 94(11), 5611-5616.

Douglas, M. E., Ali, F. A., Costa, A., & Diffley, J. F. X. (2018). The mechanism of eukaryotic CMG helicase activation. Nature, 555(7695), 265-268. doi:10.1038/nature25787

Douglas, M. E., & Diffley, J. F. X. (2016). Recruitment of Mcm10 to Sites of Replication Initiation Requires Direct Binding to the Minichromosome Maintenance (MCM) Complex. J Biol Chem, 291(11), 5879-5888. doi:10.1074/jbc.M115.707802

Dovrat, D., Stodola, J. L., Burgers, P. M., & Aharoni, A. (2014). Sequential switching of binding partners on PCNA during in vitro Okazaki fragment maturation. Proc Natl Acad Sci U S A, 111(39), 14118-14123. doi:10.1073/pnas.1321349111

Driscoll, R., Hudson, A., & Jackson, S. P. (2007). Yeast Rtt109 promotes genome stability by acetylating histone H3 on lysine 56. Science, 315(5812), 649-652. doi:10.1126/science.1135862

Eder, P. S., Walder, R. Y., & Walder, J. A. (1993). Substrate specificity of human RNase H1 and its role in excision repair of ribose residues misincorporated in DNA. Biochimie, 75(1-2), 123-126.

Edwards, M. C., Tutter, A. V., Cvetic, C., Gilbert, C. H., Prokhorova, T. A., & Walter, J. C. (2002). MCM2-7 complexes bind chromatin in a distributed pattern surrounding the origin recognition complex in Xenopus egg extracts. J Biol Chem, 277(36), 33049-33057.

English, C. M., Adkins, M. W., Carson, J. J., Churchill, M. E., & Tyler, J. K. (2006). Structural basis for the histone chaperone activity of Asf1. Cell, 127(3), 495-508. doi:10.1016/j.cell.2006.08.047

Evrin, C., Clarke, P., Zech, J., Lurz, R., Sun, J., Uhle, S., . . . Speck, C. (2009). A double-hexameric MCM2-7 complex is loaded onto origin DNA during licensing of eukaryotic DNA replication. Proc Natl Acad Sci U S A, 106(48), 20240-20245. doi:0911500106 [pii] 10.1073/pnas.0911500106

Evrin, C., Maman, J. D., Diamante, A., Pellegrini, L., & Labib, K. (2018). Histone H2A-H2B binding by Pol alpha in the eukaryotic replisome contributes to the maintenance of repressive chromatin. EMBO J. doi:10.15252/embj.201899021

Fachinetti, D., Bermejo, R., Cocito, A., Minardi, S., Katou, Y., Kanoh, Y., . . . Foiani, M. (2010). Replication termination at eukaryotic chromosomes is mediated by Top2 and occurs at genomic loci containing pausing elements. Mol Cell, 39(4), 595-605. doi:10.1016/j.molcel.2010.07.024

Fangman, W. L., & Brewer, B. J. (1992). A question of time: replication origins of eukaryotic chromosomes. Cell, 71(3), 363-366.

Fazly, A., Li, Q., Hu, Q., Mer, G., Horazdovsky, B., & Zhang, Z. (2012). Histone chaperone Rtt106 promotes nucleosome formation using (H3-H4)2 tetramers. J Biol Chem, 287(14), 10753-10760. doi:10.1074/jbc.M112.347450

Fillingham, J., Recht, J., Silva, A. C., Suter, B., Emili, A., Stagljar, I., . . . Greenblatt, J. F. (2008). Chaperone control of the activity and specificity of the histone H3 acetyltransferase Rtt109. Mol Cell Biol, 28(13), 4342-4353. doi:10.1128/MCB.00182-08

Foltman, M., Evrin, C., De Piccoli, G., Jones, R. C., Edmondson, R. D., Katou, Y., . . . Labib, K. (2013). Eukaryotic replisome components cooperate to process histones during chromosome replication. Cell Rep, 3(3), 892-904. doi:10.1016/j.celrep.2013.02.028

Formosa, T. (2012). The role of FACT in making and breaking nucleosomes. Biochim Biophys Acta, 1819(3-4), 247-255. doi:10.1016/j.bbagrm.2011.07.009

Formosa, T., & Nittis, T. (1999). Dna2 mutants reveal interactions with Dna polymerase alpha and Ctf4, a Pol alpha accessory factor, and show that full Dna2 helicase activity is not essential for growth. Genetics, 151(4), 1459-1470.

Frank, P., Braunshofer-Reiter, C., & Wintersberger, U. (1998). Yeast RNase H(35) is the counterpart of the mammalian RNase HI, and is evolutionarily related to prokaryotic RNase HII. FEBS Lett, 421(1), 23-26.

Franz, A., Orth, M., Pirson, P. A., Sonneville, R., Blow, J. J., Gartner, A., . . . Hoppe, T. (2011). CDC-48/p97 coordinates CDT-1 degradation with GINS chromatin dissociation to ensure faithful DNA replication. Mol Cell, 44(1), 85-96. doi:10.1016/j.molcel.2011.08.028

Frigola, J., Remus, D., Mehanna, A., & Diffley, J. F. X. (2013). ATPase-dependent quality control of DNA replication origin licensing. Nature, 495(7441), 339-343. doi:10.1038/nature11920

Fullbright, G., Rycenga, H. B., Gruber, J. D., & Long, D. T. (2016). p97 Promotes a Conserved Mechanism of Helicase Unloading during DNA Cross-Link Repair. Mol Cell Biol, 36(23), 2983-2994. doi:10.1128/MCB.00434-16

Fumasoni, M., Zwicky, K., Vanoli, F., Lopes, M., & Branzei, D. (2015). Error-free DNA damage tolerance and sister chromatid proximity during DNA replication rely on the Polalpha/Primase/Ctf4 Complex. Mol Cell, 57(5), 812-823. doi:10.1016/j.molcel.2014.12.038

Gambus, A. (2017). Termination of Eukaryotic Replication Forks. Adv Exp Med Biol, 1042, 163-187. doi:10.1007/978-981-10-6955-0_8

Gambus, A., Jones, R. C., Sanchez-Diaz, A., Kanemaki, M., van Deursen, F., Edmondson, R. D., & Labib, K. (2006). GINS maintains association of Cdc45 with MCM in replisome progression complexes at eukaryotic DNA replication forks. Nat Cell Biol, 8(4), 358-366. doi:ncb1382 [pii] 10.1038/ncb1382

Ganai, R. A., Zhang, X. P., Heyer, W. D., & Johansson, E. (2016). Strand displacement synthesis by yeast DNA polymerase epsilon. Nucleic Acids Res, 44(17), 8229-8240. doi:10.1093/nar/gkw556

Garg, P., Stith, C. M., Sabouri, N., Johansson, E., & Burgers, P. M. (2004). Idling by DNA polymerase delta maintains a ligatable nick during lagging-strand DNA replication. Genes Dev, 18(22), 2764-2773. doi:10.1101/gad.1252304

Ge, X. Q., Jackson, D. A., & Blow, J. J. (2007). Dormant origins licensed by excess Mcm2-7 are required for human cells to survive replicative stress. Genes Dev, 21(24), 3331-3341. doi:10.1101/gad.457807

Georgescu, R. E., Langston, L., Yao, N. Y., Yurieva, O., Zhang, D., Finkelstein, J., . . . O'Donnell, M. E. (2014). Mechanism of asymmetric polymerase assembly at the eukaryotic replication fork. Nat Struct Mol Biol, 21(8), 664-670. doi:10.1038/nsmb.2851

Georgescu, R. E., Schauer, G. D., Yao, N. Y., Langston, L. D., Yurieva, O., Zhang, D., . . . O'Donnell, M. E. (2015). Reconstitution of a eukaryotic replisome reveals suppression mechanisms that define leading/lagging strand operation. Elife, 4, e04988. doi:10.7554/eLife.04988

Gerik, K. J., Li, X., Pautz, A., & Burgers, P. M. (1998). Characterization of the two small subunits of Saccharomyces cerevisiae DNA polymerase delta. J Biol Chem, 273(31), 19747-19755.

Green, B. M., Finn, K. J., & Li, J. J. (2010). Loss of DNA replication control is a potent inducer of gene amplification. Science, 329(5994), 943-946. doi:329/5994/943 [pii] 10.1126/science.1190966

Gros, J., Devbhandari, S., & Remus, D. (2014). Origin plasticity during budding yeast DNA replication in vitro. EMBO J, 33(6), 621-636. doi:10.1002/embj.201387278

Groth, A., Corpet, A., Cook, A. J., Roche, D., Bartek, J., Lukas, J., & Almouzni, G. (2007). Regulation of replication fork progression through histone supply and demand. Science, 318(5858), 1928-1931. doi:10.1126/science.1148992

Guy, C. P., Atkinson, J., Gupta, M. K., Mahdi, A. A., Gwynn, E. J., Rudolph, C. J., . . . McGlynn, P. (2009). Rep provides a second motor at the replisome to promote duplication of protein-bound DNA. Mol Cell, 36(4), 654-666. doi:10.1016/j.molcel.2009.11.009

Hammond, C. M., Stromme, C. B., Huang, H., Patel, D. J., & Groth, A. (2017). Histone chaperone networks shaping chromatin function. Nat Rev Mol Cell Biol, 18(3), 141-158. doi:10.1038/nrm.2016.159

Han, J., Zhou, H., Horazdovsky, B., Zhang, K., Xu, R. M., & Zhang, Z. (2007). Rtt109 acetylates histone H3 lysine 56 and functions in DNA replication. Science, 315(5812), 653-655. doi:10.1126/science.1133234

Hanna, J. S., Kroll, E. S., Lundblad, V., & Spencer, F. A. (2001). Saccharomyces cerevisiae CTF18 and CTF4 are required for sister chromatid cohesion. Mol Cell Biol, 21(9), 3144-3158.

Harvey, K. J., & Newport, J. (2003). CpG methylation of DNA restricts prereplication complex assembly in Xenopus egg extracts. Mol Cell Biol, 23(19), 6769-6779.

Hathaway, N. A., Bell, O., Hodges, C., Miller, E. L., Neel, D. S., & Crabtree, G. R. (2012). Dynamics and memory of heterochromatin in living cells. Cell, 149(7), 1447-1460. doi:10.1016/j.cell.2012.03.052

Heller, R. C., Kang, S., Lam, W. M., Chen, S., Chan, C. S., & Bell, S. P. (2011). Eukaryotic Origin-Dependent DNA Replication In Vitro Reveals Sequential Action of DDK and S-CDK Kinases. Cell, 146(1), 80-91. doi:S0092-8674(11)00654-4 [pii] 10.1016/j.cell.2011.06.012

Hoek, M., & Stillman, B. (2003). Chromatin assembly factor 1 is essential and couples chromatin assembly to DNA replication in vivo. Proc Natl Acad Sci U S A, 100(21), 12183-12188. doi:10.1073/pnas.1635158100

Holm, C., Goto, T., Wang, J. C., & Botstein, D. (1985). DNA topoisomerase II is required at the time of mitosis in yeast. Cell, 41(2), 553-563.

Huang, H., Stromme, C. B., Saredi, G., Hodl, M., Strandsby, A., Gonzalez-Aguilera, C., . . . Patel, D. J. (2015). A unique binding mode enables MCM2 to chaperone histones H3-H4 at replication forks. Nat Struct Mol Biol, 22(8), 618-626. doi:10.1038/nsmb.3055

Huggins, C. F., Chafin, D. R., Aoyagi, S., Henricksen, L. A., Bambara, R. A., & Hayes, J. J. (2002). Flap endonuclease 1 efficiently cleaves base excision repair and DNA replication intermediates assembled into nucleosomes. Mol Cell, 10(5), 1201-1211.

Indiani, C., McInerney, P., Georgescu, R., Goodman, M. F., & O'Donnell, M. (2005). A sliding-clamp toolbelt binds high- and low-fidelity DNA polymerases simultaneously. Mol Cell, 19(6), 805-815. doi:10.1016/j.molcel.2005.08.011

Ivessa, A. S., Lenzmeier, B. A., Bessler, J. B., Goudsouzian, L. K., Schnakenberg, S. L., & Zakian, V. A. (2003). The Saccharomyces cerevisiae helicase Rrm3p facilitates replication past nonhistone protein-DNA complexes. Mol Cell, 12(6), 1525-1536.

Jackson, V., & Chalkley, R. (1981). A reevaluation of new histone deposition on replicating chromatin. J Biol Chem, 256(10), 5095-5103.

Jasencakova, Z., Scharf, A. N., Ask, K., Corpet, A., Imhof, A., Almouzni, G., & Groth, A. (2010). Replication stress interferes with histone recycling and predeposition marking of new histones. Mol Cell, 37(5), 736-743. doi:10.1016/j.molcel.2010.01.033

Johnston, L. H., & Nasmyth, K. A. (1978). Saccharomyces cerevisiae cell cycle mutant cdc9 is defective in DNA ligase. Nature, 274(5674), 891-893.

Kanemaki, M., & Labib, K. (2006). Distinct roles for Sld3 and GINS during establishment and progression of eukaryotic DNA replication forks. EMBO J, 25(8), 1753-1763.

Kang, H. Y., Choi, E., Bae, S. H., Lee, K. H., Gim, B. S., Kim, H. D., . . . Seo, Y. S. (2000). Genetic analyses of Schizosaccharomyces pombe dna2(+) reveal that dna2 plays an essential role in Okazaki fragment metabolism. Genetics, 155(3), 1055-1067.

Kang, Y. H., Lee, C. H., & Seo, Y. S. (2010). Dna2 on the road to Okazaki fragment processing and genome stability in eukaryotes. Crit Rev Biochem Mol Biol, 45(2), 71-96. doi:10.3109/10409230903578593

Katan-Khaykovich, Y., & Struhl, K. (2011). Splitting of H3-H4 tetramers at transcriptionally active genes undergoing dynamic histone exchange. Proc Natl Acad Sci U S A, 108(4), 1296-1301. doi:10.1073/pnas.1018308108

Kaya, H., Shibahara, K., Taoka, K., Iwabuchi, M., Stillman, B. and Araki, T.(2001) *FASCIATA* genes for Chromatin Assembly Factor-1 in Arabidopsis maintain the cellular organization of apical meristems. *Cell*, **104**, 131–142.

Kim, D., Setiaputra, D., Jung, T., Chung, J., Leitner, A., Yoon, J., . . . Song, J. J. (2016). Molecular Architecture of Yeast Chromatin Assembly Factor 1. Sci Rep, 6, 26702. doi:10.1038/srep26702

Koc, K. N., Singh, S. P., Stodola, J. L., Burgers, P. M., & Galletto, R. (2016). Pif1 removes a Rap1-dependent barrier to the strand displacement activity of DNA polymerase delta. Nucleic Acids Res, 44(8), 3811-3819. doi:10.1093/nar/gkw181

Krogan, N. J., Cagney, G., Yu, H., Zhong, G., Guo, X., Ignatchenko, A., . . . Greenblatt, J. F. (2006). Global landscape of protein complexes in the yeast Saccharomyces cerevisiae. Nature, 440(7084), 637-643. doi:10.1038/nature04670

Krude, T. (1995). Chromatin assembly factor 1 (CAF-1) colocalizes with replication foci in HeLa cell nuclei. Exp Cell Res, 220(2), 304-311.

Krude, T., & Knippers, R. (1991). Transfer of nucleosomes from parental to replicated chromatin. *Mol Cell Biol, 11*(12), 6257-6267.

Kubota, T., Katou, Y., Nakato, R., Shirahige, K., & Donaldson, A. D. (2015). Replication-Coupled PCNA Unloading by the Elg1 Complex Occurs Genome-wide and Requires Okazaki Fragment Ligation. Cell Rep, 12(5), 774-787. doi:10.1016/j.celrep.2015.06.066

Kurat, C. F., Yeeles, J. T., Patel, H., Early, A., & Diffley, J. F. X. (2017). Chromatin Controls DNA Replication Origin Selection, Lagging-Strand Synthesis, and Replication Fork Rates. Mol Cell, 65(1), 117-130. doi:10.1016/j.molcel.2016.11.016

Lee, L., Rodriguez, J., & Tsukiyama, T. (2015). Chromatin remodeling factors Isw2 and Ino80 regulate checkpoint activity and chromatin structure in S phase. Genetics, 199(4), 1077-1091. doi:10.1534/genetics.115.174730

Lei, M., Kawasaki, Y., & Tye, B. K. (1996). Physical interactions among MCM proteins and effects of MCM dosage on DNA-replication in Saccharomyces cerevisiae. Mol. Cell. Biol., 16(9), 5081-5090.

Levikova, M., & Cejka, P. (2015). The Saccharomyces cerevisiae Dna2 can function as a sole nuclease in the processing of Okazaki fragments in DNA replication. Nucleic Acids Res, 43(16), 7888-7897. doi:10.1093/nar/gkv710

Levikova, M., Klaue, D., Seidel, R., & Cejka, P. (2013). Nuclease activity of Saccharomyces cerevisiae Dna2 inhibits its potent DNA helicase activity. Proc Natl Acad Sci U S A, 110(22), E1992-2001. doi:10.1073/pnas.1300390110

Leyser, H.M. and Furner, I.J. (1992) Characterisation of three shoot apical meristem mutants of *Arabidopsis thaliana*. *Development*, **116**, 397–403.

Li, J. J., & Kelly, T. J. (1985). Simian virus 40 DNA replication in vitro: specificity of initiation and evidence for bidirectional replication. Mol Cell Biol, 5(6), 1238-1246.

Li, Q., Burgess, R., & Zhang, Z. (2013). All roads lead to chromatin: multiple pathways for histone deposition. Biochim Biophys Acta, 1819(3-4), 238-246.

Li, Q., Zhou, H., Wurtele, H., Davies, B., Horazdovsky, B., Verreault, A., & Zhang, Z. (2008). Acetylation of histone H3 lysine 56 regulates replication-coupled nucleosome assembly. Cell, 134(2), 244-255. doi:10.1016/j.cell.2008.06.018

Liu, S., Xu, Z., Leng, H., Zheng, P., Yang, J., Chen, K., . . . Li, Q. (2017). RPA binds histone H3-H4 and functions in DNA replication-coupled nucleosome assembly. Science, 355(6323), 415-420. doi:10.1126/science.aah4712

Liu, Y., Kao, H. I., & Bambara, R. A. (2004). Flap endonuclease 1: a central component of DNA metabolism. Annu Rev Biochem, 73, 589-615. doi:10.1146/annurev.biochem.73.012803.092453

Lu, X., Tan, C. K., Zhou, J. Q., You, M., Carastro, L. M., Downey, K. M., & So, A. G. (2002). Direct interaction of proliferating cell nuclear antigen with the small subunit of DNA polymerase delta. J Biol Chem, 277(27), 24340-24345. doi:10.1074/jbc.M200065200

Lucas, I., Germe, T., Chevrier-Miller, M., & Hyrien, O. (2001). Topoisomerase II can unlink replicating DNA by precatenane removal. EMBO J, 20(22), 6509-6519. doi:10.1093/emboj/20.22.6509

Maga, G., Villani, G., Tillement, V., Stucki, M., Locatelli, G. A., Frouin, I., . . . Hubscher, U. (2001). Okazaki fragment processing: modulation of the strand displacement activity of DNA polymerase delta by the concerted action of replication protein A, proliferating cell nuclear antigen, and flap endonuclease-1. Proc Natl Acad Sci U S A, 98(25), 14298-14303. doi:10.1073/pnas.251193198

Mahbubani, H. M., Chong, J. P., Chevalier, S., Thommes, P., & Blow, J. J. (1997). Cell cycle regulation of the replication licensing system: involvement of a Cdk-dependent inhibitor. J Cell Biol, 136(1), 125-135.

Maric, M., Maculins, T., De Piccoli, G., & Labib, K. (2014). Cdc48 and a ubiquitin ligase drive disassembly of the CMG helicase at the end of DNA replication. Science, 346(6208), 1253596. doi:10.1126/science.1253596

Masuda-Sasa, T., Imamura, O., & Campbell, J. L. (2006). Biochemical analysis of human Dna2. Nucleic Acids Res, 34(6), 1865-1875. doi:10.1093/nar/gkl070

Masumoto, H., Hawke, D., Kobayashi, R., & Verreault, A. (2005). A role for cell-cycle-regulated histone H3 lysine 56 acetylation in the DNA damage response. Nature, 436(7048), 294-298. doi:10.1038/nature03714

Mattiroli, F., Gu, Y., Yadav, T., Balsbaugh, J. L., Harris, M. R., Findlay, E. S., . . . Luger, K. (2017). DNA-mediated association of two histone-bound complexes of yeast Chromatin Assembly Factor-1 (CAF-1) drives tetrasome assembly in the wake of DNA replication. Elife, 6. doi:10.7554/eLife.22799

McKnight, S. L., & Miller, O. L. (1977). Electron microscopic analysis of chromatin replication in the cellular blastoderm *Drosophila melanogaster* embryo. *Cell, 12*, 795-804.

Mejlvang, J., Feng, Y., Alabert, C., Neelsen, K. J., Jasencakova, Z., Zhao, X., . . . Groth, A. (2014). New histone supply regulates replication fork speed and PCNA unloading. J Cell Biol, 204(1), 29-43. doi:10.1083/jcb.201305017

Mello, J. A., Sillje, H. H., Roche, D. M., Kirschner, D. B., Nigg, E. A., & Almouzni, G. (2002). Human Asf1 and CAF-1 interact and synergize in a repair-coupled nucleosome assembly pathway. EMBO Rep, 3(4), 329-334. doi:10.1093/embo-reports/kvf068

Meyer, H., Bug, M., & Bremer, S. (2012). Emerging functions of the VCP/p97 AAA-ATPase in the ubiquitin system. Nat Cell Biol, 14(2), 117-123. doi:10.1038/ncb2407

Moggs, J. G., Grandi, P., Quivy, J. P., Jonsson, Z. O., Hubscher, U., Becker, P. B., & Almouzni, G. (2000). A CAF-1-PCNA-mediated chromatin assembly pathway triggered by sensing DNA damage. Mol Cell Biol, 20(4), 1206-1218.

Mohanty, B. K., Bairwa, N. K., & Bastia, D. (2006). The Tof1p-Csm3p protein complex counteracts the Rrm3p helicase to control replication termination of Saccharomyces cerevisiae. Proc Natl Acad Sci U S A, 103(4), 897-902. doi:10.1073/pnas.0506540103

Moreno, S. P., Bailey, R., Campion, N., Herron, S., & Gambus, A. (2014). Polyubiquitylation drives replisome disassembly at the termination of DNA replication. Science, 346(6208), 477-481. doi:10.1126/science.1253585

Morgan, D. (2007). The cell cycle : principles of control. Oxford: Oxford University Press.

Murante, R. S., Henricksen, L. A., & Bambara, R. A. (1998). Junction ribonuclease: an activity in Okazaki fragment processing. Proc Natl Acad Sci U S A, 95(5), 2244-2249.

Nabatiyan, A., & Krude, T. (2004). Silencing of chromatin assembly factor 1 in human cells leads to cell death and loss of chromatin assembly during DNA synthesis. Mol Cell Biol, 24(7), 2853-2862.

Natsume, R., Eitoku, M., Akai, Y., Sano, N., Horikoshi, M., & Senda, T. (2007). Structure and function of the histone chaperone CIA/ASF1 complexed with histones H3 and H4. Nature, 446(7133), 338-341. doi:10.1038/nature05613

Nguyen, V. Q., Co, C., & Li, J. J. (2001). Cyclin-dependent kinases prevent DNA re-replication through multiple mechanisms. Nature, 411(6841), 1068-1073.

Nishiyama, A., Frappier, L., & Mechali, M. (2011). MCM-BP regulates unloading of the MCM2-7 helicase in late S phase. Genes Dev, 25(2), 165-175. doi:10.1101/gad.614411

Okazaki, R., Okazaki, T., Sakabe, K., Sugimoto, K., & Sugino, A. (1968). Mechanism of DNA chain growth. I. Possible discontinuity and unusual secondary structure of newly synthesized chains. Proc Natl Acad Sci U S A, 59(2), 598-605.

On, K. F., Beuron, F., Frith, D., Snijders, A. P., Morris, E. P., & Diffley, J. F. X. (2014). Prereplicative complexes assembled in vitro support origin-dependent and independent DNA replication. EMBO J, 33(6), 605-620. doi:10.1002/embj.201387369

Osmundson, J. S., Kumar, J., Yeung, R., & Smith, D. J. (2017). Pif1-family helicases cooperatively suppress widespread replication-fork arrest at tRNA genes. Nat Struct Mol Biol, 24(2), 162-170. doi:10.1038/nsmb.3342

Paeschke, K., Bochman, M. L., Garcia, P. D., Cejka, P., Friedman, K. L., Kowalczykowski, S. C., & Zakian, V. A. (2013). Pif1 family helicases suppress genome instability at G-quadruplex motifs. Nature, 497(7450), 458-462. doi:10.1038/nature12149

Paeschke, K., Capra, J. A., & Zakian, V. A. (2011). DNA replication through G-quadruplex motifs is promoted by the Saccharomyces cerevisiae Pif1 DNA helicase. Cell, 145(5), 678-691. doi:10.1016/j.cell.2011.04.015

Papamichos-Chronakis, M., & Peterson, C. L. (2008). The Ino80 chromatin-remodeling enzyme regulates replisome function and stability. Nat Struct Mol Biol, 15(4), 338-345. doi:10.1038/nsmb.1413

Pellegrini, L., & Costa, A. (2016). New Insights into the Mechanism of DNA Duplication by the Eukaryotic Replisome. Trends Biochem Sci, 41(10), 859-871. doi:10.1016/j.tibs.2016.07.011

Petryk, N., Dalby, M., Wenger, A., Stromme, C. B., Strandsby, A., Andersson, R., & Groth, A. (2018). MCM2 promotes symmetric inheritance of modified histones during DNA replication. Science. doi:10.1126/science.aau0294

Pike, J. E., Burgers, P. M., Campbell, J. L., & Bambara, R. A. (2009). Pif1 helicase lengthens some Okazaki fragment flaps necessitating Dna2 nuclease/helicase

action in the two-nuclease processing pathway. J Biol Chem, 284(37), 25170-25180. doi:10.1074/jbc.M109.023325

Podust, V. N., & Hubscher, U. (1993). Lagging strand DNA synthesis by calf thymus DNA polymerases alpha, beta, delta and epsilon in the presence of auxiliary proteins. Nucleic Acids Res, 21(4), 841-846.

Postow, L., Ullsperger, C., Keller, R. W., Bustamante, C., Vologodskii, A. V., & Cozzarelli, N. R. (2001). Positive torsional strain causes the formation of a four-way junction at replication forks. J Biol Chem, 276(4), 2790-2796. doi:10.1074/jbc.M006736200

Prior, C. P., Cantor, C. R., Johnson, E. M., & Allfrey, V. G. (1980). Incorporation of exogenous pyrene-labeled histone into Physarum chromatin: a system for studying changes in nucleosomes assembled in vivo. Cell, 20(3), 597-608.

Ptashne, M. (2007). On the use of the word 'epigenetic'. Curr Biol, 17(7), R233-236. doi:10.1016/j.cub.2007.02.030

Qiu, J., Qian, Y., Frank, P., Wintersberger, U., & Shen, B. (1999). Saccharomyces cerevisiae RNase H(35) functions in RNA primer removal during lagging-strand DNA synthesis, most efficiently in cooperation with Rad27 nuclease. Mol Cell Biol, 19(12), 8361-8371.

Quan, Y., Xia, Y., Liu, L., Cui, J., Li, Z., Cao, Q., . . . Lou, H. (2015). Cell-Cycle-Regulated Interaction between Mcm10 and Double Hexameric Mcm2-7 Is Required for Helicase Splitting and Activation during S Phase. Cell Rep, 13(11), 2576-2586. doi:10.1016/j.celrep.2015.11.018

Radman-Livaja, M., Verzijlbergen, K. F., Weiner, A., van Welsem, T., Friedman, N., Rando, O. J., & van Leeuwen, F. (2011). Patterns and mechanisms of ancestral histone protein inheritance in budding yeast. PLoS Biol, 9(6), e1001075. doi:10.1371/journal.pbio.1001075

Randall, S. K., & Kelly, T. J. (1992). The fate of parental nucleosomes during SV40 DNA replication. *J Biol Chem, 267*(20), 14259-14265.

Reagan, M. S., Pittenger, C., Siede, W., & Friedberg, E. C. (1995). Characterization of a mutant strain of Saccharomyces cerevisiae with a deletion of the RAD27 gene, a structural homolog of the RAD2 nucleotide excision repair gene. J Bacteriol, 177(2), 364-371.

Recht, J., Tsubota, T., Tanny, J. C., Diaz, R. L., Berger, J. M., Zhang, X., . . . Allis, C. D. (2006). Histone chaperone Asf1 is required for histone H3 lysine 56 acetylation, a modification associated with S phase in mitosis and meiosis. Proc Natl Acad Sci U S A, 103(18), 6988-6993. doi:10.1073/pnas.0601676103

Reinholz, E. (1966) Radiation induced mutants showing changed inflorescence characteristics. *Arab. Inf. Serv.* **3**, 19–20.

Remus, D., Beuron, F., Tolun, G., Griffith, J. D., Morris, E. P., & Diffley, J. F. X. (2009). Concerted loading of Mcm2-7 double hexamers around DNA during DNA replication origin licensing. Cell, 139(4), 719-730. doi:S0092-8674(09)01303-8 [pii] 10.1016/j.cell.2009.10.015

Ricke, R. M., & Bielinsky, A. K. (2004). Mcm10 regulates the stability and chromatin association of DNA polymerase-alpha. Mol Cell, 16(2), 173-185.

Ritzi, M., Baack, M., Musahl, C., Romanowski, P., Laskey, R. A., & Knippers, R. (1998). Human minichromosome maintenance proteins and human origin recognition complex 2 protein on chromatin. J Biol Chem, 273(38), 24543-24549.

Romanowski, P., Madine, M. A., & Laskey, R. A. (1996). XMCM7, a novel member of the Xenopus MCM family, interacts with XMCM3 and colocalizes with it throughout replication [see comments]. Proceedings of the National Academy of Sciences of the United States of America, 93(19), 10189-10194.

Rossi, M. L., & Bambara, R. A. (2006). Reconstituted Okazaki fragment processing indicates two pathways of primer removal. J Biol Chem, 281(36), 26051-26061. doi:10.1074/jbc.M604805200

Rossi, M. L., Pike, J. E., Wang, W., Burgers, P. M., Campbell, J. L., & Bambara, R. A. (2008). Pif1 helicase directs eukaryotic Okazaki fragments toward the two-nuclease cleavage pathway for primer removal. J Biol Chem, 283(41), 27483-27493. doi:10.1074/jbc.M804550200

Rowles, A., Chong, J. P., Brown, L., Howell, M., Evan, G. I., & Blow, J. J. (1996). Interaction between the origin recognition complex and the replication licensing system in Xenopus. Cell, 87(2), 287-296.

Sabouri, N., McDonald, K. R., Webb, C. J., Cristea, I. M., & Zakian, V. A. (2012). DNA replication through hard-to-replicate sites, including both highly transcribed RNA Pol II and Pol III genes, requires the S. pombe Pfh1 helicase. Genes Dev, 26(6), 581-593. doi:10.1101/gad.184697.111

Samora, C. P., Saksouk, J., Goswami, P., Wade, B. O., Singleton, M. R., Bates, P. A., . . . Uhlmann, F. (2016). Ctf4 Links DNA Replication with Sister Chromatid Cohesion Establishment by Recruiting the Chl1 Helicase to the Replisome. Mol Cell, 63(3), 371-384. doi:10.1016/j.molcel.2016.05.036

Sauer, P. V., Timm, J., Liu, D., Sitbon, D., Boeri-Erba, E., Velours, C., . . . Panne, D. (2017). Insights into the molecular architecture and histone H3-H4 deposition mechanism of yeast Chromatin assembly factor 1. Elife, 6. doi:10.7554/eLife.23474

Schalbetter, S. A., Mansoubi, S., Chambers, A. L., Downs, J. A., & Baxter, J. (2015). Fork rotation and DNA precatenation are restricted during DNA replication to

prevent chromosomal instability. Proc Natl Acad Sci U S A, 112(33), E4565-4570. doi:10.1073/pnas.1505356112

Selth, L., & Svejstrup, J. Q. (2007). Vps75, a new yeast member of the NAP histone chaperone family. J Biol Chem, 282(17), 12358-12362. doi:10.1074/jbc.C700012200

Sengupta, S., van Deursen, F., de Piccoli, G., & Labib, K. (2013). Dpb2 integrates the leading-strand DNA polymerase into the eukaryotic replisome. Curr Biol, 23(7), 543-552. doi:10.1016/j.cub.2013.02.011

Shibahara, K., & Stillman, B. (1999). Replication-dependent marking of DNA by PCNA facilitates CAF-1-coupled inheritance of chromatin. Cell, 96(4), 575-585.

Siddiqui, K., On, K. F., & Diffley, J. F. X. (2013). Regulating DNA replication in eukarya. Cold Spring Harb Perspect Biol, 5(9), a012930. doi:10.1101/cshperspect.a012930

Sikorski, R. S., & Hieter, P. (1989). A system of shuttle vectors and yeast host strains designed for efficient manipulation of DNA in Saccharomyces cerevisiae. Genetics, 122, 19-27.

Simon, A. C., Zhou, J. C., Perera, R. L., van Deursen, F., Evrin, C., Ivanova, M. E., . . . Pellegrini, L. (2014). A Ctf4 trimer couples the CMG helicase to DNA polymerase alpha in the eukaryotic replisome. Nature, 510(7504), 293-297. doi:10.1038/nature13234

Smith, D. J., & Whitehouse, I. (2012). Intrinsic coupling of lagging-strand synthesis to chromatin assembly. Nature, 483(7390), 434-438. doi:10.1038/nature10895

Smith, S., & Stillman, B. (1989). Purification and characterization of CAF-I, a human cell factor required for chromatin assembly during DNA replication in vitro. Cell, 58(1), 15-25.

Sofueva, S., Osman, F., Lorenz, A., Steinacher, R., Castagnetti, S., Ledesma, J., & Whitby, M. C. (2011). Ultrafine anaphase bridges, broken DNA and illegitimate recombination induced by a replication fork barrier. Nucleic Acids Res, 39(15), 6568-6584. doi:10.1093/nar/gkr340

Sogo, J. M., Stahl, H., Koller, T., & Knippers, R. (1986). Structure of replicating simian virus 40 minichromosomes. The replication fork, core histone segregation and terminal structures. *J Mol Biol, 189*(1), 189-204.

Sonneville, R., Moreno, S. P., Knebel, A., Johnson, C., Hastie, C. J., Gartner, A., . . . Labib, K. (2017). CUL-2(LRR-1) and UBXN-3 drive replisome disassembly during DNA replication termination and mitosis. Nat Cell Biol, 19(5), 468-479. doi:10.1038/ncb3500

Steinacher, R., Osman, F., Dalgaard, J. Z., Lorenz, A., & Whitby, M. C. (2012). The DNA helicase Pfh1 promotes fork merging at replication termination sites to ensure genome stability. Genes Dev, 26(6), 594-602. doi:10.1101/gad.184663.111

Stillman, B. (1986). Chromatin assembly during SV40 DNA replication in vitro. Cell, 45(4), 555-565.

Stillman, B., Gerard, R. D., Guggenheimer, R. A., & Gluzman, Y. (1985). T antigen and template requirements for SV40 DNA replication in vitro. EMBO J, 4(11), 2933-2939.

Stillman, B. W., & Gluzman, Y. (1985). Replication and supercoiling of simian virus 40 DNA in cell extracts from human cells. Mol Cell Biol, 5(8), 2051-2060.

Stith, C. M., Sterling, J., Resnick, M. A., Gordenin, D. A., & Burgers, P. M. (2008). Flexibility of eukaryotic Okazaki fragment maturation through regulated strand displacement synthesis. J Biol Chem, 283(49), 34129-34140. doi:10.1074/jbc.M806668200

Stodola, J. L., & Burgers, P. M. (2016). Resolving individual steps of Okazaki-fragment maturation at a millisecond timescale. Nat Struct Mol Biol, 23(5), 402-408. doi:10.1038/nsmb.3207

Straube, K., Blackwell, J. S., Jr., & Pemberton, L. F. (2010). Nap1 and Chz1 have separate Htz1 nuclear import and assembly functions. Traffic, 11(2), 185-197. doi:10.1111/j.1600-0854.2009.01010.x

Su, D., Hu, Q., Li, Q., Thompson, J. R., Cui, G., Fazly, A., . . . Mer, G. (2012). Structural basis for recognition of H3K56-acetylated histone H3-H4 by the chaperone Rtt106. Nature, 483(7387), 104-107. doi:10.1038/nature10861

Sun, X., Thrower, D., Qiu, J., Wu, P., Zheng, L., Zhou, M., . . . Shen, B. (2003). Complementary functions of the Saccharomyces cerevisiae Rad2 family nucleases in Okazaki fragment maturation, mutation avoidance, and chromosome stability. DNA Repair (Amst), 2(8), 925-940.

Sundin, O., & Varshavsky, A. (1980). Terminal stages of SV40 DNA replication proceed via multiply intertwined catenated dimers. Cell, 21(1), 103-114.

Suski, C., & Marians, K. J. (2008). Resolution of converging replication forks by RecQ and topoisomerase III. Mol Cell, 30(6), 779-789. doi:10.1016/j.molcel.2008.04.020

Swygert, S. G., & Peterson, C. L. (2014). Chromatin dynamics: interplay between remodeling enzymes and histone modifications. Biochim Biophys Acta, 1839(8), 728-736. doi:10.1016/j.bbagrm.2014.02.013

Takahashi, T. S., Wigley, D. B., & Walter, J. C. (2005). Pumps, paradoxes and ploughshares: mechanism of the MCM2-7 DNA helicase. Trends Biochem Sci, 30(8), 437-444.

Tanaka, S., & Araki, H. (2013). Helicase activation and establishment of replication forks at chromosomal origins of replication. Cold Spring Harb Perspect Biol, 5(12), a010371. doi:10.1101/cshperspect.a010371

Tanaka, S., Umemori, T., Hirai, K., Muramatsu, S., Kamimura, Y., & Araki, H. (2007). CDK-dependent phosphorylation of Sld2 and Sld3 initiates DNA replication in budding yeast. Nature, 445(7125), 328-332. doi:nature05465 [pii] 10.1038/nature05465

Tishkoff, D. X., Boerger, A. L., Bertrand, P., Filosi, N., Gaida, G. M., Kane, M. F., & Kolodner, R. D. (1997). Identification and characterization of Saccharomyces cerevisiae EXO1, a gene encoding an exonuclease that interacts with MSH2. Proc Natl Acad Sci U S A, 94(14), 7487-7492.

Todorov, I. T., Attaran, A., & Kearsey, S. E. (1995). BM28, a human member of the MCM2-3-5 family, is displaced from chromatin during DNA replication. J Cell Biol, 129(6), 1433-1445.

Tsao, C. C., Geisen, C., & Abraham, R. T. (2004). Interaction between human MCM7 and Rad17 proteins is required for replication checkpoint signaling. EMBO J, 23(23), 4660-4669. doi:10.1038/sj.emboj.7600463

Tsubota, T., Berndsen, C. E., Erkmann, J. A., Smith, C. L., Yang, L., Freitas, M. A., . . . Kaufman, P. D. (2007). Histone H3-K56 acetylation is catalyzed by histone chaperone-dependent complexes. Mol Cell, 25(5), 703-712. doi:10.1016/j.molcel.2007.02.006

Tsukuda, T., Fleming, A. B., Nickoloff, J. A., & Osley, M. A. (2005). Chromatin remodelling at a DNA double-strand break site in Saccharomyces cerevisiae. Nature, 438(7066), 379-383. doi:10.1038/nature04148

Tsurimoto, T., & Stillman, B. (1990). Functions of replication factor C and proliferating-cell nuclear antigen: functional similarity of DNA polymerase accessory proteins from human cells and bacteriophage T4. Proc Natl Acad Sci U S A, 87(3), 1023-1027.

Tyler, J. K., Adams, C. R., Chen, S. R., Kobayashi, R., Kamakaka, R. T., & Kadonaga, J. T. (1999). The RCAF complex mediates chromatin assembly during DNA replication and repair. Nature, 402(6761), 555-560. doi:10.1038/990147

Uemura, T., & Yanagida, M. (1984). Isolation of type I and II DNA topoisomerase mutants from fission yeast: single and double mutants show different phenotypes in cell growth and chromatin organization. EMBO J, 3(8), 1737-1744.

van Attikum, H., Fritsch, O., & Gasser, S. M. (2007). Distinct roles for SWR1 and INO80 chromatin remodeling complexes at chromosomal double-strand breaks. EMBO J, 26(18), 4113-4125. doi:10.1038/sj.emboj.7601835

Vassileva, I., Yanakieva, I., Peycheva, M., Gospodinov, A., & Anachkova, B. (2014). The mammalian INO80 chromatin remodeling complex is required for replication stress recovery. Nucleic Acids Res, 42(14), 9074-9086. doi:10.1093/nar/gku605

Vijayakumar, S., Chapados, B. R., Schmidt, K. H., Kolodner, R. D., Tainer, J. A., & Tomkinson, A. E. (2007). The C-terminal domain of yeast PCNA is required for physical and functional interactions with Cdc9 DNA ligase. Nucleic Acids Res, 35(5), 1624-1637. doi:10.1093/nar/gkm006

Villa, F., Simon, A. C., Ortiz Bazan, M. A., Kilkenny, M. L., Wirthensohn, D., Wightman, M., . . . Labib, K. (2016). Ctf4 Is a Hub in the Eukaryotic Replisome that Links Multiple CIP-Box Proteins to the CMG Helicase. Mol Cell, 63(3), 385-396. doi:10.1016/j.molcel.2016.06.009

Wang, J. C. (2002). Cellular roles of DNA topoisomerases: A molecular perspective. Nature Reviews Molecular Cell Biology, 3(6), 430-440.

Wanrooij, P. H., & Burgers, P. M. (2015). Yet another job for Dna2: Checkpoint activation. DNA Repair (Amst), 32, 17-23. doi:10.1016/j.dnarep.2015.04.009

Wilson, M. A., Kwon, Y., Xu, Y., Chung, W. H., Chi, P., Niu, H., . . . Ira, G. (2013). Pif1 helicase and Poldelta promote recombination-coupled DNA synthesis via bubble migration. Nature, 502(7471), 393-396. doi:10.1038/nature12585

Winkler, D. D., Muthurajan, U. M., Hieb, A. R., & Luger, K. (2011). Histone chaperone FACT coordinates nucleosome interaction through multiple synergistic binding events. J Biol Chem, 286(48), 41883-41892. doi:10.1074/jbc.M111.301465

Xu, M., Long, C., Chen, X., Huang, C., Chen, S., & Zhu, B. (2010). Partitioning of histone H3-H4 tetramers during DNA replication-dependent chromatin assembly. Science, 328(5974), 94-98. doi:10.1126/science.1178994

Yadav, T., & Whitehouse, I. (2016). Replication-Coupled Nucleosome Assembly and Positioning by ATP-Dependent Chromatin-Remodeling Enzymes. Cell Rep, 15(4), 715-723. doi:10.1016/j.celrep.2016.03.059

Yang, J., Zhang, X., Feng, J., Leng, H., Li, S., Xiao, J., . . . Li, Q. (2016). The Histone Chaperone FACT Contributes to DNA Replication-Coupled Nucleosome Assembly. Cell Rep, 16(12), 3414. doi:10.1016/j.celrep.2016.08.070

Ye, X., Franco, A. A., Santos, H., Nelson, D. M., Kaufman, P. D., & Adams, P. D. (2003). Defective S phase chromatin assembly causes DNA damage, activation of the S phase checkpoint, and S phase arrest. Mol Cell, 11(2), 341-351.

Yeeles, J. T., Deegan, T. D., Janska, A., Early, A., & Diffley, J. F. X. (2015). Regulated eukaryotic DNA replication origin firing with purified proteins. Nature, 519(7544), 431-435. doi:10.1038/nature14285

Yeeles, J. T., Janska, A., Early, A., & Diffley, J. F. X. (2017). How the Eukaryotic Replisome Achieves Rapid and Efficient DNA Replication. Mol Cell, 65(1), 105-116. doi:10.1016/j.molcel.2016.11.017

Yu, C., Gan, H., Han, J., Zhou, Z. X., Jia, S., Chabes, A., . . . Zhang, Z. (2014). Strand-specific analysis shows protein binding at replication forks and PCNA unloading from lagging strands when forks stall. Mol Cell, 56(4), 551-563. doi:10.1016/j.molcel.2014.09.017

Yu, C., Gan, H., Serra-Cardona, A., Zhang, L., Gan, S., Sharma, S., . . . Zhang, Z. (2018). A mechanism for preventing asymmetric histone segregation onto replicating DNA strands. Science. doi:10.1126/science.aat8849

Zechiedrich, E. L., & Cozzarelli, N. R. (1995). Roles of topoisomerase IV and DNA gyrase in DNA unlinking during replication in Escherichia coli. Genes Dev, 9(22), 2859-2869.

Zegerman, P., & Diffley, J. F. X. (2007). Phosphorylation of Sld2 and Sld3 by cyclin-dependent kinases promotes DNA replication in budding yeast. Nature, 445(7125), 281-285. doi:10.1038/nature05432

Zhang, Z., Shibahara, K., & Stillman, B. (2000). PCNA connects DNA replication to epigenetic inheritance in yeast. Nature, 408(6809), 221-225.

Zheng, L., Zhou, M., Guo, Z., Lu, H., Qian, L., Dai, H., . . . Shen, B. (2008). Human DNA2 is a mitochondrial nuclease/helicase for efficient processing of DNA replication and repair intermediates. Mol Cell, 32(3), 325-336. doi:10.1016/j.molcel.2008.09.024

Zhou, H., Madden, B. J., Muddiman, D. C., & Zhang, Z. (2006). Chromatin assembly factor 1 interacts with histone H3 methylated at lysine 79 in the processes of epigenetic silencing and DNA repair. Biochemistry, 45(9), 2852-2861. doi:10.1021/bi0521083

Zou, L., & Stillman, B. (1998). Formation of a preinitiation complex by S-phase cyclin CDK-dependent loading of Cdc45p onto chromatin. Science, 280(5363), 593-596.